



**Enhancing Structural Performance of Concrete Structures with
Recycled Steel Fibers through improved Mechanical, Dynamic,
and Shear Properties**

By

Xia Qin

A thesis submitted to the University of Birmingham for the degree of
Doctoral of Philosophy

School of engineering

Department of civil engineering

University of Birmingham

August 2024

UNIVERSITY OF
BIRMINGHAM

University of Birmingham Research Archive

e-theses repository

This unpublished thesis/dissertation is copyright of the author and/or third parties. The intellectual property rights of the author or third parties in respect of this work are as defined by The Copyright Designs and Patents Act 1988 or as modified by any successor legislation.

Any use made of information contained in this thesis/dissertation must be in accordance with that legislation and must be properly acknowledged. Further distribution or reproduction in any format is prohibited without the permission of the copyright holder.

© 2023 University of Birmingham

All rights reserved. This copyright is held by the author. No part of this thesis may be reproduced or transmitted in any form or by any means, electronic or mechanical, including photocopying, recording, or by any information storage and retrieval system, without permission in writing from the author.

Abstract

This thesis explores the potential of recycled steel fibres (RSF) as an innovative and environmentally friendly reinforcement material for concrete, addressing the urgent need for cost-effective and sustainable alternatives in the construction industry. RSF, sourced from discarded tires and construction waste, can partially replace industrial steel fibres (ISF), offering benefits such as cost reduction, lower carbon emissions, and enhanced structural strength. This dual advantage not only mitigates environmental pollution but also conserves resources.

The first part of the thesis involves a comprehensive study of the engineering characteristics of RSF, including its mechanical properties, dynamic performance, and structural shear resistance. An essential part of the study is the development of a set of improved shear capacity prediction formulas for high strength steel fibre concrete (HSFRC) beams, based on modifications to the TR63 standard. Additionally, the cradle-to-grave life cycle analysis was conducted to evaluate the carbon footprint of RSF. In the second part, the thesis focuses on modelling and predicting the overall performance of HSFRC beams using experimental data and machine learning techniques. Various machine learning (ML) models were employed to predict key parameters, and finite element modelling (FEM) was used to establish the mechanical behaviour model. Surrogate models were developed to streamline the modelling process, ensuring quick and accurate parameter estimation. With the help of reliable collected experimental database, the study provides a thorough analysis of the reliability of HSFRC beams, offering

recommendations to balance safety and economic efficiency. The research also presents a simplified model for assessing the performance of HSFRC beams in corrosive environments, highlighting the material's time-dependent reliability. In summary, RSF emerges as a possible, low-cost, and sustainable substitute for ISF, which has enormous implications for the construction sector.

Acknowledgment

First and foremost, I would like to extend my sincerest gratitude to my supervisor, Dr. Sakdirat Kaewunruen, for his exceptional guidance and unwavering support throughout my Ph.D. journey. His profound expertise and rigorous academic standards have been invaluable to my research.

I am deeply thankful to laboratory members Jonathan Briggs, Mark Carter, and Rachel Kennedy for their indispensable assistance in the experimental process. Their support was crucial in enabling me to complete the experiments successfully. I also wish to express my appreciation to the members of the TOFU research group, especially Dan Li, Rucheng Liu, Xu Huang, Hao Fu, Junhui Huang, Yang Li, Ruihua Liang, Chayut Ngamkhanong, Panrawee Rungskunroch, Zhichao Huang, Jessada Sresakoolchai and Pasakorn Sengsri. Your friendship and support during my time in Birmingham have made my research journey more enriching and enjoyable.

Finally, I am profoundly grateful to my family. My parents and wife unwavering encouragement and support have been my constant source of strength, and special thanks go to my uncle for providing the invaluable experimental materials. Your steadfast belief in me has been the driving force behind my perseverance and achievements.

List of Publications

The doctoral dissertation adopts a structure akin to an amalgamation of published articles. Its composition primarily comprises scientific articles that have already been published or are currently under submission to scholarly journals.

Published:

Qin, X., & Kaewunruen, S. (2022). Environment-friendly recycled steel fibre reinforced concrete. *Construction and Building Materials*, 327, 126967.

Qin, X., & Kaewunruen, S. (2023). Eco-Friendly Design and Sustainability Assessments of Fibre-Reinforced High-Strength Concrete Structures Automated by Data-Driven Machine Learning Models. *Sustainability*, 15(8), 6640.

Qin, X., Huang, X., Li, Y., & Kaewunruen, S. (2024). Sustainable design framework for enhancing shear capacity in beams using recycled steel fiber-reinforced high-strength concrete. *Construction and Building Materials*, 411, 134509.

Qin, X., Huang, X., & Kaewunruen, S. (2024). Sustainable design and carbon-credited application framework of recycled steel fibre reinforced concrete. *Developments in the Built Environment*, 100404.

Qin, X., & Kaewunruen, S. (2024, May). Circular Economy in Construction: Harnessing Secondary Materials from End-of-Life Tires for Sustainable Building. In *International Conference" Coordinating Engineering for Sustainability and Resilience"* (pp. 302-311).

Cham: Springer Nature Switzerland.

Qin, X., & Kaewunruen, S. (2024). Machine Learning and Traditional Approaches in Shear Reliability of Steel Fiber Reinforced Concrete Beams. *Reliability Engineering & System Safety*, 110339.

In Progress:

Qin, X., & Kaewunruen, S. (2024). Surrogated Modelling for Structure Reliability and Safety Assessments of High-Strength Concrete Beams with Industrial and Recycled Steel Fibers. *Engineering Structures*.

Qin, X., & Kaewunruen, S. (2024). Time-Dependent Reliability Assessment and Durability Analysis of Industrial and Recycled Steel Fiber Reinforced Concrete Beams. *Reliability Engineering & System Safety*.

Co-published:

Wu, H., Qin, X., Huang, X., & Kaewunruen, S. (2023). Engineering, mechanical and dynamic properties of basalt fiber reinforced concrete. *Materials*, 16(2), 623.

Huang, X., Sresakoolchai, J., Qin, X., Ho, Y. F., & Kaewunruen, S. (2022). Self-healing performance assessment of bacterial-based concrete using machine learning approaches. *Materials*, 15(13), 4436.

Glossary

ABBREVIATIONS	DEFINITION
ISF	Industrial Steel Fibre
RSF	Recycled Steel Fibre
SFRC	Steel Fibre Reinforced Concrete
ISFRC	Industrial Steel Fibre Reinforced Concrete
RSFRC	Recycled Steel Fibre Reinforced Concrete
PC	Plain Concrete
HSF	Hybrid Steel Fibre
HSFRC	Hybrid Steel Fibre Reinforced Concrete
ELT	End-of-life Tires
HSC	High Strength Concrete
CTOD	Crack Tip Opening Displacement
CMOD	Crack Mouth Opening Displacement
CO₂	Carbon dioxide

GWP	Global Warming Potential
SHM	Structural Health Monitoring
SEM	Scanning Electron Microscopy
LOP	Limit of Proportionality
AVG	Average Value
SD	Standard Deviation
COV	Coefficient of Variation
ML	Machine Learning
AI	Artificial Intelligence
ANN	Artificial Neural network
XGBOOST	eXtreme Gradient Boosting
RF	Random Forest
AAE	Average Absolute Error
R²	Coefficient of Determination
MAE	Mean Absolute Error

MSE	Mean Squared Error
FEM	Finite Element Model
CDP	Concrete Damage Plasticity
RSM	Response Surface Methodology
KSM	Kriging Surrogate Models
LRFD	Load and Resistance Factor Approach
FORM	First-order Reliability Method
SORM	Second-order Reliability Method
LRFD	Load and Resistance Factor Approach

Content

Abstract	I
Acknowledgment.....	III
List of Publications.....	IV
Glossary.....	VI
Content	IX
List of Figures	XIV
List of Table.....	XVIII
1. Introduction	1
1.1 Background of the Research.....	1
1.2 Research Significance.....	3
1.3 Thesis Structure and Research Methodology	4
2. Literature Review	6
2.1 Review Methodology	6
2.2 Data Integrity Assessment	7
2.2 Fibres from End-of-life Tire and Recyclability	10
2.3 Fresh Concrete Properties.....	15
2.4 Mechanical Properties	20

2.5 Sustainability Analysis	48
2.6 Research Gap.....	52
2.7 Conclusion Remark	54
3. Experimental Study of Mechanical and Dynamic Properties.....	56
3.1 Experimental Design	57
3.2 Experimental Facilities	61
3.3 Results Analysis.....	66
3.4 Dynamic Properties	80
3.5 Microstructural Analysis.....	84
3.6 Conclusion Remark	86
4. Shear Capacity Experiments with Large Scale Beams.....	88
4.1 Background.....	88
4.2 Experimental Programmes	89
4.3 Results Analysis of Shear Capacity	91
4.4 Loading and Displacement Analysis	93
4.5 The Strain of Longitudinal Reinforcement.....	98
4.6 Failure Mode Analysis.....	98
5. Modified TR63 Standard.....	103

5.1 Existing Formulas Analysis	103
5.2 Modify the TR63	104
5.3 Conclusion Remark	113
6. Sustainable Development	115
6.1 Recycling Processing of RSF	115
6.2 GHG Emissions of Beams	116
6.3 Sustainability Assessments	118
6.4 Conclusion Remark	126
7. Structure Prediction Methodology of Machine Learning	128
7.1 Literature Review	128
7.2 Research Methods	131
7.3 Data Preparation	134
7.4 Research Analysis	135
7.5 Shapley Additive Explanations	142
7.6 Conclusion Remark	144
8. Structure Prediction Methodology of Finite Element Modelling	146
8.1 Numerical Modelling	146
8.2 Materials Definition	147

8.3 Analysis Results of the Reference Beam	150
8.4 Parametric Studies	154
8.5 Sensitivity Analysis by Surrogated Finite Element Analysis.....	160
8.6 Application of FEM for Flexural Strength Prediction	167
8.7 FEM application in flexural prediction.....	168
8.8 Validation Analysis	171
8.9 Conclusion Remark	173
9. Reliability Analysis of Different Perdition Methodology	175
9.1 Datasets Analysis	175
9.2 Uncertainty Analysis.....	177
9.3 Reliability Analysis.....	190
9.4 Reliability Results.....	194
9.5 Sensitivity Analysis	207
9.6 Conclusion Remark	208
10. Time-Dependent Reliability Analysis.....	211
10.1 Corrosion Mechanisms Analysis	212
10.2 Study of Parameters.....	212
10.3 Design Space	217

10.4 Case Study	220
10.5 Conclusion Remark	229
11. Conclusion and Recommendations	230
11.1 Experimental Analysis	230
11.2 Numerical Analysis	232
11.3 Reliability Analysis.....	233
11.4 Advice for Future Research	235
Appendix A.....	238
Reference.....	248

List of Figures

Figure 1-1 Research route of thesis	5
Figure 2-1 Data flow diagrams	9
Figure 2-2 Results of aspect ratio	12
Figure 2-3 Comparison between RSF and ISF	13
Figure 2-4 Results of fibre tensile strength.....	14
Figure 2-5 Results of slump test	17
Figure 2-6 Results of air content	18
Figure 2-7 Results of compressive strength.....	28
Figure 2-8 Strength improvement between RSFRC and PC	29
Figure 2-9 Results of splitting strength	33
Figure 2-10 Results of splitting strength of RSFRC.....	34
Figure 2-11 Flexural strength improvement with RSF	48
Figure 2-12 Compressive strength relative ratio.....	48
Figure 2-13 Structure of tire	50

Figure 3-1 Research route.....	57
Figure 3-2 Fibre tensile strength test	59
Figure 3-3 Fibre properties	60
Figure 3-4 Test setup	63
Figure 3-5 Loading and CMOD curve.....	73
Figure 3-6 Correlation models.....	83
Figure 3-7 Microstructure analysis	86
Figure 4-1 Experimental beam dimension.....	91
Figure 4-2 Shear span of 1.5 (Group I beams)	94
Figure 4-3 Shear span of 2.5 (Group II)	95
Figure 4-4 Shear span of 3.5 (Group III).....	96
Figure 4-5 Shear span of 4 (Group IV).....	97
Figure 4-6 Loading strain curve.	102
Figure 5-1 Prediction results versus experimental results	111
Figure 5-2 Box and whisker analysis.....	113

Figure 6-1 Manufacturing process of RSF	115
Figure 7-1 ML used in shear capacity	137
Figure 7-2 ML used in flexural capacity	140
Figure 7-3 ML used in shear stiffness.....	142
Figure 7-4 SHAP explanation models.	144
.....	145
Figure 8-1 Modelling.....	147
Figure 8-2 Stress-strain diagram.....	149
Figure 8-3 Failure model	154
Figure 8-4 Research route of surrogate model.....	161
Figure 8-5 3D smooth graph.....	166
Figure 8-6 Reliability indices	167
Figure 8-7 Stress-strain distribution graph	168
Figure 8-8 Stress-strain distribution in TR63	168
Figure 8-9 Formula validation.....	172

Figure 9-1 Model uncertainty analysis	179
Figure 9-2 PDF and CDF graph for different models.....	188
Figure 9-3 FORM and SORM	193
Figure 9-4 HSFRC with live and dead loading combination.....	196
Figure 9-5 NSFRC with live and dead loading combination.....	197
Figure 9-6 Reliability Index for different load combination	206
Figure 10-1 Detail of case study	221
Figure 10-2 Experimental case study	223
Figure 10-3 Proposed case study	224
Figure 10-4 Effect of concrete cover depth	225
Figure 10-5 Effect of longitudinal ratio.....	227
Figure 10-6 Effect of fibre content	228
Figure 10-7 Effect of adding RSF in concrete	229

List of Table

Table 2-1 Results of tests with standard of UNI-11039.....	37
Table 2-2 Results of tests with standard of ASTM C78.....	40
Table 2-3 Results of tests with standard of EN 14651 standard	44
Table 2-4 Global warming potential	51
Table 2-5 Price between RSF and ISF	52
Table 3-1 Fibre properties.....	59
Table 3-2 Detail of Mixes	61
Table 3-3 Test results of ISFRC and RSFRC.....	66
Table 3-4 CMOD test results	71
Table 3-5 Failure mode of RSF and ISF concrete.....	77
Table 3-6 Results of dynamic properties.....	83
Table 4-1 Results of shear strength test	92
Table 5-1 Review of collected existing formulas.....	103
Table 5-2 Results of formula design analysis	107

Table 6-1 GHG emissions and budget price of raw materials.	117
Table 6-2 GHG emissions and budget price analysis	117
Table 6-3 Component of different tires.....	120
Table 6-4 GHG emissions and cost benefit analysis.....	123
Table 7-1 Review analysis	129
Table 7-2 Overview of the datasets.....	134
Table 7-3 ML used in shear capacity	136
Table 7-4 ML used in flexural strength.....	138
Table 7-5 ML used in stiffness.....	141
Table 8-1 Mesh analysis.....	151
Table 8-2 Results analysis.....	153
Table 8-3 Comparison between referenced beams and FEM results	156
Table 8-4 Comparison between ISF and RSF reinforced concrete beams.....	159
Table 8-5 Stress calculation results.....	171
Table 9-1 Statistical properties of the dataset	176

Table 9-2 Anderson-Darling test results.....	189
Table 9-3 Load combinations.....	192
Table 9-4 Results for HSFRC group.....	194
Table 9-5 Results for NSFRC group.....	195
Table 9-6 Reliability Index for HSFRC Beams with Different Load Combination.....	201
Table 9-7 Reliability Index for NSFRC Beams with Different Load Combination.....	201
Table 9-8 Sensitivity analysis	207
Table 10-1 Environmental deterioration	217
Table 10-2 Parameters of random variable	219
Table A-1 Failure mode analysis.....	238
Table A-2 Datasets for shear capacity analysis.....	241
Table A-3 Datasets for ML analysis.....	242
Table A-4 Datasets for ML analysis.....	244
Table A-5 NSFRC beams datasets for reliability analysis	245

1. Introduction

1.1 Background of the Research

According to the research of ref[1], more than a billion tires are replaced globally each year, with over half abandoned and awaiting disposal. This "black pollution" is difficult to biodegrade, posing significant environmental risks and health threats to workers in scrap zones [2-4]. Traditionally, waste tires have been disposed of through burning followed by landfilling, typically without undergoing any treatment [5, 6]. The European Tire and Rubber Manufacturers Association reports that untreated tires in landfills degrade at a very slow rate. In light of this, the European Union has forbidden getting rid of waste tires through open air burning or disposal in landfills from the 16th of July 2003 [7-9].

In Europe, a number of civil engineers are concentrating on the management of waste tires, leading to 46% of waste tires being recycled into material form [10]. In ref[11], waste tires yield three primary materials: rubber, steel, and scrap. However, the process of reheating waste steel in factories is associated with considerable costs and carbon emissions [12, 13]. Despite these challenges, the high tensile strength of waste steel has motivated researchers to investigate its potential applications in construction. Research has indicated that incorporating industrial steel fibres (ISF) into concrete can greatly enhance the original brittle matrix, particularly in regard to strength and performance after cracking [14-17].

In ref[27], adding ISF to concrete helps control crack development and can partially replace steel bars, increasing the concrete's shear and tensile strength while reducing construction costs. Researchers have reported that ISF creates a bridge effect in concrete, maintaining structural

integrity even when cracks occur [18-21]. The use of steel fibre-reinforced concrete (SFRC) in construction has been steadily growing over the past few decades, owing to its effectiveness in improving the mechanical properties of concrete [22, 23]. Given the impressive performance of ISF, there is increasing interest in the feasibility of using recycled steel fibre (RSF) as an environmental-friendly alternative.

Recently, as people became increasingly conscientious about environmental protection, the emphasis on secondary raw materials applications in civil engineering considerably increased. RSF, derived from waste tires, have emerged as a viable alternative to ISF [24, 25]. Research by [26] highlights RSF's efficacy as a substitute for ISF in concrete applications. Studies indicate that incorporating RSF in concrete can achieve comparable improvements to ISF, while offering advantages such as lower greenhouse gas emissions and reduced costs [4, 27, 28]. Moreover, RSF demonstrates economic benefits, with a 1.5% inclusion contributing approximately 35% to construction budgets, compared to ISF's contribution of over 50% [27].

Despite the acknowledged benefits of RSF, gaps persist in understanding its comparative mechanical performance with industrial steel fibre-reinforced concrete (ISFRC). The existing literature points to improvements in various mechanical properties of recycled steel fibre-reinforced concrete (RSFRC). However, comprehensive insights into these enhancements and their implications remain limited. This study seeks to fill these gaps by systematically analysing literature from a range of sources, with a focus on the impact of RSF on the mechanical and structural properties with concrete. To extensively confirm the viability of RSF as a novel eco-friendly substance, this thesis rigorously investigates its attributes via meticulous review,

hands-on experimentation, and various modelling. The overall aim is to comprehend RSF's role in mechanical properties, fresh properties, structural properties, and sustainability contribution as compared to ISF. It aims to highlight the prospects for additional advancement and research in this RSF research domain.

1.2 Research Significance

Worldwide, getting rid of waste tires is an urgent environmental problem with far-reaching impacts on sustainability and public well-being. These tires often end up in landfills or are incinerated, contributing to long-term pollution and health hazards. In response to these challenges, there has been a concerted effort to recycle waste tires, particularly focusing on materials like steel, which can be reclaimed and repurposed. ISF have proven effective in reinforcing concrete, improving its toughness and ability to withstand cracks. This has spurred interest in exploring Derived from waste tires as a potential substitute for ISF, RSF offer better mechanical performance and environmental benefits, such as reduced greenhouse gas emissions and cost savings. Despite the potential advantages of RSF, there remains a critical gap in understanding how its performance compares to ISF in applications. This study aims to fill this gap by systematically reviewing and evaluating on the impact of RSF on the mechanical and structural characteristics with concrete. By analysing findings from various studies and locations, this research aims to provide insights into RSF's role in improving concrete performance while promoting sustainable practices in construction. The findings from this research are anticipated to provide valuable insights for industry professionals, policymakers, and researchers regarding the feasibility and benefits of incorporating RSF into concrete production.

1.3 Thesis Structure and Research Methodology

This thesis aims to comprehensively explore the potential applications of RSF in the construction industry through a comparative study with ISF. The thesis is structured into eleven chapters, including an introduction and conclusion. Beyond the introduction and conclusion, the research and analysis are conducted on four key levels.

The first part provides a systematic literature review, discussing the current use of traditional ISF and analysing the potential benefits of RSF, including cost savings and environmental friendliness. A comparative study highlights the strengths and weaknesses of RSF and ISF in terms of performance enhancement, carbon footprint reduction, and cost control. The next section presents an empirical study of RSF through experimental research. This section details the process of extracting RSF from waste tires and construction debris and outlines the experimental design used to evaluate its mechanical properties, dynamic performance, and structural shear capacity. To provide a clear and effective comparison, ISF are used as a control group in these experiments. The chapter also describes the methodology for conducting a life cycle assessment of RSF, analysing its environmental footprint from production to disposal. In addition to basic mechanical performance tests, this thesis includes a separate study on HSFRC beams, a critical structural component. Based on the experimental results and collected data, and referencing the TR63 standard, an improved shear capacity prediction formula is proposed. The third and fourth parts focus on a detailed study of HSFRC, assessing the contributions of RSF and ISF within the structure. The third part provides technical analysis, using experimental data and machine learning models to predict key performance parameters. This includes finite element analysis to simulate the mechanical behaviour of concrete reinforced with RSF and ISF,

and the development of simplified surrogate models to enhance simulation efficiency. The fourth part primarily investigates the reliability of the structure, offering a comprehensive evaluation of the reliability and effectiveness of HSFRC based on collected data. This section also verifies the shear capacity model and examines the performance of ISF and RSF under corrosive conditions.

The final chapter, Chapter Eleven, presents the conclusions and recommendations. It discusses the overall findings of the thesis and offers suggestions for future research, which can be improved upon based on this study's content. The overall structure of the thesis is illustrated in

Figure 1-1.

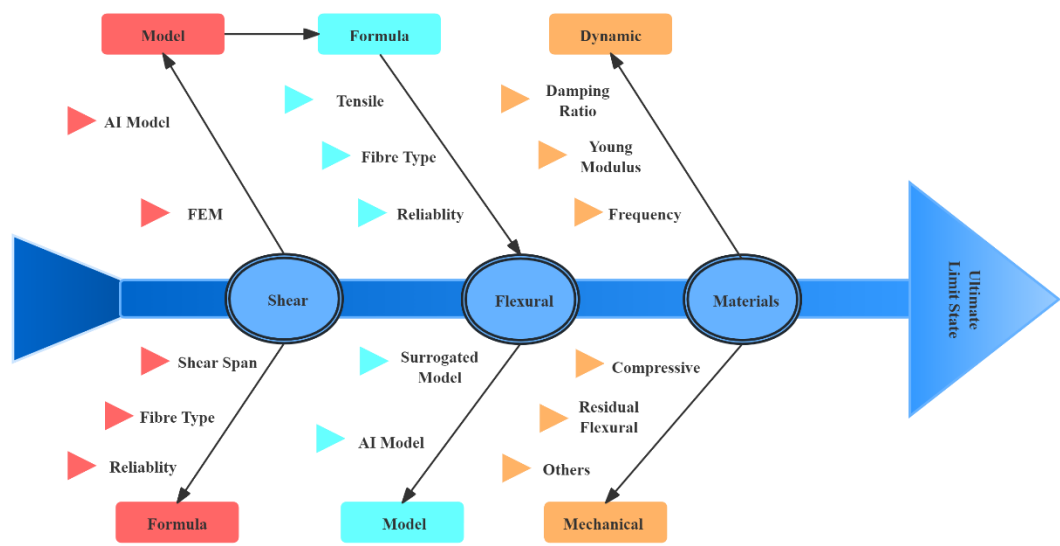


Figure 1-1 Research route of thesis

2. Literature Review

2.1 Review Methodology

This review aims to critically assess the mechanical properties of RSFRC through a thorough examination of pertinent literature. The research involved utilizing bibliometric databases like ScienceDirect, Google Scholar, and Web of Science, with key search terms such as "recycled steel fibre," "fibre-reinforced concrete," and "mechanical properties." A total of thirty-six publications were selected after thorough screening and are the basis for detailed data analysis.

The research process is structured into four main steps and been described in **Figure 2-1**:

Literature Collection and Review: The initial phase involved systematically gathering papers related to RSFRC, with a focus on conducting a thorough literature review. This step was crucial for identifying the methodologies used in the studies and understanding the analytical frameworks employed.

Data Compilation: Detailed forms were created to systematically compile information related to material properties, characteristics of fresh concrete, and harden properties as documented in the reviewed literature.

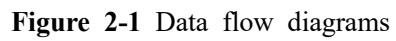
Analysis of RSF Content: Special attention was given to examining the relationship between RSF content and various concrete properties. This analysis aimed to elucidate how varying levels of RSF impact mechanical performance of SFRC, such as strength, durability, and crack resistance, within concrete compositions.

Contribution to Sustainable Development: The final step involved evaluating the broader implications of RSF in terms of sustainable development. This included assessing its environmental benefits, such as reduced carbon footprint and potential economic advantages compared to conventional materials like ISF. By comparing RSF with ISF, the study sought to highlight its role in promoting sustainable practices in construction.

2.2 Data Integrity Assessment

In scientific research, the quality and integrity of data are critical to the accuracy and reproducibility of research findings. Therefore, a rigorous assessment of data integrity is essential when conducting a literature review. This assessment should encompass not only the reliability of data sources but also the completeness of key parameters during data collection and the transparency of data processing. First, data sources must be highly credible, preferably from peer-reviewed literature or widely recognized databases, to ensure their reliability. During data collection, the completeness of key parameters is a crucial indicator of data quality. For instance, in studies involving experimental research, data sets that lack essential parameters such as curing time, testing rate, or standard requirements should be considered incomplete and excluded from the analysis. The absence of these parameters can lead to significant biases in data interpretation, rendering the results less meaningful. Moreover, the handling of outliers is another critical aspect of data integrity assessment. If the authors of a study attribute certain outliers to substantial deviations caused by experimental conditions or procedures, such data should be carefully scrutinized and typically excluded from further analysis. These outliers could introduce systematic errors, thereby undermining the robustness of the study's

conclusions. By applying these stringent criteria, this study can ensure the selection of high-quality data, thereby enhancing the credibility and scientific value of their findings. Conducting a systematic data integrity assessment during a literature review helps in filtering out studies that are representative and reliable, thereby avoiding analytical errors and biased conclusions due to low-quality data.



2.2 Fibres from End-of-life Tire and Recyclability

2.2.1 Production Process

RSF are extracted from discarded tires and made two ways: mechanical recycling and thermo-chemical decomposition [29]. Mechanical recycling is further categorized into shredding and cryogenic processes [30]. In the shredding process, scrap tires are initially shredded into chips, resulting in a mixture of RSF and rubber particles [31, 32]. These particles are subsequently separated from magnetic materials. The cryogenic process, more complex than shredding, begins by cooling the material below -80°C , making the rubber brittle due to the glass transition temperature [33]. In ref[34], found that cryogenic processing yields finer rubber particles and higher quality RSF than shredding, albeit at a higher cost.

Thermal technologies include pyrolysis and microwave treatment. Pyrolysis starts by creating an oxygen-free environment filled with inert gas [35]. The technology entails exposing the substance to high temperatures (surpassing 430°C) and pressure to produce RSF, tire-derived activated carbon, carbon black, fuel gas, and many other organic substances as their derivatives [36, 37]. The gases generated during pyrolysis can be used to sustain the process, thereby lowering carbon emissions [38, 39]. Microwave treatment, carried out in a nitrogen-rich environment, prevents the formation of undesirable combustion products and efficiently preserves valuable materials [40].

The primary distinction between mechanical recycling and thermal technologies lies in the treatment of the rubber component. Thermal methods typically produce purer RSF, whereas mechanical recycling results in RSF mixed with rubber particles. After combustion in thermal

processing, the steel surface is coated with ash and combustion by-products rather than rubber, facilitating a cleaner separation of the steel [38, 41]. In ref[4] note that rubber particles can fill gaps between fibres and aggregates, enhancing the elastic modulus of concrete. However, the residual rubber ($\leq 1\%$) from mechanical recycling has minimal impact on RSF performance in concrete due to its small quantity [42]. Overall, the impact of rubber particles on the mechanical properties of concrete is minimal, and shredding technology is favoured over thermal methods due to its lower cost.

2.2.2 Physical Characteristics

Ref [43] highlighted the critical roles that fibre aspect ratio and content play in determining the performance of SFRC. The aspect ratio is calculated as the length divided by the equivalent diameter and typically ranges from 50 to 100 for ISF used in concrete construction. However, a higher aspect ratio can make concrete compaction more challenging [44, 45]. This section discusses the different characteristics of ISF and RSF in reinforcing concrete. **Figure 2-2** presents a comparison of aspect ratios between RSF and ISF from thirteen different studies.

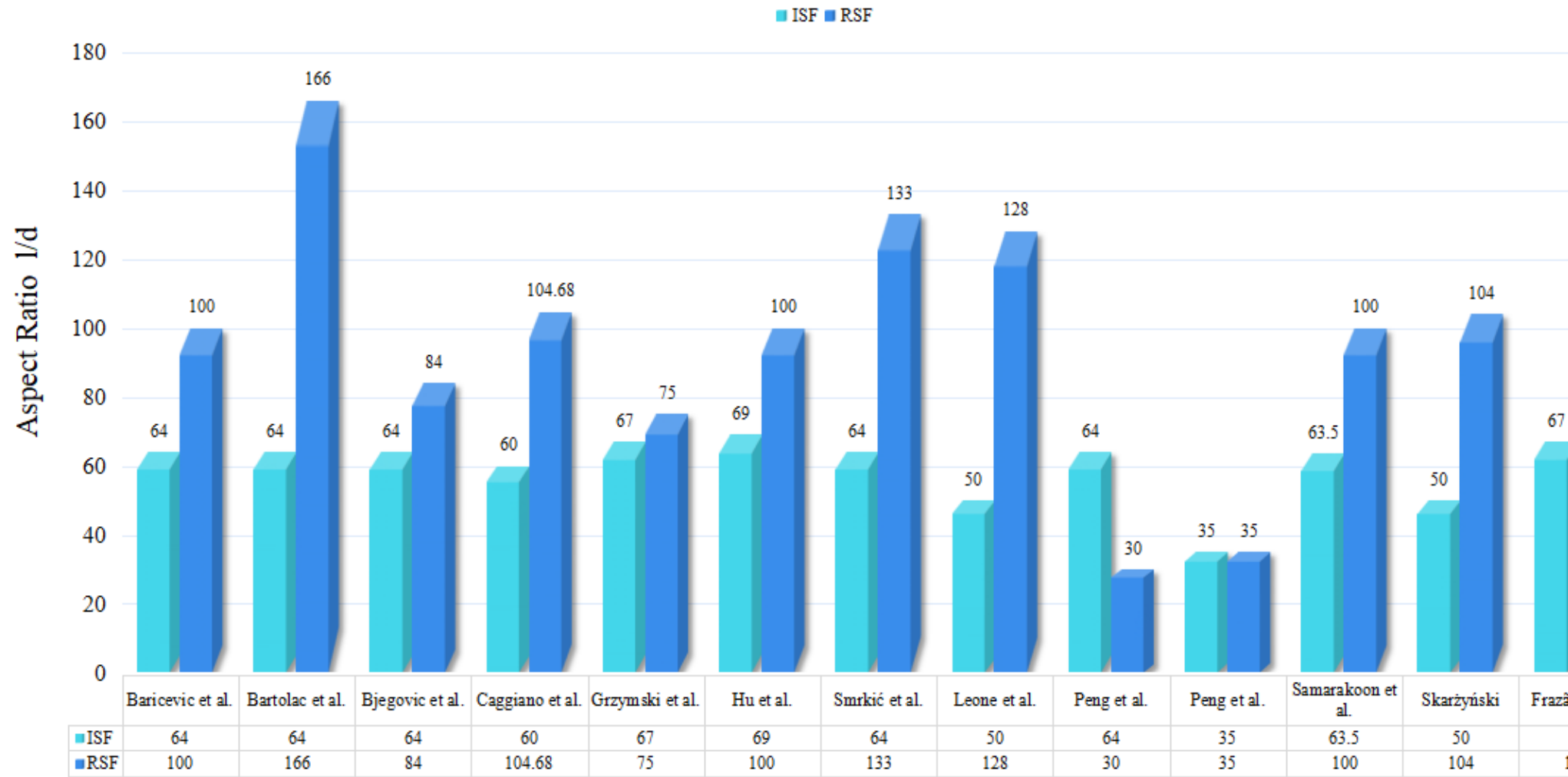


Figure 2-2 Results of aspect ratio

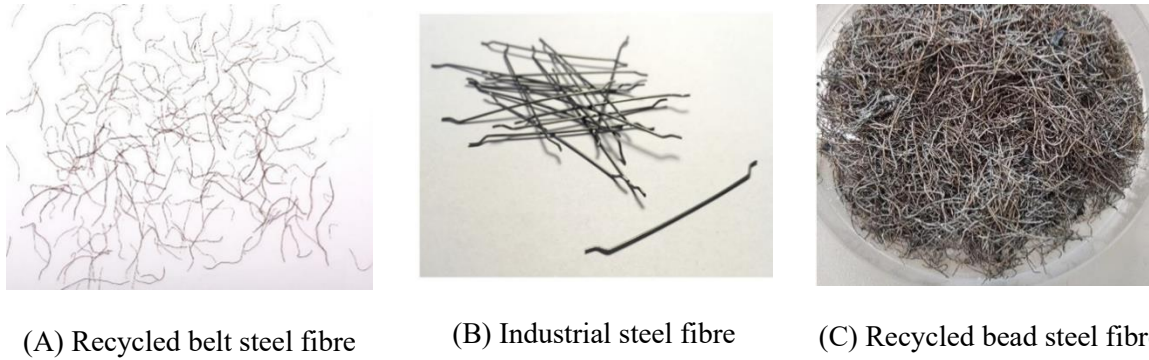


Figure 2-3 Comparison between RSF and ISF

Figure 2-3 shows that RSF are more akin to micro-fibres with irregular shapes and smaller diameters compared to ISF, resulting in a higher aspect ratio for RSF[46, 47]. According to **Table 2-1**, the aspect ratio of RSF can reach up to 133, while the maximum aspect ratio for ISF is 69. In addition, in ref [48] indicates that ISF with lower aspect ratios contribute to higher compressive strength and greater energy absorption, which subsequently enhance flexural strength, toughness indices, and impact strength. Earlier studies have shown that RSF improves the splitting tensile strength and flexural strength of concrete to the same degree as ISF [5, 46, 49-51]. This is because the strong performance of RSF in concrete can be linked to its high tensile strength [52]. **Figure 2-4** presents data from twelve studies discussing the different fibre properties between ISF and RSF.

Figure 2-4 identifies a significant tensile strength advantage for recycled steel fibers (RSF) over industrial steel fibers (ISF), nearly two-fold greater. This compensates for the adverse impact of their higher aspect ratio. Mechanical shredding is the primary method for RSF recycling, although the authors of ref[5] employed pyrolysis. Based on Figure 2-4, no meaningful tensile strength difference exists between RSF obtained via mechanical recycling and those derived via pyrolysis. The better tensile performance of RSF in comparison to ISF can be attributable to their distinct raw materials. RSF comes from waste tires, which have automotive applications that necessitate high-strength steel. ISF, on the other hand, is produced using less durable materials to reduce costs. The tensile strength of the steel wires in tires exceeds 2900 MPa, with some reaching up to 3300 MPa [35]. In contrast, ISF typically has a tensile strength of no more than 1600 MPa, to balance cost with strength requirements [53].

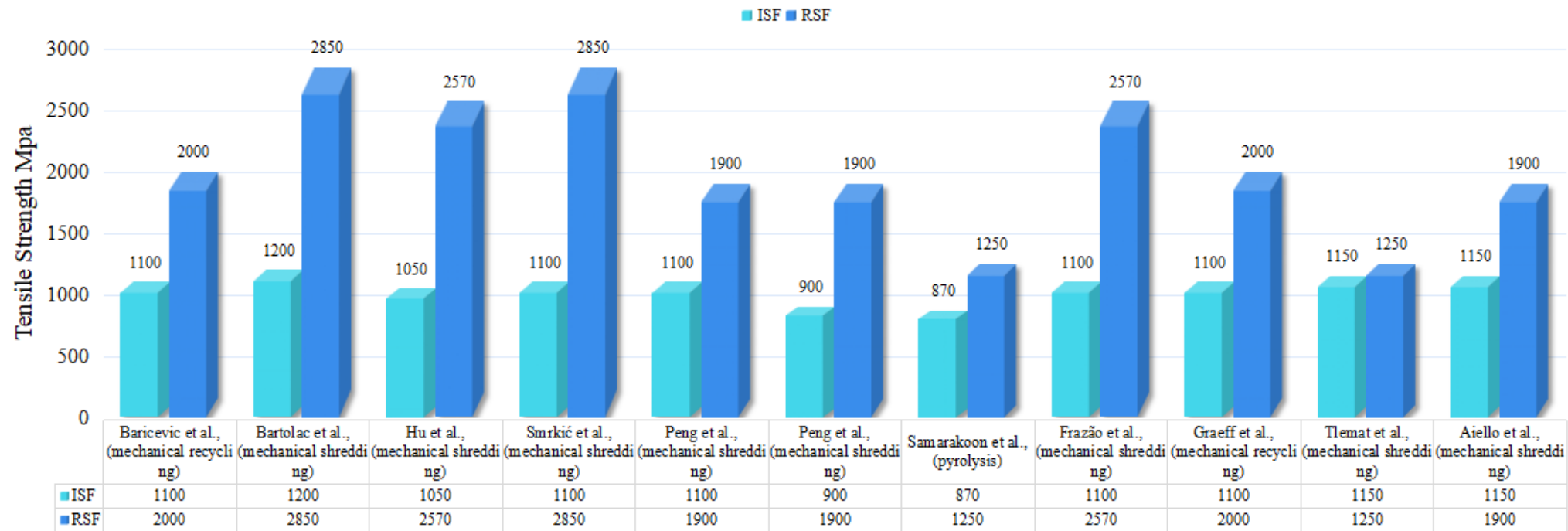


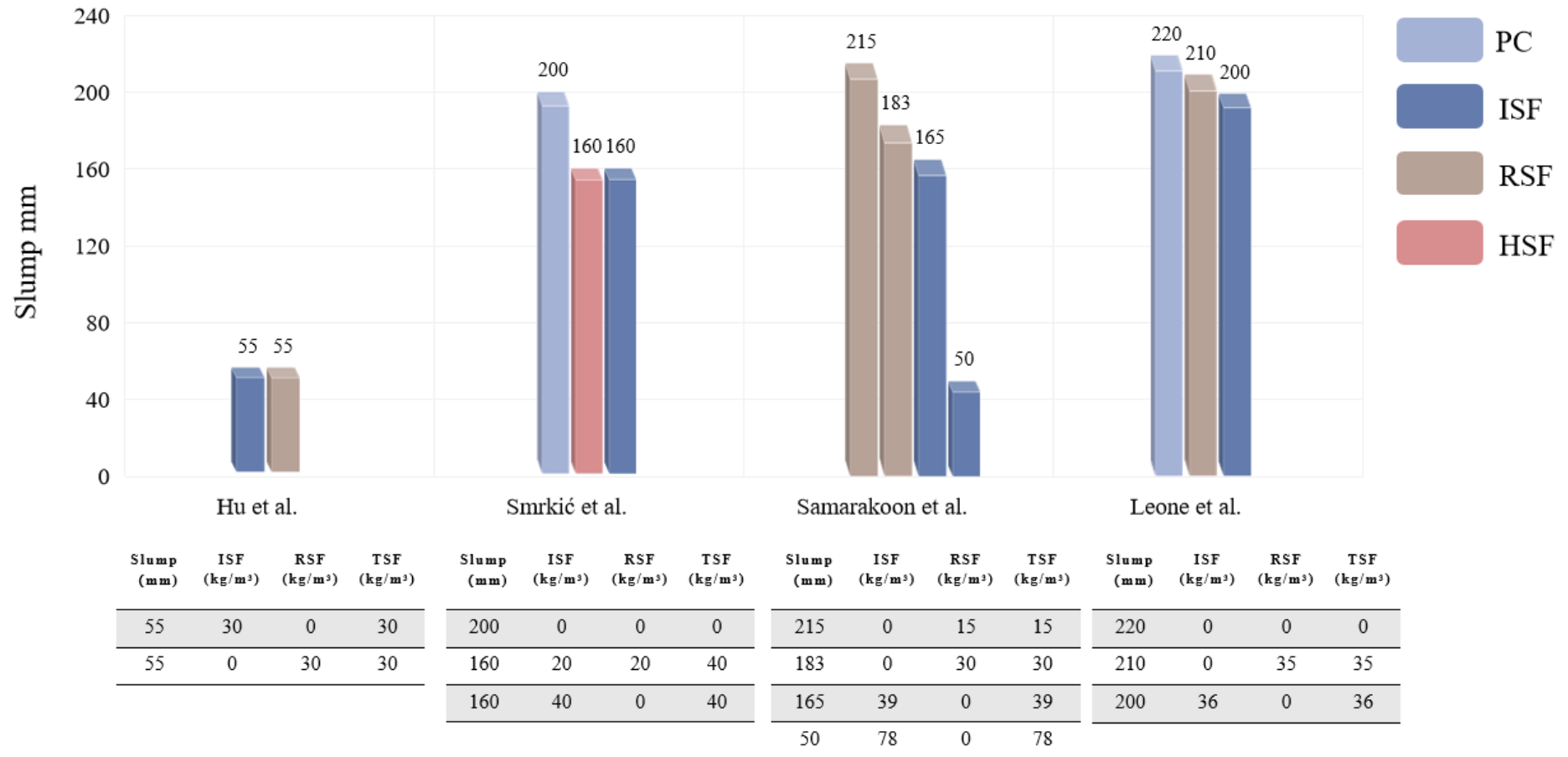
Figure 2-4 Results of fibre tensile strength

2.3 Fresh Concrete Properties

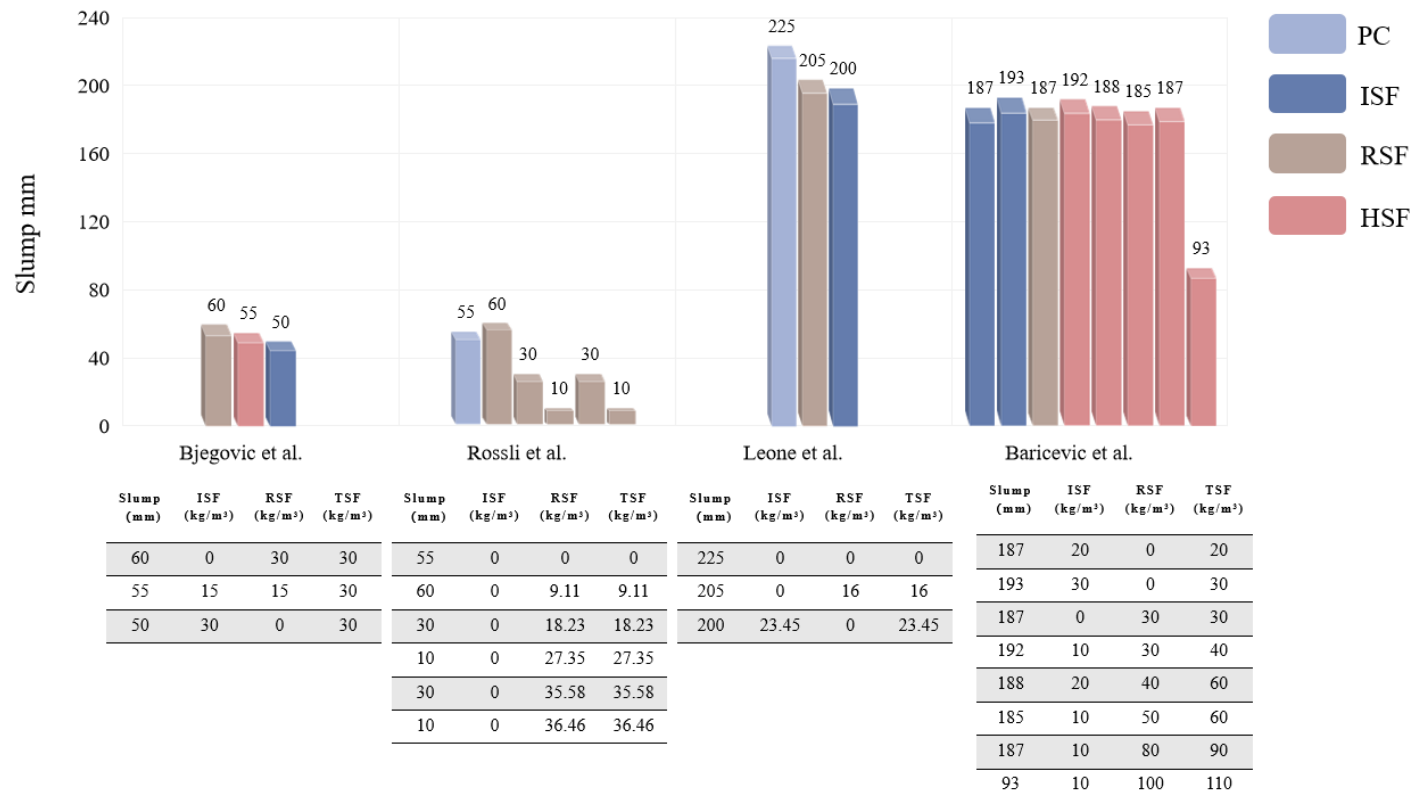
According to ref [54], adding ISF reduces the material's fluidity, meaning the workability of concrete decreases as the ISF content increases. ISF introduces mini-holes between the concrete combination and fibres, resulting in a higher proportion of voids. The next part analyses the characteristics of fresh concrete with RSF and ISF added, concentrating on slump and air content tests.

2.3.1 Workability

The slump test is significant because it affects consistency, manoeuvrability, and compact ability of concrete mixes, as well as their workability [55]. Although fibres can enhance the mechanical properties of concrete, the potential decrease in workability during the mixing of fibre with concrete should be taken into account [56]. **Figures 2-5(A) to (B)** represent the relationship between a variety of SFRC types and the outcomes of the slump test. In these figures, PC refers to plain concrete, while HSF means hybrid steel fibre, which contains both ISF and RSF in the concrete mix.



(A)



(B)

Figure 2-5 Results of slump test

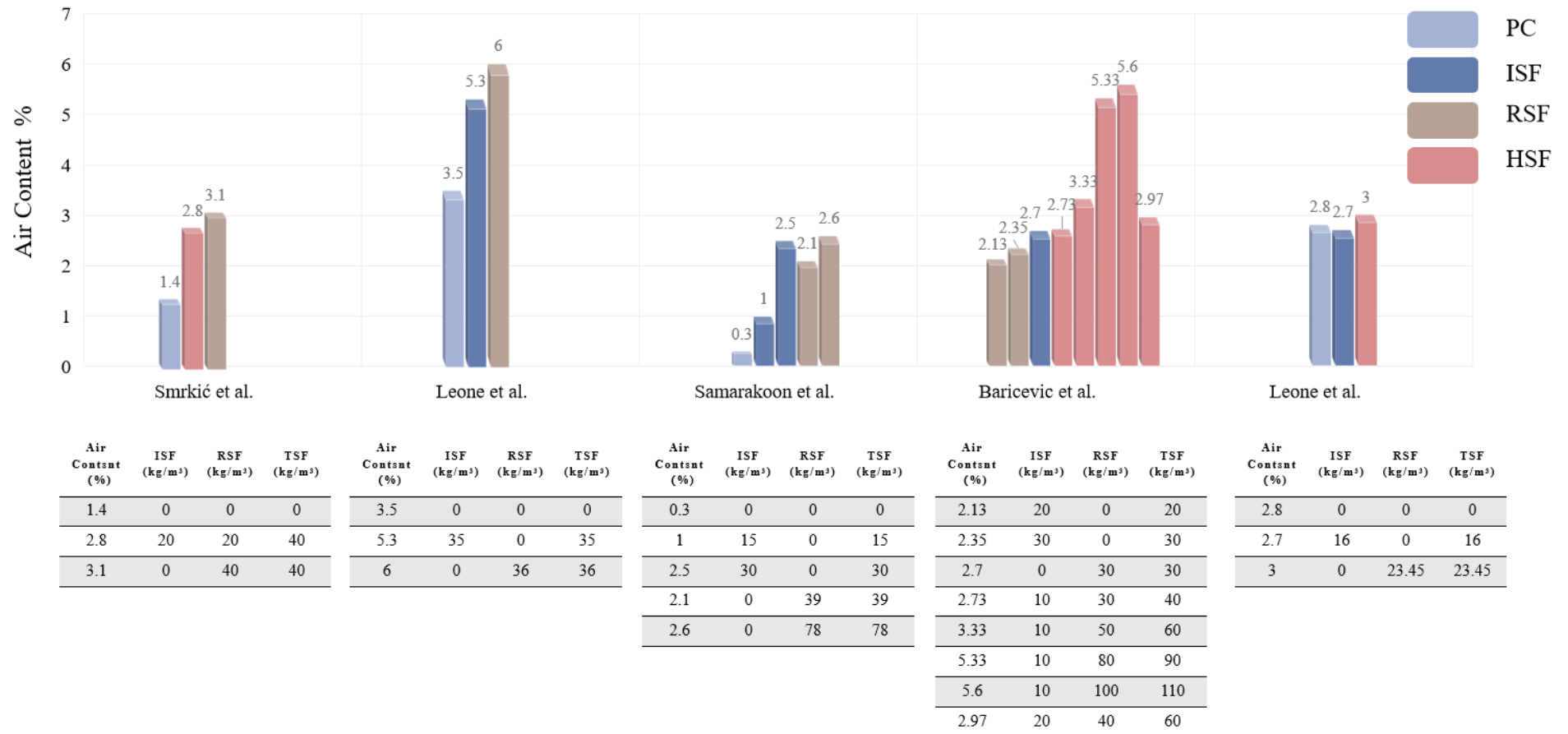


Figure 2-6 Results of air content

In all mixes, the addition of RSF and ISF has been observed to decrease workability. However, RSF typically results in less reduction in workability compared to ISF as reported in [5, 51, 57, 58]. In ref[26] increased the dosage of superplasticizer to maintain consistent slump values across PC, RSFRC (1.19 kg/m³), and ISFRC (2.07 kg/m³). ISFRC required more superplasticizer compared to RSFRC to achieve the same slump. Furthermore, RSF often have irregular shapes and higher aspect ratios compared to ISF, which complicates fibre fusion during mixing processes. The increased admixture dosage suggests that fibre inclusion reduces workability. **Figures 2-5** demonstrate that replacing part of ISF with RSF in concrete, termed Hybrid Steel Fiber (HSF) concrete, can improve workability. However, RSF's contribution to improvement is limited, and there are no synergistic effects observed between ISF and RSF in concrete.

In experiments conducted by ref [58], it was observed that RSF can cause an unusual increase in slump when the fibre content exceeds 0.6%. Specifically, the slump increased to 30 mm at a fibre dosage of 35.58 kg/m³ (0.8%). The rise is mostly caused by the particular way in which the fibres ball up. The chance of fibres balling up goes up when RSF includes asymmetrical forms. Researchers can prevent these fibre intertwining problems in concrete by using small-size aggregates and superplasticizers. [59, 60]. Additionally, self-compacting concrete shows better compatibility with RSF compared to PC [61].

2.3.2 Air Content

Air content is a crucial factor in determining concrete's ability to endure freeze-thaw cycles effectively. Keeping air content within a reasonable range ($\leq 6\%$) is vital for improving

concrete's resistance to freeze-thaw damage [62]. In ref [63], increasing fibre dosages can slightly raise the air content. This is because the addition of fibres complicates the consolidation of the concrete mix, resulting in increased voids between fibres and aggregates [43]. Five studies have reported air content values for RSFRC and ISFRC, detailed in **Figures 2-6**.

All results indicate an increasing trend in air content with higher fibre additions, generally reflecting improved overall air content. According to **Figure 2-6**, most studies suggest that RSF contributes less to air content improvement compared to ISF [5, 26, 57, 64]. This discrepancy is often attributed to the use of unsorted RSF, which has a more irregular shape than standard RSF, leading to increased micro-voids in concrete. Experimental findings demonstrate that an increase in air content correlates with a decrease in compressive strength, suggesting potential risks of micro-crack development and strength loss [65, 66]. Studies on HSFRC indicate that adding RSF to ISFRC results in increased air content. Furthermore, the total volume fraction of fibres significantly influences air content, with a threshold value observed around 60kg/m³ [67].

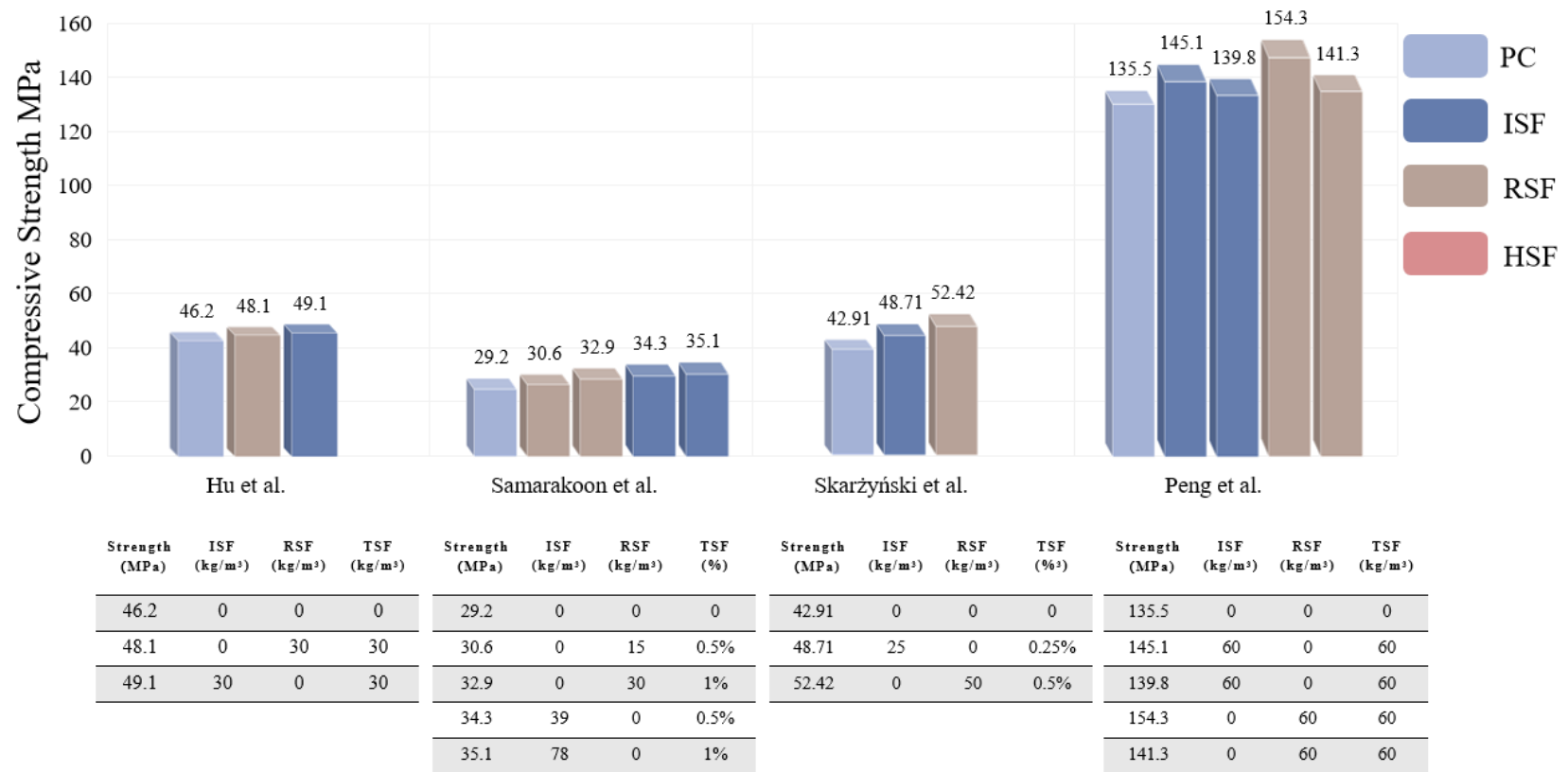
2.4 Mechanical Properties

2.4.1 Compressive Strength

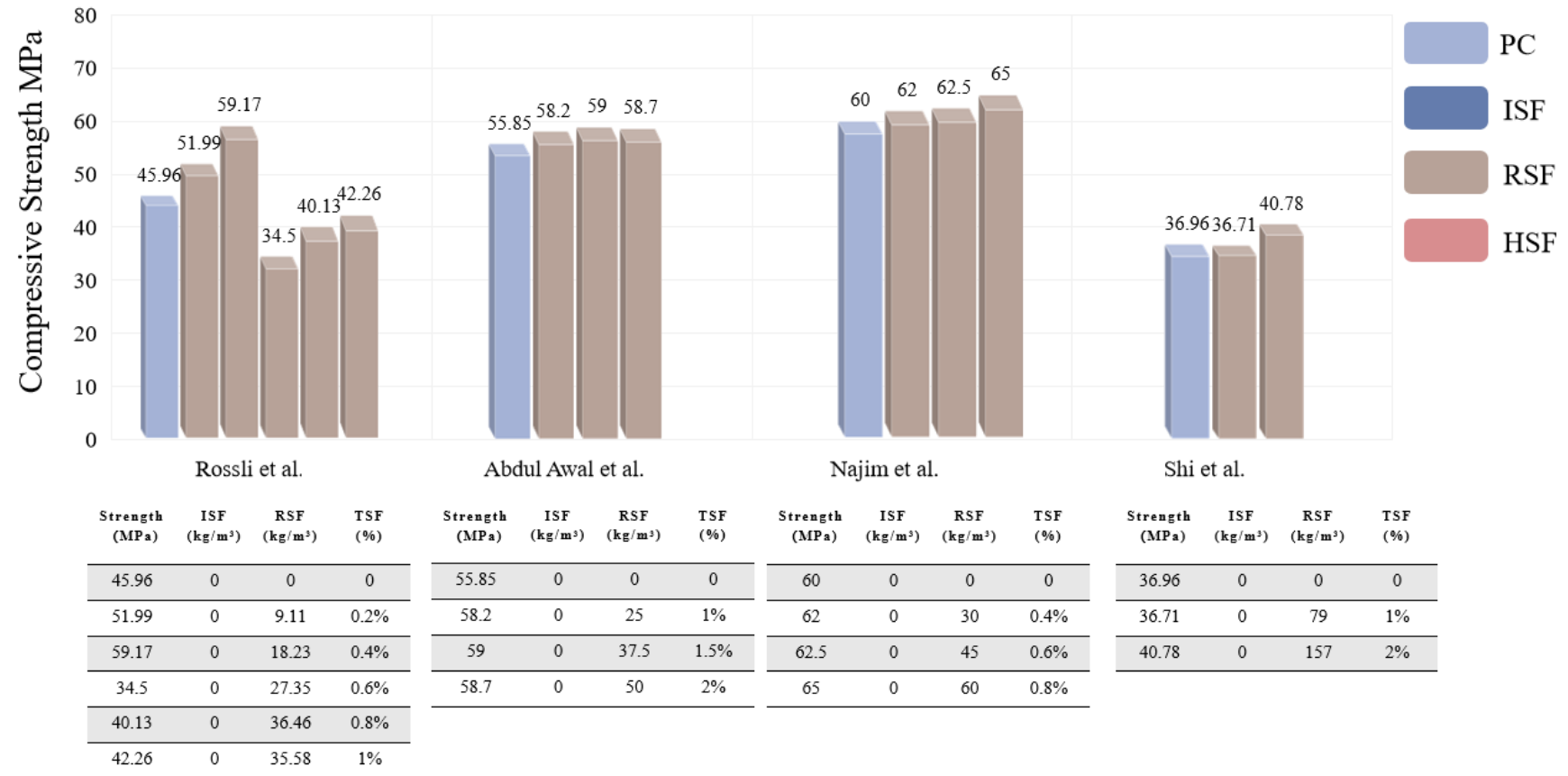
Generally, the impact of fibers on enhancing compressive strength is considered negligible. In ref [68] found that ISF slightly increases its contribution to compressive strength. Additionally, in ref [69] noted that ISFRC shows an increasing trend in compressive strength at low content of ISF [70]. This anomalous increase is attributed to the toughness and ductility provided by ISF, which contribute to a modest improvement in compressive strength [71-73]. **Figures 2-7**

illustrate the enhancement of compressive strength with increasing fibre content.

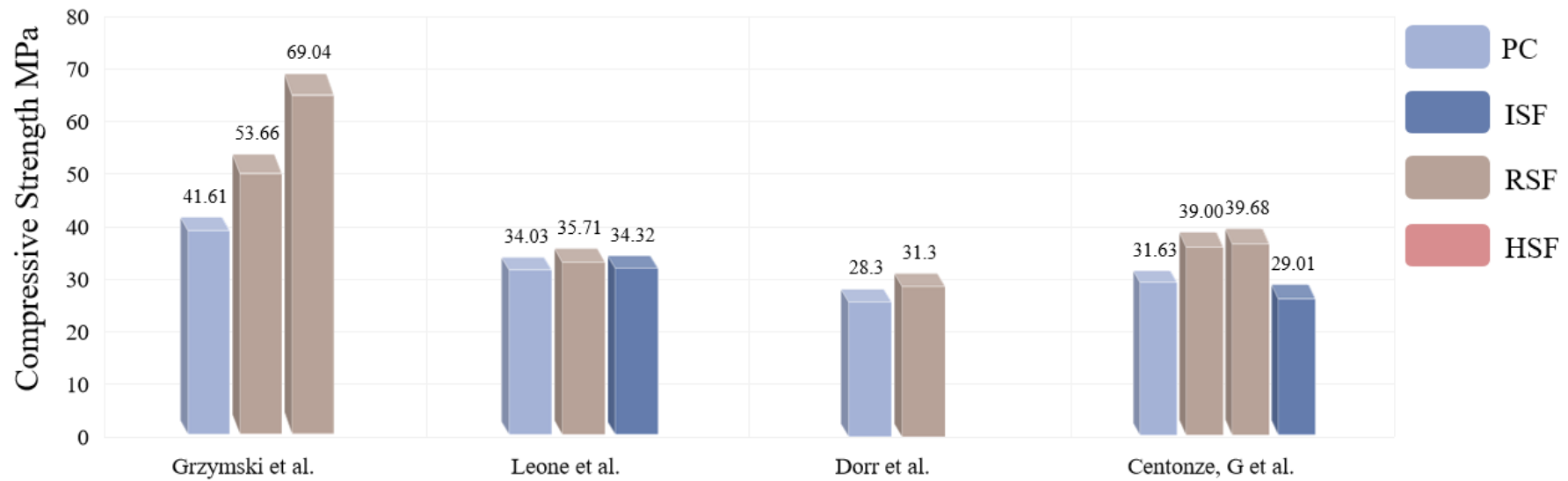
Figures 2-7 indicate that incorporating RSF and ISF fibres into concrete slightly enhances strength capacity when the fiber content is maintained below 1%. Notably, RSF outperforms ISF in boosting compressive strength, with a maximum strength gain of approximately 64% observed at a fibre dosage of around 25 kg/m³ RSF [47]. This modest strength improvement is attributed to the fibers' ability to reduce capillary porosity, thereby suppressing the development of micro-cracks. However, this enhancement is not substantial enough to significantly elevate the mechanical properties of concrete. The general consensus is that adding fibres typically decreases compressive strength. According to the results from Figures 2-7, the compressive strength of RSFRC and ISFRC is greater than PC, particularly when the fibre content is lower than 0.5%. The majority of research indicates that as fibre consumption grows beyond 1%, the compressive strength diminishes. Results are mixed for the range of 0.5% to 1% fibre content. In ref[74], compressive strength peaks at 1% RSF, whereas in ref [58] the highest compressive strength at 0.6% RSF. These conflicting results are mainly due to differences in compaction efficiency. The balling effect was recorded when fibre content is greater than 0.6% in ref[58], while siliceous sand and a superplasticizer were utilized in ref[74] to enhance the bond between fibres and the concrete mix.



(A)

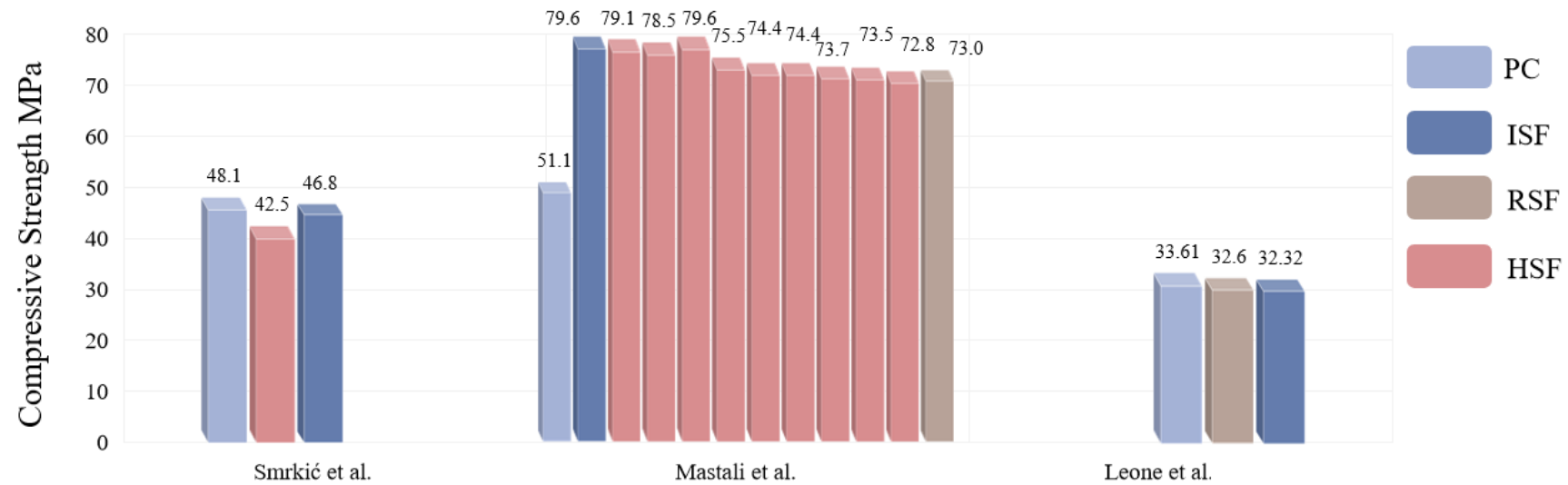


(B)



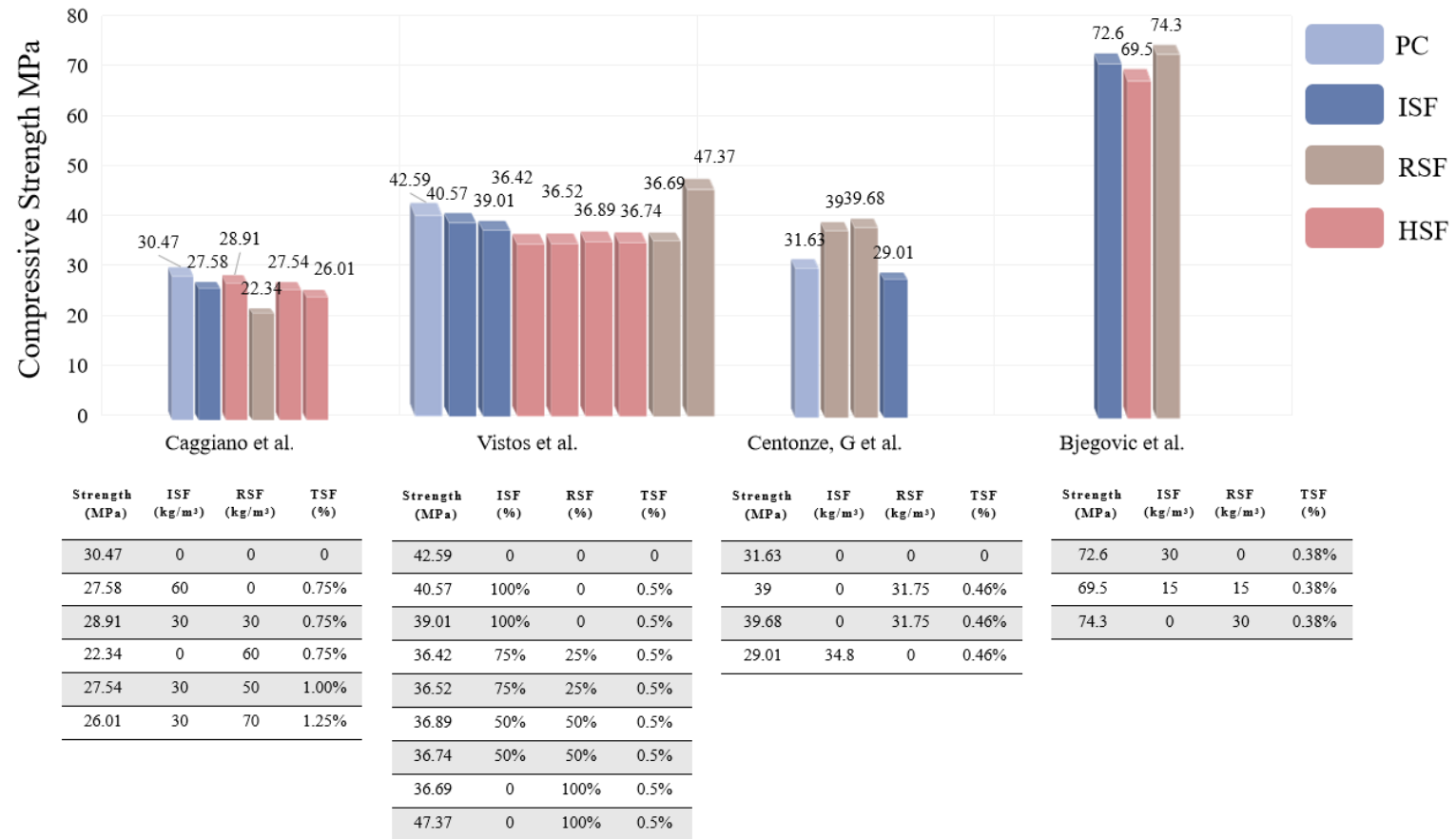
Strength (MPa)	ISF (kg/m ³)	RSF (kg/m ³)	TSF (kg/m ³)	Strength (MPa)	ISF (kg/m ³)	RSF (kg/m ³)	TSF (%)	Strength (MPa)	ISF (kg/m ³)	RSF (%)	TSF (%)	Strength (MPa)	ISF (kg/m ³)	RSF (kg/m ³)	TSF (%)
41.61	0	0	0	34.03	0	0	0	28.3	0	0	0	31.63	0	0	0
53.66	25	0	25	35.71	0	16	0.30%	31.3	0	0.50%	0.50%	39.00	0	31.75	0.46%
69.04	0	25	25	34.32	23.45	0	0.30%					39.68	0	31.75	0.46%
												29.01	34.8	0	0.46%

(C)

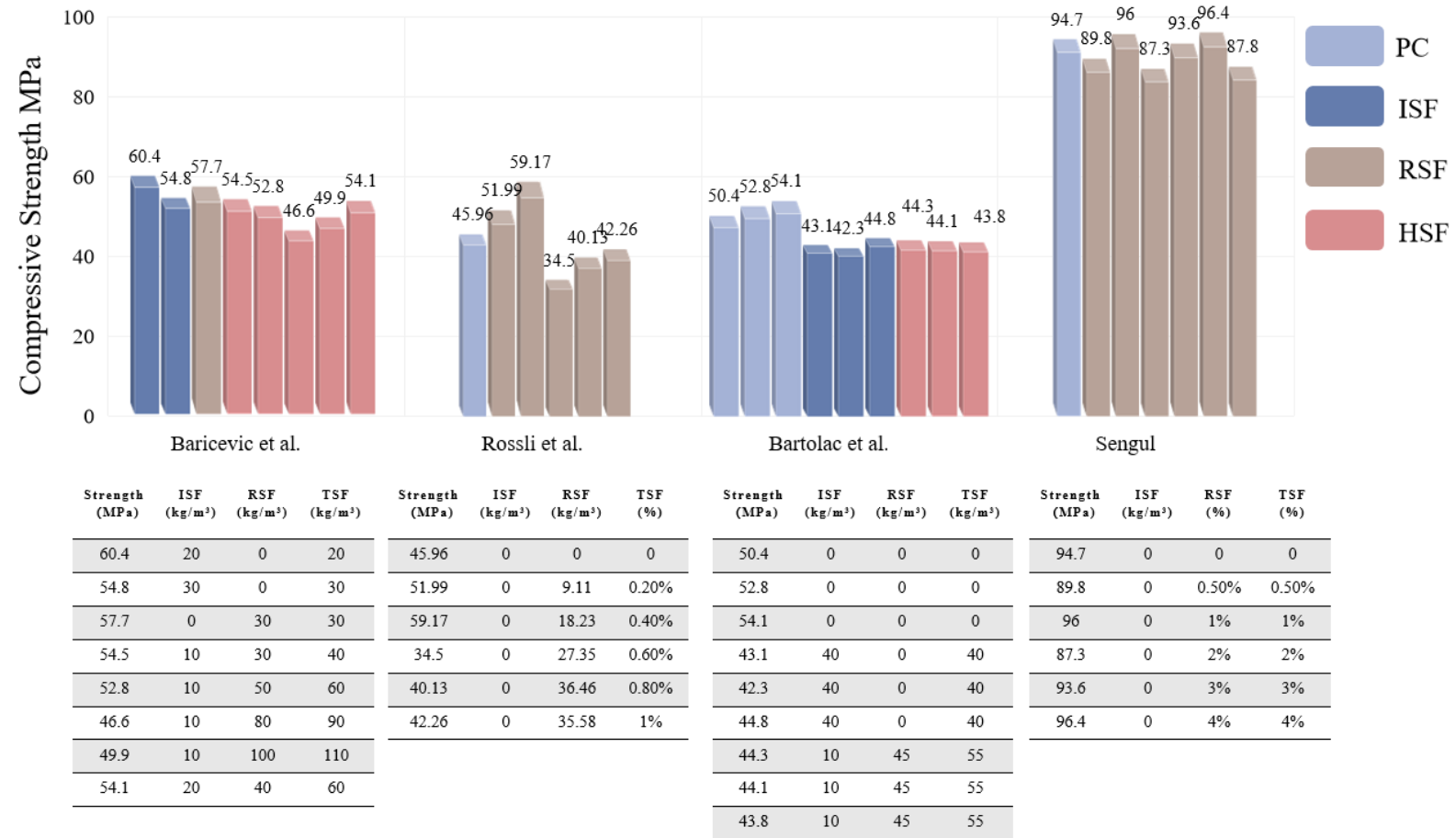


Strength (MPa)	ISF (kg/m ³)	RSF (kg/m ³)	TSF (%)	Strength (MPa)	ISF (kg/m ³)	RSF (kg/m ³)	TSF (%)	Strength (MPa)	ISF (kg/m ³)	RSF (kg/m ³)	TSF (%)	Strength (MPa)	ISF (kg/m ³)	RSF (kg/m ³)	TSF (%)
48.1	0	0	0	51.1	0	0	0	74.4	58.5	58.5	1.50%	33.61	0	0	0
42.5	20	20	0.50%	79.6	117	0	1.50%	74.4	46.8	70.2	1.50%	32.6	0	35	0.46%
46.8	40	0	0.50%	79.1	105.3	11.7	1.50%	73.7	35.1	81.9	1.50%	32.32	36	0	0.46%
				78.5	93.6	23.4	1.50%	73.5	23.4	93.6	1.50%				
				79.6	81.9	35.1	1.50%	72.8	11.7	105.3	1.50%				
				75.5	70.2	46.8	1.50%	73.0	0	117	1.50%				

(D)



(E)



(F)

Figure 2-7 Results of compressive strength

Ref [27] and [75] evaluated HSF performance in strength compression while retaining the same concentration of TSF. They found that increasing the RSF content leads to a consistent decrease in compressive strength. However, concrete with 100% RSF exhibits better performance in enhancing compressive strength compared to concrete with 100% ISF. Efficiency of compacting concrete decreases with increasing RSF in HSFRC. There is no significant synergetic effect in the improvement of compressive strength for both ISF and RSF. The addition of different types of fibres causes void sizes between the fibres and the concrete mix to become more irregular, which conventional compaction methods cannot easily rectify. Despite these challenges, the impact of fibre addition on compressive strength is generally limited, typically not deviating more than $\pm 30\%$ from the properties of PC. To illustrate the improvement provided by RSF compared to plain concrete, **Figure 2-8** was created based on data from **Figure 2-7**.

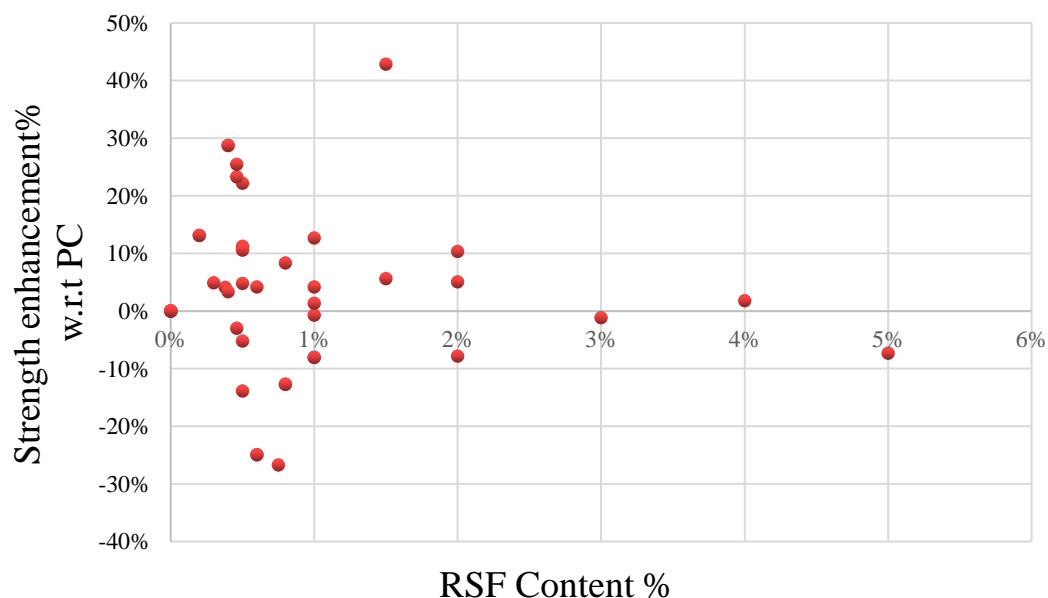


Figure 2-8 Strength improvement between RSFRC and PC

According to **Figure 2-8**, in most cases, RSF contributes to a less than 1% improvement in

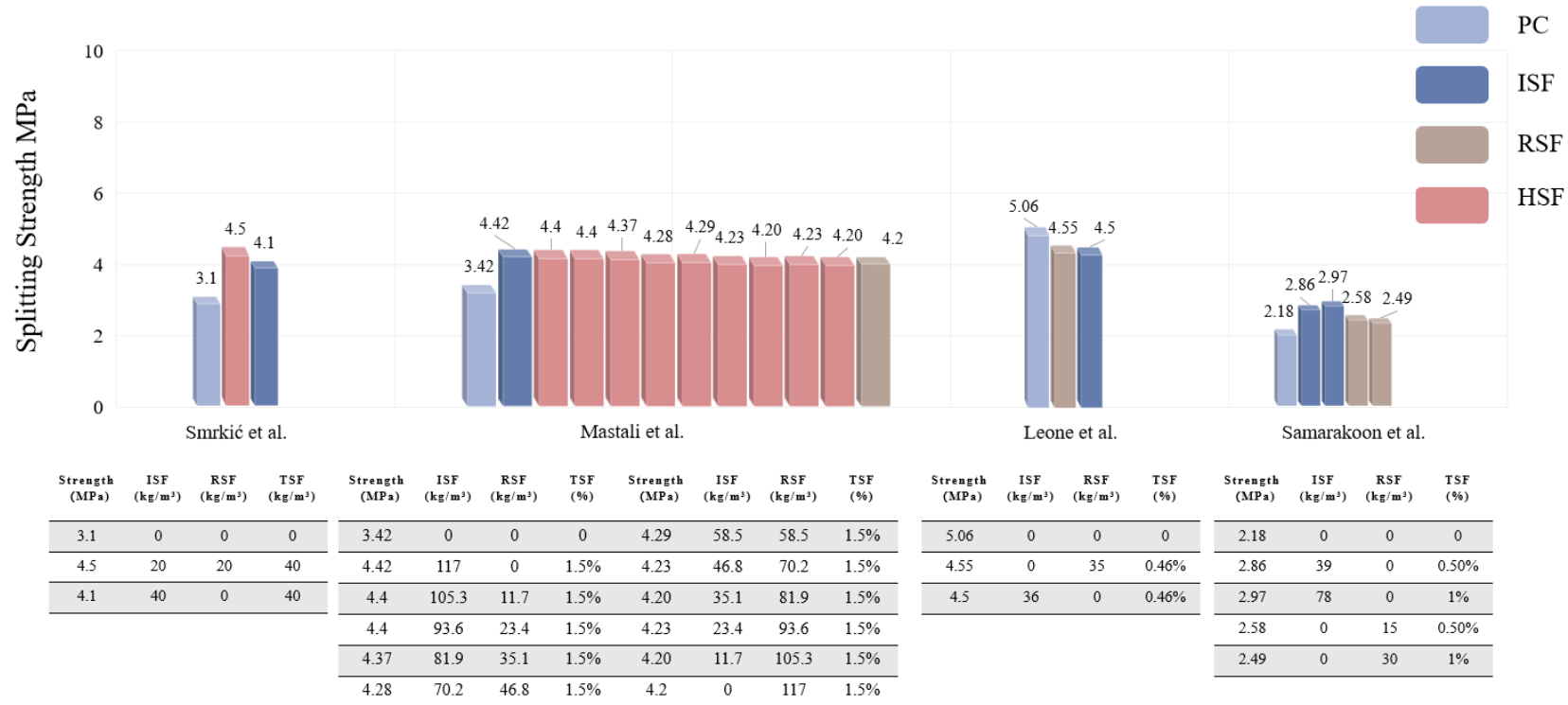
compressive strength compared to PC. All data for RSF content below 0.5% indicate an increase in compressive strength. Overall, the effect of RSF on compressive strength is modest, with variations typically within $\pm 30\%$ compared to PC. When fibre content is kept low, the compressive strength of ISF and RSF concrete tends to increase almost linearly, although the rate of increase is limited. However, when fibre content exceeds a moderate volume (1% to 2%), the improvement in compressive strength with RSF begins to show a slight decline. This trend can be explained by the size of the voids between fibres and aggregates. At low fibre content, fibres help fill these voids, enhancing the internal structure. However, as more fibres are added, air content increases, leading to larger gaps between different concrete mix parameters and promoting micro-crack development. ISF tends to increase air content more than RSF, which explains why RSF performs better in enhancing compressive strength and causes less reduction beyond the optimal fibre level. To prevent the loss of compressive strength, use sophisticated concrete compaction techniques like self-compacting concrete and high-performance superplasticizers, especially when utilizing a high fibre percentage level [76-78].

2.4.2 Splitting strength

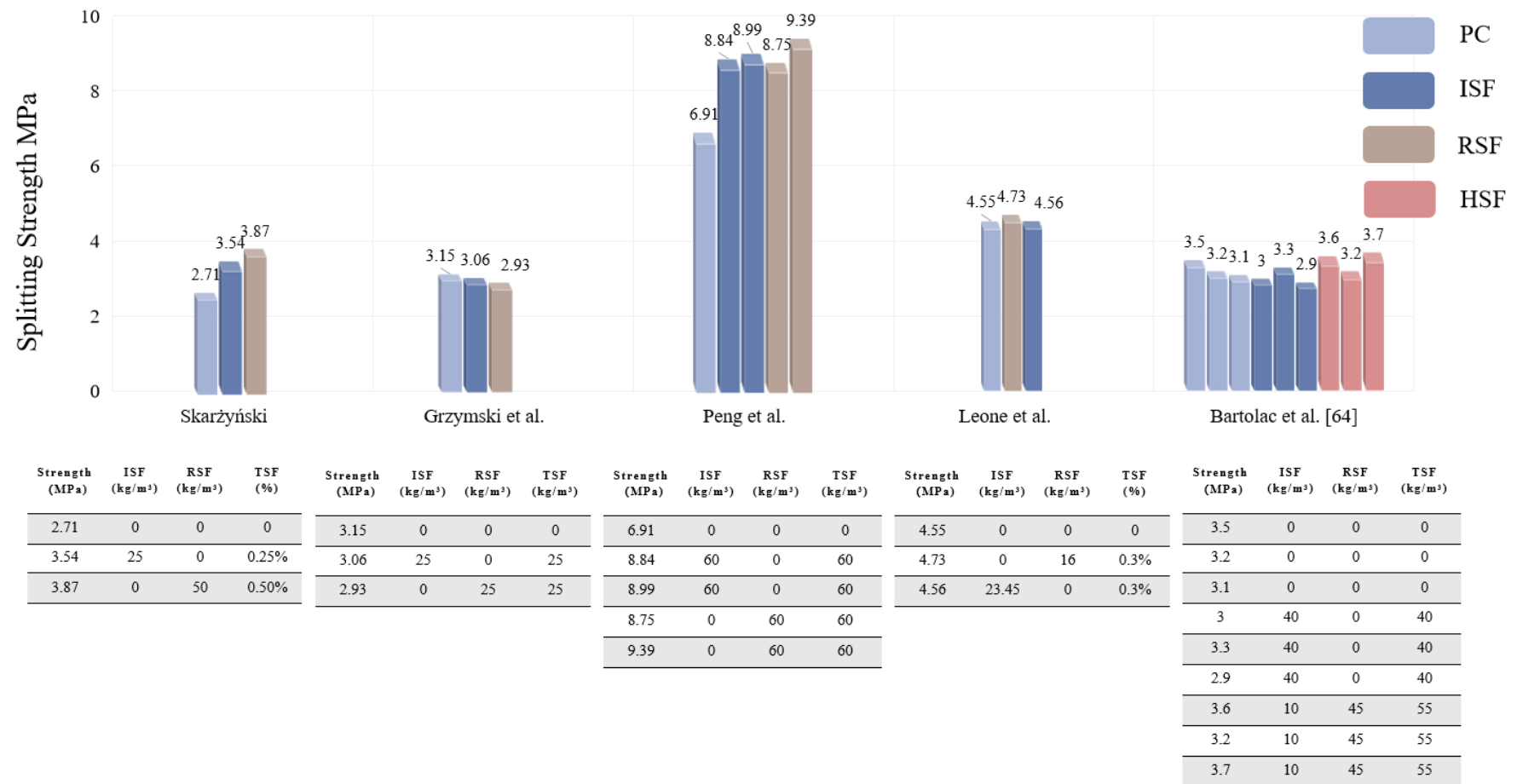
According to **Figure 2-9**, ISFRC shows better performance in strength improvement compared to RSFRC, with ISF concrete achieving the maximum splitting strength. However, the difference between ISF and RSF in enhancing splitting strength is minimal. Ref [49] indicated that RSFRC has higher splitting strength than ISFRC at a fibre dosage of 60 kg/m^3 . Additionally, qualitative studies in ref [26] and [47] revealed that both ISF and RSF can reduce splitting strength. This reduction may be attributed to the random distribution of fibres, leading to discontinuous crack development.

HSFRC shows significant improvement in splitting strength, achieving more than a 45.1% enhancement compared to plain concrete [27, 64, 79]. However, ref [27] found no synergistic effect between RSF and ISF in enhancing splitting strength when the TSF content was maintained at 1.5%. In their experiment, as the proportion of RSF increased within the TSF content, there was no significant trend in splitting strength. The splitting strength exhibited a gradual decline with the increased RSFRC in ISFRC, but the reduction was limited to less than 5% compared to 100% ISFRC.

Figure 2-10 illustrates the improvement in splitting strength with the addition of RSF compared to PC. With the inclusion of RSF, splitting strength significantly increases, reaching a maximum improvement of 213% with a 5% RSF addition [74]. When the fibre content is controlled around 1%, the increases in splitting strength range from 13.1% to 86.8% [58, 74, 80, 81]. The efficiency of improvement does not decline with increasing fibre dosage. These results suggest that RSF incorporation curbs crack development, enhancing tensile strength with higher RSF dosages.



(A)



(B)

Figure 2-9 Results of splitting strength

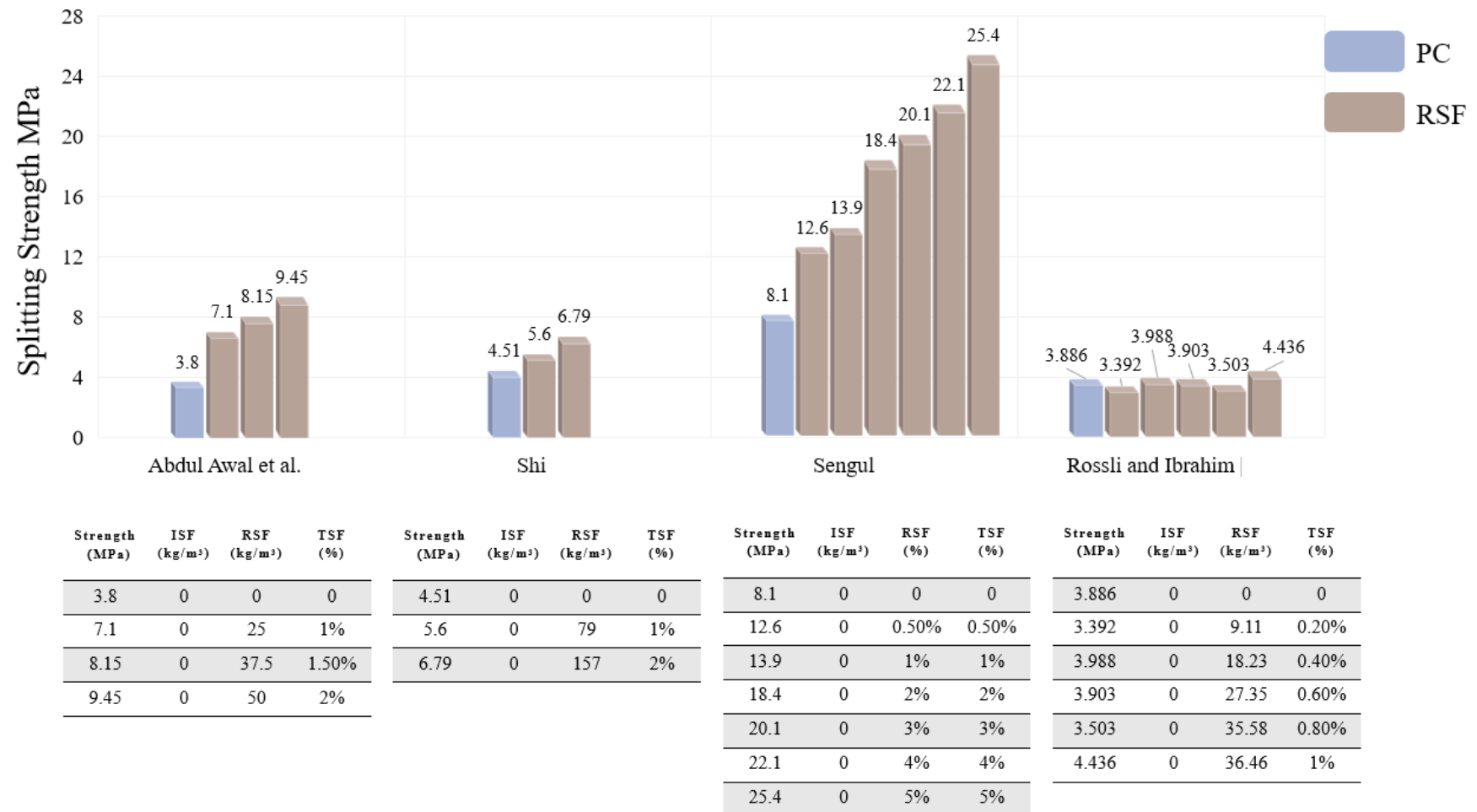


Figure 2-10 Results of splitting strength of RSFRC

2.4.3 Flexural strength

2.4.3.1 Standard of UNI-11039

The Crack Tip Opening Displacement (CTOD) test is a fracture toughness test that monitors crack development prior to failure, assisting in the evaluation of the flexural strength of concrete structures [82]. **Table 2-1** compiles data related to RSF and ISF concrete. **Table 2-1** demonstrate that the first crack strength (f_{1f}) slightly increases with the addition of fibres, with RSFRC exhibiting higher f_{1f} values than ISFRC. Similarly, the strength of $f_{eq(0-0.6)}$ follows the same trend, indicating that RSF provides a better bridging effect at the onset of cracking. However, ISFRC appears to offer higher post-crack strength compared to RSFRC. The differing performance between $f_{eq(0-0.6)}$ and $f_{eq(0.6-3.0)}$ with the addition of RSF is likely due to the shorter average length of the RSF used, which is more effective at controlling micro-cracks rather than macro-cracks. **Table 2-1** indicate that the toughness of concrete with added RSF primarily tends towards softening, while ISF tends towards both softening and plastic behaviour. Ref [75] and [83] compared HSFRC, and noted that HSF improves flexural strength and outperforms both ISF and RSF individually. In contrast, Ref [75] argued that the performance of HSF depends on the fibre content. If ISF content is higher than RSF in HSRC, the performance will more closely resemble ISFRC.

The differing opinions on the performance HSF can be attributed to the TSF content. When the content of RSF or ISF is low (below 0.5%), the synergistic effect between them is negligible. Generally, RSF is more effective in the early stages of cracking, while ISF is better at controlling larger cracks. The synergistic effect between ISF and RSF mainly arises from the

hybridization of fibres with different geometries. As discussed in Chapter 2.3, RSF functions similarly to micro-fibres with varying shapes and aspect ratios compared to ISF. These different geometries help create a bridging effect for cracks of different lengths. Additionally, the inclusion of RSF results in a softening structure, reducing the risk of brittle damage. Overall, the results indicate that HSF is effective in controlling both micro-cracks and macro-cracks, making it a suitable option for balancing strength improvement and economic benefits.

Table 2-1 Results of tests with standard of UNI-11039

Authors	Year	Fibre Properties				RSF	ISF	Total	CTOD ₀	f_{lf}	$f_{eq(0-0.6)}$	$f_{eq(0.6-3.0)}$	D ₀	D ₁
		Tensile Strength		Aspect Ratio										
		Mpa		l/d										
		RSF	ISF	RSF	ISF									
Vistos et al. [75]	2018	-	1200	104.68	60	25%	75%	0.50%	-	3.84	3.27	2.78	0.85	0.84
						50%	50%	0.50%	-	3.42	2.57	2.19	0.75	0.83
						75%	25%	0.50%	-	4.24	2.64	2.07	0.61	0.76
						100%	0	0.50%	14.28	4.45	2.67	1.37	0.6	0.51
Caggiano	2017	-	1200	104.68	60	0	60	0.75%	14.28	3.26	3.46	4.34	1.06	1.24
et al.						30	30	0.75%	14.28	3.93	4.07	4.36	1.02	1.06
[83]						50	30	1%	14.28	3.83	4.04	4.13	1.06	0.99

						70	30	1.25%	14.28	4.22	4.6	4.84	1.08	1.06
						60	0	0.75%	14.28	3.68	3.74	4.01	1.01	1.08
						0	0	0	18.85	3.25	-	-	-	-
Leone et	2018	-	-	58	50	35	0	0.46%	18.85	3.29	2.01	2.09	0.6	0.83
al. [26]						0	36	0.46%	18.85	3.09	2	2.3	0.64	1.34
						0	0	0	15.5	3.32	-	-	-	-
Leone et	2016	-	-	128	50	16	0	0.30%	15.5	3.35	2.21	1.92	0.67	0.85
al. [57]						0	23.45	0.30%	15.5	3.13	2.6	2.25	0.84	0.86

2.4.3.2 ASTM C78

Table 2-3 presents the flexural strength with standard of ASTM C78. ISF shows a slightly better performance in increasing flexural strength compared to RSF, with the improvement gap ranging from 7.7% to 12.4%. However, the addition of RSF still significantly enhances flexural strength, with a maximum improvement of 75.3% over PC [84]. Focusing on the toughness indices (I_5 - I_{20}), higher fibre content in concrete reinforcement leads to increased toughness indices. Ref [27] investigated the performance of HSF in terms of flexural strength and found that the toughness indices reach their lowest point at 46.7 kg/m³ (40%) RSF and 70.2 kg/m³ (60%) ISF, as the proportion of RSF decreases. The toughness indices decrease by approximately 50% with an increased RSF content, indicating a reduction in post-cracking strength and the concrete's energy absorption capacity. Despite this decline, the maximum toughness indices are observed at the initial addition of RSF to ISF concrete, suggesting some synergistic effects between ISF and RSF.

Ref [85] noted that concrete tends to soften when the residual strength factor is below 100. The addition of ISF in HSF concrete slightly reduces the residual strength factor. In contrast, RSF contributes to a greater softening effect, which aligns with findings from the CTOD test. When equal amounts of RSF and ISF are used in concrete, ISF concrete shows better performance in terms of energy absorption and residual flexural strength. Moreover, the energy absorption efficiency in RSF concrete is relatively low at low fiber content levels ($\leq 0.5\%$). However, the efficiency increases rapidly for fiber content above 0.5% and stabilizes after reaching 1%. This indicates that while RSF can significantly enhance energy absorption, its efficiency becomes more notable at higher fibre contents.

Table 2-2 Results of tests with standard of ASTM C78

Author	Year	Fibre Properties				RSF (kg/m³)	ISF (kg/m³)	Total (kg/m³) and (%v)	f_{ct} (MPa)	I ₅	I ₁₀	I ₂₀	R _{5,10}	R _{10,20}
		Tensile Strength Mpa		Aspect Ratio										
				l/d										
		RSF	ISF	RSF	ISF									
Bjegovic et al. [51]	2014	-	-	83	63	0	30	30	6.47	3.72	6.46	12.03	54.7	55.7
						15	15	30	6.53	3.41	5.65	9.72	44.8	40.7
						30	0	30	5.74	3.36	5.38	8.67	40.4	32.8
Najim et al. [84]	2018	781.3	-	50	-	0	0	0	9.51	4.15	9.27	20.43	102.4	111.6
						30	0	30	14.21	4.9	10.52	22.91	112.4	124
						45	0	45	15.40	5.1	11.05	24.06	119	130
						60	0	60	16.67	5.24	11.24	24.35	120	131
Mastali et al. [27]	2018	-	1300	111~333	47	0	0	0	6.55	1	1	1	0	0
						0	117	117	8.89	5.53	9.66	15.54	82.57	58.79

(1.5%)									
11.7	105.3	117	8.84	6.74	12.94	21.7	124.06	87.6	
23.4	93.6	117	8.74	6.05	10.91	18.47	97.29	75.56	
35.1	81.9	117	8.66	4.9	8.37	13.15	69.45	47.82	
46.7	70.2	117	8.51	4.62	7.56	11.64	58.89	40.75	
58.5	58.5	117	8.41	4.92	7.87	11.59	58.94	37.16	
70.2	46.8	117	8.34	5.06	8.17	12.59	62.23	44.2	
81.9	35.1	117	8.24	5.87	9.71	15.49	76.77	57.86	
93.6	23.4	117	8.21	5.01	7.94	11.91	58.71	39.62	
105.3	11.7	117	8.19	6.24	9.71	15.23	69.32	55.28	
117	0	117	8.2	5.06	7.7	11.62	52.77	39.24	

Author	Year	Fibre Properties		RSF (kg/m ³)	ISF (kg/m ³)	Total (kg/m ³) and (%v)	f_{ct} (MPa)	I_5	I_{10}	I_{20}	$R_{5,10}$	$R_{10,20}$
		Tensile Strength Mpa	Aspect Ratio									

						I/d					
						RSF	ISF	RSF	ISF		
Mastali et al.[78]	2017	1200	-	333	-	0	0	0	4.41	1	1
						0.35%	0	0.35%	4.89	4.32	8.17
						0.70%	0	0.70%	4.98	9.93	28.3
						1.05%	0	1.05%	5.31	5.89	9.68
Tlemat et al. [86]	2003	1250	1150	-	50	1.0%	0	1.0%	10.7	2.58	4.44
						1.5%	0	1.5%	12.7	4.75	8.34
						0	1.5%	1.5%	14.5	5.97	12.2

2.4.3.3 EN 14651

This testing technique involves evaluating SFRC tensile characteristics by calculating the area under its load-deflection plot or measuring the load-carrying capacity at a specific deflection or crack mouth opening displacement (CMOD) point. This is achieved via evaluating a simply backed notched beam under three-point bending [87]. **Table 2-3** presents the results of experiments conducted according to the EN 14651 standard. The results for the limit of proportionality ($f_{ct,L}$) indicate that concrete with added RSF generally does not achieve the same tensile strength improvements as concrete with ISF. However, the strength loss of RSF concrete relative to ISF concrete is approximately 3.1%. The differences between ISF and RSF reinforced concrete are minor, and with increasing RSF content, similar strengths can be achieved. Furthermore, the residual flexural strength values ($f_{R,1}$ - $f_{R,4}$) reported by ref [67] indicate that the combination of ISF and RSF can delay crack development, resulting in a more controlled failure process. However, RSF concrete still provides less post-crack strength support compared to ISF, and the gap in residual strength increases as cracks develop.

Table 2-3 Results of tests with standard of EN 14651 standard

Author	Year	Fibre Properties				RSF (kg/m³)	ISF (kg/m³)	Total (kg/m³) and (%v)	$f_{ct,L}$ (MPa)	$f_{R,1}$ (MPa)	$f_{R,2}$ (MPa)	$f_{R,3}$ (MPa)	$f_{R,4}$ (MPa)
		Tensile Strength		Aspect Ratio									
		Mpa		l/d									
		RSF	ISF	RSF	ISF								
Hu et al. [46]	2018	2570	1050	100	69	0	30	30	3.9	4.1	4.2	3.7	3.2
						30	0	30	3.7	3.4	2.7	2.1	1.7
Smrkić et al. [64]	2017	2850	1100	133	64	0	0	0	4.25	0.56	0.15	0	0
						20	20	40	5.00	4.59	4.50	3.94	3.46
						0	40	40	5.57	5.74	5.3	4.78.	4.16
Skarżyńs ki [50]	2018	-	-	104	50	0	0	0	3.59	-	-	-	-
						0	25	0.25%	4.82	2.29	-	-	0.98
						50	0	0.5%	4.67	4.67	-	-	2.45
Bjegovic	2014	-	-	83	63	0	30	30	6.47	-	-	-	-

et al. [51]						15	15	30	6.53	-	-	-	-
						30	0	30	5.74	-	-	-	-
Zamanza deh et al. [88]	2015	-	-	-	-	45	0	45	4.73	4.16	3.94	3.69	3.43
						60	0	60	5	5.36	5.17	4.86	4.41
						90	0	90	4.56	6.62	6.56	5.9	5.55
						0	45	45	5.14	8.61	8.36	6.83	5.64
						0	60	60	6.62	10.43	7.39	4.8 6	3.4
						0	90	90	5.99	12.37	12	9.71	7.38

Author	Year	Fibre Properties				RSF	ISF	Total (kg/m³) (%v)	$f_{ct,L}$ (MPa)	$f_{R.1}$ (MPa)	$f_{R.2}$ (MPa)	$f_{R.3}$ (MPa)	$f_{R.4}$ (MPa)
		Tensile Strength		Aspect Ratio									
		Mpa		l/d									
		RSF	ISF	RSF	ISF								
Tlemat et	2006	1250	1150	-	50	0%	0	0%	3.45	-	-	-	-

al. [89]						0.50%	0	0.50%	4.26	1.1	-	-	0.8
						1%	0	1%	5.32	3.9	-	-	1.7
						2%	0	2%	6.24	6	-	-	2.5
						0	20	20	4.6	1.47	0.83	0.59	0.44
						0	30	30	5.1	2.54	2.36	1.59	1.09
						30	0	30	4.4	3.55	3.77	3	2.38
Baricevic						30	10	40	4.9	2.49	1.86	1.24	0.88
et al.						50	10	60	4.9	3.12	2.61	1.94	1.4
[67]						80	10	80	4.4	3.05	2.32	1.81	1.42
						100	10	100	5.9	5.8	4.47	3.32	2.49
						40	20	40	4.7	3.47	3.23	2.41	1.85

2.4.3.4 Flexural strength of RSFRC

Figure 2-11 and 2-12 aims to illustrate the improvement in flexural strength between RSFRC with respect to PC.

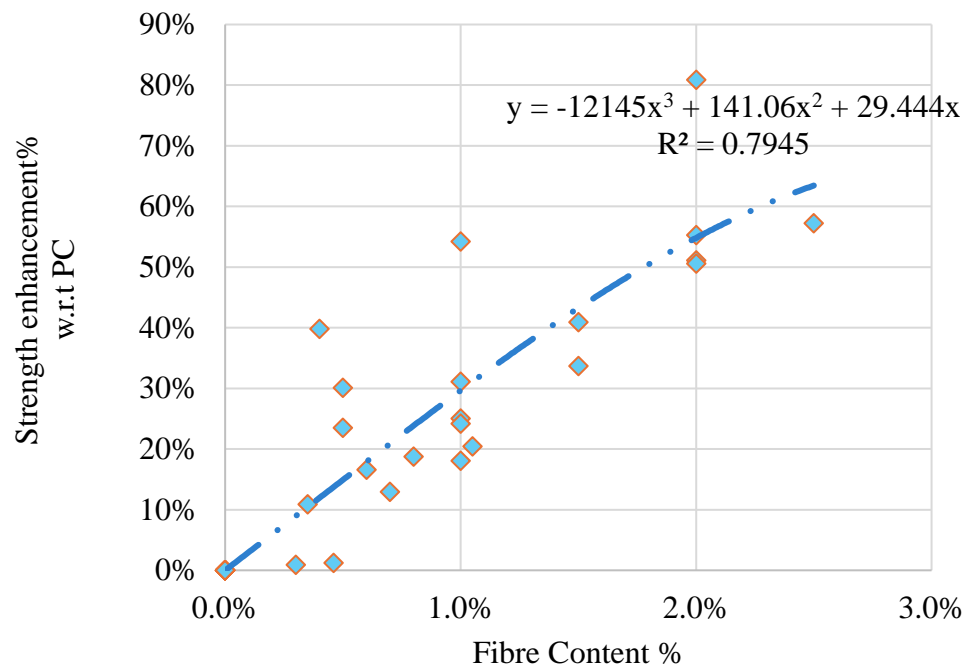
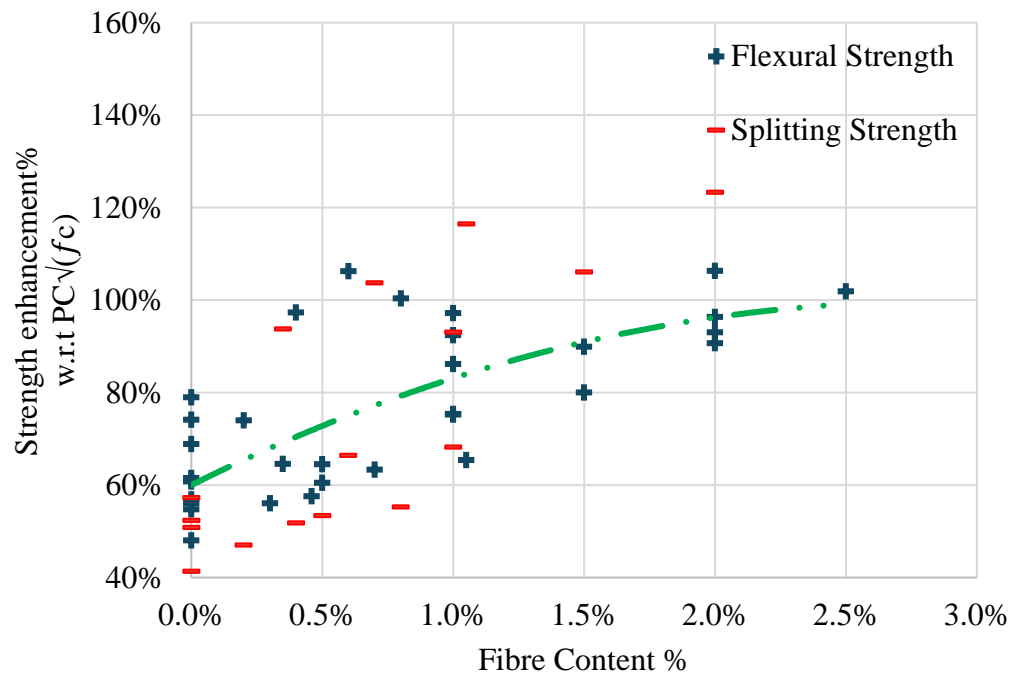


Figure 2-11 Flexural strength improvement with RSF**Figure 2-12** Compressive strength relative ratio

According to **Figure 2-12**, relations between the flexural and splitting strengths indicate a probable link with $\sqrt{f_c}$. This data shows that the ratio of the $f_r/\sqrt{f_c}$ and $f_{sp}/\sqrt{f_c}$ rose upon fiber addition, implying that RSF enhances tensile strength. Additionally, a fiber content-over 1% stabilized the escalation of tensile strength increase, delineating its zenith tendency to enhance tensile robustness. Even though there are conflicting trends in compressive strength increase with RSF addition [78, 89], $f_r/\sqrt{f_c}$ ratio and $f_{sp}/\sqrt{f_c}$ ratio retained an upward trajectory. The statement aggregates that even when RSF use influences compressive strength differently, its efficiency at increasing tensile strength remains constant.

2.5 Sustainability Analysis

Waste tires, as materials with substantial recycling potential, have garnered significant attention

due to their potential contributions to environmental sustainability and economic value. RSF are one such material, derived from waste tires. To understand the origin and structure of RSF, it is essential to examine the composition of a tire, illustrated in **Figure 2-13**. A typical tire consists of several layers, each with specific functions and materials:

- **Tread:** The outer layer of the tire, providing traction and durability. It is usually made from natural and synthetic rubber compounds.
- **Belts:** Beneath the tread, steel belts enhance strength and puncture resistance. These belts are the primary source of RSF.
- **Sidewall:** This part protects the tire from impacts and abrasions. It is also made from rubber compounds but does not contain steel.
- **Body Ply:** Layers of textile cords (often polyester, nylon, or rayon) embedded in rubber provide the tire's flexibility and strength.
- **Bead:** The innermost part that ensures the tire stays securely on the rim. It consists of steel wires encased in rubber.

By understanding these layers, particularly the steel belts, we can appreciate the origin of RSF [90]. The recycling process involves extracting these steel components from waste tires, cleaning them, and processing them into usable fibres for concrete reinforcement. This not only helps in waste management but also adds value by enhancing the mechanical properties of concrete, making RSF an environmentally friendly and economically viable material.

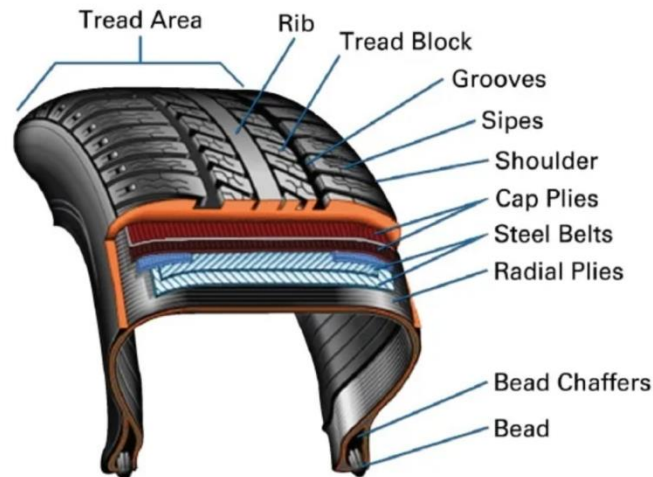


Figure 2-13 Structure of tire

2.5.1 Sustainability

Carbon dioxide (CO₂) footprint is among the major criteria utilized for evaluating the ecological impact. The CO₂ footprint is a significant metric for evaluating environmental impact, crucially influencing sustainable development. Over 13% of steel can be reclaimed from discarded passenger tires, and the recycling process for truck tires in the European Union reclaims 25% of the steel with minimal carbon emissions [91]. Therefore, the proper recycling of waste steel, such as substituting RSF for ISF in concrete, holds practical importance in reducing carbon emissions from civil construction activities. Table 6 has been constructed to compare the global warming potential (GWP) of RSF and ISF, aiming to assess RSF's contribution to sustainable development. Additionally, due to limited information on RSF's GWP, two studies detailing the GWP value in tire recycling processes have been reviewed as in **Table 2-4**.

Table 2-4 Global warming potential

ISF (kg CO ₂ eq)		RSF (kg CO ₂ eq)	
Mastali [27]	2.15	Mastali [27]	0.5(RSF)
Isa et al.[28]	2.68	Isa et al.[28]	0.083(RSF)
Mehdipour et al.[92]	1.6	Piotrowska et al.[93]	-2.116(T)
Yepes et al.[94]	2.35	Turner et al.[95]	-1.17±1.047(T)
Mean Value	2.2	Max Value	0.5

In general, tire recycling is considered environmentally friendly, primarily contributing to reduced carbon emissions. The positive impact noted by ref [27] is largely attributed to transportation rather than the recycling process itself. The average GWP of ISF is 2.2 kg CO₂ eq, nearly four times higher than the maximum GWP value of RSF, based on data from ref [5]. Annually, Europe discards over 500,000 tonnes of RSF from waste tires. Therefore, if RSF is reused in concrete instead of ISF, it could potentially save over 1 billion kg CO₂ eq per year in terms of maximum GWP reduction.

2.5.2 Economics

In addition to RSF's impact on reducing GWP, its affordability is another significant factor to consider. Three studies have compared the price difference between ISF and RSF, with detailed results presented in **Table 2-5**.

Table 2-5 Price between RSF and ISF

ISF (€/kg)		RSF (€/kg)	
Mastali [27]	0.8	Mastali [27]	0.5
Neocleous et al.[96]	0.7	Neocleous et al.[96]	0.05-0.2
Samarakoon et al.[5]	1.5	Samarakoon et al.[5]	0.15
Mean Value	1.0	Mean Value	0.24

Based on the findings from **Tables 2-5** and **2-6**, it is evident that using RSF instead of ISF offers significant benefits in terms of both economic and environmental considerations. Additionally, the social impact of RSF cannot be overstated. As noted in the paper, discarded tires are a major environmental hazard that could badly harm human health and water resources if burned or disposed of improperly. When used these recycled components materials from waste tires in civil construction projects, these materials are a sustainable material that can make the building more environmentally friendly and durable. Concrete made with recycled tires demonstrates significant improvement in its mechanical traits. Even though tire-mix concrete does not always exceed traditional concrete in performance and can sometimes underperform, its advantages in terms of economics, environmental sustainability, greenhouse gas reduction, and societal advancement are substantial.

2.6 Research Gap

Based on the comprehensive review conducted, it is evident that RSF can effectively replace

ISF in concrete applications. However, there are several areas that require further research and development:

Compressive Strength: Future studies could explore the use of self-compacting concrete techniques with added RSF to enhance compressive strength. Currently, there are limited studies on different compacting technologies to optimize RSF concrete's compressive strength.

Shear Strength: RSF has shown promise in improving flexural and splitting strengths of concrete. Research should now focus on its potential to enhance shear strength in SFRC. Previous studies using ISF as transverse reinforcement have been successful, but RSF's specific contribution to shear capacity needs detailed exploration, including the development of semi-empirical or empirical formulas.

Dynamic Properties and Impact Resistance: Research gaps exist regarding the dynamic properties of RSF concrete and its application in structures subjected to impact. Understanding these properties is crucial for applications requiring resilience to dynamic loading.

Durability Properties: Properties such as chloride resistance and freeze-thaw resistance of RSF concrete require more investigation. Enhancing these durability aspects would broaden the applicability of RSF concrete in various environmental conditions.

In conclusion, while RSF has demonstrated its capability to replace ISF in concrete effectively, future research should prioritize advancing its compressive strength through self-compacting techniques, exploring its role in enhancing shear strength, investigating dynamic properties and impact resistance, evaluating high-strength concrete, and improving durability properties.

These efforts will contribute to expanding the practical applications and sustainability of RSF concrete in construction and infrastructure projects.

2.7 Conclusion Remark

In this study, RSF concrete is meticulously appraised, and its mechanical properties are contrasted with those of ISF concrete, highlighting its sustainability. The findings are condensed as follows:

RSF concrete has far superior tensile strength due to the high-strength steel in its fibres compared to ISF concrete, resulting in improved bending and splitting resilience. The workability of RSF concrete, when compared to ISF concrete, diminishes as the RSF content rises. Nonetheless, this problem can be addressed by using superplasticizers and smaller aggregates. With increasing fibre proportions, the RSF concrete's resistance to compression is optimized. However, strength may decline after 0.5% because of air pocket development. This situation should improve by upgrading the self-compacting or vibration process to decrease voids. RSF concrete can enhance splitting resistance at higher dosages without achieving peak efficiency, with ISF being somewhat more effective. When it relates to flexural strength, although RSF can control early crack construction, and ISF is better at preventing macro-cracks. Both types of fibres provide essential enhancements in tensile resistance, and their results are accomplished over 1% of the blend. RSF contributes significantly to sustainability, with potential negative GWP if transportation distances are minimized. RSF is also cost-effective, being priced at a quarter of ISF, offering substantial budget savings.

In summary, RSF concrete demonstrates significant potential due to its extremal high

performance of tensile strength, cost-effectiveness, and contributions to sustainability. However, several challenges remain, particularly its non-stable performance. These unresolved issues highlight the need for further investigation. In the next chapter, this paper will explore the differences between RSF and ISF concrete, focusing on their mechanical properties and dynamic performance, to better understand the potential applications and limitations of RSF in concrete technology.

3. Experimental Study of Mechanical and Dynamic Properties

Literature review on the challenges of systematically evaluating SFRC's performance due to inherent uncertainty. Existing literature has confirmed the potential advantage of adding RSF in concrete. Still, results have exhibited significant variability due to RSF source quality and the methods used in recycling processing. This aspect contrasts with ISF, which are formulated with high-quality steel wire exclusively for concrete reinforcement. ISF are offered in a variety of shapes, sizes, and orientations to meet specific criteria as well as in compliance with international standards such as ASTM A820, presenting consistent execution through strict quality control processes. The section is intended to narrow the significant divide between ISF and RSF by focusing on a more dependable variant of RSF. Furthermore, many contemporary designs use prevalent vibration-based monitoring solutions in long-span bridges, footbridges, and historic structures [97]. Each of these monitoring systems for concrete structure has three interconnected dynamic features: dynamic elasticity modulus, natural frequency, and vibration damping. For the further field application, this section will focus on non-destructive testing techniques, with a particular emphasis on the structural health monitoring (SHM) involves the continuous vibration sensing [98]. For a better understanding of the research route of this study,

Figure 3-1 was built.

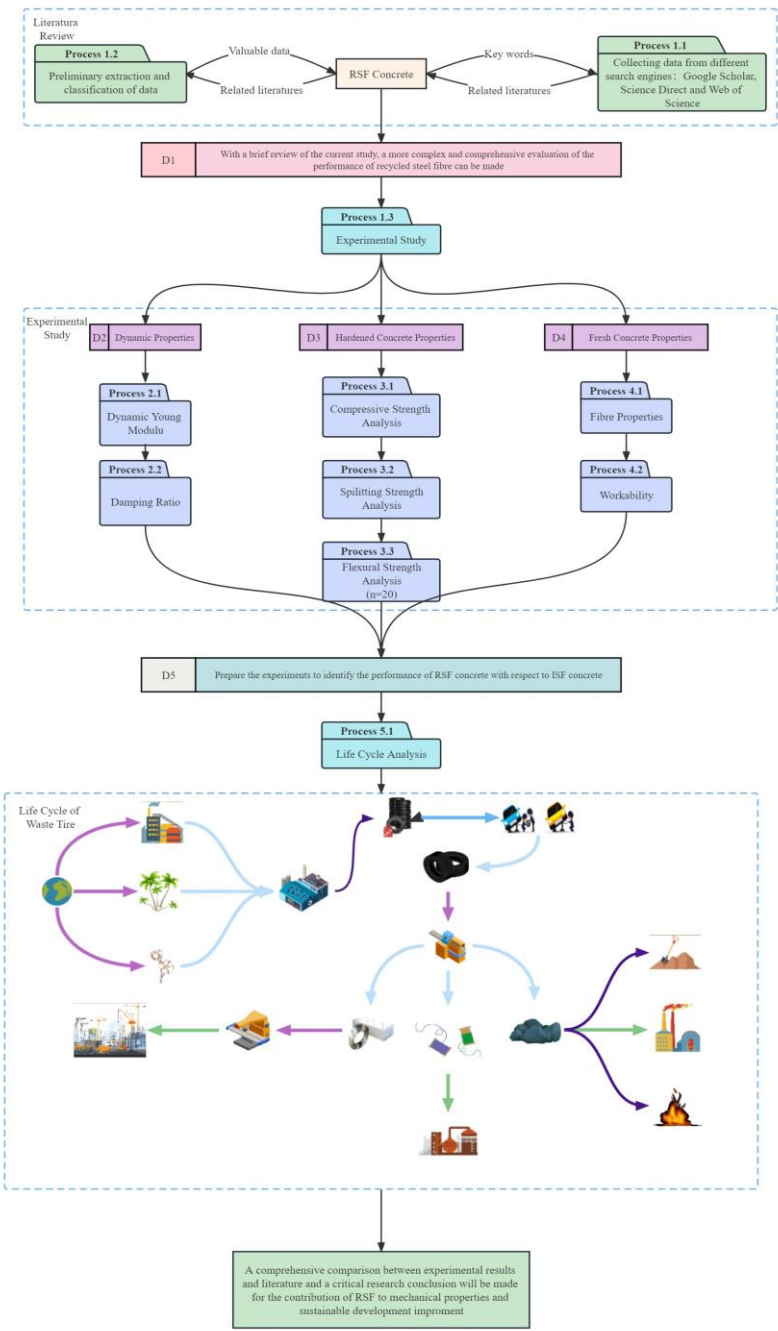


Figure 3-1 Research route

3.1 Experimental Design

3.1.1 Materials Preparation

This study would use Rugby High Strength Cement CEM/I, which meets UK BS EN 197-1 standards for construction due to its physical and mechanical properties. The coarse and fine

concrete components would be purchased from Tarmac Trupak of Plumtree Farm Industrial Estate in Birmingham, UK. The concrete components have a specific gravity of 2.5, and their bulk density is 1700 kg/m^3 . The coarse material is granite that was crushed and has a specific gravity of 2.5 and a bulk density of 1650 kg/m^3 . For comparative purposes, Novocon® HE 1050 from ControlLiner, a unit of Milliken Infrastructure Solutions, LLC, will be used as Interface Surface Fibre (ISF) to compare the performance of this RSF. Based on the characteristics of Novocon® HE 1050 in **Table 3-1**, it has an average diameter of 1 mm, a length of 50 mm, and an average axial tensile strength of 1150 MPa. In comparison, recycled steel fibre (RSF) has a specific gravity of 2.5 and 1700 kg/m^3 of bulk density. Coarse aggregate is crushed granite with an average grain size of 10 mm and a specific gravity of 2.5 and bulk density of 1650 kg/m^3 . The RSF showed in **Figure 3-3**, the bead wires were obtained from tires scrapped and collected by the Xiang He Tire Retreading Factory. An optimal bead wire shredding method was developed to create RSF with a hook shape at the ends. A total of 50 RSF were randomly selected for length and diameter measurements. The average diameter of the RSF is 1.62 mm, and the average length is 50.1 mm. In addition, five RSF samples were randomly selected for tensile strength testing, as shown in **Figure 3-2**. The average tensile strength of RSF is 2072.94 MPa with a coefficient of variation of 6.47%. By comparing the appearance of RSF and the ISF in **Figure 3-3**, the surface of the RSF is covered by black powder. This is due to some particles of tire rotation dust form on the steel-wire surface during the recovery of steel wire.



Figure 3-2 Fibre tensile strength test

Table 3-1 Fibre properties

RSF		ISF	
Tensile Strength	2072.94MPa	Tensile Strength	1150MPa
Raw Material	Scarp bead wire	Raw Material	Steel plate
Diameter	1.62mm	Diameter	1mm
Length	50.1mm	Length	50mm
Aspect Ratio	30.92	Aspect Ratio	50
Surface	Covered by Rubber Dust	Surface	Clean



(a) RSF

(b) ISF(left) and RSF(Right)

Figure 3-3 Fibre properties

3.1.2 Concrete Mixes

The M0 group serves as a reference for evaluating various fibre replacement ratios: 0% (reference), 0.4%, 0.8%, and 1.2%. The concrete mix has a mass ratio of cement, water, sand, and stone of 1:0.54:1.7:2.3. All mixtures maintain a water/cement ratio of 0.54, with a cement dosage of 317.3 kg/m³. **Table 3-2** presents the design of combination schemes featuring these four different content levels.

In the conducted experiment, the optimal fibre content was determined to be 1.2%. This selection was based on recommendations from the ISF manufacturer (SIKA company) and existing literature on RSF [99]. Research indicates that while increasing RSF content above 1% enhances flexural strength, the efficiency of this improvement decreases significantly beyond the 0.5% to 1% range [99]. Additionally, SIKA's guidelines suggest an ISF content below 60 kg, which corresponds to approximately 0.8%. Additionally, higher fibre content introduces a risk of causing balling effect, which can adversely affect the consistency and general performance of the concrete. After a detailed assessment of ISF and RSF traits, 1.2% fibre

content was picked for the study. This ratio was chosen to achieve the ideal structural improvement and prevent problems related to increased fibre content - for example, decreased workability and potential for uneven distribution in the concrete.

Fibre reinforced concrete's key concern compared to conventional reinforced concrete is the "balling effect." This problem arises when concrete fibres clump together, forming aggregates. Concrete consistency is compromised by these aggregations. To prevent the balling effect, the most critical step is to adhere to BS EN 12350-1 and 12350-2. These guidelines help to achieve a uniform concrete mix [100]. This strategy for ensuring uniform concrete mixing is intended to prevent the clustering of fibres. Additionally, it improves concrete durability, which is also crucial for the overall performance of the SFRC.

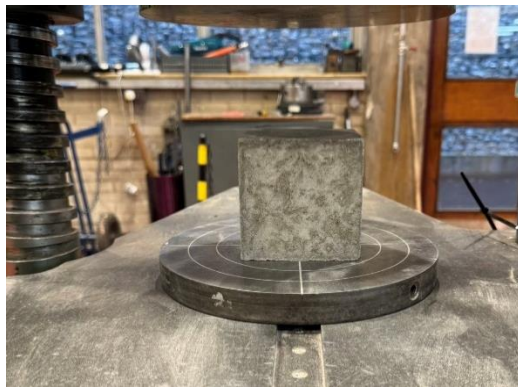
Table 3-2 Detail of Mixes

Group	Cement (kg/m ³)	Water (kg/m ³)	Sand (kg/m ³)	Gravel (kg/m ³)	Fibre (kg/m ³)
M0	317.3	171.34	983.63	713.925	0
M1-ISF	317.3	171.34	983.63	713.925	24(0.4%)
M2-ISF	317.3	171.34	983.63	713.925	48(0.8%)
M3_ISF	317.3	171.34	983.63	713.925	24(0.4%)
M1-RSF	317.3	171.34	983.63	713.925	48(0.8%)

3.2 Experimental Facilities

This study explores the mechanical and dynamic characteristics of RSFRC and ISFRC.

Cylindrical specimens measuring 200mm in height and 100mm in diameter were produced to conduct splitting tests, while 100mm cube specimens were made to carry out compressive strength tests. In addition, beam specimens with a 600 mm length and 150 mm x 150 mm cross-section, including a notch, were developed to enable residual flexural strength and dynamic tests. Three samples were extensively studied for each trial type, except for the CMOD test, to ensure that the findings were trustworthy and repeatable. **Figure 3-4** illustrates the configurations of each examination in more detail.



(a) Compressive Tests



(b) Splitting Test



(c) CMOD Test



(d) Modal Test

Figure 3-4 Test setup**3.2.3.1 Compressive Strength**

As shown in **Figure 3-4(a)**, following the procedures given in BS EN 12390-3:2009, the compressive strength in this research was done on concrete cubes of dimensions 100 mm × 100 mm × 100 mm. These cubes were kept in a water reservoir and tested after 28 days. The test was done at 0.6 MPa/s loading rate, and the procedure for concrete specimens was as explained in Section 3.1. The specimens were held in sealed, moist-tight containers at 20°C in the laboratory before the test. The report lists the average value of the compressive strengths of three concrete specimens.

3.2.3.2 Splitting Test

Three cylindrical samples of the same size are created for each mix. Their diameter stands at 100mm, and they measure 200 mm in height. Their tensile strength is examined to split them at 28 days following cure, as shown in **Figure 3-4(b)**, **Equation 3-1** is utilized to compute the split tensile strength of each cylinder.

$$f_{sp} = \frac{2P}{\pi DL} \quad (3 - 1)$$

Here, f_{sp} denotes the split tensile strength, P represents the maximum applied splitting load, L denotes the length of the specimen, and D represents the diameter of the samples.

3.2.3.3 Flexural Test

The CMOD test is acknowledged for its ability to describe material fracture, particularly among those that behave malleably, it is important to note its versatility, as many metals and polymers

are commonly used in a variety of industries, from aerospace to automotive to civil engineering. By calculating the point of displacement at the crack tip of a sample under applied strain, the CMOD test allows determination of material integrity in a variety of contexts, offering a significant edge in investigating the complexities of these laterally flexible substances.

For instance, concrete beams measuring $150\text{mm} \times 150\text{mm} \times 600\text{mm}$ are notched with a 25mm depth and 5mm width at mid-span. Subsequently, this study test the notched beams under different loading at different stage. For the sampling setup, this study used a 500 kN hydraulic testing device to arrange a three-point setup. Gauges linked to the notch gather CMOD readings. These devices, complying with BS EN 14651 standards, run at different loading rates. The test commences at 0.05 mm/min, advancing to 0.2 mm/min after the CMOD measures 0.1 mm.

Figure 3-4(c) illustrates the test setup.

Equation 3-2 is applied to calculate the limit of proportionality, while **Equation 3-3** defines the flexural residual strength ($f_{R,j}$).

$$\sigma = \frac{3PL}{2bh_{sp}^2} \quad (3 - 2)$$

$$f_{R,j} = \frac{3F_jL}{2bh_{sp}^2} \quad (3 - 3)$$

3.2.3.4 Modal Test

Modal analysis is a non-damaging process employed to evaluate the dynamic performance of structures and materials. It includes independently exciting the structure using a fixed vibration or force and monitoring its response to determine its natural frequencies and damping ratios [101]. The technique is vital to assess the structural integrity and functioning of SFRC without

impacting the specimens' condition. It also plays a vital role in monitoring the quality of SFRC applications.

Three primary results from the modal test are apparent. They are natural frequency, damping ratio, dynamic Young's modulus. Dynamic Young's modulus is significant because it refers explicitly to the material's capability to withstand deformation due to oscillatory and cyclical stress. Accordingly, this is a critical factor when designing structures that endure vibration, seismic events, and impacts.

The modal test setup in this study follows ASTM C215 guidelines, and **Equation 3-4** from ASTM C215 is employed to calculate the dynamic Young's modulus (E):

$$E = CMn^2 \quad (3 - 4)$$

Where M denotes the mass of the specimen, n represents the fundamental transverse frequency, and C is defined as $0.9464(L^3T/bt^3)$ for the prism specimen. To ensure a free-free condition during testing, as illustrated in **Figure 3-4(d)**, two sponge mats, each with a thickness of 500mm, have been placed above all tests. This setup aligns with similar modal test examples found in the literature.

3.2.3.5 Micro-Structure Analysis

In this study, a scanning electron microscope (SEM) will be used to explore the physical structure of SFRC, based on the technique delineated by the ASTM C1723-2010 standard [102]. First, a small fragment of SFRC will be acquired and dried in a 40°C oven. The sample will then be coated with gold before SEM examination. The produced electron-backscattered

images will be magnified to 1000 times their original size. The SEM images will range from 200 to 500 micrometres in clarity, with a resolution of 1280 x 1040 pixels.

3.3 Results Analysis

This chapter gives a thorough assessment of the performance of RSFRC and ISFRC. The objective is to establish the extent of the performance gain as a result of comparing these two kinds of SFRC. The fresh and mechanical properties of RSF and ISF concrete are detailed in **Table 3-3**.

Table 3-3 Test results of ISFRC and RSFRC

Group	Slump (mm)	Compressive		Splitting		Flexural
		Strength (MPa)		Strength (MPa)		Strength
		Avg \pm SD	COV	Avg \pm SD	COV	(MPa)
M0	65	58.69 \pm 1.15	1.96%	3.35 \pm 0.10	2.87%	2.04
M1-ISF	54	64.15 \pm 0.39	0.61%	4.25 \pm 0.12	2.83%	3.05
M2-ISF	49	66.14 \pm 2.01	3.03%	4.35 \pm 0.3	6.96%	3.31
M3_ISF	47	66.90 \pm 2.29	3.43%	5.20 \pm 0.25	4.76%	4.59
M1-RSF	56	62.16 \pm 1.25	2.01%	3.85 \pm 0.07	1.91%	2.94
M2-RSF	49	64.62 \pm 0.74	1.14%	4.24 \pm 0.14	3.26%	3.25
M3_RSF	48	65.26 \pm 0.39	0.60%	4.44 \pm 0.09	1.95%	3.72

3.3.1 Slump Test

Table 3-3 shows the variation in slump tests with differing fibre content. Predictably, adding

fibres reduces the slump measurement considerably. According to ref[103], the addition of fibres will negatively affect geopolymer concrete workability, while hooked-end fibres create higher flow resistance in fresh geopolymer concrete. Furthermore, the slump of ISFRC is less than that of RSFRC when the fibre content is constant. This distinction is due to the rubber dust coating on the RSF surface, which helps the fibre absorb water during hydration [104]. RSFRC exhibits slightly higher slumps than ISFRC due to its hydrophobicity due to the rubber coating.

Both ISFRC and RSFRC have lower slump values when the fibre content is constant at 1.2%, compared to traditional concrete. With a fibre content of 1.2%, ISFRC and RSFRC have notably lower slump values of 27.2% and 26.1%, respectively, compared to PC. The study results are consistent with prior research [5, 51, 57, 105]. Still, one critical finding is that the presence of RSF produced from steel wires is less likely to cause conglomeration during mixing. This differs from the action of RSF collected from steel belts, which is more prone to clustering owing to its uneven shape of tabs and inclination to get tangled. This distinction is due to the application of different recycling procedures. Fiber derived from steel wires retained its shape in our study, leading to better performance than irregular fibre. Additionally, the research findings show that the interplay of RSF with cement during mixing is more important than that between ISF and water absorption, taking into consideration that the water taken in by the rubber dust can coat the RSF.

3.3.2 Compressive Tests

Incorporating fibres boosts compressive strength irrespective of fibre shapes. However, the inclusion of fibres makes consolidation more difficult, reducing the compressive power of each

fibre form. It's been contended that incorporating fibres is not help with compressive strength because it entangles air. Ref [106] suggested that ISF influence on the process cannot substantial enough to influence the concrete strength. In this case, strength is related to the ISF qualities and quantities used in construction.

According to experimental data, the compressive strength of RSFRC after 28 days is typically 15-20% higher than plain concrete. Also, compared to RSF concrete, ISF concrete has greater compressive strength. M1-ISF concrete outperforms M1-RSF at 10% (21.10% stronger), M2-ISF at 8.86%, and M3-ISF at 9.14%. After combining similar quantities of fibres, it's clear from the test results that ISF concrete typically has better strength than RSFRC[104]. The reason for this is that the latter has a poorer hydration potential. Because the hydration reaction is constrained, the existence of rubber bits on the RSF exterior compromises it. Concrete strength is dependent on the carbonation level and hydration activity.

The compressive strength improvement seen in RSFRC is not as strong as that of ISF concrete due to the use of relative low-quality RSF. RSF is derived from waste tires, which have already been weakened by fatigue and lack of malleability. The rubber dust encasing the fibre adversely affects fibre-paste bonding. Additionally, the rubber dust affects the transition zone between the fibre and the cement paste, thereby spoiling the interfacial transition zone, which undermines the strength improvement [107]. The compressive strength improvement rate in ISF concrete shows only a slight change when the fibre content increases from 0.4 to 1.2 %. This particular pattern is also observed in RSFRC, hinting at a slow rate of growth. As a result, increasing the fibre content in this range has little effect on the compressive strength of these types of concrete.

Prior research has shown that incorporating RSF or ISF into concrete leads to a substantial increase in compressive strength by making the concrete matrix [47]. The higher-strength concrete in this study, on the other hand, behaves differently. In general, the introduction of RSF or ISF only produces a small strength increase, indicating a minor effect. In contrast to common concrete, this is an intriguing finding. The increased density of HSC restricts fibres' ability to improve its compressive strength.

3.3.3 Splitting Test

Based on **Table 3-3** results, the splitting tension strength for ISFRC grew from 4.25 MPa to 5.2 MPa in cases where the fibre was increased from 0.4% to 1.2%. Also, the 1.2% RSF content improved the splitting tensile strength of RSFRC to 4.44 MPa – showing a notable 32.5% increase from PC. Notably, ISFRC had a higher tensile strength than RSFRC across different fibre types, differing from the compressive strength pattern. Including fibres resulted in a 17% improvement in power, regardless of fibre kind.

Fibre quality has a substantial impact on the splitting strength improvement efficacy in view of the compressive strength test results. The fibre's hook end in the splitting test is a critical factor in boosting splitting strength. A strong hook end can prevent minor crack formation and growth, improving the concrete's overall resistance to cracks [108].

It is essential to consider that steel strands in RSF material are a key ingredient sourced from tires. Steel strands are vulnerable to long-term fatigue, which could compromise the RSF clamp's clamping force and splitting strength improvement [109]. In previous trials, it was noted that RSF marginally decreases concrete's split strength [47, 110]. This decrement is

typically caused by inconsistent and uneven fibres' role in forming internal cracks, particularly from steel belt recycling. These irregular fibres make the crack development appear disordered and fragmented, which in turn disrupts the concrete's overall performance.

In this context, the test was conducted using RSF that had been produced in a uniform mold instead of the randomly shaped RSF typically obtained from steel belt recycling. This consistent shape and structure of the RSF lead to greater uniformity in the resulting hardened concrete. This, consequently, supports the rational development of cracks within the concrete, enhancing its overall strength and structural integrity.

3.3.4 CMOD Test

3.3.4.1 CMOD-deflection Curve

The CMOD tests were conducted conforming to the BS EN 14651-2005+A1-2007 standard to investigate the post-cracking performance of RSFRC and ISFRC beams. The description of the experimental findings is highlighted in **Table 3-4** and **Figure 3-5**.

Table 3-4 demonstrates the notable impact of the volume fractions of ISF and RSF on the mechanical properties of SFRC. The bridging effect of the fibre prevents sharp decreases in load capacity in SFRC examples. As fibre content grows, the flexural strength of RSFRC and ISFRC rises as expected. Nonetheless, ISFRC outperforms RSFRC in terms of residual strength and maximum flexural strength [88].

At 1.2% fibre volume, ISF concrete shows a 225% higher maximum peak load than PC. Similarly, RSFRC has a higher maximum peak load of around 182.3% compared to PC with

the same fibre volume. In contrast, although the ISFRC and RSFRC significantly increases both the post-crack and overall energy absorption capacities, the ISFRC excels in enhancing the post-crack and overall energy absorption capacities for bending strength. Regarding the load behaviour post peak stress and sharp decline, the ISF concrete with 0.8% fibre content shows a slight uptick before attaining a plateau. Perhaps the most notable difference is that LOP (load of proportionality) for RSFRC and ISFRC is pretty similar. This is because the LOP, which is primarily influenced by the friction between concrete matrix and fibres within the uncracked concrete beams and shows signs of flexural tensile strength, or capability to resist forces causing tension, remains consistent between ISFRC and RSFRC. The hooks at the end of these reinforcing fibres play a central role in controlling cracking after the beams have cracked fully and continue to bear the load. This hooked end ensures that the residual flexural tensile strength of the composite is adequate to maintain its indented functionality following cracking [111].

Table 3-4 CMOD test results

Result	Residual Flexural Strength (MPa) 28days						
	Plain		ISF		RSF		
	0%	0.40%	0.80%	1.2%	0.40%	0.80%	1.2%
Peak Load	2.04	3.05	3.31	4.59	2.94	3.25	3.72
Fct 0.5	-	2.08	3.50	4.54	1.12	2.90	3.48
Fct 1.5	-	2.01	3.70	4.00	1.21	2.69	3.07
Fct 2.5	-	1.87	3.40	3.60	1.30	2.17	2.72
Fct 3.5	-	1.57	2.84	3.23	1.29	1.90	2.25

Fracture Work							
W_f^T (N/m)	-	20.32	38.47	31.32	47.37	55.18	61.91
W_f^{pre} (N/m)	-	0.43	0.52	0.59	1.16	0.55	1.72
W_f^{post} (N/m)	-	19.89	37.94	30.73	46.21	54.63	60.19
Fracture Energy							
G_f^T (J/mm ²)	-	5.42	10.26	8.35	12.63	14.71	16.51
G_f^{pre} (J/mm ²)	-	0.12	0.14	0.16	0.31	0.15	0.46
G_f^{post} (J/mm ²)	-	5.30	10.12	8.20	12.32	14.57	16.05

* W_f^T and G_f^T is the total fracture work and energy, W_f^{pre} and G_f^{pre} the fracture work and energy before peak and W_f^{post} and G_f^{post} is the fracture work and energy after peak.

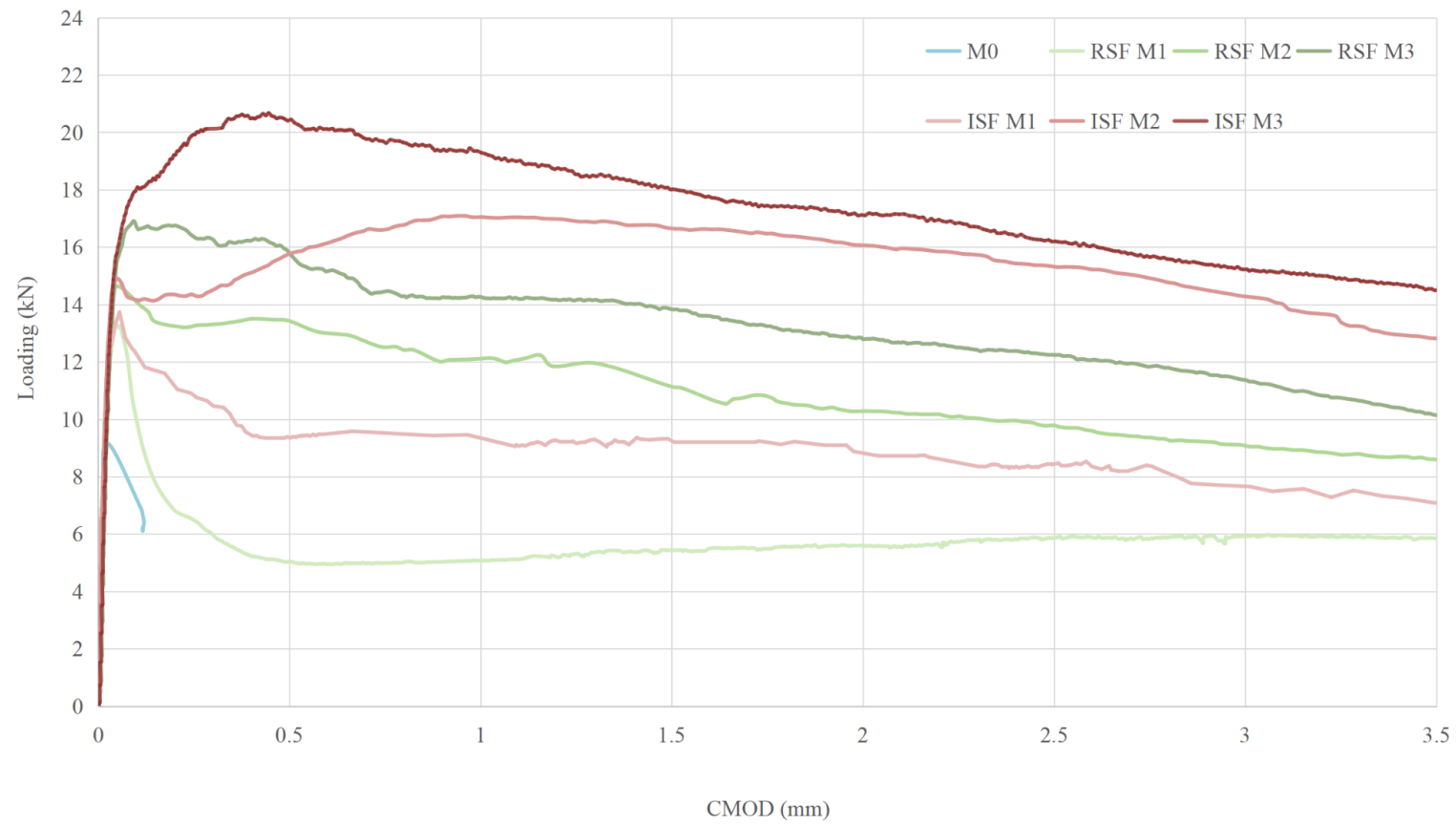


Figure 3-5 Loading and CMOD curve

3.3.4.2 Fracture Energy Analysis

The term "fracture energy" refers to a material's ability to take in supplemental energy following splitting. It indicates the amount of energy a structure can withstand as it fails. The specific fracture G_f (J/mm^2) can be estimated from the area under the splitting force–displacement line. Earlier experiments have found that adding fibres enhances the concrete matrix's split resistance. This research compares the capability of ISF and RSF to boost the concrete matrix's capacity to absorb crack initiation energy, as shown in **Table 3-4**.

The research findings show that the incorporation of fibres into concrete results in a concrete type that offers higher energy needed to propagate a fracture in conventional concrete. The reason is that cracks can't spread without the fibres undergoing stretching and surface stripping. In comparison with unreinforced concrete samples, SFRC specimens demonstrate the most remarkable improvement in fracture energy, notably for the M3-ISF specimens, reaching $16.51 \text{ J}/\text{mm}^2$. Including RSF in the concrete results in a less significant increase in the fracture energy compared to ISF, with values of 5.42, 10.26, and $12.63 \text{ J}/\text{mm}^2$ at fibre levels of 0.4%, 0.8%, and 1.2%, respectively.

The differing effects of ISF and RSF on the enhancement of concrete's flexural strength are attributed to the various ways in which they amplify the material's capacity to absorb point load-induced fractures (or fracture energy). This difference arises from how the two types of SF respond to and make losing strength, instead of just focusing on the initial stage. The

improvement of the flexural strength of concrete mainly results from the interaction between the fibres and the concrete as it relates to different phases of the material's development. In the initial cracking stage, fibres increase the flexural strength of concrete due to the friction they establish with the concrete matrix, which is especially notable in the micro-cracking stage. As the concrete matrix starts to form significant fractures and experiences a reduction in flexural strength, the role played by the fibres changes. Following the formation of substantial fractures and the loss of strength, the fibres begin to pull out, and the ability of the hooked ends to anchor becomes critical [112].




The fracture energy of the sample can be determined from the graph, which depicts the area under the curve up to the X-axis[113], and compared to the ISF. The initial behaviour of ISF overlaps with that of the RSF until the LOP (least order point) is reached. The difference in the post-peak behaviour, particularly in residual strength progression, distinguishes the two types of fibre concrete. RSF's inferior post-peak performance is ascribed to the reduced strength of their hooked ends. RSF is subject to further processing and shows signs of extended fatigue, resulting in naturally weaker hooks. Despite the minor difference between RSF and ISF at lower fiber amounts due to the weak hooks' limited capacity, the difference is more pronounced at increased fibre proportions. The ISF, with its durable extended hooks, offers substantial strength benefits that the RSF cannot match. Consequently, the gap in fracture energy between RSF and ISF widens because of the weakened integrity of RSF hooks in the post-cracking phase.



3.3.4 Failure Mode Analysis

Table 3-5 shows a number of crack patterns noticed in different specimens after stretching trials, with most of the samples showing a solitary crack originating from the precut notches. Furthermore, most specimens do not undergo complete fracturing even after a 4-millimeter deformation, indicating that fibres have a resilient response under serious harm levels. As the fibre content expands, the beam's method of breakdown changes to become more durable. For example, beams with 1.2% of RSF and ISF may have surface failure under the bridge effect, but they still keep a specific residual pressure. This suggests that integrating steel fibres enhances structural reliability.

Both RSF and ISF materials show an effective bonding action when their performance is compared. Hence, there is not much difference between them just by the rupture mode. On the other hand, in terms of the load-deflection curves and breaking mode, it was observed that the bonding effect provided by ISFs is better at higher fibre contents and after completion of cracking. At the same time, it does not make much difference at less than 0.8% fibre content, with almost no separation between them at a 0.4% fibre content level

Table 3-5 Failure mode of RSF and ISF concrete

	Failure model	Analysis
M1-ISF		Like PC, the main cracks develop at the notch, but the cracks also show the onset of fibres bridging
M2-ISF		The primary crack was notably slower to appear in the cement beam containing 0.8% of fibers compared to the one which had 0.4% of fibre content.
M3-ISF		Compared to the concrete beam with an 0.8% fibre content, there are vast micro-cracks around the main cracks. And the micro-cracks appear in tandem with the continuous development of the main cracks. In addition, the concrete

Failure model	Analysis
M1-RSF	floor spalls as micro-cracks increase.
	Similar crack progression as the reinforced concrete beams with 0.4% ISF
M2-RSF	The main crack didn't form quickly in comparison to the concrete beam with 0.4% RSF. Because of the small cracks surrounding the main cracks, the main cracks finally appeared.
	

Failure model	Analysis
<p data-bbox="255 507 353 539">M3-RSF</p> 	<p data-bbox="1144 467 2000 665">Many micro-cracks, similar to those in the case with ISF containing 0.8%, appeared next to the primary cracks in the concrete beam that included 0.8% fibre content.</p>

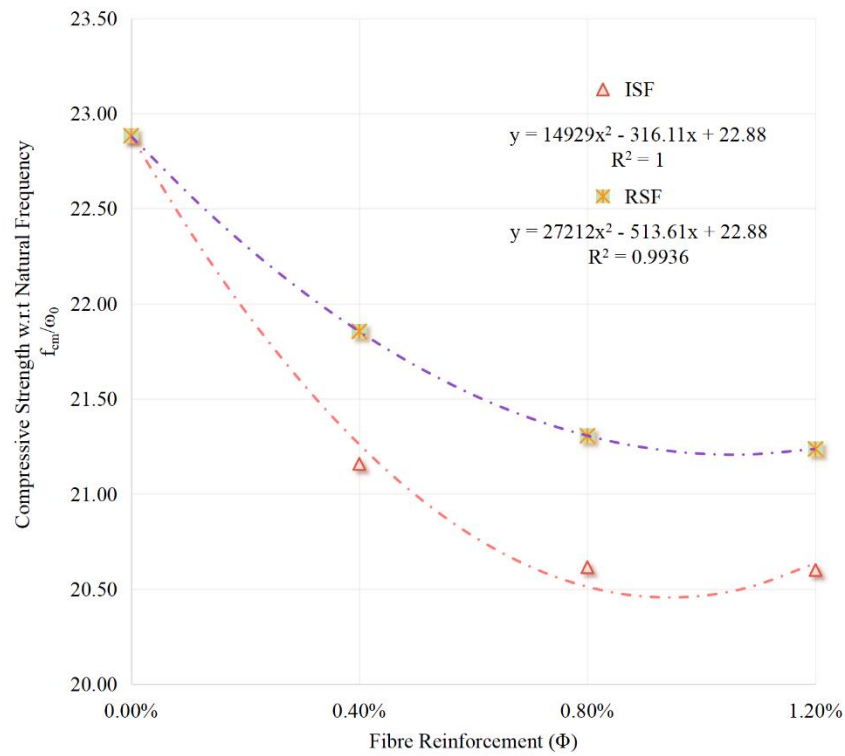
3.4 Dynamic Properties

The dynamic properties of RSFRC and ISFRC can be observed in **Table 3-6**. Adding fibres to the concrete mix would mean changes to its fundamental characteristics, which would ultimately affect its natural frequencies and mechanics. Since adding fibres to the concrete mix can result in it being stiffer, which would allow it to bear more dynamic loads, studies indicate that it can also assist the concrete in becoming more resistant to dynamic loads by increasing its natural frequency. It is quite transparent that increasing the fibre content in the mix improves the dynamic modulus of elasticity, which is critical in making it more resilient to dynamic loads. Unlike ISF, RSF has a higher sensitivity to natural frequency. For example, increasing the fibre content in M1-RSF to 1.2% increased the natural frequency to 1385.9 Hz. Furthermore, there is no big change in the damping ratio as a result of adding fibre. Additionally, the trend shows a greater sensitivity in the case of RSF than ISF, with the natural frequency's growth rate increasing faster as RSF content rises. These differences will affect the comparison between RSF and ISF.

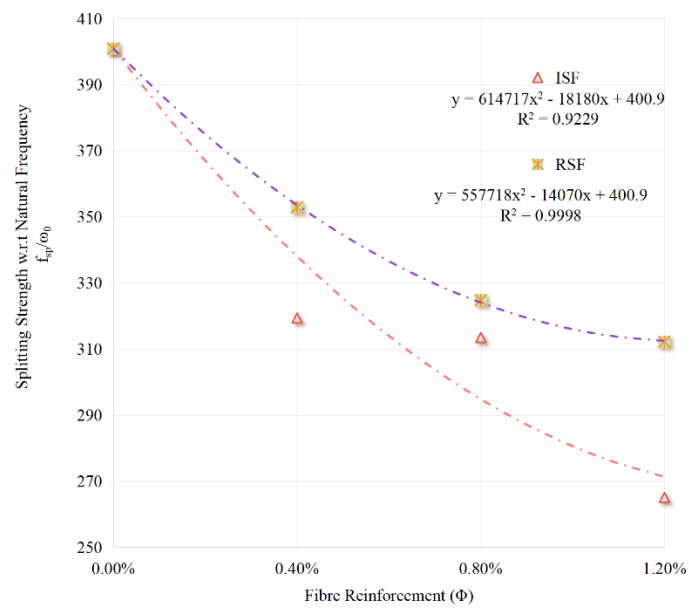
The impact of adding fibres to concrete structures on natural frequency and damping ratio is highly relevant because it depends on the structural system's stiffness and the rate of energy dissipation within the system. [114]. When fibres are mixed with concrete, structural stiffness and natural frequency increase due to the tight connection between them. Damping ratio, which measures energy release in the system, typically stays constant in systems with minimal flaws or adequate internal consistency [115]. This could be attributed to the fact that the commonly stable damping ratio is influenced by mechanisms that generate energy release within the system, which are mostly unsympathetic to the fibre addition. In contrast, the presence of flaws

or deterioration in the system allowing energy to be released could lead to an increase in the damping ratio. Despite this, the effect of adding fibers to concrete structures is generally trivial when it comes to the damping ratio because that relies heavily on the structural integrity and internal properties of the system. To summarize, adding fibers to concrete structures can augment stiffness and potentially influence natural frequency, but the impact on the damping ratio, especially in undamaged structures, is typically minimal.

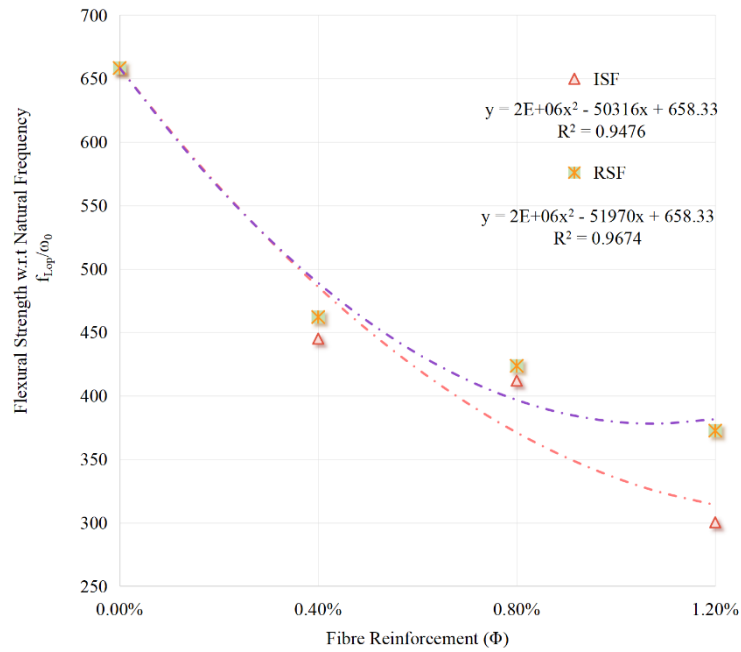
Modal testing offers insights regarding the fundamental structural properties of concrete. This test can be integrated with the SFRC properties to offer a comprehensive picture of the significant relationship between dynamic characteristics and mechanical properties. Analysing **Figure 3-6**, which indicates the potential relationship between mechanical and dynamic properties, indicates that there is an intense relationship between the natural frequency, compressive strength, splitting tensile strength, and flexural strength of the concrete. The R-squared values for these relationships stay high, typically exceeding 0.98. This high correlation implies that the dynamic properties like natural frequency derived from the modal test can indicate and be affected by the mechanical features of the concrete. Therefore, the modal test can evaluate the structural integrity and provide valuable insights into the performance and mechanical properties of SFRC in various construction conditions.



(A) Correlation model of f_{cm}/ω_0 with fiber content



(B) Correlation model of f_{sp}/ω_0 with fiber content



(C) Correlation model of f_{lop}/ω_0 with fiber content

Figure 3-6 Correlation models

Table 3-6 Results of dynamic properties

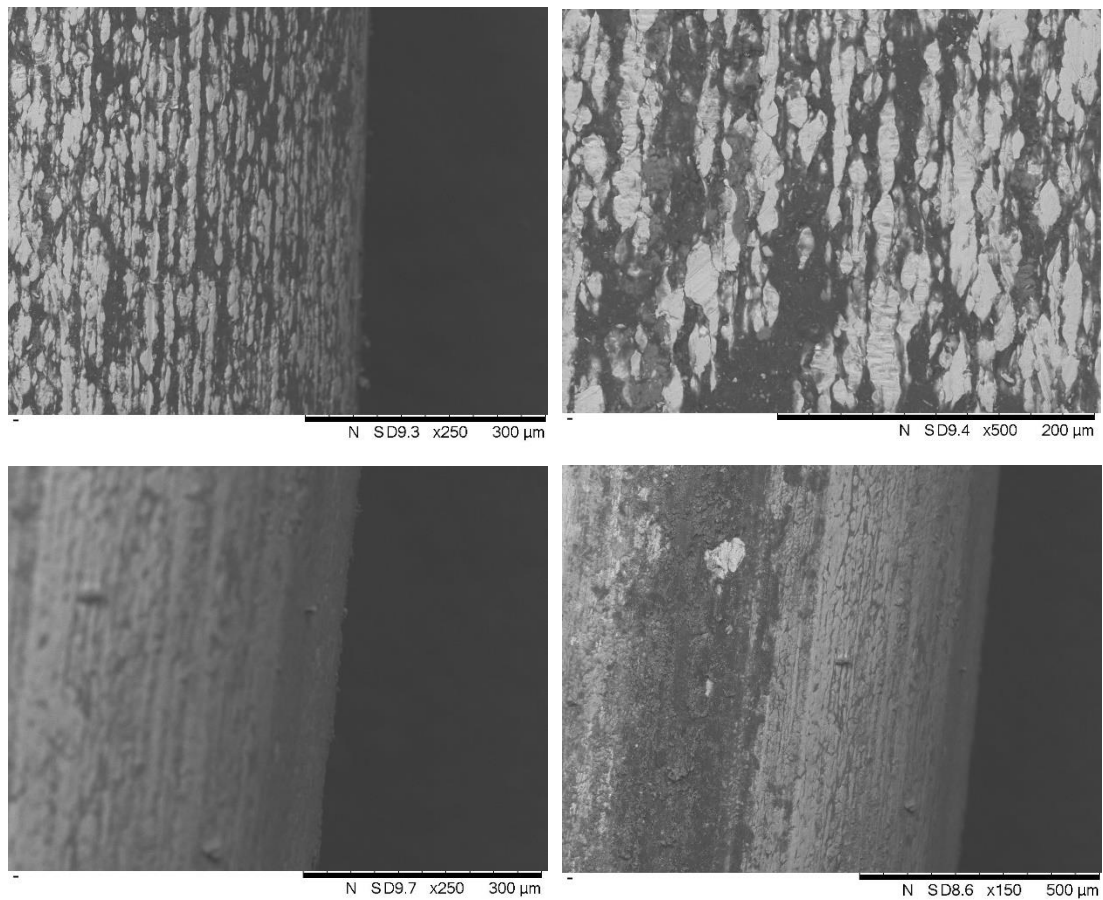
Group	Properties	Natural	Damping	Dynamic Young
	Weight (Kg)	Frequency (Hz)	Ratio (%)	Modulus (GPa)
M0	32.84	1343	0.97	20.48
M1-ISF	32.23	1357.3	0.92	20.55
M2-ISF	32.47	1363.5	1.1	21.26
M3_ISF	33.23	1378.2	0.97	21.82
M1-RSF	31.975	1358.5	0.83	20.36
M2-RSF	32.815	1376.8	0.82	21.08
M3-RSF	33.105	1385.9	0.99	21.74

3.5 Microstructural Analysis

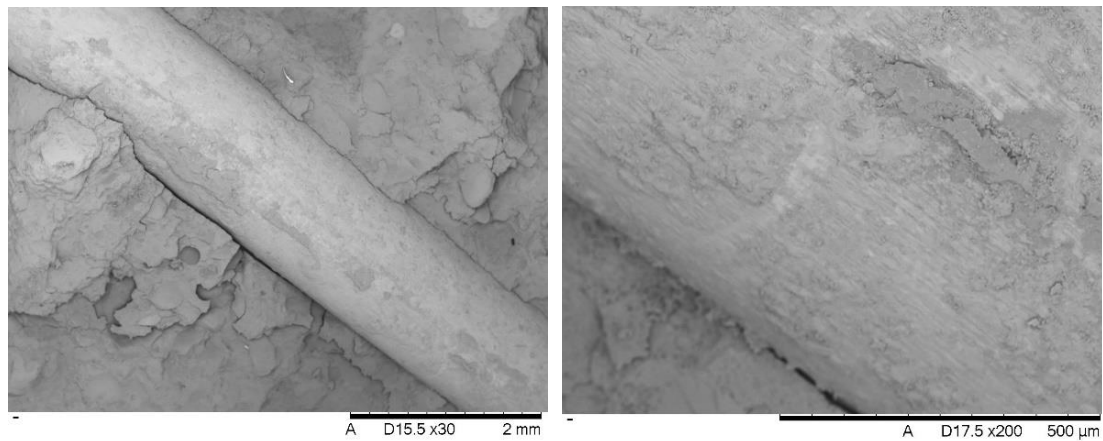
Based on the microstructural analysis using SEM of ISFRC and RSFRC mixtures, the examination focuses on three main components: cement paste, aggregate, and the ISF or RSF. According to **Figure 3-7(A)**, which compares the surface details of ISF and RSF, ISF exhibits a rougher surface texture compared to RSF. Conversely, RSF displays a smoother surface texture, although it appears darker due to a coating of rubber dust rather than having a bright metal colour. Figures **3-7(B)** and **3-7(C)** provide insights into the internal structure of RSF and ISFRC. Figure **3-7(B)** shows that the surface of ISF wires is uniform after being pulled out from the mortar, with visible regular cracks that occurred during the steel wire production stage. Additionally, there are traces of slurry cement residue visible in the surface pits, indicating a high calcium content tarnish. In contrast, RSF wires exhibit a smoother surface compared to ISF wires. This difference may suggest variations in production technology or the application of protective coatings during manufacturing.

Based on Figure 3-7(C), the SEM analysis reveals that RSF are partly coated with cement paste despite their smooth surfaces. This cement paste coating indicates a bond between the cement paste and RSF, although it may not be perfectly bonded due to potential slippage issues observed with ISF. The increased flexural and splitting tensile strengths observed with RSF further support their contribution to bond strength in concrete. However, the rougher surface texture of ISF limits the coverage of the concrete matrix by cement paste. The greater cement paste coverage on RSF is primarily attributed to the presence of rubber dust and carbon black on their surfaces. These materials, while aiding in cement encapsulation, do not necessarily enhance the bonding degree between and cement. In fact, ref[116], nanoscale particles like

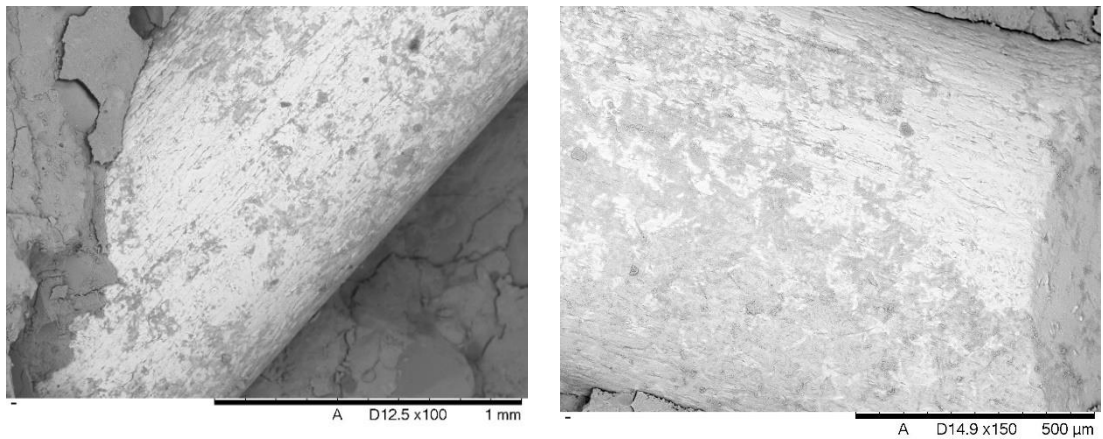
carbon black and rubber can absorb significant amounts of water, thereby hindering the hydration reaction and potentially reducing the effectiveness of cement bonding [117]. This phenomenon, as highlighted by ref[118], suggests that the involvement of rubber particles can diminish the mechanical advantages typically associated with fibre reinforcement in concrete.



(A) Surface of RSF and ISF



(B) Micro-structure of RSF concrete



(C) Micro-structure of ISF concrete

Figure 3-7 Microstructure analysis

3.6 Conclusion Remark

This research examines the benefits and drawbacks of substituting RSF for ISF in SFRC with a series of laboratory tests. It aims to investigate RSFs as a possible substitute in ISF concrete by creating seven RSF concrete mixtures with varying substitution rates and subjecting them to numerous experimental assessments such as criteria for mechanical and dynamic tests. By comparing RSF concrete and ISF concrete, including their microstructures, the study concludes that RSF concrete enhances mechanical and dynamic properties when RSF content is below

0.8%. For example, substituting 1.2% RSF enhance compressive, tensile and flexural strengths by 11.2%, 32.5%, and 82.3% over PC. However, RSF is less effective than ISF in improving residual stress following the manufacturing process, and its hook ends deteriorate quickly due to fatigue problems, reducing their ability to impede large cracks and thus harming the concrete's strength. Concrete's natural frequency increased slightly when RSF content was raised, including a 3.19% increase to 1385.9 Hz with 1.2% RSF, compared to standard concrete's 1343.0 Hz. ISF concrete also showed a 2.62% rise when its fibre concentration was raised to 1.2%, with similar behaviour. Based on the results, this study may infer a robust link (R^2 over 0.97) between dynamic performance and mechanical attributes, which should help evaluate structures and assure excellent dynamic performance over time. Studies have shown that RSF can be used as an alternative to ISF in SFRC, and RSFs with an optimal percentage of 1.2% RSF can be better balanced in terms of many of the same benefits and goals as ISFs. The use of RSF concrete improves the economic performance without possessing a significant hazard regarding bearing capacity.

However, RSF exhibit some limitations compared to ISF, such as reduced effectiveness in improving residual stress and lower resistance to fatigue damage. The next chapter will build upon these findings by evaluating the shear capacity of RSF and ISF in large-scale structural beams. This investigation aims to determine whether RSF and ISF offer comparable structural performance and effectiveness in larger beam applications. By examining their behaviour under shear loading, which aims to seek to further understand their practical implications and potential advantages in structural engineering.

4. Shear Capacity Experiments with Large Scale Beams

4.1 Background

Prior research indicates that reinforcing concrete with synthetic short fibres will help enhance concrete's innate durability and reduce the risk of ductile and low tensile capacity by strengthening stress transmission from the fibre to the paste matrix [119]. As a result of these enhancements, this extra increases the concrete's capacity to halt unnecessary paste crack development, which will stop something from happening [120]. Studies have demonstrated that supplementing concrete with ISF can increase its basic strength, reduce the likelihood of brittleness, and improve tensile capacity. This is due to enhanced stress transfer performance, as indicated in trials, in which infusing synthetic fibres into reinforced concrete beams boosted ductile properties and shear capacity while delaying aging cracks in the infrastructure [121]. The mix design includes a small amount of ISF to offer effective shear resistance and steer clear of a shear failure method. For instance, as mentioned in ref [122], fibre addition helped avert shear failure. These fibre characteristics foster the potential of the bridging system to avert shear failure: fibre type, the bond between the cementitious matrix and the fibre, fibre composition, fibre dimensions. In addition, conventional theoretical formulations do not adequately explain the behaviour of randomly distributed fibres. As a result, prior studies [123, 124] have investigated significantly improved structures with SFRC beams based on key factors that predict shear strength and highlight the benefits of randomly adding ISF.

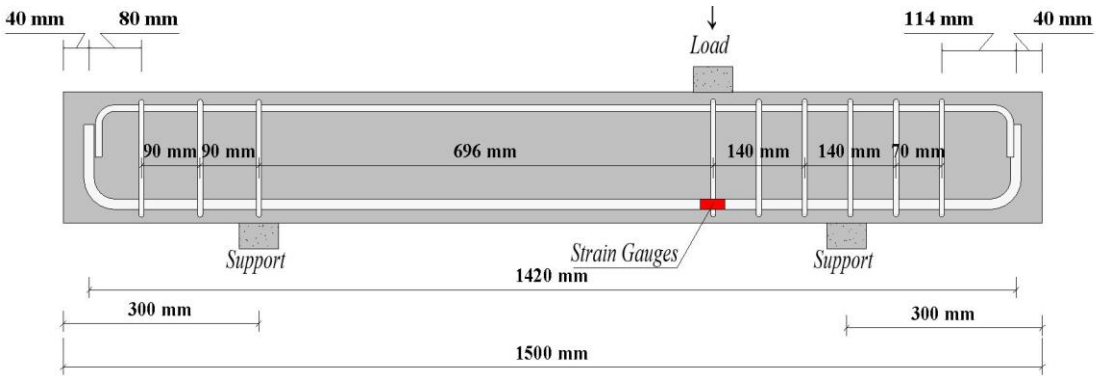
TR63 is a standard developed from Eurocode 2 that suggests using experimental data from CMOD tests to predict the tensile strength of SFRC using straightforward presumptions. However, this approach does not cover the combined effects of the three entities: composite interaction between concrete, fibre, and rebar, high strength of concrete, as well as shear span ratios. This also suggests that the synergy between different entities is not well-explicated. Additionally, the standard has not considered the rebar ratio, the width of the section, and the concrete strength, which all impact the shear capacity computation.

Existing literature has primarily focused on integrating ISF into normal strength concrete (NSC) to examine various beam shear properties in ISFRC. However, upon scrutinizing TR 63 and Eurocode 2, which were primarily formulated for NSC applications, the research community found these protocols unsuitable for studying the growing interplay between concrete and fibre in high-strength concretes (HSC). Moreover, these standards were not designed to help engineers understand changes in beam failure modes and shear capacity attributable to varying shear spans, an absence most noticeable in TR 63. Furthermore, no prior studies have delved into how RSF can boost shear capacity in SFRC. To address these shortcomings, researchers will investigate the impact of shear span and RSF and ISF in HSFRC beams without stirrups to gain insights into shear failure. This will entail conducting 20 shear tests with distinct shear span ratios to study parameters such as shear resistance capacity, strain distribution along longitudinal rebar, crack propagation, ductility, and failure patterns. The experimental measurements will be juxtaposed with predictions from various design methods and standards. There will also be suggestions for predictive formulas informed by experimental findings. The study will also investigate the above parameters using RSFRC in order to formulate design methods that account for the complex interactions between fibres and concrete in HSC. The aforementioned parameters will be studied based on the experimental results of ISFRC and RSFRC beams. Predictions will also be made considering various models and formulas noted in the TR63 and Eurocode 2.

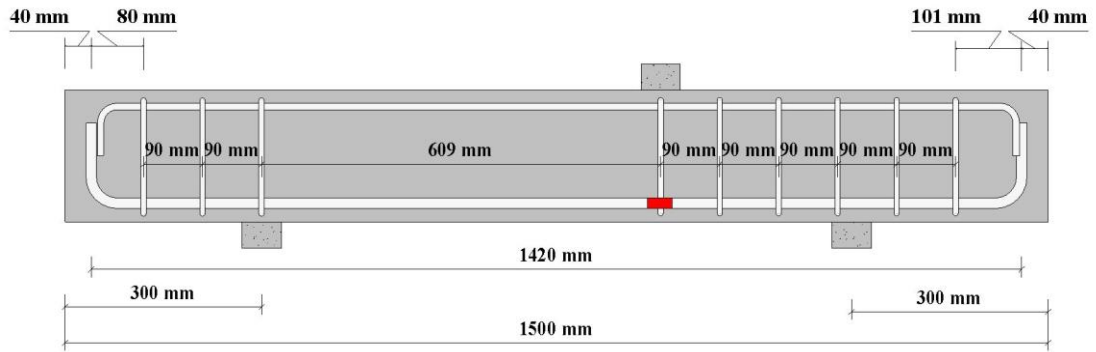
4.2 Experimental Programmes

4.2.1 Test Specimen and Setup

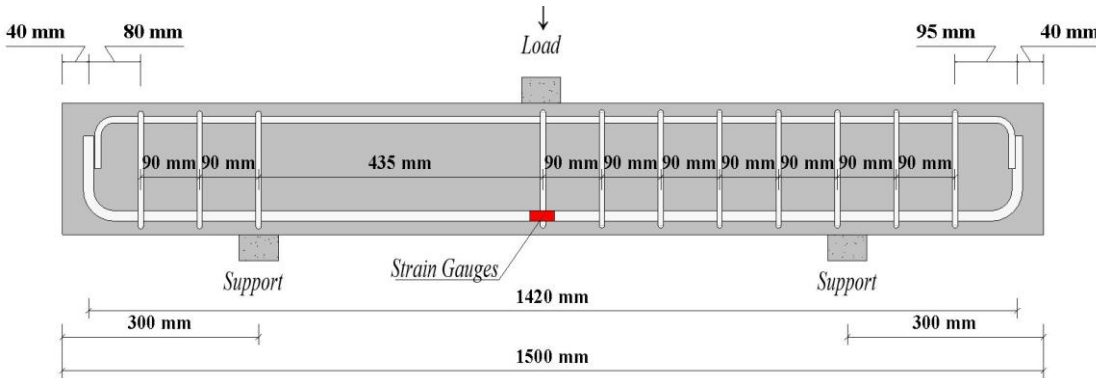
A testing speed of 0.5 MPa/s was utilized. The schematic diagrams of the beam cross-section and its reinforcements were highlighted in Figure 4-1. Appropriate beams were put through a three-point loading test to induce failure. A 500 kN capacity hydraulic machine was used for the three-point loading test. The test was controlled for deflection with 0.1mm/s. Laser displacement monitor was put under the loading points to measure vertical deflection.



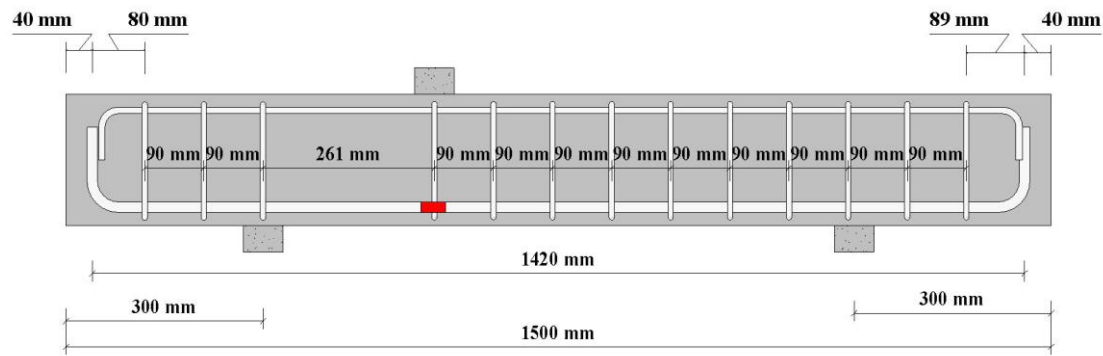
(a) Shear span ratio of 4



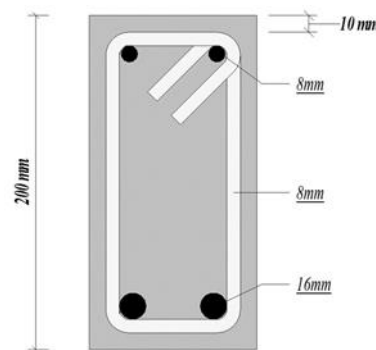
(b) Shear span ratio of 3.5



(c) Shear span ratio of 2.5



(d) Shear span ratio of 1.5



(e) Cross section

Figure 4-1 Experimental beam dimension

To clarify, the bottom longitudinal reinforcement of the beams incorporates two Ø16 mm rods, while the top reinforcement consists of two Ø8 mm rods. Both the top and bottom reinforcements are layered into one. The bottom reinforcement has a concrete covering of 10mm. The information about the beam samples is represented in **Table 4-1**. The ambition of the study is to investigate shear behaviour for ISFRC and RSFRC beams with no stirrups.

4.3 Results Analysis of Shear Capacity

4.3.1 Shear Strength Test

This chapter focuses on the ISF and RSF impact on cracking and shear improvement of 20 reinforced concrete beams built without stirrups. The beams were constructed using different types and volume fractions of fibre, including 0%, 0.4%, and 0.8%. **Table 4-1** summarizes the experimental results, where P_u and Δ_u represent the ultimate shear force and the corresponding deflection at mid-span. Also, τ_u and ϵ_u denote the ultimate shear capacity and the surface strain

of the longitudinal bars at mid-span. %u and %P indicate the ultimate shear capacity and the related displacement improvement ratio relative to plain concrete beams, respectively.

Table 4-1 Results of shear strength test

Beam	P _u	Δu	ε _u	%u	%P	V _{cr}
M0-1.5	86.65	6.21	1037.5	-	-	3.54
M0-2.5	45.86	3.41	926.47	-	-	1.36
M0-3.5	84.58	5.16	1469.76	-	-	1.57
M0-4	119.78	7.94	1663.98	-	-	1.56
M1- ISF-1.5	100.8	7.41	1537.2	16.33%	19.32%	4.11
M1-ISF-2.5	77.67	5.59	1639.09	69.36%	63.93%	2.31
M1- ISF-3.5	110.28	6.86	1394.77	30.39%	32.95%	2.05
M1- ISF-4	186.51	8.09	1845.83	55.71%	1.89%	2.43
M2- ISF-1.5	129.92	7.889	1823.6	49.94%	27.04%	5.30
M2- ISF-2.5	101.09	5.87	1645.47	120.43%	72.14%	3.00
M2- ISF-3.5	126.16	7.60	1737.7	49.16%	47.29%	2.34
M2- ISF-4	235.42	9.05	7.59	96.54%	13.98%	3.07
M1- RSF-1.5	93.94	7.17	1180.3	8.41%	15.46%	3.83
M1-RSF-2.5	64.60	3.84	1110.22	40.86%	12.61%	1.92
M1- RSF-3.5	109.49	5.44	1574.42	29.45%	5.43%	2.03

M1- RSF-4	150.74	9.67	1362.46	25.85%	21.79%	1.96
M2- RSF-1.5	118.07	8.10	1322.8	36.26%	30.43%	4.82
M2- RSF-2.5	78.42	5.59	1289.98	71.00%	63.93%	2.33
M2- RSF-3.5	121.67	6.85	1577.79	43.85%	32.75%	2.26
M2- RSF-4	200.09	9.61	2796.47	67.05%	21.03%	2.61

4.4 Loading and Displacement Analysis

In this research, load versus mid-span deflection curves for various beam specimens have been divided into several sub-classes in Figures 4-2 to 4-5 based on the relevant researched variables. Stiffness within the beam's elastic range was established using the load-displacement curves from experimental data.

According to the data depicted in **Figure 4-2**, the shear span ratio of 1.5 reinforced beams with various fibres demonstrate improvements in stiffness and load-carrying capacity compared to control beams that are not supplemented with fibres. The experiments illustrate that introducing ISF and RSF substantially increases the beams' capacity to resist shear forces. However, incorporating ISF or RSF materials in the concrete mix can boost the structural capacity to a different degree. Specifically, when RSF constitutes 0.8% of the fibre by volume, the load-carrying capacity of the beams jumps by 36.26% compared to the control beams. This improvement is strong but lower than that observed due to the combination of ISF. The load-carrying capacity of the concrete beams increases by 49.94% when the fibre rebars constitute 0.8% by volume in level beams. Experience reveals that incorporating fibres in a concrete composite, whether ISF or RSF, enhances its ability to resist shear forces in the composite material. However, the rate of enhancement was not significantly different between the two types of fibre. It is noted that the limited surface area available for reinforcing fibres in

traditional beams containing a shear span ratio of 1.5 may be a significant factor limiting the reinforcement effects of fibres. In such instances, the performance of fibre-reinforced composite beams with a lower shear span ratio is likely not as impressive as those containing fibre in the mix, regardless of the type of fibre.

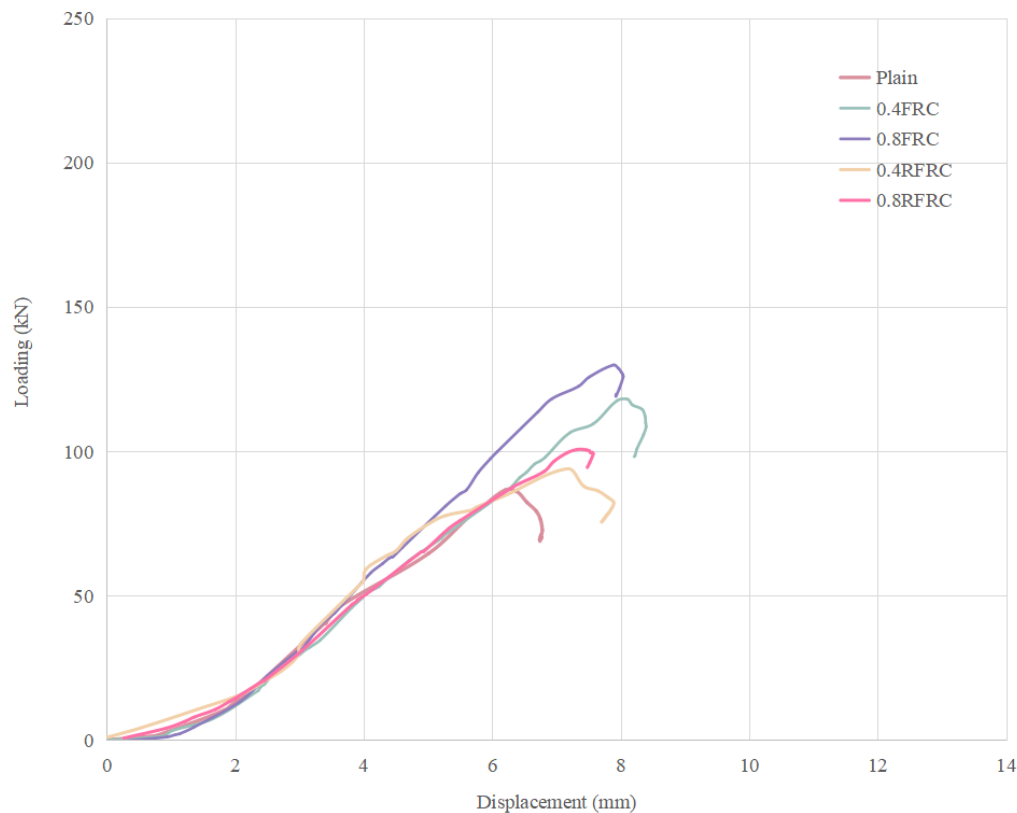


Figure 4-2 Shear span of 1.5 (Group I beams)

The investigation of Group II into the shear strength of SFRC beams with a span ratio of 2.5, specifically the control sample M0-2.5 which failed in shear, established that the specimen developed shear cracks at midspan when a load (P) of 40 kN was applied, with the majority of the cracks forming perpendicular to the load application point and the support. In addition, the stiffness of the beam progressively decreased as the number of cracks rose. M1-ISF-2.5 reached a maximum strength of 77.67 kN at a deflection (δ) of 5.59 mm, after which it began to fail dramatically. Ultimately, the load-bearing capacity increased by 220.6% with 0.8% ISF content and 171.3% with 0.8% RSF content compared to the peak strength. When compared to the control sample, the shear capacities of the M1-ISF-2.5 and M1-RSF-2.5 increased by around

120.43% and 71.00%, correspondingly.

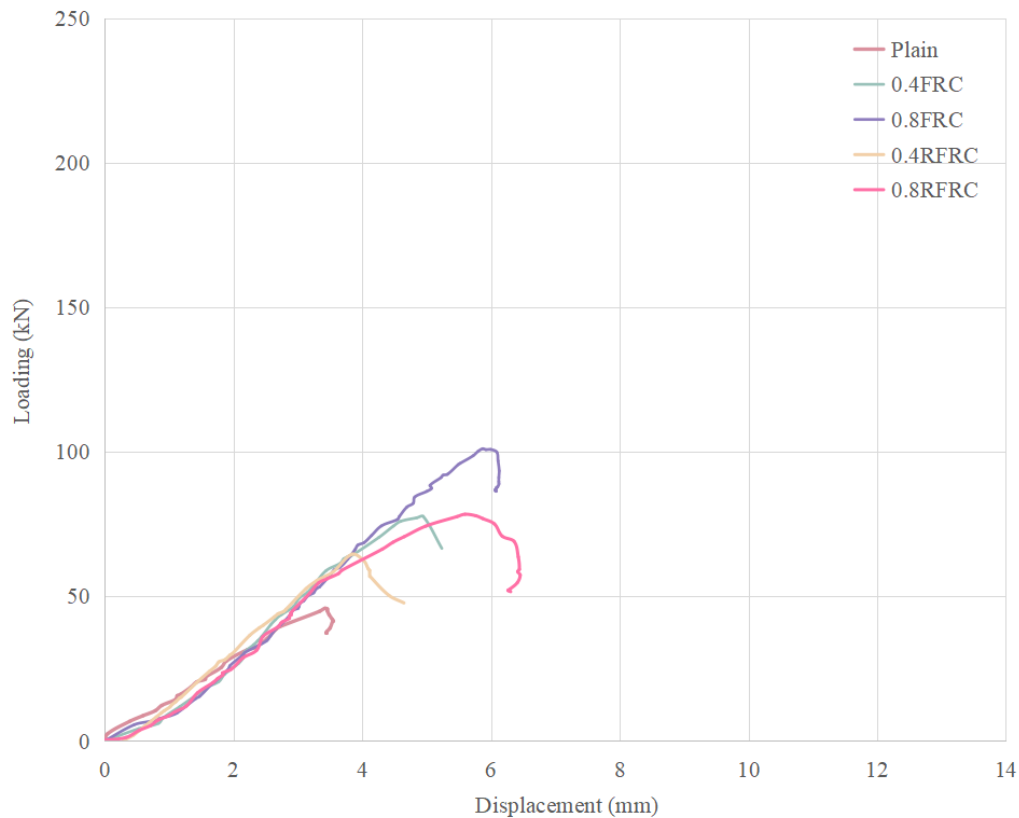


Figure 4-3 Shear span of 2.5 (Group II)

The deviation of the load-deflection curve from the initial stiffness curve at the cracking point emphasizes the cracking load in Groups IV and III, particularly in beams with a shear span ratio of 4. The stiffness of SFRC concrete beams changes gradually with the addition of fibres, indicating that steel fibres produce more significant bridging effects as the shear span-to-effective depth ratio increases. As a result, compared to the control beam, the shear capacity improvements for Group IV's beams M1-ISF-3.5, M2-ISF-3.5, M1-RSF-3.5, and M2-RSF-3.5 are 30.39%, 49.16%, 29.45%, and 43.85%, respectively. Beam displacements were severely enhanced at maximum shear capacity for Group IV beams with added steel fibres because of their high shear span-to-effective depth ratios. Beams that included steel fibres had shear capacity improvements of 55.71%, 96.54%, 25.85%, and 67.05%, respectively. Compared to beam M0-4, the M1-ISF-4 beams demonstrated a 1.89% deflection increase, the M2-ISF-4 beams a 13.98% increase, the M1-RSF-4 beams a 23.43% increase, and the M2-RSF-4 beams

a 22.19% increase.

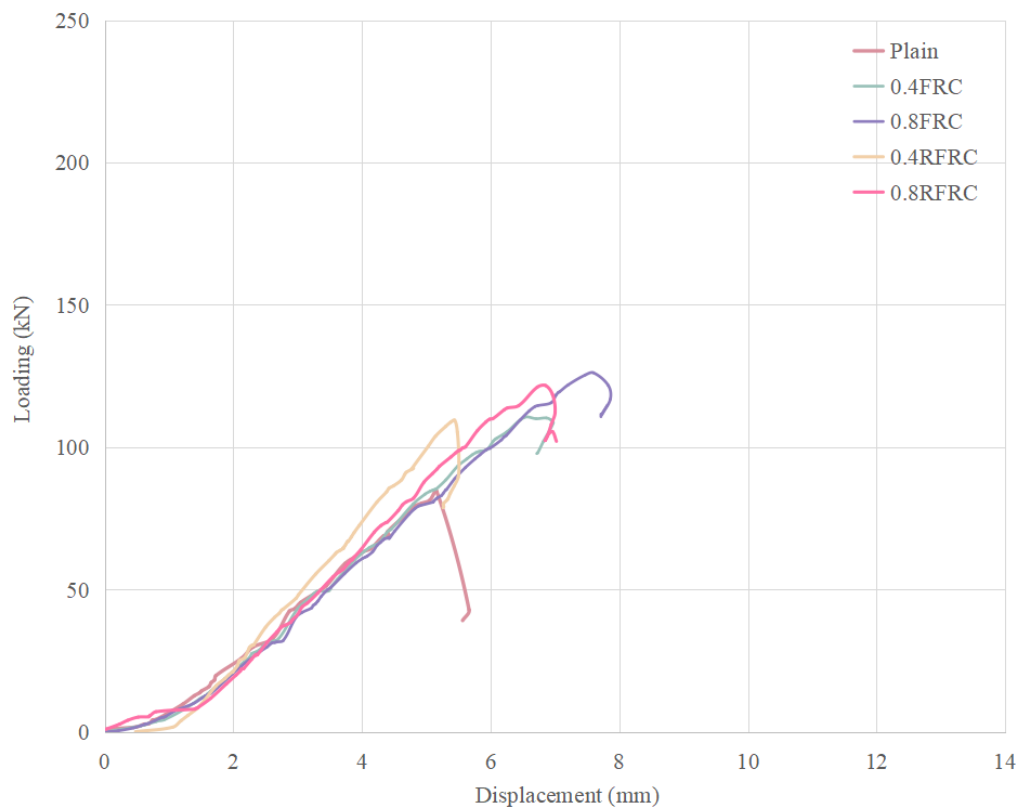


Figure 4-4 Shear span of 3.5 (Group III)

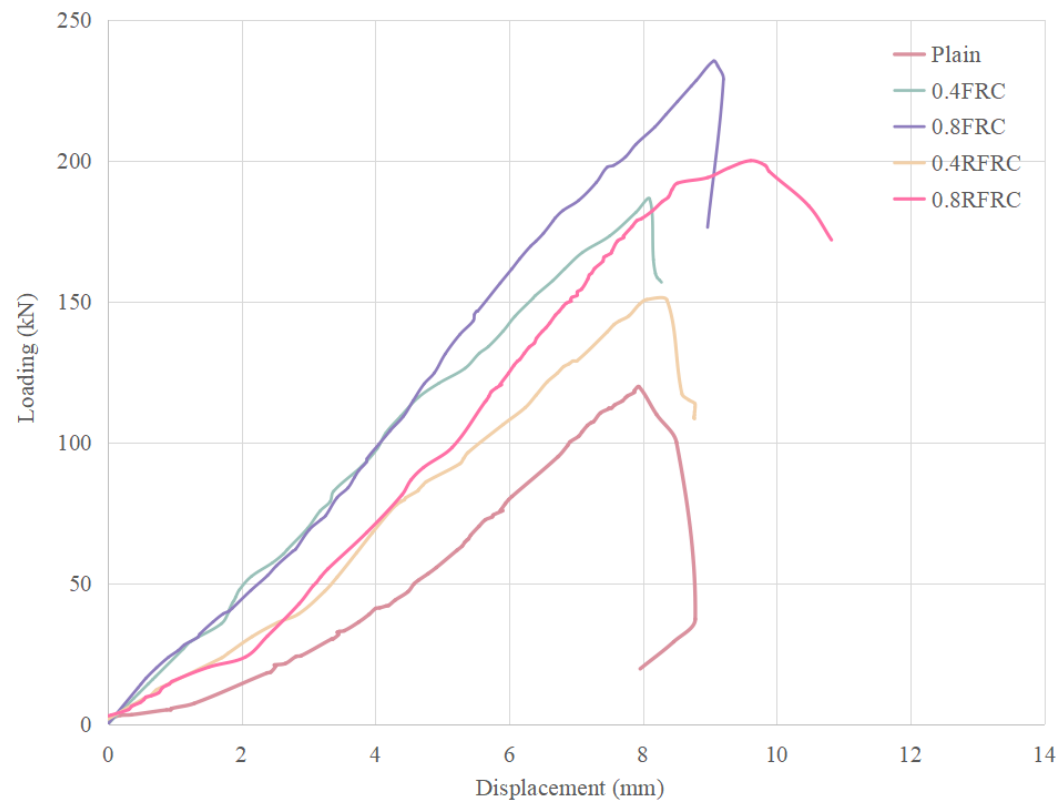


Figure 4-5 Shear span of 4 (Group IV)

The whole load-deflection curve evaluation can be broken down into several stages: shear cracking, shearing load growth, and drop-down stages. The first phase involves forming the initial curve, during which fiber's bridging influence is minor. Typically, all beams behave almost linearly. As the load increases toward its maximum, the fiber proportion, loading rate, and related deflection rise. Additionally, with an increasing shear span ratio, the performance differences between the control and RSF and ISF-reinforced samples in terms of maximum load and deflection in all figures become more distinct. It's worth noting that RSF beams' load-deflection response at the midspan is almost identical to ISFRC beams with an equivalent fiber concrete content, implying that RSFRC beams with the same fiber content exhibit similar macro-mechanical qualities as ISFRC beams. All the beams experience a brittle shear failure, but the decline in the load-deflection curve for the ISF- and RSF-reinforced beams isn't immediately sharp. It's vital to point out that when the shear span ratio is 4 in the SFRC beams, the load grows as it approaches the maximum capacity with a more significant deflection. Also, this implies that a greater shear span-to-depth ratio can offer early warnings with more significant deformation, which might mean more energy dissipation as the load approaches its peak.

The improvement in shear strength has been especially remarkable within a narrow range from 1.5 to 2.5 in the ratio of shear span. Even though beams strengthened with steel fiber are theoretically equally effective for shear resistance, those strengthened with ISF can achieve marginally better shear resistance compared to RSFRC beams. As one might anticipate, the shear resistance upgraded by steel fiber rises in a linear fashion in line with the increased fiber content. However, there is no significant increase in shear resistance as the ratio of shear span to depth increases from 2.5 to 4. To put it simply, the shear resistance is significantly influenced by both the ratio of shear span and the content of fiber. Additionally, the effectiveness of RSF and ISF in improving shear resistance is similar when their content is the same.

4.5 The Strain of Longitudinal Reinforcement

The electric resistance strain gauges measured the maximum stress of $1823.6 \mu\epsilon$ applied to the beams in Group I with a shear span ratio of 1.5, as demonstrated in **Figure 4-6** and **Table 4-1** at the point of load application. **Figure 4-6** and **Table 4-1** depict the stress perceived on the steel reinforcement bars at the beam's centre point. The $1823.6 \mu\epsilon$ is the maximum value identified at the application of the load radius to the short span Group I beams. Moreover, the addition of fibres to the longitudinal rebar reinforces the shear resistance, mainly caused by beneficial interactions between the fibre and steel rebar. The introduction of fibres creates a steeper diagonal shear crack profile, enlarging the functional area of the longitudinal rebar. Notably, improved shear capacity does not imply a cooperative link with steel rebars' performance. This primarily relates to RSF's weak hooked finish. Moreover, the production of RSF after waste tire recycling, which results in a soft and weak state and exposes the rebar to severe tire wear, increases the hazard of joint failure due to the fatigue effect after taking the hooked form.

According to **Figure 4-6**, the longitudinal bars showed significant stress increments with higher loading, just as in Group I rebar and RSF beams. There is no surprise that the maximum strain in the rebar did not surpass the ISF bar's ultimate strain in the reinforced concrete beams. The maximum strain recorded as $1,645.47 \mu\epsilon$ for M2-ISF-2.5. In the case of Group III beams with an aspect ratio of 3.5, and Group IV beams with a shear span ratio of 4, the maximum strain in the longitudinal bars of a shear span ratio of 2.5 increased significantly. Such considerable strain increment is plainly observable in a shear span ratio increase.

4.6 Failure Mode Analysis

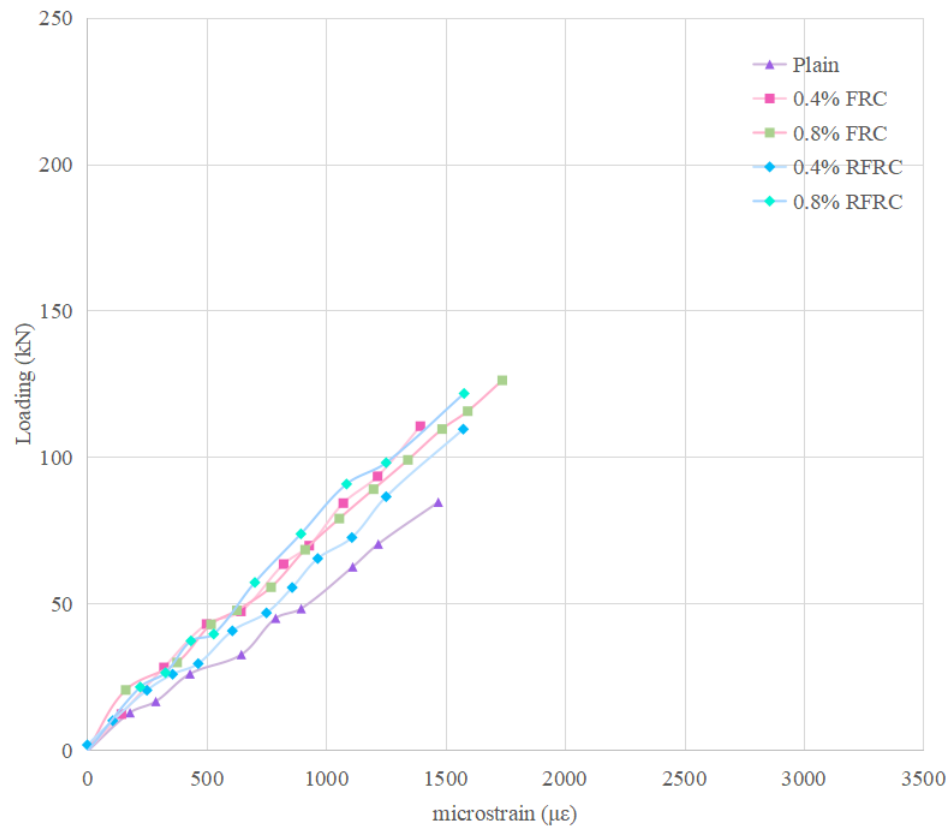
From the cracking patterns observed in the Group I beams during the test, which is provided in **Appendix A-1**, the deep beam failure model is represented by the shear span ratio of 1.5. These results portray the failure mode characterized by a set of inclined cracks in the shear zone obstructing the transfer of horizontal shear from the longitudinal bars into the compression zone.

The resistance mechanism of shear is significantly supported by standard arch action in this scenario, which entails inclined breaks and concrete division contributing to the collapse cycle. The primary crack appears as soon as a heap-induced load is supported by a portion of uncracked concrete. As the load is increased, breaches develop on the shear span zones and expand diagonally towards vital loading areas, at angles between 32 and 40 degrees. Suddenly, the design experiences failure stemming from a single significant shear crack. Differently, B7 and B8, i.e., the beams with 0.4% and 0.8% ISF, develop a major diagonal break thus failing in a shear pattern similar to RSF reinforced beams. The crack distribution is smaller with the fibre incorporation. Moreover, the use of 0.8% ISF and RSF is highly effective in reducing the crack openings due to the fiber's stitching power, which incites tensile tension over the cracks and results in delayed localized crack growth. When the single diagonal crack is developed, the extension of the current cracks becomes more evident as the load increases. Subsequently, these cracks interact, gradually forming a primary crack accountable for the failure.

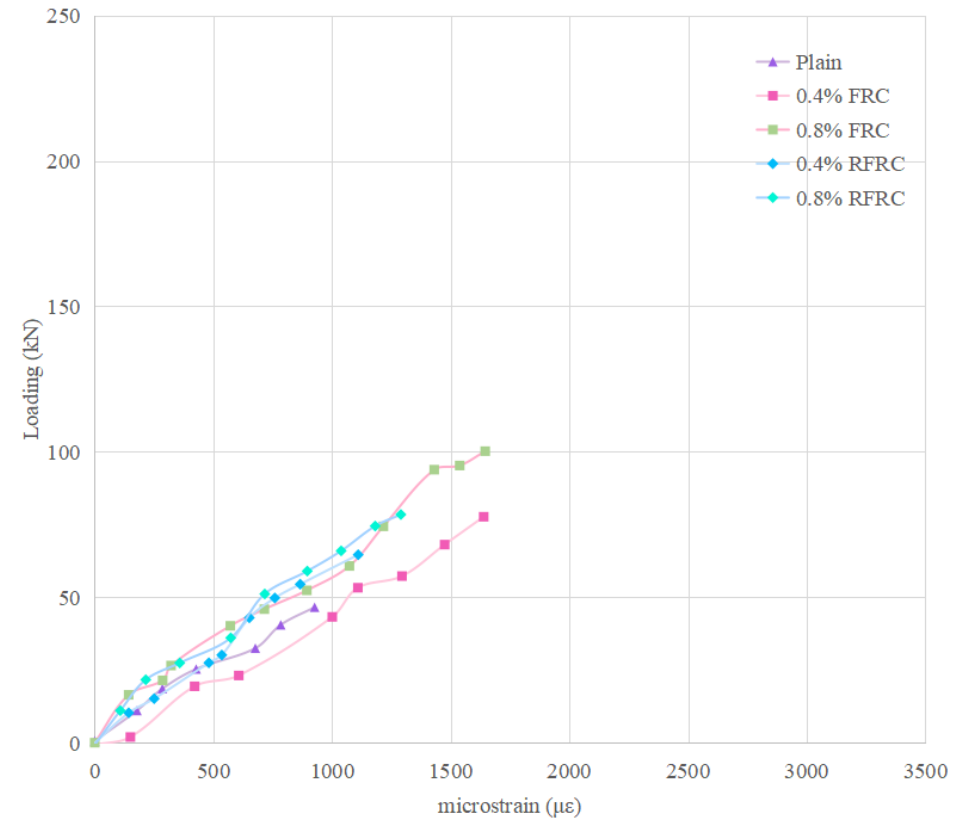
Although Group II beams typically experience a fragile shear failure mechanism, the ones reinforced with steel fibres display more lenient failure compared to the control beams during the experiment. As the shear reinforcement level climbs, the SFRC beams achieved more shear load at an advanced stage due to the resistance to the tensile force by the steel fibres at the crack interface, enhancing the resistance to both cracking and shear. In the specimens with a shear span ratio of 2.5, macro cracks originate on the line connecting the support and loading point when the load reaches the ultimate state. Nonetheless, most of these cracks tend to merge and develop around the primary diagonal crack. The results indicate a minor rise in the number of cracks and a crack width decline, with a significant decrease in the crack angle due to the addition of ISF, in comparison to the Group I beams with a shear span to depth ratio of 1.5. The same pattern happens in beams with RSFRC, which indicates certain crack angles.

As shown in **Appendix A-1**, all of the Group III and Group IV beams broke because of a mix of bending and shear forces. First, diagonal shear fractures typically happen in the core section of the concrete web. As the shear load rises, the width of these cracks widens significantly, and

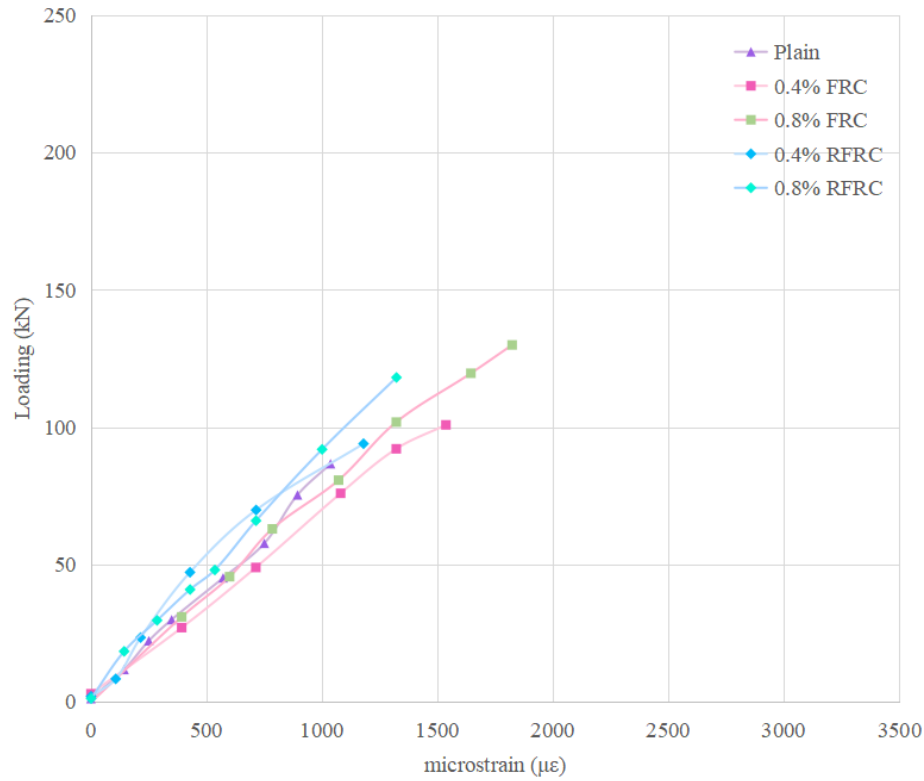
additional cracks happen beside the initial ones. Similar to the Group II beams, the M0-4 examples had a milder failure mode than the M0-2.5 and M0-3.5 ones. This differs from the failures of the Group I beam, where the primary cause of failure was the collapse of the concrete compression strut. The significant rise in shear resistance when the maximum shear span ratio rises from 2 to 4 compared to the maximum shear span ratio of 2 to 3 is attributed to the increased vertical stress that results from the steeper angle of the diagonal shear split, which does not collapse in short shear span reinforced concrete beams and beams with low shear span ratios.



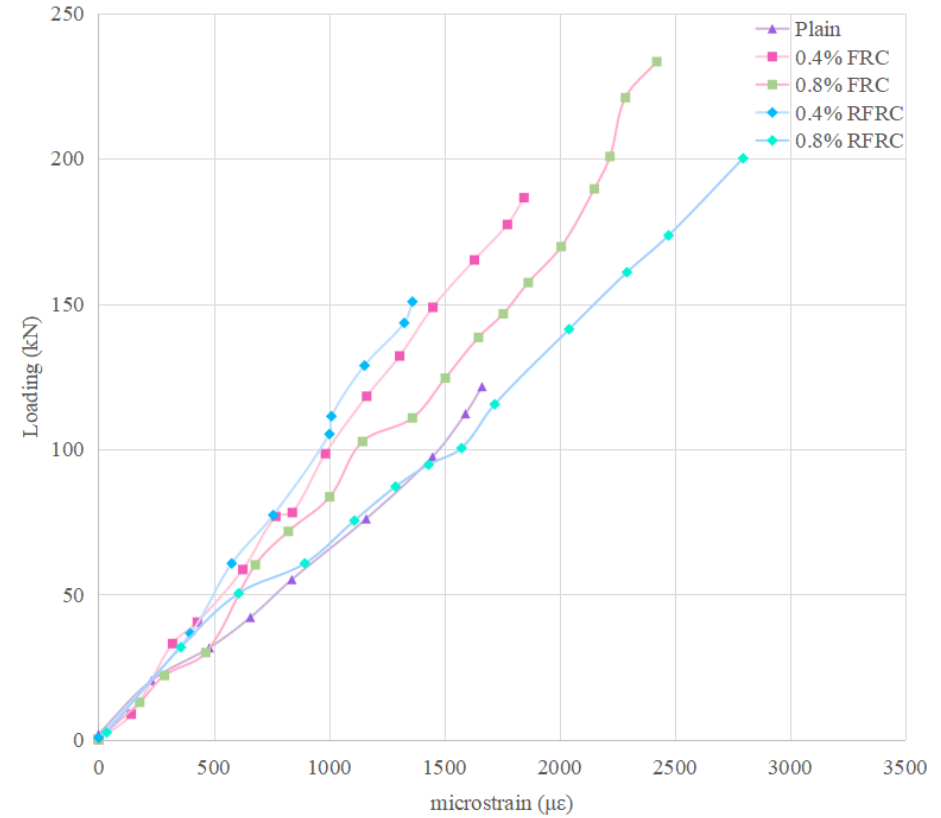
Shear span ratio of 1.5 (Group I)



(b) Shear span ratio of 2.5 (Group II)



(c) Shear span ratio of 3.5 (Group III)



(c) Shear span ratio of 4 (Group IV)

Figure 4-6 Loading strain curve.

5. Modified TR63 Standard

5.1 Existing Formulas Analysis

In SFRC beam structures, the additional fibres have different functional and spatial benefits that assist in optimizing the structure's performance. Several studies found a critical relationship between the shear span ratio and the shear capacity of concrete beams without stirrups. This section presents and summarizes five empirical, analytical, and theoretical shear capacity prediction methods for ISFRC beams from past research. The review suggests that the existing prediction models do not correctly account for the combined effect of ISF and HSC and therefore might be inadequate. Ref [120] highlights that the steel fibres significantly affect the interaction of cement, fibres, and aggregates and thus challenges the accuracy of employing NSC formulas for HSC. **Table 5-1** presents various models from current standards and includes the ISF impact on HSC.

Table 5-1 Review of collected existing formulas

	Formula
Mansur et al.	$V_{frc} = \left(0.16\sqrt{f_{ck}} + 17.2\frac{\rho V_d}{M}\right) \leq 0.29\sqrt{f_{ck}}bd$
Al-Ta'an et al.	$v_{frc} = (1.6\sqrt{f_{ck}} + 960\rho_1\frac{d}{a}e + 8.5\beta V_f\frac{l_f}{d_f})/9$
Khuntia et al.	$v_{frc} = (0.167\alpha + 0.28V_f\frac{l_f}{d_f})\sqrt{f_{ck}}$
Swamy et al.	$v_{frc} = v_c + v_w = 3.75\tau_r + 0.9\sigma_{cu}$
Kara et al.	$v_{frc} = \left(\frac{\rho_1 d}{c_0 c_1 \left(\frac{a}{d}\right)}\right)^3 + \frac{F_1 d^{\frac{1}{4}}}{c_2} + \frac{c_3^{\frac{1}{2}} \sqrt{f_{ck}}}{d^{\frac{1}{2}}}$
	$v_{frc} = \left[\left(2.11\sqrt[3]{f_{ck}} + 7V_f\frac{l_f}{d_f}\right) \left(\rho\frac{d}{a}\right)^{0.333} \right] \text{ for } a/d \geq 2.5$
Ashour et al.	$v_{frc} = \left[\left(2.11\sqrt[3]{f_{ck}} + 7V_f\frac{l_f}{d_f}\right) \left(\rho\frac{d}{a}\right)^{0.333} \right] \left(\frac{2.5}{a}\right) +$ $(0.41\tau V_f\frac{l_f}{d_f})(2.5 - \frac{d}{a}) \text{ for } a/d < 2.5$

* V_{frc} is the shear capacity of fibre reinforced concrete beams; f_{ck} is the compressive strength of fibre reinforced concrete; ρ is the longitudinal ratio; b is the width of concrete beams; d is the depth of concrete beams; V_f is the fibre content and $\frac{l_f}{d_f}$ is the aspect ratio.

5.2 Modify the TR63

Several critical formulation parameters contribute to the compressive strength, longitudinal ratio, fibre content, and aspect ratio. Despite the importance of shear span ratios in previous research, the investigation concerning the shear capacity of SFRC is varied and lacks necessary equations and explanations. Through this research, we aim to explore the impact of the shear span ratio upon the shear capacity of HSFRC beams. We also derive a novel empirical formula to quantify the shear capacity, incorporating the shear span ratio in our research. Said formulae are subsequently confirmed, and adjustments to existing standards are proposed, specifically Eurocode 2 and TR63 recommendations. Such proposals will lead to more comprehensive predictive methodologies for shear strength for the given dataset of beams. Additionally, regression analyses will be conducted using 164 beams selected from previous HSFRC beams studies to improve predictability, which shown in **Appendix A-2**.

5.2.1 RC beams

According to the design standard of TR63 and Eurocode 2, the shear capacity of RC beams should follow **Equation 5-1**:

$$V_{Rd,c} = C_{Rd,d} k (100 \rho_1 f_{ck})^{\frac{1}{3}} \quad (5 - 1)$$

The effect of shear span ratios hasn't been independently verified. Through regression analysis, formulas were developed based on Eurocode 2 and experimental data found in published studies for this development: **Equations 5-2 and 5-2**:

$$V_{Rd.c} = 1.9C_{Rd.c}k\sqrt{100\rho f_{ck}\frac{d}{a}} \quad \frac{a}{d} > 2.5 \quad (5-2)$$

$$V_{Rd.c} = \left[1.9C_{Rd.c}k\sqrt{100\rho f_{ck}\frac{d}{a}} \right] \left(\frac{2.5}{\frac{a}{d}} \right) \quad \frac{a}{d} \leq 2.5 \quad (5-3)$$

where $C_{Rd.c}$ is the $0.18/\gamma_c$; k is the size effect which is $1 + \sqrt{200}/d \leq 2.0$; f_{ck} refers to the compressive strength in MPa, and a/d stands for the shear span ratio.

5.2.2 HSFRC Beams

Most of the investigations considered when deriving the fiber contributions in TR63 did not include residual strength data. Therefore, this thesis selected the pattern proposed by in-source ref [113] to determine the fibre strength in this research.

$$f_{R,4k} = \psi[0.177(f_{ck})^{0.5} + 6.151(RI) + 0.137N^2] \quad (5-4)$$

where $\psi = (1 + \frac{L_f}{100})^{0.5}$ and L_f are the fibre length; RI refers to the fibre factors, and $(V_f L_f / D_f)$ and N stands for the number of hooked ends in steel fibre.

In this study, a regression analysis was conducted and utilized to improve the predictive power of **Equations 5-5 to 5-8**, capturing how different parameters affect HSFRC beam shear capacity with different fibre type. The analysis factored in the shear-span ratio, which was crucial, and tailored the coefficients using available experimental data.

ISFRC beams:

$$V_{Rd.c} = 1.15 C_{Rd.c} k \sqrt{100 \rho f_{ck} \frac{d}{a}} + 5 \frac{f_{R.4}}{\psi \sqrt{f_{ck}}} \left(\rho \frac{d}{a} \right)^{\frac{1}{3}} \quad \frac{a}{d} > 2.5 \quad (5-5)$$

$$V_{Rd.c} = \left(\frac{2.5}{\frac{a}{d}} \right) * \left[C_{Rd.c} k \sqrt{100 \rho f_{ck} \frac{d}{a}} + 5 \frac{f_{R.4}}{\psi \sqrt{f_{ck}}} \left(\rho \frac{d}{a} \right)^{\frac{1}{3}} \right] \quad \frac{a}{d} \leq 2.5 \quad (5-6)$$

RSFRC beams:

$$V_{Rd.c} = 1.15 C_{Rd.c} k \sqrt{100 \rho f_{ck} \frac{d}{a}} + 3 \frac{f_{R.4}}{\psi \sqrt{f_{ck}}} \left(\rho \frac{d}{a} \right)^{\frac{1}{3}} \quad \frac{a}{d} > 2.5 \quad (5-7)$$

$$V_{Rd.c} = \left(\frac{2.5}{\frac{a}{d}} \right) * \left[C_{Rd.c} k \sqrt{100 \rho f_{ck} \frac{d}{a}} + 3 \frac{f_{R.4}}{\psi \sqrt{f_{ck}}} \left(\rho \frac{d}{a} \right)^{\frac{1}{3}} \right] \quad \frac{a}{d} \leq 2.5 \quad (5-8)$$

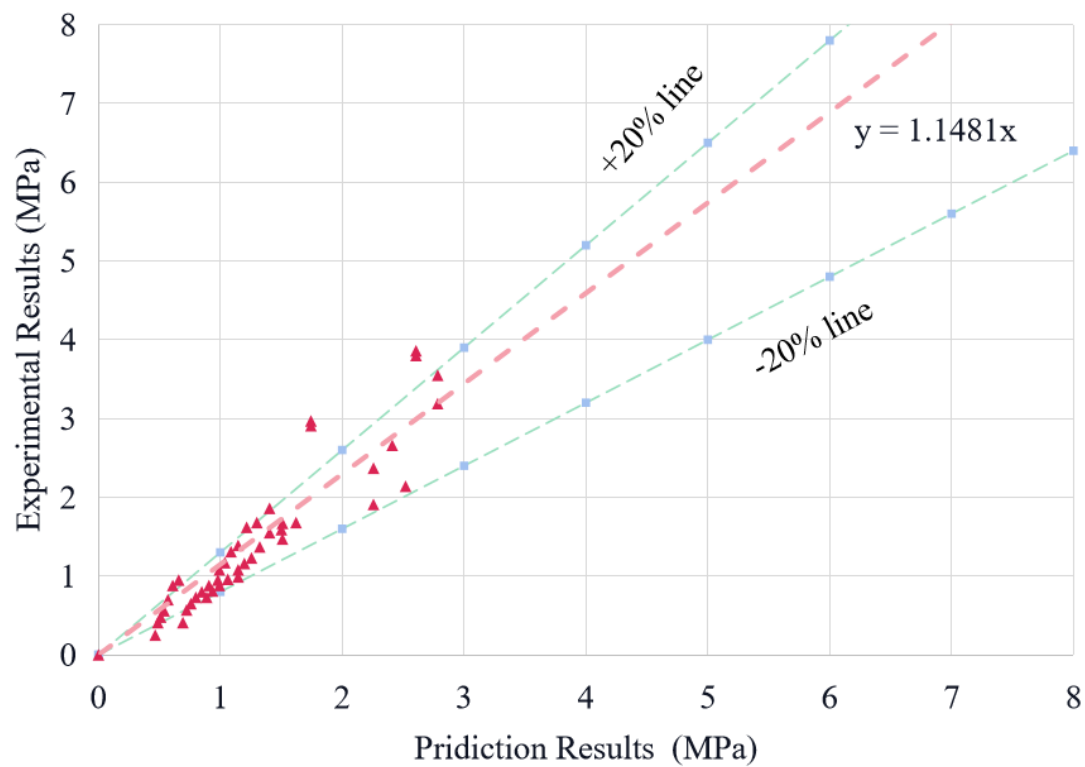
Table 5-2 Results of formula design analysis

Shear Span Ratio	1.5			2.5			3.5			4		
Fibre Content	0 %	0.40%	0.80%	0 %	0.40%	0.80%	0 %	0.40%	0.80%	0 %	0.40%	0.80%
Ratio between Prediction Results and Experimental Result for ISFRC												
Khuntia	0.59	1.87	1.91	0.81	0.41	0.92	0.62	0.69	0.40	0.42	0.72	0.69
Swamy	0.36	1.18	1.24	0.81	0.39	0.84	0.62	0.66	0.37	0.42	0.68	0.63
Mansur	0.47	1.50	1.53	0.86	0.42	0.91	0.64	0.69	0.39	0.43	0.71	0.66
Ashour	0.92	3.26	3.58	1.06	0.50	1.05	0.72	0.75	0.41	0.47	0.74	0.68
Ilker Fatih Kara	0.63	1.90	1.88	1.18	0.54	1.12	0.87	0.88	0.47	0.59	0.91	0.81
Al-Ta	0.84	2.34	2.17	1.53	0.64	1.23	0.96	0.91	0.46	0.62	0.90	0.76
Proposed Formulas in this Study	1.13	1.37	1.00	0.94	1.36	1.16	1.12	0.89	1.15	0.98	1.08	0.78
Ratio between Prediction Results and Experimental Result for RSFRC												
RSF Pre (MPa)	-	4.44	2.11	-	2.02	1.90	-	4.74	2.26	-	2.16	2.03
RSF Exp (MPa)	-	3.83	1.92	-	2.03	1.96	-	4.82	2.33	-	2.26	2.61

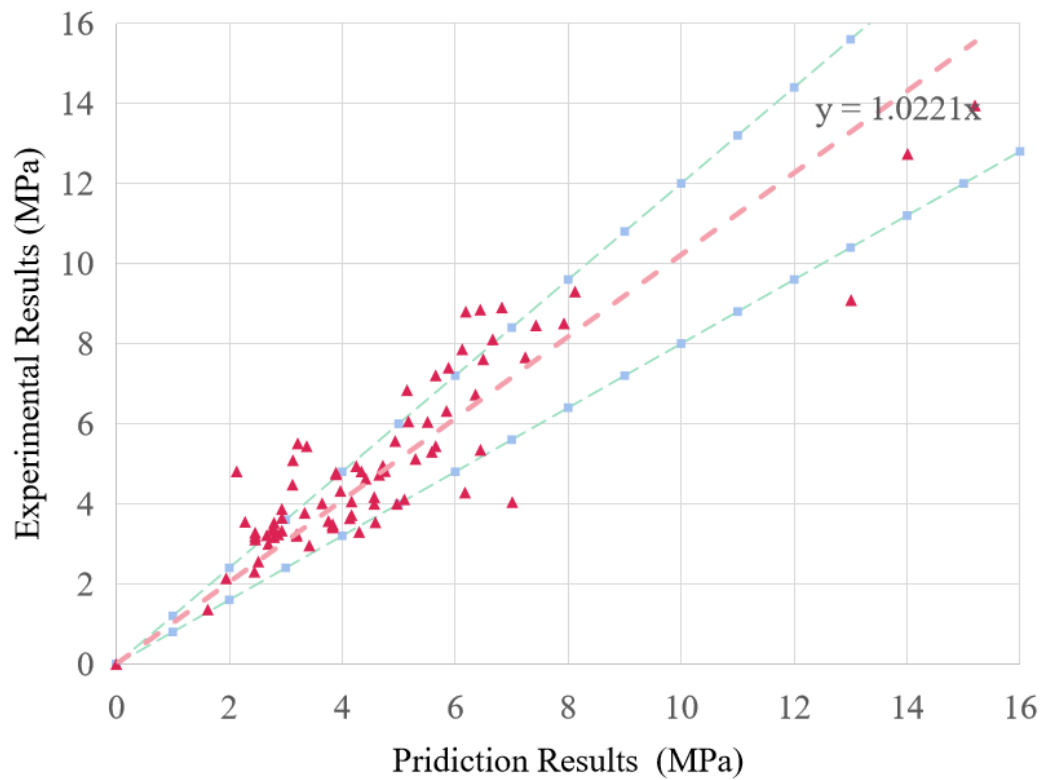
Pre/Exp	-	1.16	1.10	-	0.99	0.97	-	0.98	0.97	-	0.95	0.78
---------	---	------	------	---	------	------	---	------	------	---	------	------

5.2.3 Proposed Model Analysis

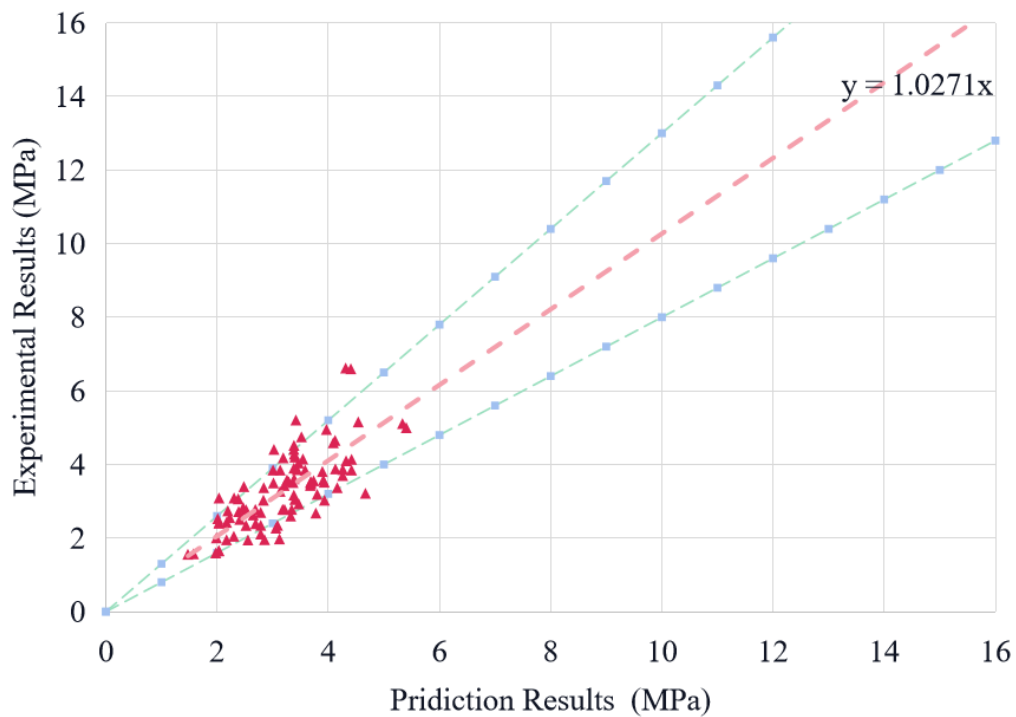
The proposed shear capacity prediction model is assessed by aligning its projected shear capabilities with results from 164 beam tests. The trials cover different ratios of shear span and incorporate ISF with hooked ends and diverse fibre volume proportions (0 to 4%). The calculations for projecting the shear capacity of HSFRC beams have been fine-tuned with reference to Eurocode 2 and TR63 standards. The chart in **Figure 5-1** establishes the predictability of each formula, enabling an assessment of its consistency with comprehensive experimental results.



(a) RC beams



(b) ISF reinforced concrete beams with shear span ratio higher than 2.5



(c) ISF reinforced concrete beams with shear span ratio lower than 2.5

Figure 5-1 Prediction results versus experimental results

The statistical analysis showed that the mean forecast-to-research value for the whole dataset was 0.98, with the majority of data points having a standard deviation below 20%. The model proposed in this study was effective, resulting in forecasted shear strengths that were somewhat conservative, and it proved to be a valuable and accurate predictive tool, as seen by the R-squared value of 0.95 and the standard deviation of only 0.10. In a graph displaying shear strengths produced by **Equation 5-1** versus the corresponding experimental values, the average forecast-to-research ratios for the RC, $a/d < 2.5$, and $a/d \geq 2.5$ datasets were 0.965, 0.980, and 0.993, respectively, with standard deviations of 0.222, 0.225, and 0.200, respectively.

Moreover, to evaluate the f_{Exp}/f_{Pre} distributions in the datasets, box and whisker diagrams are drawn in **Figure 5-2**, in which the calculated results are in an acceptable agreement with experimental values. In this type of plot, known as a box plot or box-and-whisker plot, data are summarized using five key statistics: minimum, first quartile (Q1), median (Q2), third quartile (Q3), and maximum. The "box" in the plot spans from Q1 to Q3, representing the interquartile range (IQR) which contains the middle 50% of the data. The "whiskers" extend from the minimum to the maximum values within 1.5 times the IQR from Q1 and Q3, respectively. Data points lying beyond the whiskers are considered outliers and are typically marked individually on the plot. This method of data representation is widely favored in statistical analysis for its ability to quickly identify potential outliers based on a standardized criterion. In this study, most outliers were observed to occur at higher shear strength values in experimental tests. To ensure conservative design practices and enhance predictive accuracy, the study deliberately chose to underestimate shear strengths. This cautious approach prioritizes the inclusion of data from

beams with lower shear values, thereby promoting safety in design predictions. During extensive experimentation, the occurrence of outliers is common. The study's conservative estimation strategy inadvertently categorizes some data points as outliers, despite these points not necessarily representing exceptionally high experimental values. This approach reflects a preference for safety and reliability in predicting shear strengths for reinforced concrete beams.

Hence, the equations proposed in this paper are designed to predict more accurately than previous versions and are consistent with safe design principles. As a result, the methodology reduces the risk of overemphasizing beams with exceptional shear resistance characteristics, resulting in safer design results. Despite the cautious approach to handling atypical cases, the recommended theory accurately forecasts the shear strength of ISFRC and RSFRC beams across a range of shear span ratios, demonstrating its reliability and robustness in shear strength prediction.

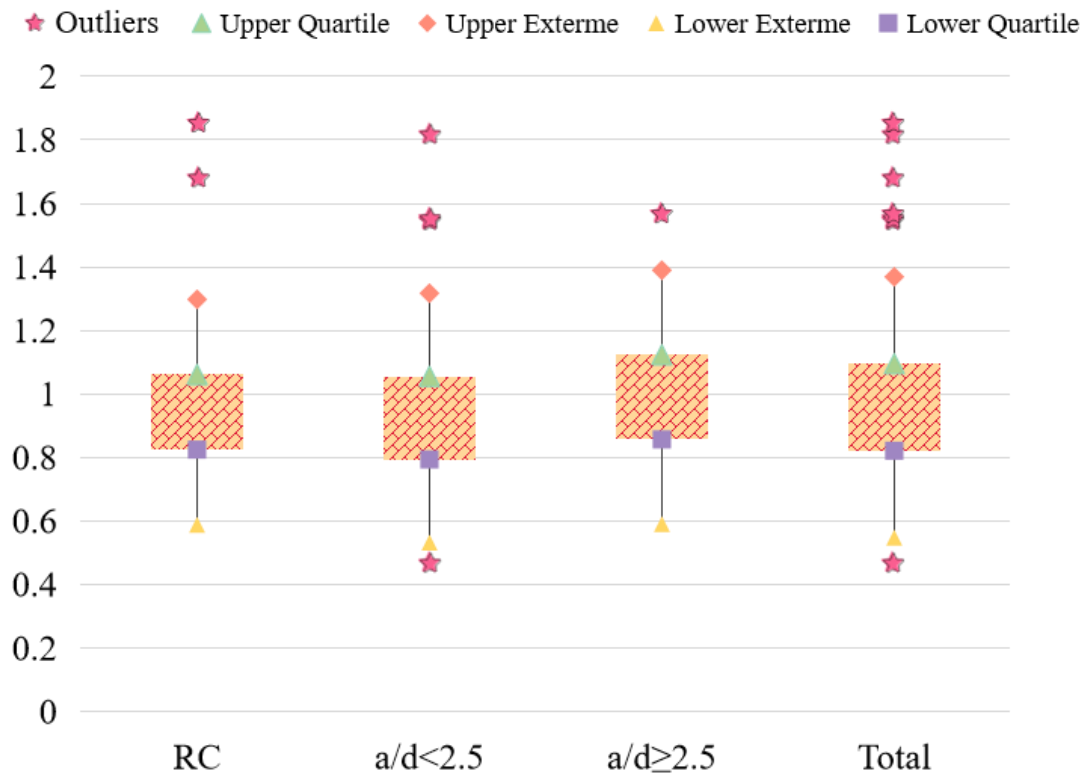


Figure 5-2 Box and whisker analysis

5.3 Conclusion Remark

RSFRC beams are a promising development in SFRC structural applications, demonstrating shear performance similar to ISFRC beams. This study focus on beams reinforced with ISF and RSF in three-point shear tests, taking into account different variables such as shear span ratios and fibre characteristics. Empirical formulas were developed based on the results of these tests and regression analysis.

Comparing the large-scale beam of ISFRC and RSFRC experiments, beams with smaller shear span ratios ($\lambda = 1.5$) often experience shear and compression failure when unreinforced. However, adding ISF or RSF shifts their failure mode to shear and flexural, significantly boosting peak loads. For beams with greater λ values (2.5, 3.5, and 4), diagonal tension failures

are common. Midpoint displacement increases when fibres are added, but the differences between ISF and RSF are minor. The bridging effect of fibres greatly improves the load-carrying capacity and deformation of concrete beams. In this regard, ISFRC and RSFRC beams show comparable performance enhancements. SFRC beams have significantly greater load-carrying capacity than non-reinforced samples, with the bridging effect being particularly noticeable. The introduction of RSF in SFRC beams represents a significant advancement in civil engineering applications due to the high ductile behaviour RSFRC beams.

In summary, the experimental analysis confirms that RSF-reinforced concrete beams exhibit comparable mechanical and structural performance to ISF-reinforced beams, with notable improvements in shear capacity and load-carrying capacity. While these results highlight the effectiveness of RSF in enhancing concrete properties, it is essential to consider the broader advantages of RSF, particularly in terms of sustainability and cost-effectiveness. As discussed in the literature review, RSF's most significant benefits lie in its potential for reducing environmental impact and lowering costs. Therefore, the next chapter will focus on a detailed comparison of RSF and ISF regarding their economic benefits and contributions to carbon emissions, providing a comprehensive assessment of RSF's role in sustainable construction practices.

6. Sustainable Development

6.1 Recycling Processing of RSF

The raw materials for RSF are sourced from Xiang He's tire-recycling facility in Shanghai.

Figure 6-1 illustrates the manufacturing process, detailing that the cost of bead wires is 411€ per ton. The recycling process involves four primary steps: 1) Collection of waste tires; 2) Splitting of bead wires; 3) Cleaning; and 4) Shaping and application.



Figure 6-1 Manufacturing process of RSF

According to Ref [125], the average processing capacity for tires is 40 pieces per hour, consuming 16.5 kWh per hour. Each recycled tire weighs approximately 9 kg. Additionally, steel wires constitute 10-15% of a tire's composition [126]. Therefore, **Formula 6-1** can be applied to compute the greenhouse gas (GHG) emissions of RSF:

$$Q_{RSF} = Q_e \rho_e * \theta * \gamma \quad (6 - 1)$$

Where Q_{RSF} represents the GHG emissions for recycling waste wires produced from tires, which are measured in kg CO₂ eq; Q_e denotes the power consumed by the tire-spun machine, measured in kw/h; ρ_e represents the percentage of waste wires from the tires; θ represents the number of tires that can be processed per hour, and the unit of measuring is pc/h; and γ refers to the greenhouse gas conversion factor.

6.2 GHG Emissions of Beams

To assess the feasibility of substituting ISF with RSF in sustainable construction development, **Table 6-1** summarizes the GHG emissions and material costs per beam. Meanwhile, **Table 6-2** presents the GHG emission values for beams made with concrete mixes as describe before. Notably, beams with varying shear span ratios exhibit GWP ranging from 1.85 to 5.04 kg CO₂ eq without additional fibre incorporation. Substituting ISF with RSF results in GWP reductions ranging from 0.33 to 1.73 kg CO₂ eq. For instance, replacing ISF with RSF in beams with a shear span ratio of 4 using HSC leads to a GHG reduction of approximately 14.61% (M1-RSF-4 versus M1-ISF-4), along with an 18.30% reduction in building costs. Conversely, in beams with low-strength reference concrete, GHG emissions increase by about 17.99% (M1-ISF-4 versus M0-4) and by only 0.5% (M1-RSF-4 versus M0-4). However, replacing ISF with 0.8% RSF results in a GHG reduction of about 25.39% (M2-RSF-4 versus M2-ISF-4), accompanied by corresponding cost savings. Moreover, a more significant decrease in GHG emissions occurs with a 100% replacement of ISF by RSF compared to a 50% replacement. Additionally, as the shear span ratio increases, RSF's contribution to GHG emission reduction becomes more

pronounced.

Table 6-1 GHG emissions and budget price of raw materials.

Component of Concrete	GWP/ kg CO ₂ eq	Price/ \$/kg	Resource
Basic Concrete Composition			
Cement	0.884	0.125	[127]
Coarse Aggregates	0.00429	0.0099	[128]
Fine Aggregates	0.0024	0.0099	[128]
Water	0.00015	0.0016	[128]
Fibres			
ISF	2.2	1	[99]
Steel Rebar	0.72	1.2	[129]
Raw RSF	0.07	0.4	Proposed by Author

Table 6-2 GHG emissions and budget price analysis

GHG Emission of Each Beams/ kg CO ₂ eq				
Shear Span	1.50	2.50	3.50	4.00
Plain	1.89	3.15	4.41	5.04
0.4% ISF	2.23	3.71	5.19	5.93
0.8% ISF	2.56	4.27	5.98	6.83
0.4% RSF	1.90	3.17	4.43	5.07
0.8% RSF	1.91	3.19	4.46	5.10

GHG Emission Saving				
			-14.61%	
w.r.t 0.4% ISF beams				
GHG Emission Saving				
			-25.39%	
w.r.t 0.8% ISF beams				
Building Budgets of Each Beams/ \$				
Shear Span	1.50	2.50	3.50	4.00
Plain	0.35	0.58	0.81	0.93
0.4% ISF	0.50	0.83	1.17	1.34
0.8% ISF	0.65	1.09	1.52	1.74
0.4% RSF	0.41	0.68	0.95	1.09
0.8% RSF	0.47	0.78	1.10	1.25
Price Saving				
			-18.30%	
w.r.t 0.4% ISF beams				
Price Saving				
			-28.04%	
w.r.t 0.8% ISF beams				

6.3 Sustainability Assessments

The above research illustrates the potential of RSF as a substitute for ISF, highlighting both its ability to reduce carbon emissions and its economic advantages, making it a dependable alternative material. However, current studies have exclusively focused on RSF, neglecting its role as a component of the broader tire recycling processes. A more comprehensive approach to utilizing tires could provide greater economic benefits and significantly impact the

construction sector. Consequently, this chapter aims to thoroughly and systematically examine the role of RSF within the entire tire recycling process, conducting a detailed industry-chain analysis and exploring its potential.

Dealing with waste tires on a global scale is challenging [130].. Reusing these tires and making them into useful resources is a complete solution. This has a lot of advantages: it cuts waste, preserves natural resources, and eliminates pollution. When recycling waste tires, there are extract materials like rubber fillers, steel wires, carbon black, and textiles can be recycled. These recycled materials can be used as raw materials in various application, such as construction, biofuel production, and tire remaking. Furthermore, this reveals that recycling initiatives are possible and promising [131].

Due to mounting worries about the environment and more extreme weather problems, nations worldwide are making efforts to push the agenda of a circular economy, which entails moving from a consumer-centric perspective to one stressing the importance of sustainability and promoting environmental conservation. This approach advocates for processes that safeguard ecosystems while simultaneously propelling economic expansion. Despite the fact that spent tires pose a major environmental danger, their recycling potential is largely untapped. Many studies have looked into tire recycling opportunities, but there is still a shortage of comprehensive conversations and evaluations incorporating economic and environmental consequences. This paper looks at circular economy fundamentals and economic tactics in recycled solid fuels production to address this gap. The intent is to thoroughly investigate tire recycling and use and illustrate its critical role in a sustainable circular economy. To evaluate

the role of recycled tire production in the circular economy, the document explores the RSF generating method and calculates its recycling potential relative to other tire-derived secondary materials by conducting an extensive tire recycling and deployment analysis.

6.3.1 Pre-treatment of Waste Tires

The necessity to effectively recycle and repurpose tires can be succeeded by adequately comprehending the composition of tires. This is explicitly detailed in Ref [132], which dissects the fundamental elements of passenger car and truck tires, delineated in **Table 6-3**. Inspecting the two classifications helps in understanding their unique resources. A key observation is that, even though truck tires are unique, they contain more natural rubber and less carbon black as a reinforcement filler than passenger vehicle tires. This disparity is attributed to passenger car tires needing superior performance characteristics, such as low rolling resistance, enhanced skid resistance, and optimal wear [133].. In the preliminary examination of the tires, reusable components include steel, rubber, and textile fibres, which are both valuable and abundant. A thorough sustainability scrutiny of these three materials is needed to assess their business potential and environmentally friendly benefits in tire recycling. By pursuing this two-point evaluation of parts, significant insights into the economic and ecological benefits of tire recycling are attained.

Table 6-3 Component of different tires

Composition	Passenger car tire	Truck tire
Natural rubber	22%	30%
Synthetic rubber	23%	15%

Carbon black	28%	20%
Other additives (e.g. curing agents, textiles)	14%	10%
Steel	13%	25%
Estimated average weight of new tire	8.5 kg	65 kg

The most essential machines used in tire recycling preparation include the Wire Pulling Machine [134] and the Rubber Shredder [134, 135]. Wire Pulling Machine pulls steel strings from used or scrap tires and is crucial for tire recycling. This happens as steel wires get separated from the other materials and complete recycling and reuse processes.

The second essential component is the rubber shredder machine, designed to recycle rubber materials. The equipment reduces the waste produced by rubber by breaking it into smaller pieces. This makes it simpler to manage and recycle the product. The machine primarily functions in the classification of tire components to enable proper recycling. After shredding, it allows for separating fibers and rubber in tires most efficiently. This process aids in achieving maximum material recovery during recycling and preserves the tire's valuable parts.

6.3.2 Steel Wires

The study utilizes recycled steel wires as the raw material for RSF. After separating the wires from tires using a Wire Drawing Machine, a Wire Forming Machine bends, coils, shapes, cuts, and joins the metal wires into specific configurations tailored to various industrial and manufacturing requirements.

Apart from employing steel wires from waste tires as steel fibers, another prevalent recycling approach involves recasting. However, this method typically incurs significant fuel

consumption. As indicated by ref [136], the standard CO₂ emissions for the basic oxygen and electric furnace routes are approximately 1770 and 380 kg CO₂ per ton of liquid steel, respectively. Additionally, the typical total energy consumption is about 4900 and 1100 kWh per ton of liquid steel, respectively. Compared to remanufacturing, this straightforward utilization of existing materials enhances recycling efficiency while reducing costs associated with labor, material resources, and time.

6.3.3 Rubber

[132] describes rubber as a predominant component of tire composition, constituting 46% in car tires and 45% in truck tires. This substantial proportion of waste rubber offers broader recycling opportunities compared to the more limited options for recycling scrap steel [137]. Recycling rubber, whether from tires or shoes, presents a sustainable solution with inherent advantages and challenges. Renewing rubber reduces the demand for new materials, thereby promoting resource efficiency and saving energy. This approach is environmentally friendly, mitigating the impact of rubber waste. However, challenges such as cost factors and maintaining product quality persist. Variations in recycled rubber materials can lead to inconsistent product quality, affecting overall performance and impeding significant cost reductions. Addressing these challenges is essential to maximize the environmental benefits of rubber recycling.

6.3.4 Textile

While the proportion of textile fibre in tires is relatively small compared to steel and other wastes, its potential should not be overlooked. Converting textile fibres into new products, such

as insulation materials or industrial fabrics, plays a crucial role in waste reduction and promotes sustainability. The thermal and mechanical properties of textile fibres enhance their value for insulation in buildings, thereby improving energy efficiency and reducing heating and cooling costs. However, challenges persist in maintaining textile fibre quality and ensuring safety. Variations in textile fibre types and treatments can impact the performance and safety of recycled fabric products. Therefore, rigorous sorting, cleaning, and quality control processes are essential to uphold the integrity and reliability of recycled textile materials across various applications.

6.3.5 Sustainable Evaluation of Waste tires

Table 6-4 compiles existing reviews on recycling methods for waste tires, offering a concise presentation of GHG emissions linked to each method. This summary enhances understanding of the environmental impacts associated with various recycling approaches, facilitating informed decisions in waste tire management within the circular economy framework.

Table 6-4 GHG emissions and cost benefit analysis.

	GHG Emission	Cost Benefit	Ref.
	kg/ CO ₂ kg eq	\$/kg	
Pre-Treatment for Tire /kg			
Tire Wire Drawing Machine	0.011	-0.0017	[134]
Tire Shredder Machine	0.007	-0.0011	[134, 135]
Steel Recycling /kg			
RSF	0.07	1.6	[99]

Rubber Recycling /kg			
Cement Production	-0.543	0.054	
Creating High-Energy Fuel	-0.613	0.054	[138]
Renew the Rubber	0.434	-	
Textile Recycling /kg			
Energy Recovery	-0.23	-	
Producing insulation materials	-8	0.5-0.6	[139, 140]
Making industrial fabrics	-8	0.5-0.6	
Polyester Recycling	-0.9	0.85	
Remark Conclusion			
Tire Type	Passenger car tire	Truck tire	
GHG Emission CO₂ kg eq/pre tire	-11.9 ~ 1.84	-67.62~13.51	
Cost Benefit \$/pre tire	2.60~3.19	30.65~32.92	

It is vital to assess the economic advantages of tire recycling and employing waste rubber in constructing playgrounds. However, it is necessary to adopt the circular economy's guidelines to highlight its worth. This research concentrated on creating playgrounds from recycled waste rubber and RSF while evaluating their economic importance. Based on the cost-effectiveness data and GHG released, it was found that the amount of electricity consumed by the refinement machine was significant, coming to 0.03 kWh and 0.046 kWh for each kilogram of enriched

tire samples. In evaluating waste rubber reuse, the energy production of rubber is scrutinized. According to ref [141], the overall electrical power output of rubber must generate 0.36 kWh/kg, and this relies on the computation of electricity produced via the tire's heat reaction (-1296.3 kJ/kg). The sale price of RSF, which is 1.5 times the cost at \$0.4 per kilogram, contrasts with the market cost of ISF at \$2.2 per kilogram. The cost assessment also considered an electricity charge of \$0.15 per kilowatt-hour from GlobalPetrolPrices. In comparison, IFS presents an opportunity to simulate the intrinsic economic value of recovering these products. These figures outline the crucial financial opportunity embedded in waste material reclamation, underscoring the possible concrete recycling in a circular economy. It should be noted that although the GHG emissions in the process for reclaiming RSF are not the most minimal, the cost benefit of \$1.6 per kilogram is substantial. This can effectively lessen building expenses while preserving structural design integrity.

Upon in-depth scrutiny and analysis of all criteria, the **Table 6-4** overviews the potential of recycling tires. Despite presenting a minor economic value, waste tire recycling has a profound positive impact on reducing GHG emissions. Even with the existence of less efficient recycling methods, the practice significantly reduces emissions [142].. For instance, even with less efficient recycling methods, waste tire recycling can reduce CO₂ emissions by 17.85 billion kg. Evaluating the economic benefits, recycling a standard passenger vehicle tire can yield \$3.19 per tire, while that of heavy truck tires can be up to \$32.92. This implies that annual replacement of 1.5 billion tires could fetch an economic value of \$4.8 billion and offset greenhouse emissions by a substantial margin—in addition, a standard tree absorbs approximately 21 kgs of carbon dioxide annually [143]. Impressively, the CO₂ abated by recycling waste tires

corresponds to what 85 million trees can absorb over a ten-year period. Furthermore, the financial benefits derived from waste tire recycling equal that of 67 million barrels of oil. This underscores the environmental and economic potential of tire recycling. The insights indicate the pivotal role of waste tire recycling in advancing a sustainable circular economy.

6.4 Conclusion Remark

RSF's role as a recyclable material offers significant environmental and economic benefits, particularly within the context of a circular economy. This chapter provides a thorough evaluation of tire recycling processes, revealing that recycling a car tire can reduce GHG emissions by 11.9 kg CO₂ equivalent per tire, while recycling a truck tire can achieve a reduction of 67.62 kg CO₂ equivalent per tire. Additionally, the economic advantages of tire recycling are noteworthy, with the process yielding approximately \$32.92 per truck tire.

The study also assesses the GWP associated with high-strength fiber-reinforced concrete materials incorporating ISF, which typically results in carbon emissions ranging from 2.23 to 6.83 kg CO₂ equivalent. Substituting 0.4% of ISF with RSF can reduce these emissions by up to 14.61% and replacing 0.8% of ISF with RSF can achieve a reduction of up to 25.39%. Moreover, the cost-effectiveness of using RSF is evident, as replacing ISF with RSF can lower the budget by up to 28.04%, assuming transportation distances are not considered.

In conclusion, RSF concrete beams demonstrate similar improvements in shear strength compared to ISF beams while offering reduced carbon emissions and lower costs. The findings of this study underscore the value of RSF in promoting sustainable construction practices by improving waste management, balancing structural performance, and reducing GHG emissions.

These insights are crucial for concrete engineers and structural designers seeking to enhance the sustainability of the construction industry, making RSF a compelling choice for future applications. While the experimental analysis provides accurate insights into the structural performance of RSF and ISF concrete beams, real-world applications often face challenges due to the time-consuming and labor-intensive nature of physical testing. To address this, improving the ability to predict structural performance efficiently becomes crucial. Therefore, the next two chapters will focus on employing cutting-edge machine learning techniques and advanced finite element modelling methods. These approaches aim to enhance the predictive accuracy of structural performance for RSF and ISF concrete beams, offering a more streamlined and effective way to evaluate and optimize their capabilities in practical scenarios.

7. Structure Prediction Methodology of Machine Learning

In modern structural design, various empirical equations are used to study shear behaviours and practical applications of SFRC beams by conducting theoretical analysis and gathering experimental data. However, most research focuses on NSFRC beams, with little consideration of the combined impact of fibres and concrete, which changes with increasing compressive strength. The **Section 5** discusses predictive capabilities based on the new formulas. Given that current models are derived from limited data, developing a data-driven way to predict HSFRC's shear strength is warranted.

In recent times, there has been a surge of interest in utilizing machine learning (ML) in civil engineering fields like developing structures, making concrete, and working with materials. Artificial intelligence (AI) models have become increasingly popular because their robust predictions and generalization capabilities help unearth hidden associations between major inputs and results. For example, ref [144] used the Artificial Neural Network (ANN) to predict the characteristics of fly ash concrete, whereas ref [145] employed a decision tree-based model known as the Xgboost to predict the failure mode of reinforced concrete shear walls. Generally, the accuracy of ML-generated predictions typically relies on the quality and amount of data used, with better outcomes met when ANN, Xgboost, or random forest (RF) models are used. Given the scenario above, this project will investigate different ML models to predict how well HSFRC beams will perform in structural engineering.

7.1 Literature Review

SFRC beams show better qualities than normal concrete in terms of post-cracking behavior and

energy absorption. Over the last 30 years, there has been a rise in the construction industry's application of the SFRC, particularly in airport runways, tunnel linings, bridge structures, and protective structures. The random distribution of fibres in the concrete mean that traditional structural analysis techniques are unreliable and show weak forecasting abilities. Some scholars focus on employing ML techniques to predict SFRC beams' shear capacity using various models. **Table 7-1** reviews the recent research on the use of ML models to predict the structural performance of SFRC beams.

Table 7-1 Review analysis

Ref	ML Technology	Results	Detailed
ML used in SFRC beams			
Qian, Sufian [146]	SVR, MLP, Gradient boosting	R^2 of 0.91 with Testing Datasets with Gradient boosting model	Flexural strength prediction of ultra- high-performance concrete
Pakzad, Roshan and Ghalehnovi [147]	MLR, KNN, SVR, RF, GB, Xgboost, AdaBoost, ANN, and CNN.	R^2 of 0.928 with Total Datasets with CNN model	Compressive strength prediction
Kang, Yoo and Gupta [148]	MLR, KNN, SVR, RF, GB, Xgboost.	RMSE of 3.6144 with Total Datasets with Xgboost	Compressive and flexural strength

		model	prediction
ML used in shear capacity prediction			Number of Datasets
Alzabeebee, Al-Hamd [149]	Evolutionary	R ² of 0.93 with	235
	polynomial	Testing and Training	
	regression analysis	Datasets	
Jesika Rahman[150]	AdaBoost,	R ² of 0.739 with	507
	CatBoost,Xgboost,	Testing Datasets with	
	ANN, SVR et al.	Xgboost model	
A Shatnawi [151]	Gradient boosting	R ² of 0.969 with	330
	regression tree	Training Datasets	
Shahnewaz and Alam [152]	Genetic Algorithm	R ² of 0.9 with total datasets	358
Kara [153]	Genetic Programming	AAE of 11.39	101
Adhikary and Mutsuyoshi [154]	Neural Networks	SEM of 0.33	85
Yaseen [155]	M5, RF and ELM	R ² of 0.87with	112
		Testing Datasets with ELM	
		model	

*AAE is the average absolute error and SEM is the standard error of mean

Following a comprehensive assessment, it is clear that the machine learning models applicable to HSFRC beams frequently lack conservatism and offer low performance prediction precision.

This article aims to overcome these flaws by using a new data-driven technique to produce a more predictive and commercially viable model of HSFRC behaviour.

According to Eurocode 2, shear capacity is only one factor in structural design. To understand the failure modes of concrete beams more clearly, we need to consider the importance of flexural strength and stiffness when designing formulas and analyzing outcomes. In structural design, flexural performance plays a vital role. The advantages of adding fibers to beams can best be shown by comparing shear strength and flexural capacity results. The stiffness of concrete beams is crucial for their seismic performance, which affects critical period identification, displacements, ductility, and internal forces distributed throughout the framework [156]. This research used three different ML techniques to model 171 HSFRC beams and predict the values of three important structural design parameters: shear strength, flexural capacity, and stiffness.

7.2 Research Methods

7.2.1 ANN Model

ANN is a well-accepted mathematical concept based on the natural biological neural network intrinsic to the human brain. Many prospective applications of ANN in engineering, specifically in predicting specific mechanical properties [157]. The model schema includes an input layer, lots of hidden layers, and an output layer, all analogous to the natural neural network [158]. Weight coefficient(w) is a critical component for input-to-output information transfer and computation processes in the model. **Equation 7-1** explicitly encapsulates the delicate interaction between input and weight coefficient as a fundamental ANN expression [159].

$$net_j = \sum_{i=1}^n (w_{ij} \times x_i + b_j) \quad (7-1)$$

The equation above is described as follows: net_j represents the total weighted input, x_i is the unit of the previous layer, w_{ij} is the weight of the connection between the previous layer and the current layer, and b_j is the bias of the current layer. This experiment chose hidden layer formulas to use the following structure: (100, 20, 20).

7.2.2 Xgboost Model

The Boosting Tree approach is derived from decision trees, which are common due to their effectiveness in statistical learning. Especially, it is well-regarded due to its ability to boost and minimize overfitting, as indicated in ref [160]. Regardless of the size of the datasets, Xgboost provides excellent performance. Its fundamental concept entails merging iterative results through a formula synthesized in **Equations 7-2 and 7-3**.

$$\hat{y}_i^{(T)} = \hat{y}_i^{(0)} + \sum_{t=1}^T f_t(x_i) \quad (7-2)$$

$$f_t(x_i) = \omega_{q(x_i)} \quad (7-3)$$

Here, \hat{y}_i represents the final predicted value for the i_{th} sample after T decision trees, where $\hat{y}_i^{(0)}$ is the initial prediction. The function $f_t(x_i)$ denotes the prediction contribution of the t_{th} decision tree to the i_{th} sample, with $\omega_{q(x_i)}$ as the weight vector corresponding to the leaf node $q(x_i)$ that x_i maps to in the decision tree. The specific Xgboost parameters, including 500 trees, a learning rate of 0.1, and a gamma of 0.01, are explicitly selected to achieve the optimal predictive performance. These parameters are vital as they can deliver accurate

predictions while efficiently managing model complexity.

7.2.3 BNN Model

Like the ANN models, BNN simulate how the human brain processes data. But instead of regularizing the model based on the magnitude of learned weights, BNNs intend to capture a distribution $p(w|D)$ over the model weights (w) after seeing the data, as shown in the following equation. This distribution consists of the dependent variable parameter values that are most likely to occur given the observed data (D), as well as the alpha and beta hyperparameters, as stated in the next equation. This formulation offers a probabilistic interpretation of the ANN training by incorporating the specific training data in the model probability space based on the BNN's architecture:

$$S(w) = \beta E_D + \alpha E_w \quad (7 - 4)$$

$$E_w(w) = \frac{\sum_{i=1}^m w_i^2}{2} \quad (7 - 5)$$

Here, m represents the total number of parameters in the network, and α and β are regularization hyperparameters. $E_w(w)$ computes the regularization term based on the L2 norm of the weights. Bayesian inference in BNNs utilizes Bayes' theorem to update prior beliefs into posterior beliefs ($p((w|D, \alpha, \beta, A))$), which states that:

$$p((w|D, \alpha, \beta, A) = \frac{p((D| w, \beta, A)p((w| \alpha, A)}{p((D| \alpha, \beta, A)} = \frac{p((D| w, \beta, A)p((w| \alpha, A)}{\int p((D| \alpha, \beta, A) p((w| \alpha, A)} \quad (7 - 6)$$

Where the $p((w| \alpha, A)$ is the prior and the $p((D| \alpha, \beta, A) = \int p((D| \alpha, \beta, A) p((w| \alpha, A)$ is the evidence, the probability distribution $p((D| w, \beta, A)$ called likelihood which represents the uncertainty on the datasets and simulates the side-effect of noise process. The individual

parameters were fixed initially, but automatically optimized based on the data gathered. The configurations of the network design are critical for how the model learns and its ability to do optimal Bayesian network modelling. The configuration of the hidden layers was deliberately selected based on the powers of 10 in the following progression: 1st layer 50, followed by 100 and then 100 again.

7.3 Data Preparation

The research used published literature data, including 171 beams in total. In this context, 171 beams were used in shear strength and flexural capacity prediction, whereas 118 were utilized in the prediction of rigidity. In line with ACI 363 standards, concrete with compressive strength equal to or greater than 55 MPa is considered high-strength concrete. A few beams with compressive strength below 55 MPa were included to ensure dataset comprehensiveness and diversity. The most important beam details and parameters are summarized in **Table 7-2**, with additional data available in **Appendix A-3**.

Table 7-2 Overview of the datasets

Parameters	Min	Max
Compressive Strength		
MPa	53.4	112
Fibre Content %	0	3
Longitudinal Ratio %	0.37	4.78
Shear Span	1	3.77
Cross Section	100*135	600*887

Fibre Type	Hooked, Crimped and Plain
------------	---------------------------

This analysis employs both Scikit-Learn and Torchbn codes within Python packages to expand the machine learning models. The existing data is split into sections: 70% for training and 30% for testing. The algorithm standardizes the input and output values, which increases the model's performance. Data standardization adjusts the attributes' distribution to feature a mean value of zero and a standard deviation of one (unit variance). Mathematically, standardized data are represented as shown in the formula:

$$\hat{y} = \frac{y - \mu}{\sigma} \quad (7 - 7)$$

where μ denotes the mean and σ represents the standard deviation of the data sets. To assess the predictive accuracy of each ML model, three commonly used metrics are applied: R-Squared (R^2), Mean Absolute Error (MAE), and Mean Squared Error (MSE).

$$R^2 = 1 - \frac{\sum_{i=1}^N (y_i - \hat{y})^2}{\sum_{i=1}^N (y_i - \bar{y})^2} \quad (7 - 8)$$

$$MAE = \frac{1}{N} \sum_{i=1}^N |y_i - \hat{y}| \quad (7 - 9)$$

$$MSE = \frac{1}{N} \sum_{i=1}^N (y_i - \hat{y})^2 \quad (7 - 10)$$

where \bar{y} is the mean value, \hat{y} is the predicted value, and y_i is the actual value.

7.4 Research Analysis

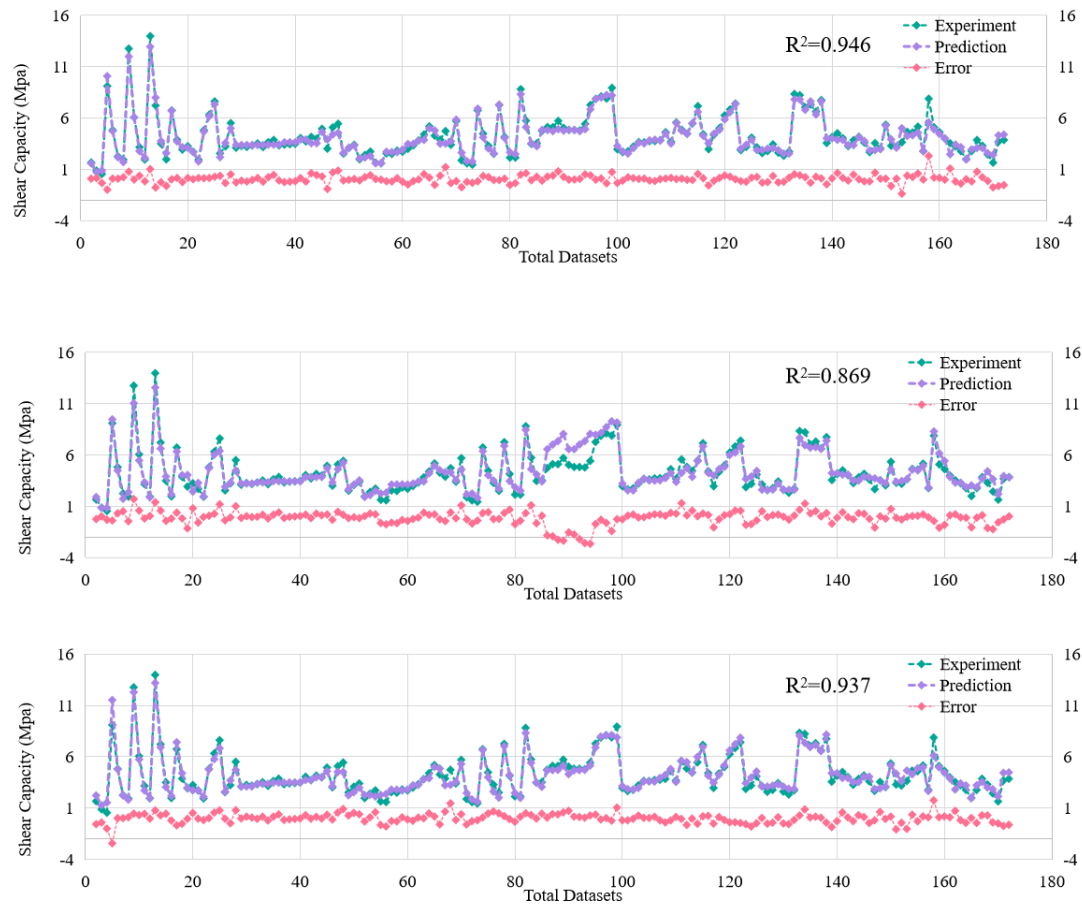
7.4.1 Shear Capacity

The study used three established ML models in this study to predict the shear strength of the

HSFRC beams that the chapter explores. A comparison of statistical metrics using different ML models for predicting shear strength is presented in **Table 7-3** in order to indicate the statistical outcomes. **Figure 7-1** shows a graphical comparison between predicted and actual results across the complete dataset. Green lines show the forecasted values of shear strength, while light purple ones represent empirical values. The results of both experimental and predicted values are displayed using red dots placed on each line. Error values are assimilated using a secondary axis to help visualize the difference between empirical and predicted results accurately.

Table 7-3 ML used in shear capacity

Results Models	Train			Test			Total		
	R^2	MSE	MAE	R^2	MSE	MAE	R^2	MSE	MAE
Xgboost	0.996	0.003	0.035	0.852	0.024	0.062	0.858	0.111	0.112
ANN	0.980	0.015	0.026	0.894	0.052	0.095	0.927	0.059	0.070
BNN	0.994	0.005	0.046	0.895	0.059	0.097	0.968	0.029	0.074



*The above figures depict the prediction error results of the ANN model, the Xgboost model and the BNN model respectively.

Figure 7-1 ML used in shear capacity

Based on the results in **Table 7-3**, the ANN model appears to have outperformed other models in shear strength prediction. The ANN model was observed to have R^2 values of 0.981, 0.888, and 0.949, as well as MSE values of 0.017, 0.095, and 0.044 for the training, test, and sum datasets, respectively. Most shear strength prediction models had statistically significant R^2 values above 0.86 for the total dataset. The Xgboost model outperformed the others in terms of prediction accuracy for the training phase, attaining an R^2 value of 0.992 and an MSE of 0.008 MPa. However, when evaluating the overall dataset, the Xgboost model did not perform as well

as the ANN and BNN models based on these statistical measures. This discrepancy is because Xgboost models operate best with unassembled data organized into tables and easy normalization, while neural networks are superior with noisier datasets. Across all categories, the models provided consistent results: Xgboost the model had an R^2 of 0.869, the ANN model 0.949 and the BNN model 0.937. The ANN model's prediction error ranged from 0.002 to 2.307 MPa, and 80.7% of predictions were within 0.5 MPa accuracy, 16.4% within 0.5 and 1 MPa accuracy while only 3% exceeded 1 MPa. The ANN model performed exceedingly well, but all three were excellent, demonstrating that they effectively identified trends within the data.

7.4.2. Flexural Capacity

Eurocode 2 guidelines on structural design indicate that it is crucial to consider flexural capacity in designing structures. To present a more detailed design, this study also computes flexural capacity, an outcome determined through pattern 2000 by Bentz, E.C at the University of Toronto [161]. This study used the same three models that help predict shear strength to determine flexural capacity. **Table 7-4** below describes the model's forecast capacities as a comparison.

Table 7-4 ML used in flexural strength

Results Models	Train			Test			Total		
	R^2	MSE	MAE	R^2	MSE	MAE	R^2	MSE	MAE
Xgboost	0.996	0.003	0.035	0.852	0.024	0.062	0.858	0.111	0.112
ANN	0.980	0.015	0.026	0.894	0.052	0.095	0.927	0.059	0.070

BNN	0.994	0.005	0.046	0.895	0.059	0.097	0.968	0.029	0.074
-----	-------	-------	-------	-------	-------	-------	-------	-------	-------

All models perform great in predicting flexural capacity values. The BNN model is specifically high-performing, outstripping the other models with a great R^2 of 0.968, MSE of 0.029, and MAE of 0.074. On the contrary, the Xgboost model is the poorest performer, yielding an R^2 of 0.858, MSE of 0.111, and MAE of 0.112. Notably, all the models show an R^2 exceeding 0.9 for the training data. The Xgboost model's results are very close to the actual data values, and it offered an MSE of 0.003 for the training dataset. Ultimately, the study indicates that the BNN model performs best with an R^2 above 0.9 for the whole dataset, while the Xgboost model is not optimal for testing because of the noise in the data. This clashes with the training trends where the model did relatively well. Specifically, the Figure 7-4 presented the Xgboost, BNN and ANN models tipping to the left in terms of error measurement. As concerns the threshold discussed earlier, 91.2% for BNN, 87.7% for Xgboost, and 91.8% for the ANN model recorded on the threshold marking error.

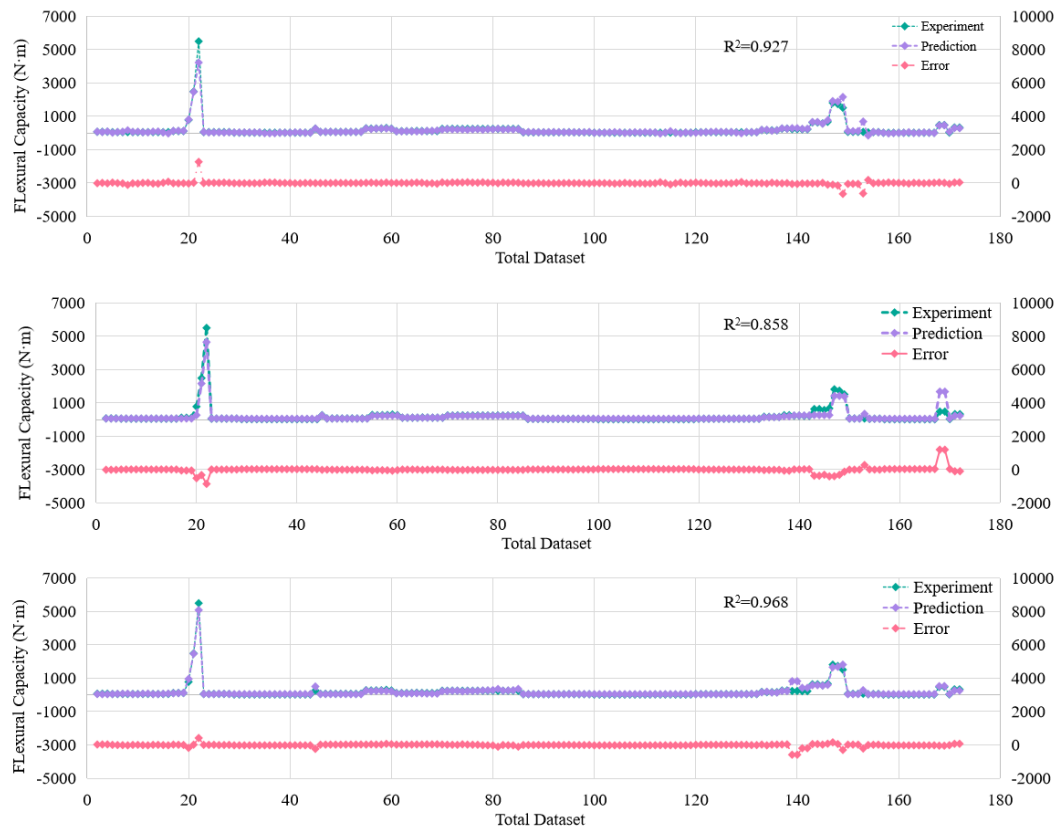


Figure 7-2 ML used in flexural capacity

7.4.3. Shear Stiffness

Shear stiffness of HSFRC was predicted using different models, as shown in **Table 7-5**. The information indicates that the predicted and experimental results for the training data were quite similar across all three models. The BNN model was established as the most accurate for all the datasets, followed by the ANN and Xgboost models. Nevertheless, the Xgboost model indicates excellent performance regarding the identification of the input-output connection, although it displayed poor generalization with the testing sets. The combination of the model evaluation and experimental results presented in **Figure 7-3** was comparable, demonstrating consistency. For the complete databases, the BNN model provided an R^2 of 0.907, indicating its excellent performance; the Xgboost model showed relatively lower performance with an R^2

of 0.714. Therefore, although the Xgboost model is effective in describing the relationships within the provided dataset, it lacks generalization capability. The distribution of the mean error shows significant differences among the models, with ANN at 5.2 kN/mm, Xgboost at 8.05 kN/mm, and BNN at 4.65 kN/mm. Noteworthy, a previous model indicated a poor performance than other models in the FNC outcome. Additionally, the distribution of the error showed that only a small proportion of the calculated errors exceeded 10 kN/mm. For the ANN, the proportion was 9.8%; show this for Xgboost - 26.8%; and for BNN was recorded as 7.69%. For this reason, although the Xgboost model could explain the input-output relations, especially on the given dataset, the BNN model showed excellent performance in predicting the shear stiffness of HSFRC.

Table 7-5 ML used in stiffness

Results Models	Train			Test			Total		
	R ²	MSE	MAE	R ²	MSE	MAE	R ²	MSE	MAE
Xgboost	0.989	0.010	0.072	0.821	0.131	0.197	0.714	0.288	0.352
ANN	0.985	0.015	0.097	0.765	0.440	0.519	0.869	0.161	0.228
BNN	0.949	0.046	0.155	0.881	0.080	0.215	0.907	0.070	0.204

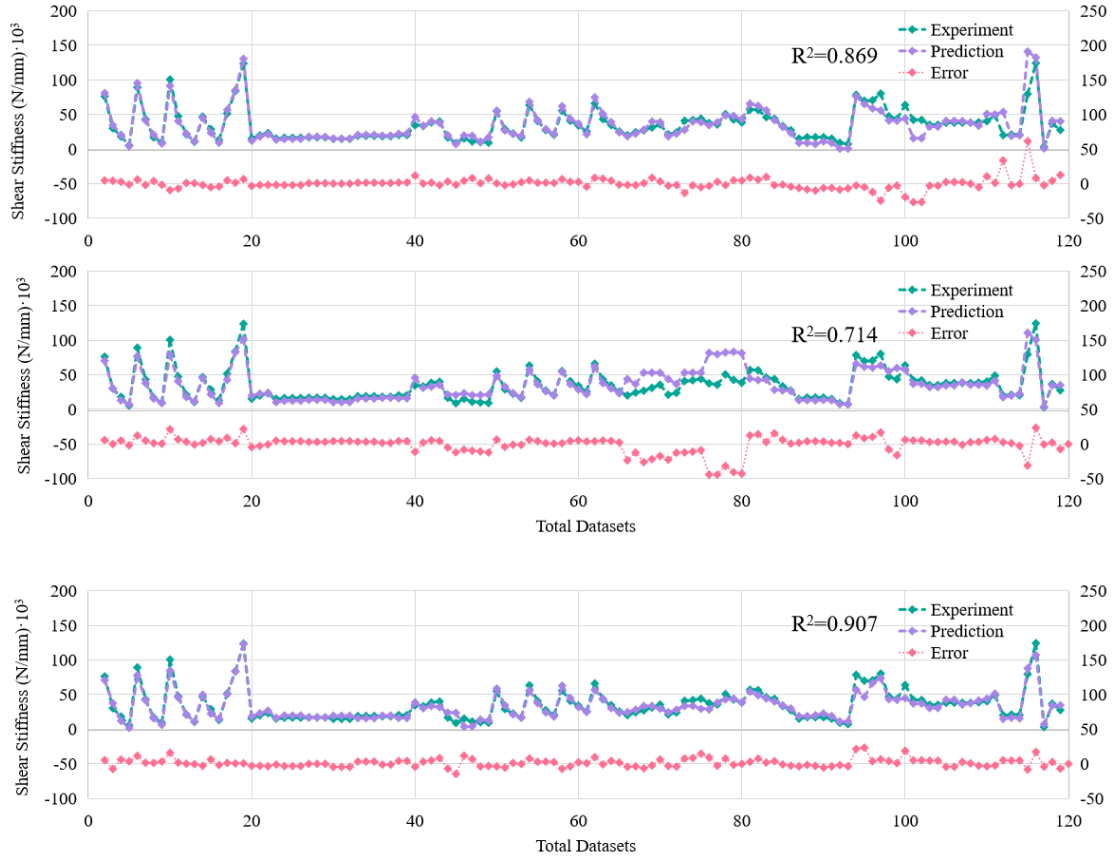


Figure 7-3 ML used in shear stiffness

7.5 Shapley Additive Explanations

In this study, the impact of each input feature on the result was investigated using the Shapley Additive Explanation Model (SHAP). SHAP is tailored to show how machine learning models work and is based on game theory. It can evaluate the impact of input parameters by determining their contribution to the output. The relevance of different input features is ranked based on their contributions to the total output [162]. This can be calculated based on **Equation 7-11**, which shows the weight $\phi^j(f)$ for the sum of the inputs' impact on the output

$$\phi^j(f) = \sum_{S \subseteq N \setminus j} \frac{|S|! (p - |S| - 1)!}{p!} [f(S \cup j) - f(S)] \quad (7 - 11)$$

where S is the feature subset, x^j is the j_{th} input, and p is the number of input variables. This

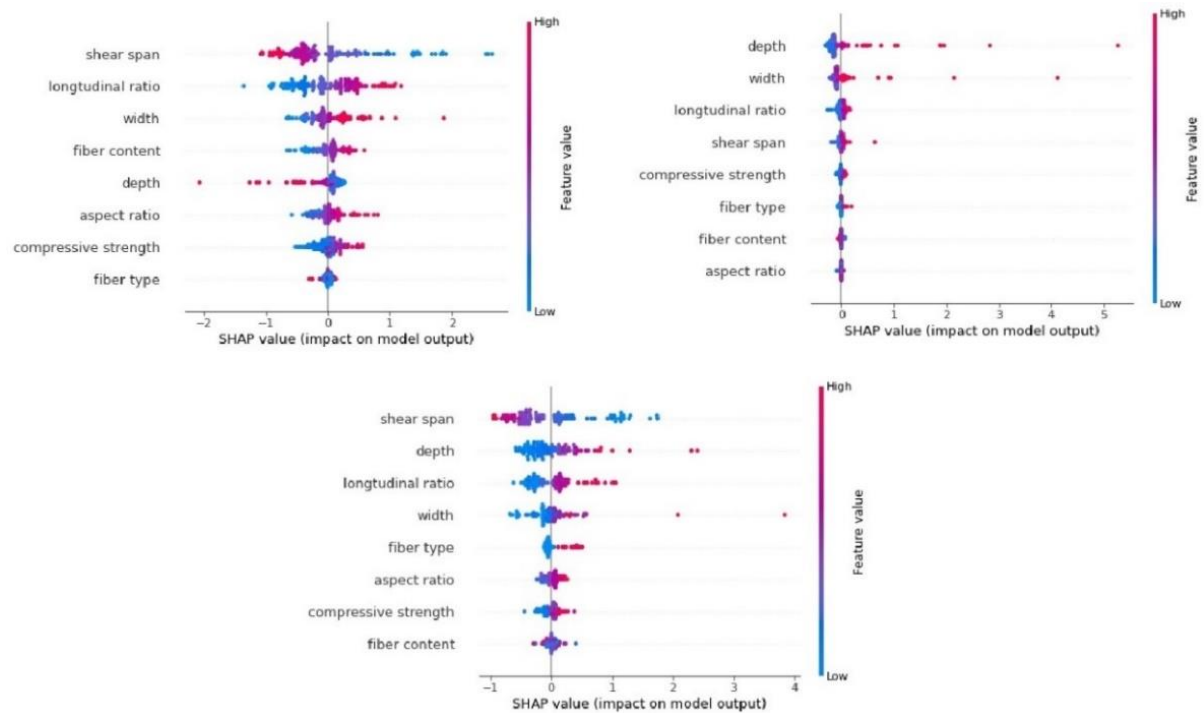
method quantifies the prediction ability of each input by evaluating estimation errors. To describe the original model $f(x)$, the explanation model $g(x')$ with inputs x^j is used in

Equation 7-12:

$$f(x) = g(x') = \phi_0 + \sum_{i=1}^M \phi_i x'_i \quad (7 - 12)$$

where M is the number of input features, and ϕ_i is the no-information constant. The BNN models were preferred over other models in this experiment, and accordingly, SHAP was employed. The SHAP values for predicting shear strength, flexural capability, and shear stiffness on BNN models are provided in **Figure 7-5**.

Using the absolute SHAP values, the input variables are ranked as follows: Shear Span > Longitudinal Ratio > Dimension Factors > Fiber Factors > Compressive Strength. The shear span has the highest impact on the prediction of shear strength and shear stiffness as well. However, the longitudinal ratio has a significant effect on stiffness estimation, showing that the presence of rebar in reinforced concrete is crucial. Furthermore, the most critical variables for predicting the flexural capacity include width and depth. However, the importance of fibre factors such as fibre type, fibre content, and aspect ratio are relatively low in this case. It can be inferred that there is a compound effect of concrete, fibres, and steel rebar leading to higher sensitivity to stiffness for longitudinal ratio, fibre factor, and compressive strength.



*The upper left figure shows the shear strength prediction of the BNN model, the upper right picture shows the flexural predicting BNN model, and the lower figure shows the shear stiffness predicting BNN model.

Figure 7-4 SHAP explanation models.

7.6 Conclusion Remark

In this study, three ML models—ANN, XgBoost, and BNN—were employed to predict the shear strength, flexural capacity, and stiffness of high-strength concrete beams. These models were compared against three empirical equations and an ML prediction formula. The predictive performance of the ML models was assessed using R^2 , MSE, and MAE criteria. Key findings include:

All ML models demonstrated robust predictive capabilities for shear strength, flexural capacity, and stiffness. The BNN model excelled with the highest R^2 values for flexural capacity and stiffness, and a close second for shear strength, proving its superior prediction ability compared

to traditional neural networks. During training, XgBoost exhibited the lowest statistical errors and highest R^2 , followed by ANN and BNN. However, XgBoost's generalization to testing datasets was less effective, indicating weaker performance in generalization. And, according to the absolute SHAP values, the input variables are ranked as follows: Shear Span > Longitudinal Ratio > Dimension Factors > Fiber Factors > Compressive Strength.

Building on the promising results from the machine learning models and their ability to predict shear strength, flexural capacity, and stiffness, the next phase of this study will delve into the application of Finite Element Modelling (FEM). While ML models provide powerful predictive insights, FEM offers a detailed simulation approach to further explore and validate the structural performance of high-strength concrete beams under various conditions. The following chapters will employ FEM to investigate the detailed behaviour of RSF and ISF concrete beams, enhancing our understanding of their performance and aiding in the development of more refined design strategies.

8. Structure Prediction Methodology of Finite Element Modelling

Numerous models have been developed for SFRC to simplify the interaction forces between concrete and fibres. Although it is more reliable and straightforward to predict shear models for large-scale beams using simple mechanical tests, relying only on basic mechanical testing might oversimplify the complex traits of these materials. The approach might not incorporate various performance aspects under different loading conditions. Moreover, using standard fibre models may not include all the subtleties of fibre-concrete interaction, such as bond strength and material discrepancies. Despite these factors, using constitutive models for simulation balances precision and efficiency and currently is the best-cost and accurate forecasting approach. This research, which addresses ISF and RSF while simulating and assessing the failure modes of ISF- and RSF-reinforced concrete beams using elementary fibre constitutive model.

This investigation delves into the mechanical characteristics of two types of SFRC and delineates their constitutive theories, closely analysing them. Moreover, it integrates 12 full-scale SFRC beams into its models to evaluate them, considering the diversity in ISF and RSF, shear span-to-depth ratios, and fibre content. This material property modelling under varying scenarios is vital for material advancement and utility improvement. The use of ABAQUS is vital to accurately predict performance and optimize it, vital in making structures that are not only safe and dependable but also economically efficient and sustainable. An accurate SFRC model promotes a deeper understanding of its properties, significantly improves the prediction of flexural capacity, and enhances the capacity to weigh its benefits against other types of reinforcing. There is, however, much work to be done in unifying advanced constitutive models with empirical data to enhance predictions in different situations. This kind of research is essential to create a framework for more efficient and sustainable structural design, thus significantly contributing to best practice in engineering.

8.1 Numerical Modelling

The 3D Finite Element Model (FEM) is acknowledged for predicting the expected shear

response in SFRC beam specimens using the ABAQUS nonlinear finite element solution. In this process, the CDP model is adopted to model concrete properties in the FEM. The stress-strain behaviour characterizes the chosen model for simulating concrete in a concrete block. The simulation uses three-dimensional eight-node linear brick elements (C3D8R) featuring reduced integration as well as hourglass control. Reinforcement is presented using a two-node linear 3D truss component type (T3D2) and applied on stirrups and aggregating reinforcement in the compression zone. The ABAQUS utilizes embedded constraint approaches to simulate truss elements contained in a set of strong components, e.g. reinforcing bars in the concrete [163].

This research uses a hard contact approach rather than one where the concrete specimen is wholly enclosed. A friction coefficient of 0.6 and a stiffness of 60 define this design [164]. This design is constructed so that the force starts at the apex of the support before being applied to the top of the concrete beam, as illustrated in **Figure 8-1**. In the support and the beam top interaction surface, compressive transformation can occur.

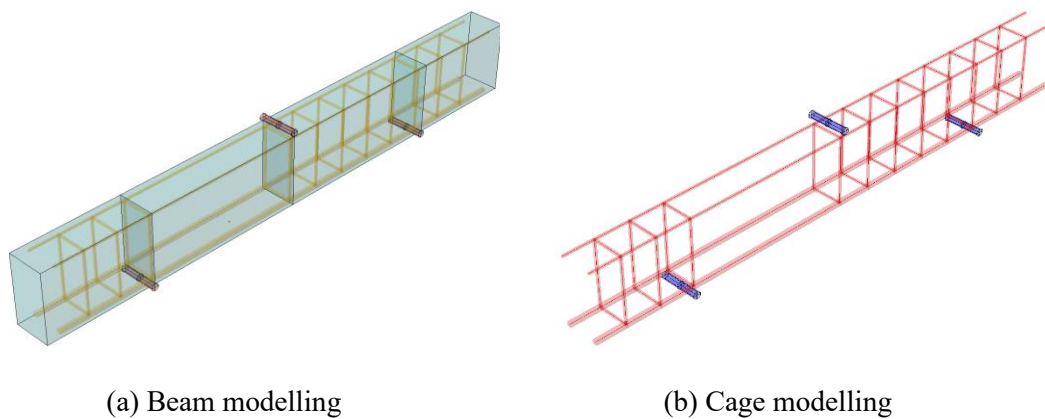


Figure 8-1 Modelling

8.2 Materials Definition

8.2.1 Compression Behaviours

The concrete damage analysis is based on using the CDP framework that centres around concrete's compressive and tension qualities. Although the inclusion of fibres can sometimes

increase concrete's compressive durability during axial compression, the precise quantification is hard since the current data is somewhat spread thin. Hence, it's accurate to suggest that the stress-strain curve aligning with concrete behaviour during uniaxial compression isn't significantly impacted by incorporating steel fibres the same way as the plain concrete curve. When analyzing the high-strength SFRC beams in this research, the material model- ABAQUS, originates from the concrete damage plasticity model suggested by ref [165] and is expressed in the formula below:

$$\sigma_c = \frac{E_0 \varepsilon_c}{1 + \left(\frac{E_0 \varepsilon_p}{\sigma_p} - 2 \right) \left(\frac{\varepsilon_c}{\varepsilon_p} \right) + \left(\frac{\varepsilon_c}{\varepsilon_p} \right)^2} \quad (8 - 1)$$

where σ_c and ε_c are the compressive stress and strain, and σ_p and ε_p refer to the experimentally determined maximum stress and its corresponding strain, which are taken to be the cylinder strength (megapascal) and 0.002, respectively. By adopting a modified Drucker-Prager yield criterion, this model considers the ref [166] and a damage plasticity model for concrete and other quasi-brittle materials. The concrete's damage plasticity model has been widely used in applying reinforced concrete and SFRC under both static and dynamic conditions.

8.2.2 Tensile Behaviours

Many theoretical models have been developed to explain the tensile behaviour of SFRC concrete. These models generally describe the stress-strain curves of the material using two branches: a rising tension and residual strength [167]. These calculations are derived from regression analysis of uniaxial tensile or spalling test data or use energy estimation techniques to evaluate variations in energy absorption (strength) levels during the bending test of SFRC prisms. Even though the models take different paths, introducing fibres into the concrete mixture, which pertains to the post-cracking behaviour of SFRC, is the most significant factor influencing the stress-strain correlation. [168].

It's essential to comprehend intricate behaviors in order to enhance SFRC structures in practical

design situations. By refining constitutive models with experimental proof, this research makes a contribution. It also gives additional information on how crack development and behaviour after cracking are influenced by various types and quantities of fibres. The key study goal is to give designers dependable tools enabling optimal SFRC integration in real-world settings, thus guaranteeing structures are long-lasting, secure, and cost-effective. Ductility and residual stress can be quantitatively analysed via approaches like CMOD and CTOD measurements. The RILEM TC 162-TDF [169] specification introduces a stress-strain relationship for SFRC based on CMOD experimental results, which is shown in **Figure 8-2**.

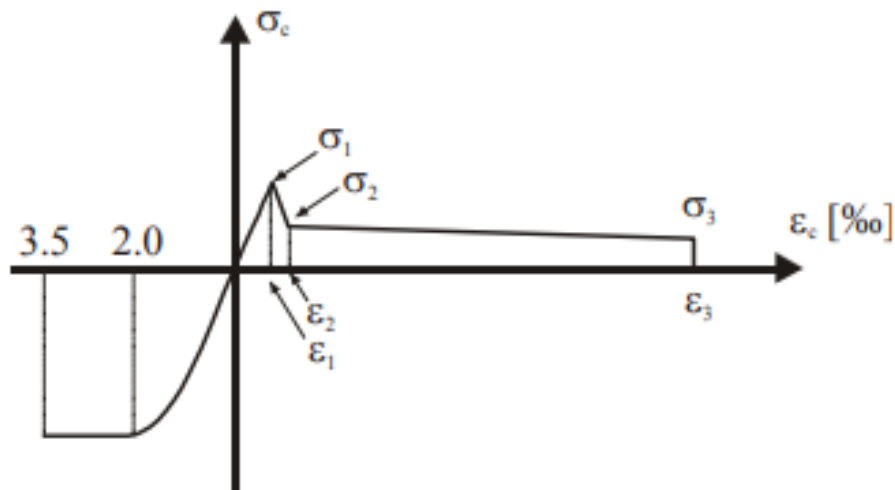


Figure 8-2 Stress-strain diagram

$$\sigma_1 = 0.7f_{actm.fl}(1.6 - d)(dinm)(N/mm^2) \quad \epsilon_1 = \sigma_1/E_c \quad (8-2)$$

$$\sigma_2 = 0.45f_{R,1}\kappa_h(N/mm^2) \quad \epsilon_2 = \epsilon_1 + 0.1‰ \quad (8-3)$$

$$\sigma_3 = 0.37f_{R,4}\kappa_h(N/mm^2) \quad \epsilon_3 = 25‰ \quad (8-4)$$

$$E_c = 9500f_{cm}^{1/3} \quad (8-5)$$

where κ_h is the size factor, which can be calculated based on Equation 5:

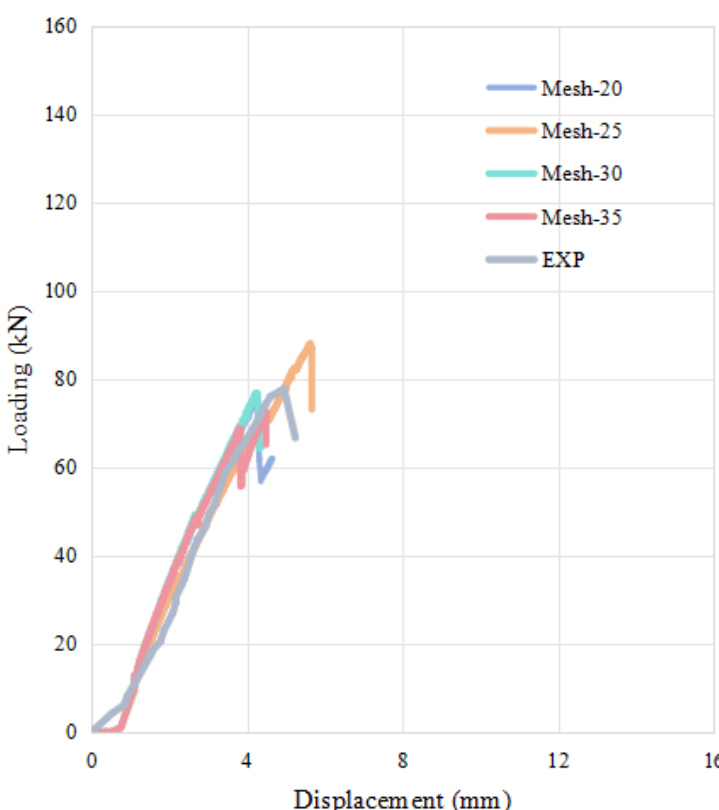
$$\kappa_h = 1.0 - 0.6 \frac{h[cm] - 12.5}{47.5} |12.5 \leq h \leq 60cm| \quad (8-6)$$

8.3 Analysis Results of the Reference Beam

8.3.1 MESH Effect

According to Table 8-1, the grid density, which is obtained by dividing the average length of the finite element edge by the height of the beam, is calculated. The grid density range is 0.2-0.35 in which aspect ratios close to 1 fall under the various elements consistent with three similarly efficient load-deflection relationship curve. The grid densities would express similar results at mesh densities ranging from 0.2 to 0.35 as they have similar properties. Mesh-30 in the grid produced a nearly perfect structured grid. It achieved 88%, 98%, and 100% experimental values in stiffness, bearing capacity, and peak displacement, respectively. In those cases, Mesh-30 was found to be suitable for impact simulation.

Table 8-1 Mesh analysis

Load-Displacement Curves	Mesh Control	Load(kN)	Displacement(mm)	Stiffness(kN/mm)
	EXP	77.68	4.95	20.82
	20.00	74.81	4.24	20.91
	25.00	87.97	5.63	20.93
	30.00	76.38	4.38	20.85
	35.00	72.49	4.51	20.82
	20/EXP	0.96	0.86	1.00
	25/EXP	1.13	1.14	1.01
	30/EXP	0.98	0.88	1.00
	35/EXP	0.93	0.91	1.00

8.3.2 Results Analysis of FEM

This analysis examines how closely the shear-midspan deflection computed from the FEM concurs with the practical findings for two SFRC reference beam specimens with a shear span-to-depth ratio of 2.5 in **Table 8-2**. While the FEM appears to simulate the shear-midspan deflection well, there are slight differences in bending resistance and midspan deflection at failure load. The FEM predicts a stiffer shear-midspan deflection curve than the actual beam prototypes during initial loading periods. This deviation in initial stiffness is linked to a few factors that could mainly include the occurrence of tiny cracks in the surface, contact surface specification, and cracking of the concrete envelope in the FEM. Due to the drying shrinkage and environmental issues, small surface cracks develop in concrete material, and such conditions are not mirrored in FEM. Additionally, the model uses a hard contact approach for the contact surfaces, which contributes to a phase of no deformation at the start of loading, signifying that the load is transferred to the supports. The load transfer happens via surface concrete cracks in the actual beams due to loading, whereas this minor crack can't be modelled in FEM since it cannot mimic soft contact. Additionally, the initial stiffness distinction in the numerical deflection response is associated with bond slip between steel bars and concrete. Although the ABAQUS software employed the constraints on the embedded region to simulate good bonding, this idealistic approach might result in a perceptibly higher initial stiffness measurement in the actual beams, as perfect bonding doesn't happen in real-world conditions.

Table 8-2 Results analysis

Load-Displacement Curves	Specimen	Load(kN)	Displacement(mm)	Stiffness(kN/mm)
	EXP-0.4	77.68	4.95	20.82
	EXP-0.8	101.70	5.55	20.50
	FEM-0.4	76.38	4.28	20.85
	FEM-0.8	103.58	5.15	20.87
	0.4-FEM/EXP	0.98	0.86	1.00
	0.8-FEM/EXP	1.02	0.93	1.02

8.3.3 Failure Mode Analysis

After comparing the crack propagation patterns in the experiments to those in the FEM, there's a clear similarity trend as shown in **Figure 8-3**. Comprehensively evaluating the final damage states using the FEM indicates the condition at which the component can no longer bear load. After the damage states of the tested experimental specimens were evaluated, it was evident that the cracks occur mainly within the unconfined regions. A loading and support locations initiate diagonal cracks, which propagate from the load locations through the supports to about 90% of the beam's depth until they lead to the beam's failure. All the reference beams specimens failed due to shear failure, which is consistent with experimental observations.

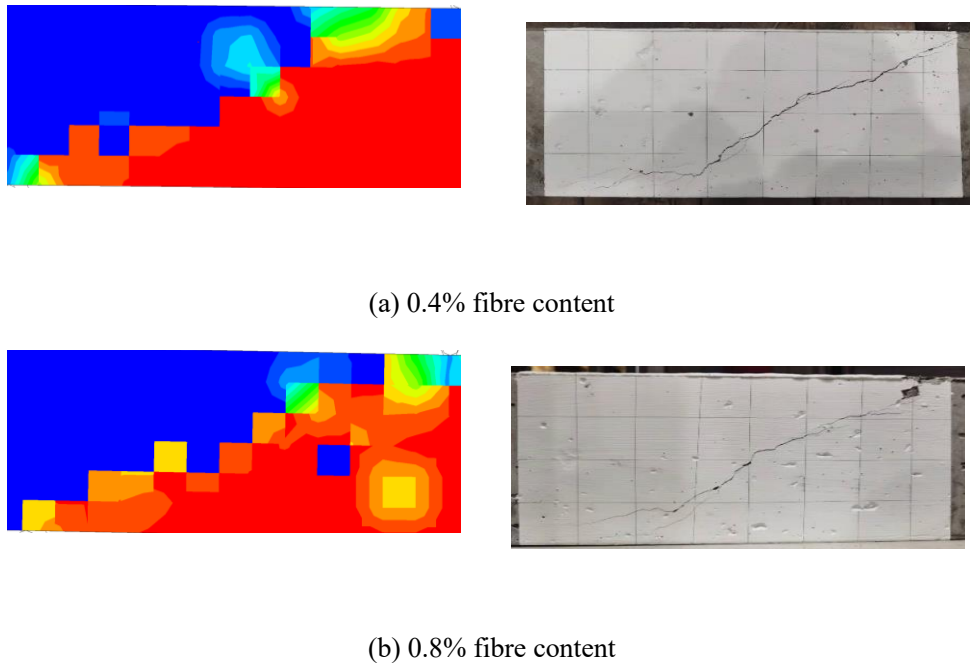


Figure 8-3 Failure model

8.4 Parametric Studies

8.4.1 Effect of Shear Span Ratio

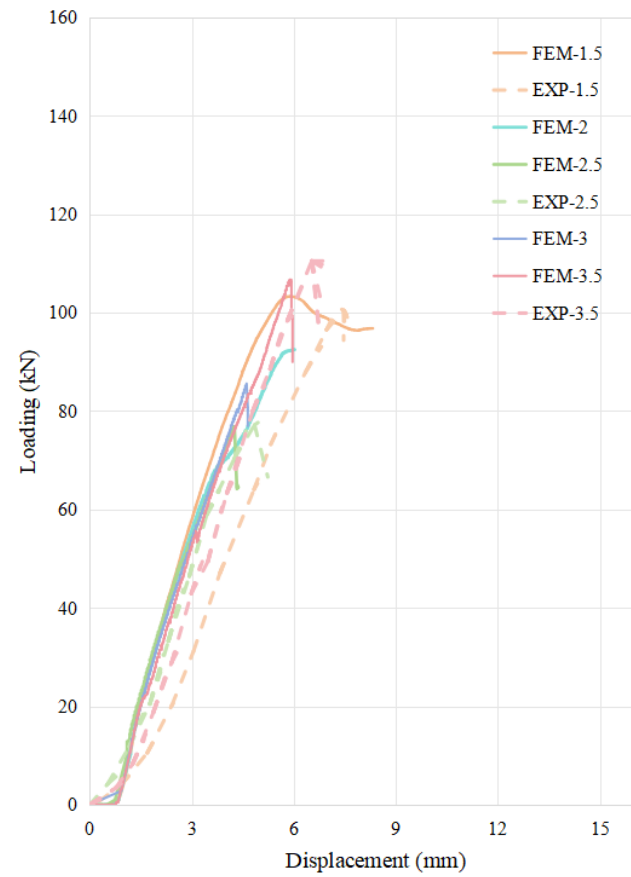
The shear capacity of the SFRC beams has varying impacts as a function of the shear span-to-depth ratio. Given constant beam measurements and an included steel fibre content of 0.4%, a range of factors, including loading positions and the size of the unconfined segment, were presented. According to data in **Table 8-3**, the expected load-displacement graph for the

different load ratios closely corresponds to the previously obtained experimental data. However, the simulation results indicated higher stiffness overall, likely due to size factors in beams with a shear span-to-depth ratio of 1.5.

Based on the FEM outcomes, the performance of SFRC beams is influenced by beam action between 2.5 to 6.0 prior to final failure, exhibiting flexural breakdown. The substantial growth in the ultimate load of SFRC beams from 10.8% to 28.4% is associated with an increase in the shear span ratio of 2.5 to 3 and 3.5. As the shear span ratio surpasses 2.5, the ultimate strength and its corresponding displacement increase, but the structure suffers from reduced stiffness. The reduced stiffness caused by the elevated shear span ratio results mainly from the increased loading zone.

Table 8-3 Comparison between referenced beams and FEM results

Load-Displacement Curves	Specimen	Load(kN)	Displacement(mm)	Stiffness(kN/mm)
	FEM-SP-1.5	106.74	5.91	19.52
	EXP-SP-1.5	100.68	7.41	22.70
	1.5-FEM/EXP	0.94	1.26	1.16
	FEM-SP-2	92.25	5.84	19.77
	FEM-SP-2.5	76.38	4.28	20.85
	EXP-SP-2.5	77.68	4.95	20.82
	2.5-FEM/EXP	1.02	1.16	1.00
	FEM-SP-3	85.59	4.65	19.81
	FEM-SP-3.5	106.64	5.91	20.01
	EXP-SP-3.5	110.52	6.53	20.25



3.5-FEM/EXP

1.04

1.10

1.01

8.4.2. Effect of Fibre Content

Table 8-4 suggests a notable improvement in ultimate strength and relative displacement of reinforced beams by increasing RSF and ISF content. Ultimate loading shows a significant 32.6% growth in the presence of 1.2% ISF content at a shear span-to-depth ratio of 2.5, while it reaches 40.7% at the same ratio when RSF increase. Nonetheless, the ultimate loading increase is more significant at a larger shear span-to-depth ratio because of the expanded steel fibre action area. Additionally, the link between fibres improves with an increase in fibre content, making their interaction smoother. This rise in RSF and ISF role in transferring concrete's internal loads can make micro-crack damage late, reducing the risk of reinforcing bar-concrete bond fracture, ultimately enhancing beam performance quality.

8.4.3 Effect of Fibre Type

Given that residual stress is a fundamental aspect that defines fibre attributes, using the constitutive model derived from residual stress experiments can effectively anticipate the behaviours of diverse fibre types in structures. This study, therefore, employed a consistent calculation formula for both ISF and RSF. The difference between the RSF-reinforced concrete beam model and the actual results was small, with slightly lower predictive accuracy compared to the ISF reinforced concrete beam (as noted in **Table 8-4**). Notably, the RSF demonstrated a comparably slightly lower ability to improve the structural shear capacity than ISF when comparing the experimental as well as simulated results. Specifically, when the fibre content was maintained at 0.4% and the shear span-to-depth ratio remained at 2.5 in the FEM, including RSF led to a percentage of ISF shear strength beams, compared to 98.2% at 0.8% fibre content and 76.5% for ISF beams and 96.2% at a fibre content of 1.2%. However, the ability to incorporate RSF beams within the structure depended on the consistency of the raw materials derived from worn tyres. It is complex because the raw materials have diverse fatigue levels and the tyre's steel wire attachments can differ. Therefore, the predictions of material uncertainties can provide insights into how hydraulic performance and enhanced land application of waste-derived residue can be achieved.

Table 8-4 Comparison between ISF and RSF reinforced concrete beams.

Load-Displacement Curves	Specimen	Load(kN)	Displacement(mm)	Stiffness(kN/mm)
	FEM-ISF-0.4	76.38	4.28	20.85
	EXP-ISF-0.4	77.68	4.95	20.82
	0.4-ISF-FEM/EXP	0.98	0.86	1.00
	FEM-ISF-0.8	103.58	5.15	20.27
	EXP-ISF-0.8	101.70	5.55	20.50
	0.8-ISF-FEM/EXP	1.02	0.93	0.99
	FEM-ISF-1.2	113.34	6.01	20.12
	FEM-RSF-0.4	75.00	4.47	19.81
	EXP-RSF-0.4	64.60	3.84	20.22
	0.4-RSF-FEM/EXP	1.16	1.16	0.98
	FEM-RSF-0.8	79.02	4.80	19.71
	EXP-RSF-0.8	78.42	5.60	20.22
	0.8-RSF-FEM/EXP	1.01	0.86	0.97
	FEM-RSF-1.2	109.01	6.03	19.53

8.5 Sensitivity Analysis by Surrogated Finite Element Analysis

This study has developed a robust FEM to predict the reliability of simply supported beams constructed from ISF and RSF concrete after evaluating the recommended model vis-à-vis experimental results. Nonetheless, using FEM in real-world applications is often computationally intensive because the relationship between parameter inputs and potential results makes finding the best solution for structural optimization or parameter regression issues solely via FEM difficult [170]. A surrogate model was therefore created based on established finite element analysis findings to minimize issues related to slow computation and FEM convergence challenges [171].

This surrogate model replaces the complex FEM, giving results close to the desired ones and augmenting computational efficiency [171]. This study looks to establish a high-dimensional Kriging Surrogate Models (KSM) based on the FEM and three key parameters. Such a system allows a broad analysis of the factors' reliability while making the sensitivity analysis of these parameters easy later. Gaussian processes' pertinence in modifying structural finite element methods has been shown by Response Surface Methodology (RSM). Using FEM data, this research intends to develop a surrogate model and investigate parameter reliability. For a better understanding of research route of this study, **Figure 8-4** was built.

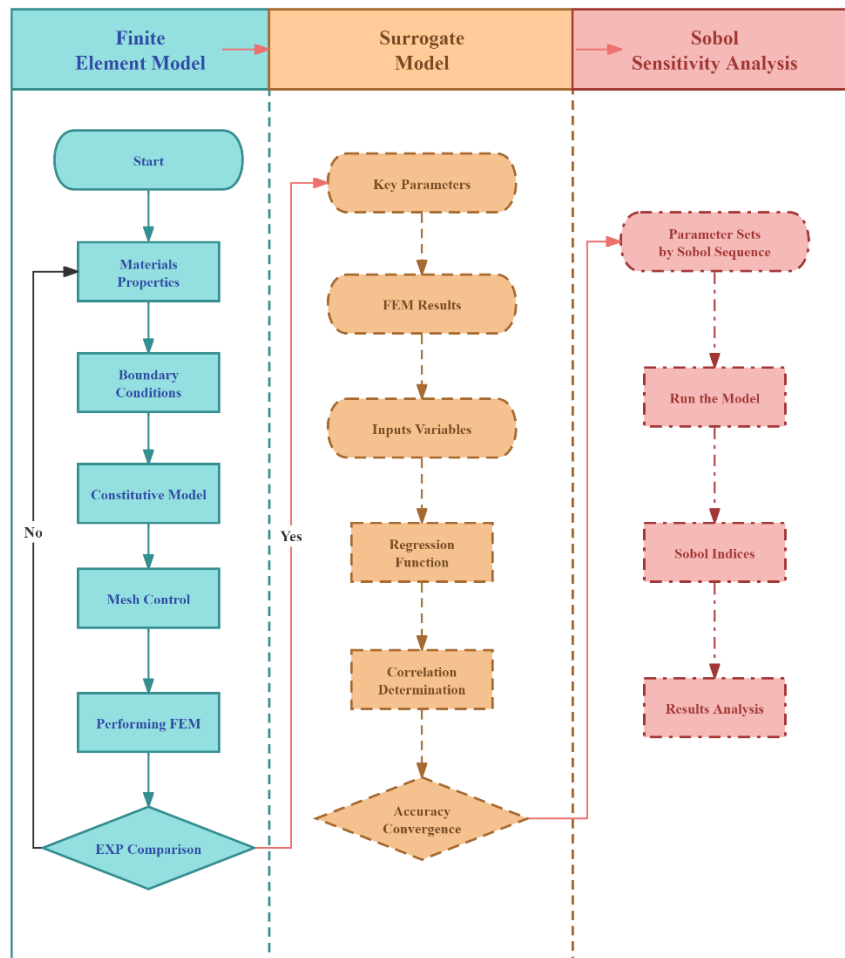


Figure 8-4 Research route of surrogate model

8.5.1 Kriging Surrogate Model

The mathematical description of the KSM is written as the following equation [172].

$$y(\mathbf{x}) = \sum_{j=1}^n \beta_j f_j(\mathbf{x}) + z(\mathbf{x}) = \mathbf{f}^T(\mathbf{x})\boldsymbol{\beta} + z(\mathbf{x}) \quad (8-7)$$

Where the function set $\mathbf{f}^T(\mathbf{x}) = [f_1, f_2, \dots, f_n]^T$ and vector set $\boldsymbol{\beta} = [\beta_1, \beta_2, \dots, \beta_n]^T$. The $z(\mathbf{x})$ used to makes the classical linear regression model become a stationary Gaussian random process model with zero mean and covariance[173].

$$Cov[z(x^i), z(x^j)] = \sigma^2 R(x^i, x^j) \quad (8-8)$$

Where the σ^2 is the process variance of the KSM and R is the correlation kernel. The valid correlation kernel $R(x^i, x^j)$ satisfies two conditions: first, the input domain is symmetrical and, second, the resulting correlation is a positive semi-definite matrix.

$$R(x^i, x^j) = R(x^j, x^i) \quad (8 - 9)$$

The correlation kernel is usually described by a function of the distance.

$$R(x^i, x^j) = R[d(x^i, x^j)] \quad (8 - 10)$$

Then, if the correlation kernel R is the power-exponential function, the covariance is computed as the equation below.

$$Cov[z(\mathbf{x}^i), z(\mathbf{x}^j)] = \sigma^2 \cdot \exp \left[- \sum_{k=1}^d \frac{|x_k^i - x_k^j|^{p_k}}{\theta_k} \right] \quad (8 - 11)$$

The array of spatial correlation kernels commonly employed includes Linear, Exponential, Gaussian, and Power-exponential[173]. The study prefers the Gaussian kernel over other choices because it offers a more stable and accurate way to reduce challenges associated with dimension reduction. This choice hinges on the fact that the Gaussian kernel has a very smooth function that can have an infinite number of derivatives. Such smoothness proves crucial for an in-depth analysis of parameters within many dimensions, making the Gaussian kernel the best choice for this study.

8.5.2 Sobol Variance-Based Sensitivity Analysis

Sobol's technique breaks down the output model's variance into the variance components that correspond to input factors across dimensions that increase [174]. It is possible to discover the

independent roles of each input factor as well as their relationships to the cumulative variance of model outcomes by using Sobol sensitivity analysis. This analysis aids in examining how changes in model output are attributable to specific parameters or their interplays [175]. Similar to traditional analysis of variance in factorial studies, this method deconstructs output variance. It is critical to understand that the primary purpose of Sobol sensitivity analysis is not to determine the sources of variability in the input. Instead, it emphasizes the significance of such variability's impact on model output and its extent.

Let $Y = g(\mathbf{X})$ is the representation of the model response function, while $\mathbf{X} = (X_1, X_2, \dots, X_n)$ denotes the n-dimensional input vector and Y signifies the scale output variable. It is assumed that all input variables are mutually independent.

$$f_{\mathbf{X}}(\mathbf{x}) = \prod_{i=1}^n f_{X_i}(x_i) \quad (8-12)$$

where $f_{\mathbf{X}}(\mathbf{x})$ stands as the joint probability density function (PDF) of X, while $f_{X_i}(x_i)$, represents the marginal PDF of x_i , respectively. With the hypothesis that all the input variables are independent with each other, the model output variance $V(Y)$ can be decomposed into $2^n - 1$ partial variance of increasing orders:

$$V(Y) = \sum_{i=1}^n V_i + \sum_{i \neq j} V_{ij} + \dots + V_{12\dots n} \quad (8-13)$$

$$\begin{aligned} V_i &= V(E(Y | X_i)) \\ \text{Where } V_{ij} &= V(E(Y | X_i, X_j)) - V_i - V_j \\ V_{ijk} &= V(E(Y | X_i, X_j, X_k)) - V_{ij} - V_{ik} - V_{jk} - V_i - V_j - V_k \end{aligned}$$

If the $S_i = V_i/V(Y)$, $S_{ij} = V_{ij}/V(Y)$, then let:

$$\sum_{i=1}^n S_i + \sum_{i \neq j} S_{ij} + \dots + S_{12\dots n} = 1 \quad (8 - 14)$$

S_i is the first order effect index of X_i and based on the Equation 8, Homma and Saltelli[176]

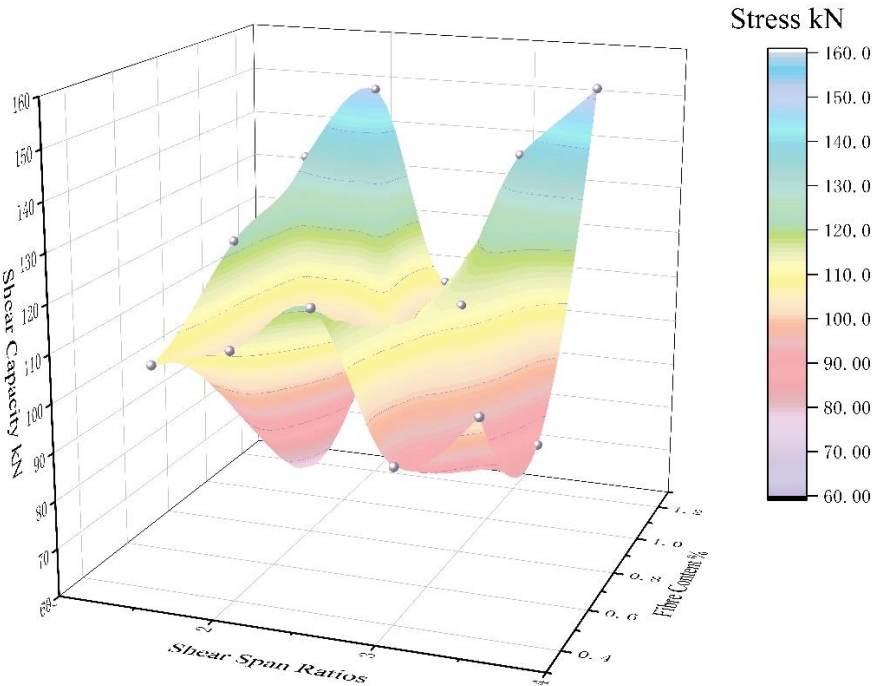
introduced the total effect index:

$$S_{Ti} = S_i + \sum_{j=1, j \neq i}^n S_{ij} + \dots + S_{12\dots n} = 1 - S_{-i} \quad (8 - 15)$$

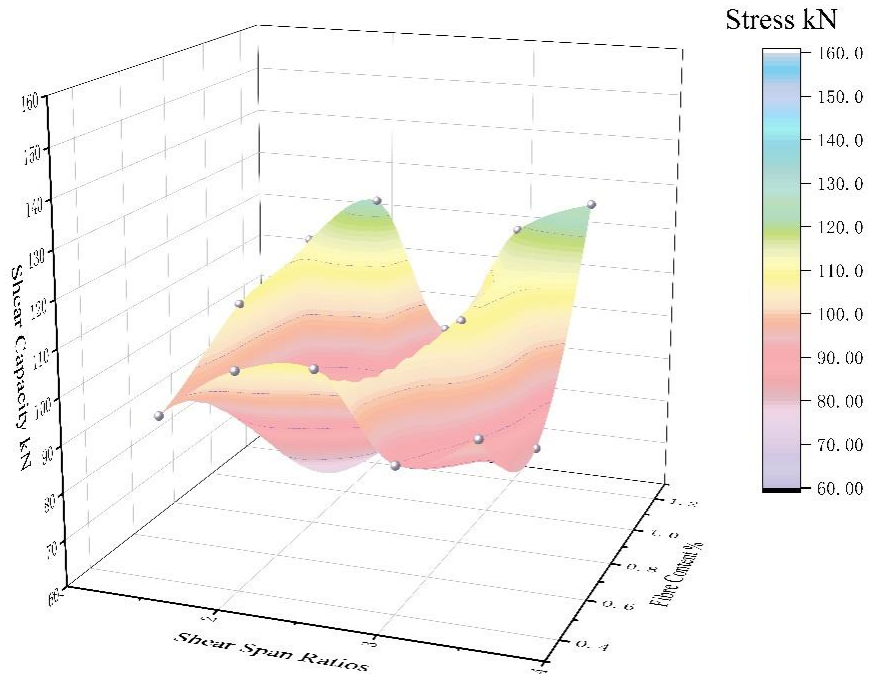
8.5.3 Result of Sensitivity Analysis

KSM reduce computational complexity and facilitate faster problem solution. The study's surrogate model greatly speeds up optimization by using simpler models that lessen computation and accelerate solution time. This specific model is highly consistent with an R^2 of 0.9997, guaranteeing accurate findings. The model's conclusions are shown in **Figure 8-5** as a smooth 3D graph, visually showing how shear strength is linked to shear span ratios and fibre content.

Figure 8-5 reveals that the RSFRC beams have less variance in shear strength compared to their ISFRC counterparts despite following similar trends. To explore the influences of shear span ratio, fibre content, and compressive strength on shear capacity further, a Sobol sensitivity analysis was carried out. This technique is beneficial in assessing the individual contributions of different parameters to shear capacity, thus enhancing the design optimization process.



(A) ISFRC



(B) RSFRC

Figure 8-5 3D smooth graph

The sensitivity matrix for the KSM is shown in **Figure 8-6**. The results include the first quartile (Q1) and the third quartile (Q3) representations. A sampling size of 5,000 points was established in this research. In a sensitivity analysis, a significance level of 0.050 differentiates variables that are relevant from those that are not. This threshold implies that if the sensitivity index is less than 0.05, the variable is not significant.

The initial sensitivity analysis and full sensitivity analysis results should be carefully considered to ensure correct parameter interplay accounting in complex models. Fiber content and shear span ratio have the most substantial impact on the shear capacity of SFRC beams, while the effect of compressive strength is relatively small. These factors' significance differs between different SFRC beam types, with RSF content resulting in weaker shear capacity and thus lower sensitivity indices. Total sensitivity analysis shows that fibre content has the most significant impact on the tensile strain distribution in ISF-reinforced beams, contributing to over three-quarters of the variation; however, its influence is less than half in RSF-reinforced beams.

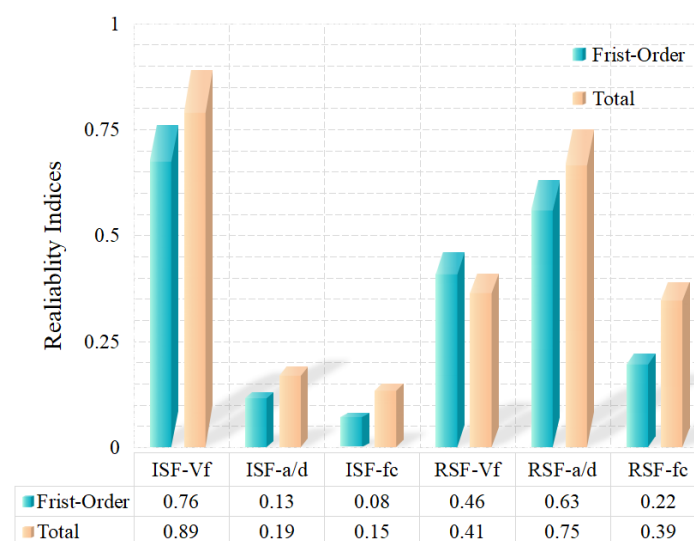


Figure 8-6 Reliability indices

8.6 Application of FEM for Flexural Strength Prediction

Once researchers develop a robust and consistent model, effectively implementing it in practice becomes the next significant challenge. This article intends to enhance the TR63 standard's current formula for estimating the flexural strength of SFRC beams by using FEM to analyse internal stress and strain distribution..

8.6.1 Evaluated the existing formula

The theoretical model for the bending strength of SFRC beams focuses on conventional reinforced concrete. Regularly reinforced concrete beams do not consider the concrete's increased tensile capacity. Additives in SFRC, on the other hand, enhance this capacity. A study of previous research showed that SFRC beam stress-strain models are formulated as shown in **Figure 8-7**. According to the TR63 guidelines, concrete's tensile strength is represented by the left residual tensile strength, showing that ISF can provide some elastic support even after the structure cracks. According to TR63, the expression for the residual tensile strength (f_{td}) is as follows[177]:

$$f_{td} = 0.37R_{e,3}f_{ctkfl}/\gamma_c \quad (8 - 16)$$

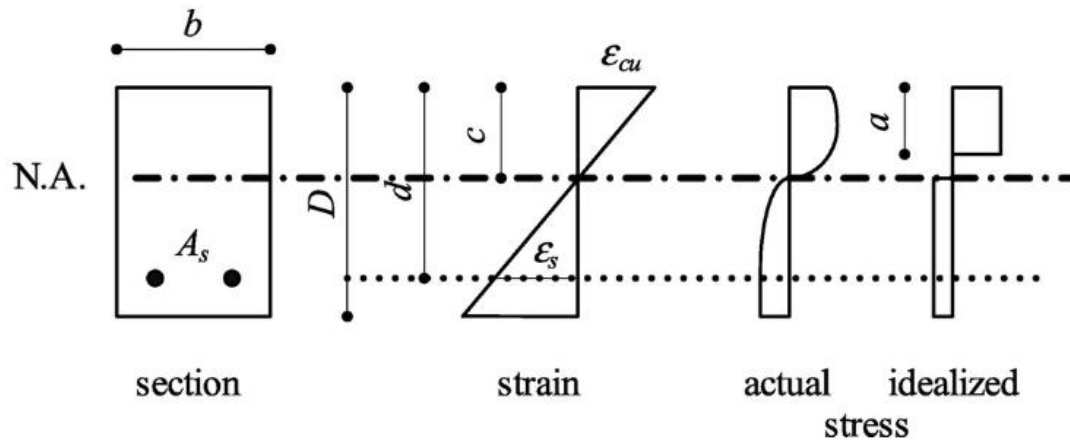
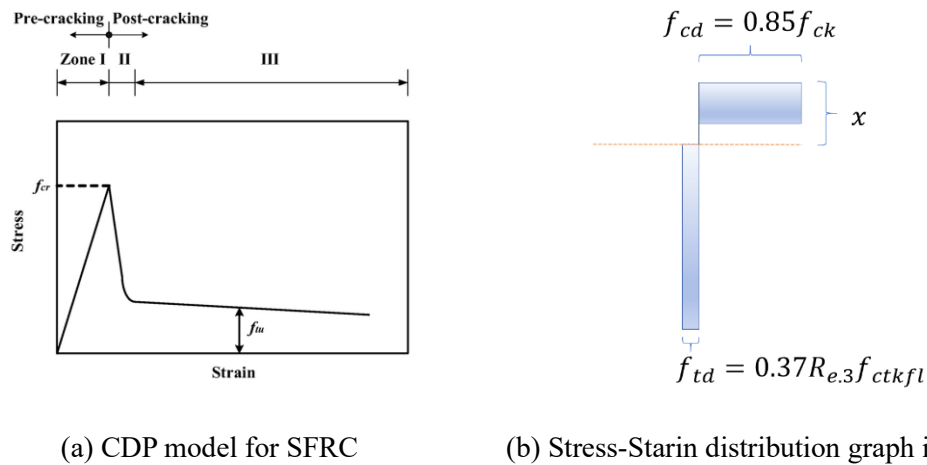


Figure 8-7 Stress-strain distribution graph



(a) CDP model for SFRC

(b) Stress-Strain distribution graph in TR63

Figure 8-8 Stress-strain distribution in TR63

The residual tensile strength suggested by TR63 is obtained from the residual tensile stress delineated in the RILEM TC 162-TDF CDP model (as highlighted in **Figure 8-8(a)**). This experiment will leverage FEM model output to authenticate the variables attributable to TR63 in line with the RILEM TC 162-TDF CDP model..

8.7 FEM application in flexural prediction

Controlling the mesh in Abaqus determines the structural stress and strain distribution. **Figure 8-9(a)** and **8-9(b)** present the flexural capacity of the beams with similar dimensions that was

attained by modifying the shear model. The interface was added to the original experimental structure to generate the model under maximum flexural load for beams with the same dimensions. **Figure 8-9(a)** shows the failure model underpinning the 2.5-0.8% Reference beam structure after it failed.

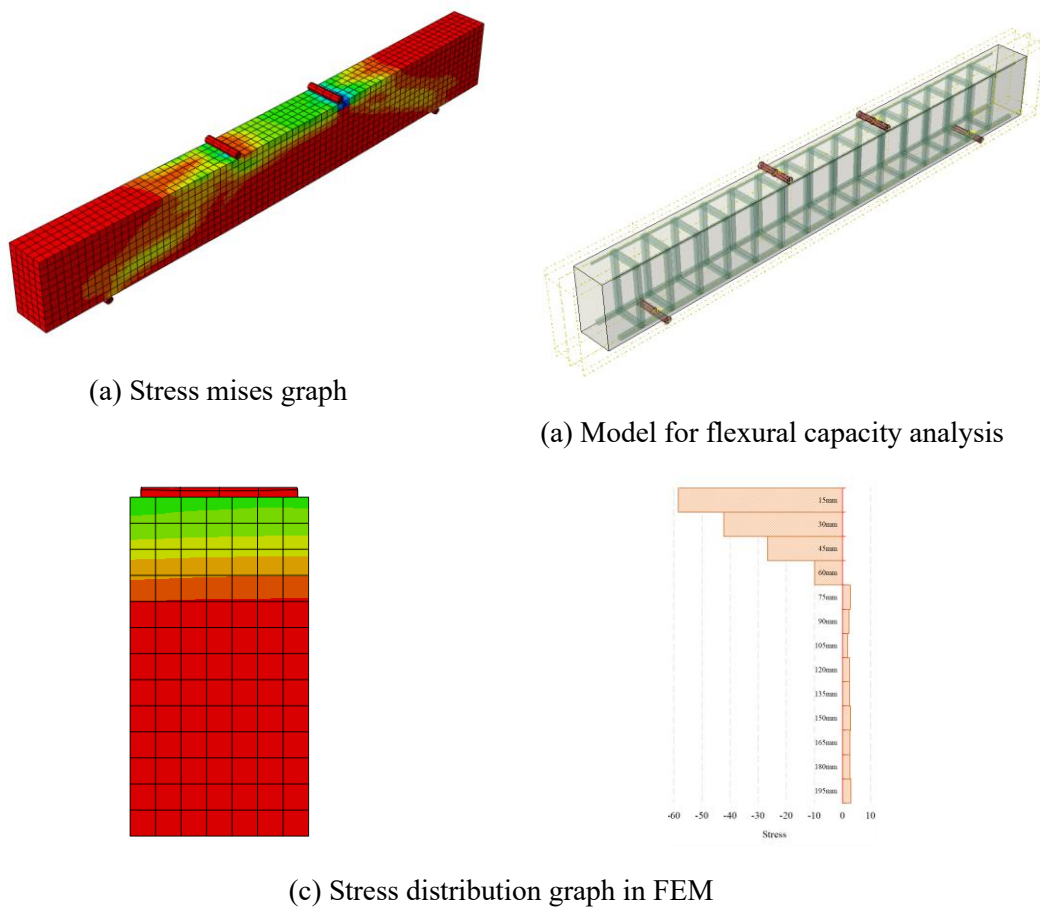


Figure 8-9 FEM model with stress plot analysis in the mid span

The clear line across the structure represents the neutral axis and separates the compression from the flexural zones in **Figure 8-9**. In the structural section beneath the neutral axis, stress values are indicated as positive, while above the neutral axis they are demonstrated as negative. Abaqus reveals that the part of the structure located below the neutral axis is under tension, while the region above it is under compression. It is possible to determine the elastic pressure

above the neutral axis since the interface stress can be obtained from the stress plot. This information is provided in **Figure 8-9(c)**, and the numerical results are compiled in **Table 8-5**.

It has been established that the stress area of the compression zone is almost the same as per the TR63 standard calculation, with computations differing by no more than 1.5%. Thus, there is no need to modify the formula for the compression zone stress calculation. However, the standard has several significant parameters related to RE that require the calculation of tensile zone stress to be handled with certain modifications. Following the acquisition of the sectional stress distribution, it is possible to perform a linear regression to determine the tensile limit of the SFRC in compliance with the TR63 standard according to the stress distribution. In this way, two different kinds of SFRC specimens were used to apply regression analysis to the tensile zone and determine the following equation:

$$T_s = A_s f_s \quad (8 - 17)$$

$$C_c = \beta_1 \beta_2 f_{ck} b c \quad (8 - 18)$$

$$T_f = (0.13 f_{R,4} \sqrt{f_{ck}} - 0.5 \sqrt{F})(D - c) \quad (8 - 19)$$

$$M_n = T_s I_1 + T_f I_2 = T_s \left(d - \frac{a}{2} \right) + T_f \left(\frac{D + c - a}{2} \right) \quad (8 - 20)$$

Where A_s is the areas of tensile reinforcement, and f_s is the yield stress of rebars. β_1 and β_2 are the compression zone factors which is 0.85 and 0.8, respectively. For this study, $f_{R,4}$ is the residual strength of SFRC, as used in Venkateshwaran, Tan and Li [113].

$$f_{R,4k} = \psi [0.177 (f_{ck})^{0.5} + 6.151 (F) + 0.137 N^2] \quad (8 - 21)$$

$$\psi = 1 + (L_f/100)^2$$

$$F = \phi V_f L_f / D_f$$

Where f_{ck} is compressive strength v_f is the fiber content, L_f is the fiber length, D_f is the fiber diameter. The reduction factor ϕ of RSF used in this study is 0.75 while for ISF, it is 1.

Table 8-5 Stress calculation results

	0.4-ISF	0.8-ISF	1.2-ISF	0.4-RSF	0.8-RSF	1.2-RSF
Compression Zone	2675.5	2694.5	2680.6	2647.4	2659.0	2649.0
Tensile Zone	259.2	362.0	515.6	227.2	252.2	291.9
Calculated Compression Zone	2549.5	2592.1	2640.9	2547.2	2587.4	2629.7
Maximum Moment						
Modified TR63	35.3	36.4	38.1	32.8	33.0	33.1
FEM Results	32.8	34.0	35.2	30.8	32.0	34.4
FEM/Calculated	1.08	1.07	1.08	1.06	1.03	0.96

8.8 Validation Analysis

To verify the suggested adjusted variation, this study documented the highest flexural resistance details for 183 SFRC beams, as presented in **Appendix A-4** and displayed in **Figures 8-9**.

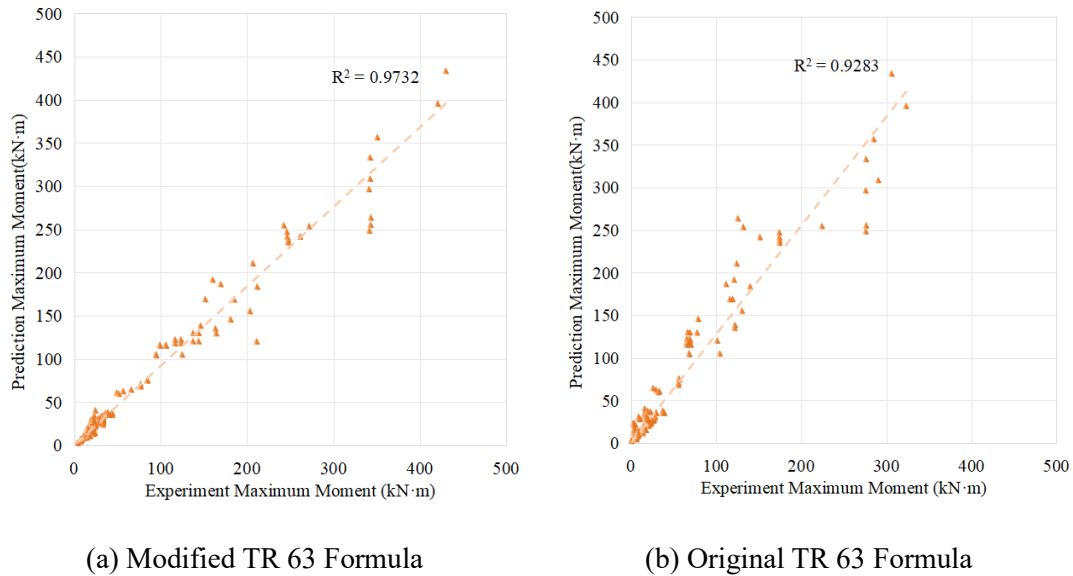


Figure 8-9 Formula validation

The TR63 modified equation, assessed using the integrated database, yielded 1.10 as the average ratio of computed to expected flexural strength. The gauge records a standard deviation of 0.152 and a coefficient of variation of 0.139, indicating variability among the tested specimens. Additionally, 12 beams exhibited a ratio of less than 0.9, equivalent to 9% of the total beams. Compared to the TR63 equation, the new equation boosted the R^2 value to 0.97, showcasing its robustness regarding correlation. The average ratio of measured to expected strength is close to 1 at 1.01.

The revised version of the TR63 equation is centered on an experimental CMOD formula. Even though the reduction factor wasn't used during the testing and forecasting, it was observed that the TR63 formula was somewhat conservative in prediction. The CMOD manufacturing process uses time-consuming and intricate procedures to prepare the specimens. A modified formula has been proposed that uses the empirical CMOD equation and is based on basic concrete characteristics and fundamental compression tests. The TR63 equation was developed

using CMOD specimens, and its forecast was found to be conservative. Due to the complex and time-consuming CMOD test specimen production process, an alternative formula based on empirical results and simpler concrete properties was developed.

8.9 Conclusion Remark

This study develops a FEM) framework for analysing SFRC beams, considering variations in fibre content, shear span ratios, and types of steel fibres (RSF and ISF). Using the RILEM TC 162-TDF CDP model, refined with residual stress testing, the research captures the interaction between SFRC and reinforcement effectively. Key findings show that beam ultimate strength improves with higher shear span ratios and increased fibre content, with RSF beams achieving 98.2% of the shear resistance of ISF beams at 0.4% fibre content. The study introduces a novel KSM based on FEM results and performs a sensitivity analysis, finding that fiber content and shear span ratio significantly affect shear strength, while compressive strength has minimal impact. A modification of the TR63 formula yields an R^2 value of 0.97, enhancing predictive accuracy.

In summary, the study provides an advanced FEM model for predicting shear resistance in SFRC structures, highlighting the importance of addressing size effects. The new model supports the practical use of RSF and contributes to sustainable construction practices by offering efficient, cost-effective methods and reducing material waste. While the developed predictive tools have demonstrated efficiency in forecasting shear strength and other key properties of SFRC beams, ensuring their safety and reliability remains crucial. Accurate predictions must be validated through rigorous reliability analysis to ensure they meet structural

safety standards. The next sections will focus on performing reliability analyses for the prediction formulas used for SFRC beams, aiming to validate their robustness and applicability in real-world scenarios.

9. Reliability Analysis of Different Perdition Methodology

Previous research has thoroughly examined and debated the shear capacity computation formula for HSFRC beams. Still, a detailed examination of the topic indicates that most predicted estimates are lower than what was witnessed in experiments [178, 179]. This apparent disagreement does not suggest a lack of accuracy in predictions; instead, it reflects a cautious analytical strategy that prioritizes structural safety. Through this rigorous strategy, the shear capacity of SFRC beams is intentionally reduced to guarantee structural longevity and dependability over theoretical potency projections.

It is argues that it is important to evaluate the formulas' predictive capability through reliability analysis to ensure the structural designs theoretically derived from them are constructed in accordance with the strictest safety and reliability codes. It outlines a detailed comparison of five significant shear capacity prediction formulas for both HSFRC and NSFRC beams, based on an extensive review of the associated literature. Moreover, it reviews the performance of these formulas across different load combinations such as seismic, snow, wind, dead, and live loads using reliability analysis methods, including Second-order Reliability Method(SORM) and First-order Reliability Method(FORM), and presents its findings.

The professional coefficients (β) inside a reliability investigation rely on data from tests on 142 HSFRC and 265 NSFRC beams leading to shear failure. The information, thought to be unparalleled in terms of uncertainty evaluation, is assembled from a comprehensive review of published research. It contains a precise evaluation of existing shear engineering standards, which are utilized as a foundation for the analysis. The most effective predictor equation model for both HSFRC and NSFRC beams is decided through a detailed examination.

9.1 Datasets Analysis

The study compiles two large collections of HSFRC and NSFRC beams for reliability analysis. Details are available in **Appendix A-3 and A-5**. Based on denoising, the dataset of SFRC was reduced to 142 beams. These collections incorporate 265 NSFRC beams and 142 HSFRC

beams' lab experiments.

Table 9-1 Statistical properties of the dataset

	NSFRC Beams			HSFRC Beams		
	Min	Mean	Max	Min	Mean	Max
Compressive Strength	53.00	75.79	154.00	9.77	38.00	61.10
Shear Span Ratio	0.70	2.71	6.00	0.90	3.07	5.00
Fibre Factor	0.00	0.65	3.82	0.06	0.59	5.73
Longitudinal Ratio	0.01	0.03	0.06	0.02	0.01	0.06

In **Table 9-1**, the empirical formula for fibre factor is expressed as follows:

$$\xi = V_f \times \frac{l_f}{d_f} \quad (9 - 1)$$

With ρ_1 representing the longitudinal steel area ratio, f_c standing for the compressive strength of concrete, and a/d as the shear span ratio. Generally, established shear capacity estimation formulas for HSFRC and NSFRC beams are classified based on three criteria: regression analysis, component contribution analysis and machine learning models. Using the initial assessment of available publications, this study identified the most effective existing formulas in each category. There are ref [180] and [181] selected for NSFRC beams; ref [182] and [183] for HSFRC beams; ref [184] and [185] for ML technology.

9.1.1 Prediction Model with ML

Shear formulas for SFRC beams without stirrups were established using a genetic tree algorithm in Ref [184]. Instead of relying on conventional mechanical analysis and theoretical derivations,

Kara's model, which differs from the traditional design approach, identifies key independent variables and determines their relationships with dependent variables using vast data analysis. The relationships between the variables are the main focus of Kara's model as opposed to mechanical principles. The approach focuses on quantitative investigations, and the formal model is as follows.

$$v_{frc} = \left(\frac{\rho_1 d}{c_0 c_1 \left(\frac{a}{d} \right)} \right)^3 + \frac{F_1 d^{\frac{1}{4}}}{c_2} + \frac{c_3^{\frac{1}{2}} \sqrt{f_{ck}}}{d^{\frac{1}{2}}} \quad (9-2)$$

with

$$F_1 = \beta V_f \frac{l_f}{d_f} \quad (9-3)$$

In the model, the constants are defined as $c_0=3.324$, $c_1=0.909$, $c_2=2.289$ and $c_3=9.436$.

Ref [185] proposed a ML based formula using a gene expression programming approach. The crucial distinction between the two models is the data source size and the model's complexity: the author expanded the sample size to 241 and simplified the formula, yielding higher accuracy:

$$v_{frc} = \left(\left(\frac{-4.83}{\rho_1} \right) \times (f_{ck} - \rho_1) \right)^{0.2} \times \left(\rho_1 + \frac{F_1}{\rho_1} \right)^{0.25} \times \frac{(F_1 \times (-2.18) - \rho_1)}{F_1 + \frac{a}{d}} \quad (9-4)$$

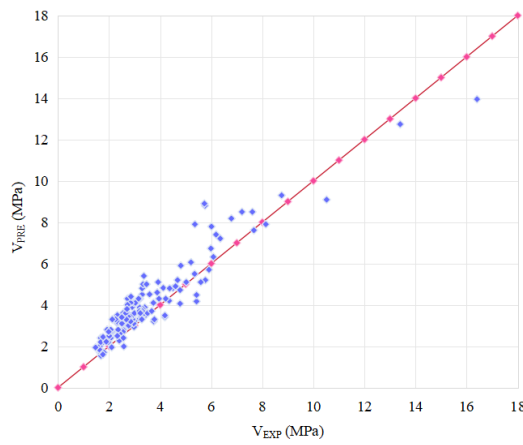
The new formula is both more accurate and easier to understand than Kara's formula. Factors of 0.667 may be used to attain the same bending capacity reduction in RC beams. This paper evaluates the formula itself but does not employ such factors.

9.2 Uncertainty Analysis

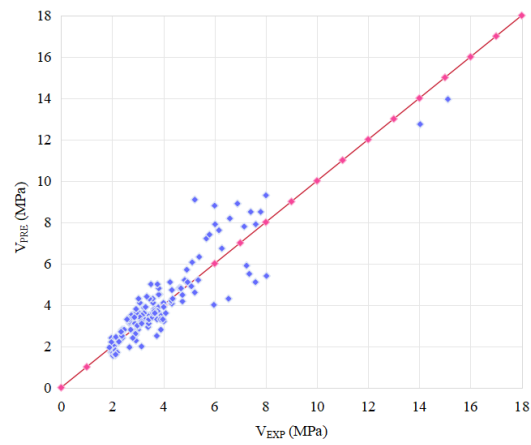
M Model uncertainty quantifies the differences between expected and actual outcomes by representing them as random variables, allowing for estimation changes. Unpredicted variation in

the behaviour of idealized conditions adds to uncertainty. Previous research has integrated model uncertainty to correct gaps between anticipated and actual results. For reliability assessment, cognitive uncertainty quantification is utilized to account for unknowns. This incorporates an overall model uncertainty value (θ_R) to quantify possible variance sources.

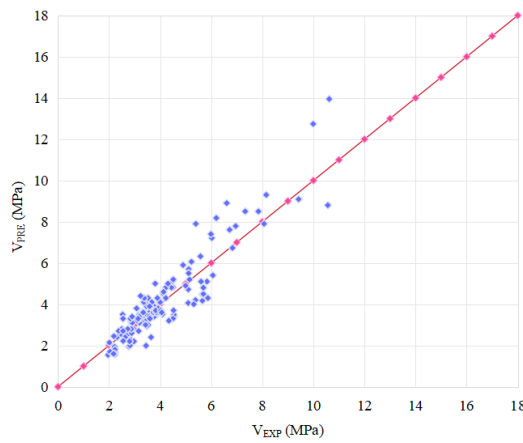
$$\theta_R = \frac{V_{EXP}}{V_{PRE}} \quad (9-5)$$



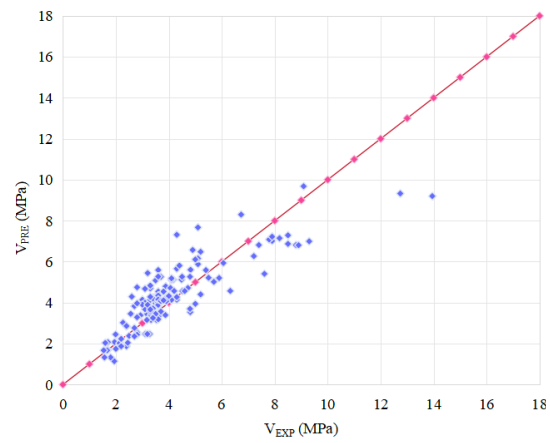
(a) HSFRC for Ashour model



(b) HSFRC for Kara model



(c) HSFRC for Al-Ta'an model



(d) HSFRC for Tarawneh model

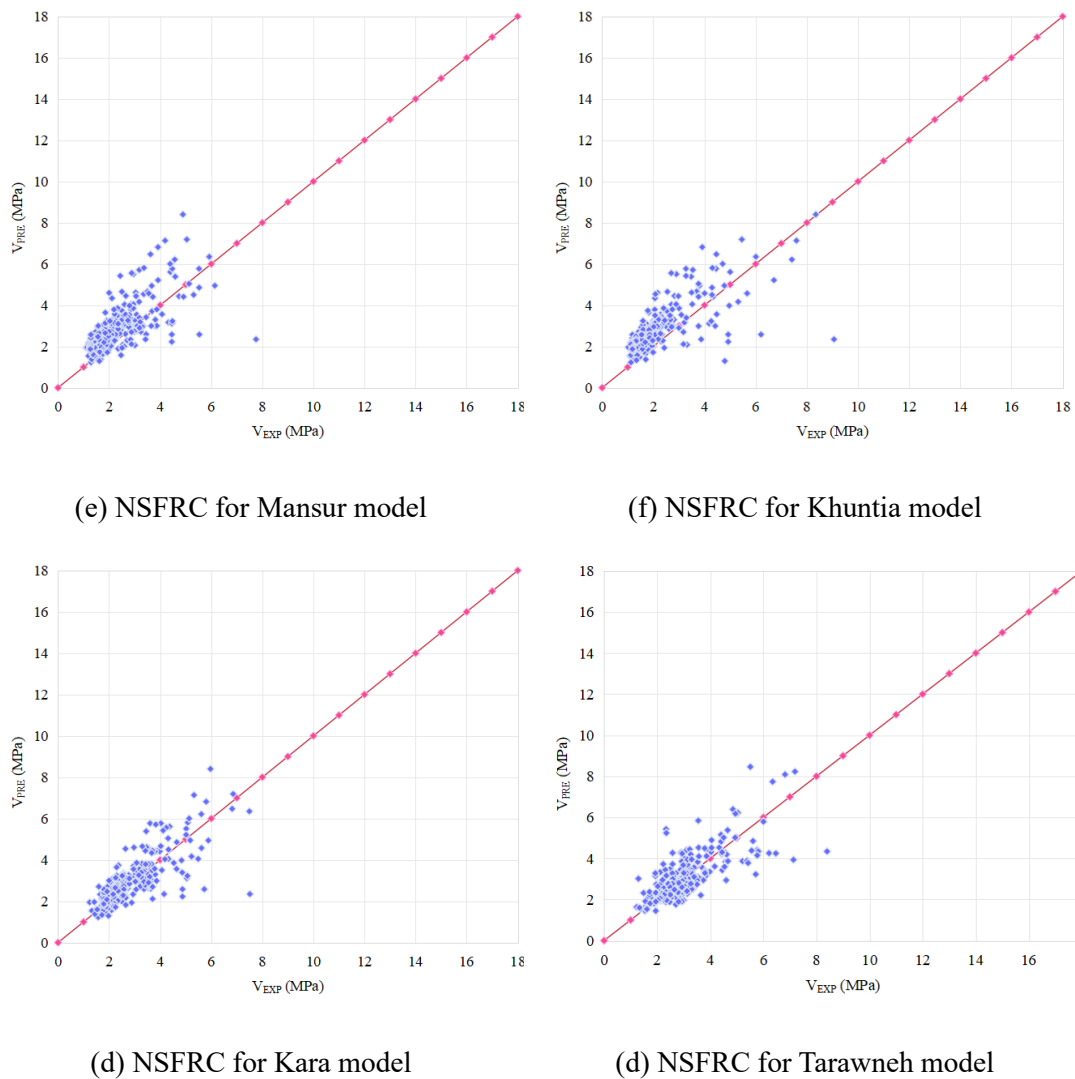


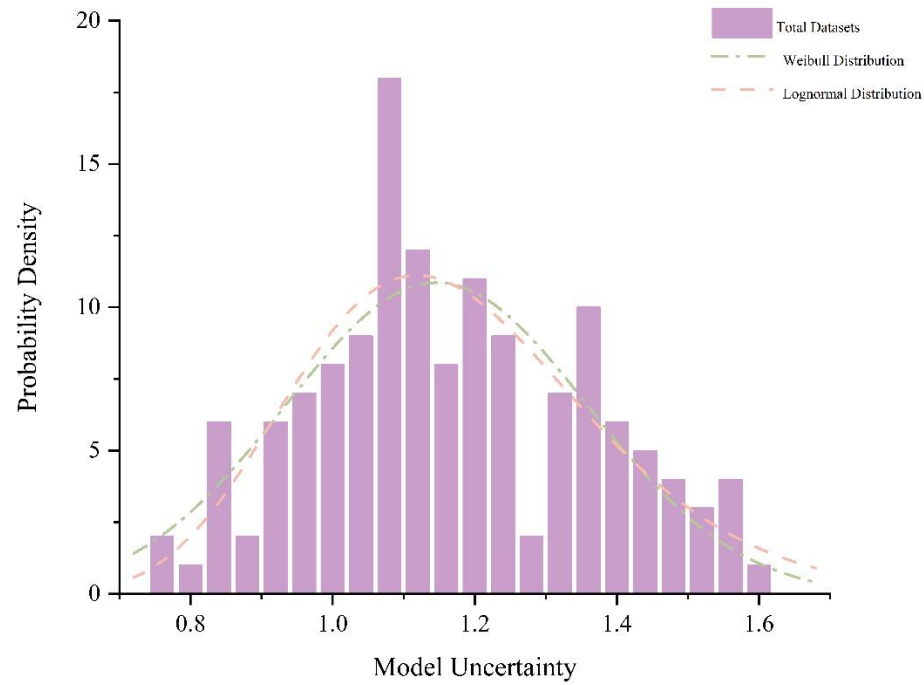
Figure 9-1 Model uncertainty analysis

The Anderson-Darling test is implemented to assess the probability distribution of θ_R for each mechanical model before conducting the reliability analysis. This article examines four widely used probability distributions—including Gaussian, lognormal, Weibull, and extreme value type I—using SciPy's data library in Python. The recommended distribution and the second-best distribution for describing the variability are taken into account based on statistical results.

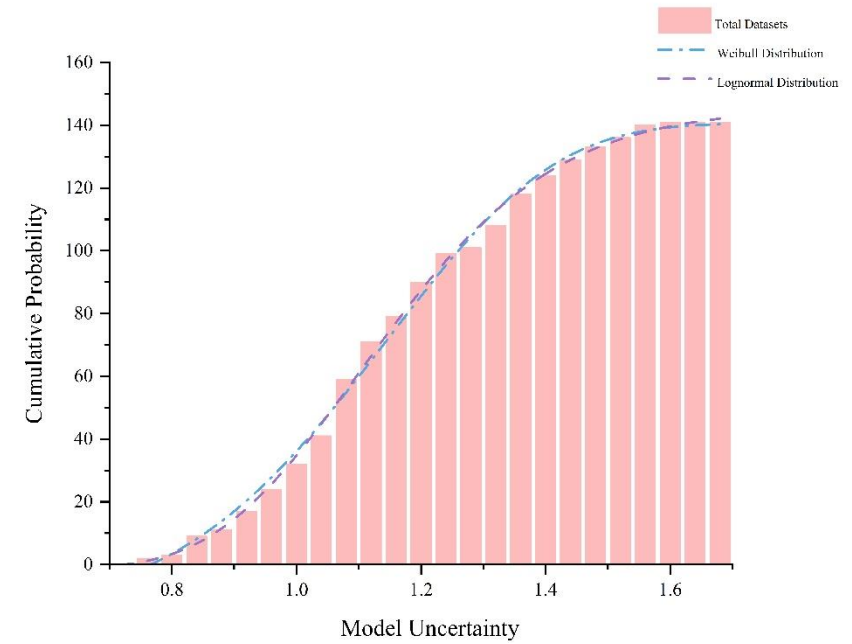
The graphs of the probability density function (PDF) and cumulative distribution function (CDF) for shear strength forecast models considering different SFRC beam strengths in **Figure 9-2** demonstrate the accuracy of the suggested distribution. A p-value greater than or equal to 0.05 highpoints to a great fit of the expected distribution to the data during Anderson-Darling test.

Therefore, a higher p-value suggests how small the inaccuracies get in the anticipated distribution, which suggests a better fit.

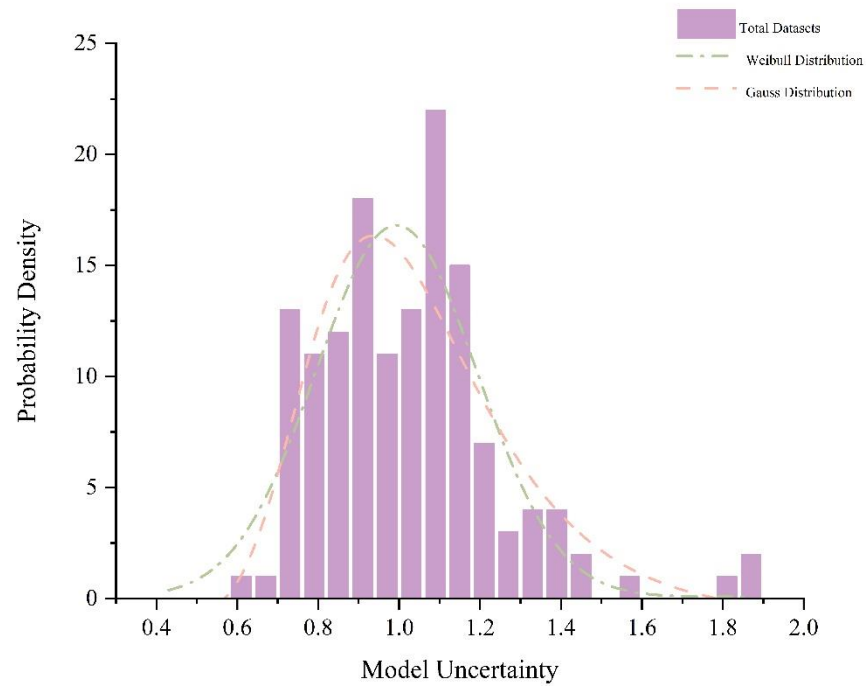
According to **Figure 9-2** and **Table 9-3**, the Weibull distribution is the most accurate for θ_R in the Ashour, Hasanain and Wafa [182] and Kara [184] models. The Al-Ta'an and Al-Feel [183] model, however, fits better with the Gaussian distribution. In the prediction models for the NSFRC beam, distributions that fit θ_R are the lognormal distribution in the Kara [184] and Khuntia, Stojadinovic and Goel [181]. The Weibull distribution aligns better with Mansur, Ong and Paramasivam [180] model in will ultimately be using the Weibull distribution. The Weibull, lognormal, and Gaussian distributions are widely used in structural reliability analysis for θ_R . The study, however, focuses on the Weibull distribution. It predicts the model values to be conservative for HSFRC beams, meaning there is an evident left skew in the CDF, PDF, and distribution histograms.



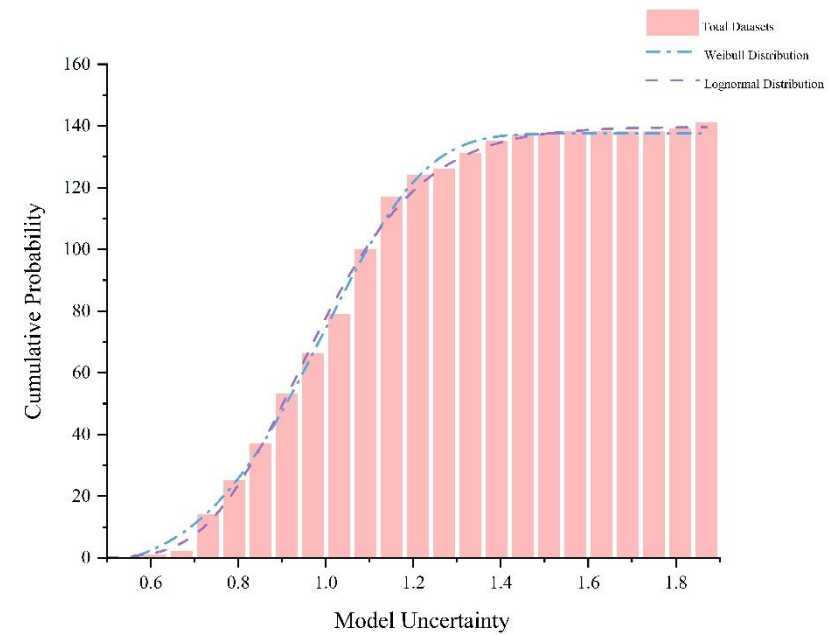
(a) HSFRC for Ashour model (PDF)



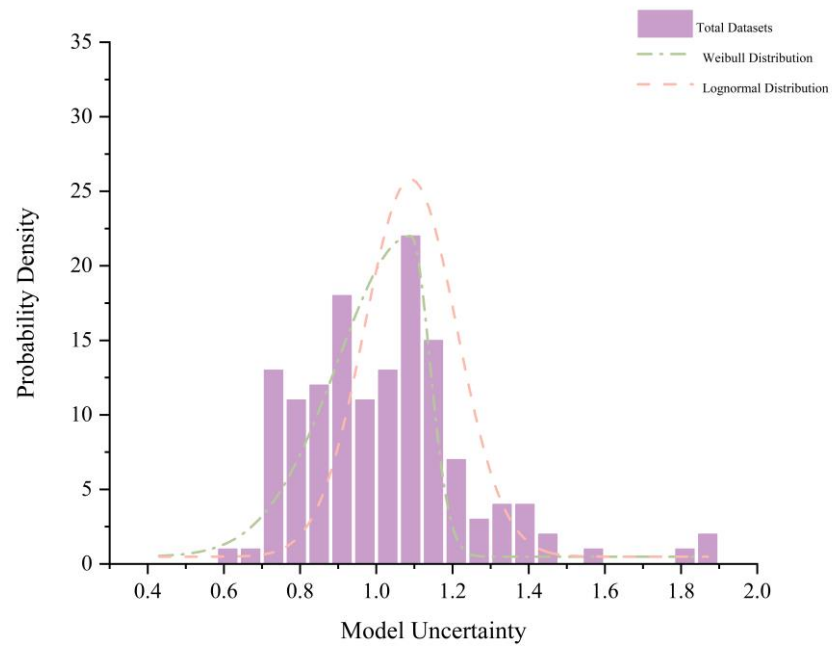
(b) HSFRC for Ashour model (CDF)



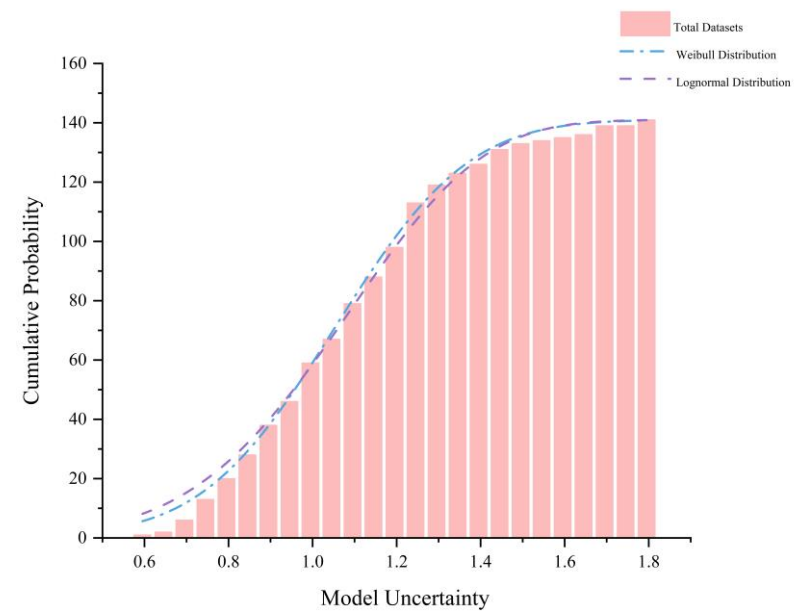
(c) HSFRC for Kara model (PDF)



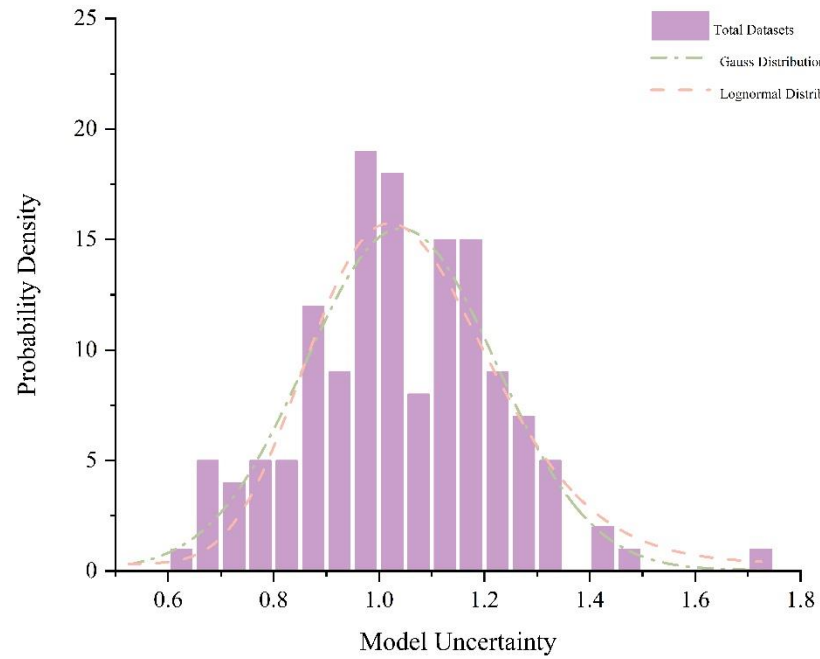
(d) HSFRC for Kara model (CDF)



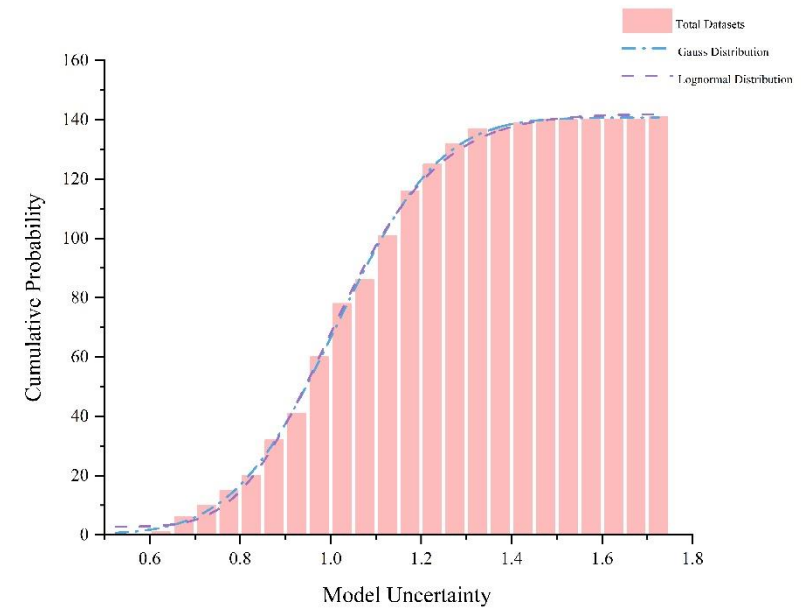
(e) HSFRC for Tarawneh model (PDF)



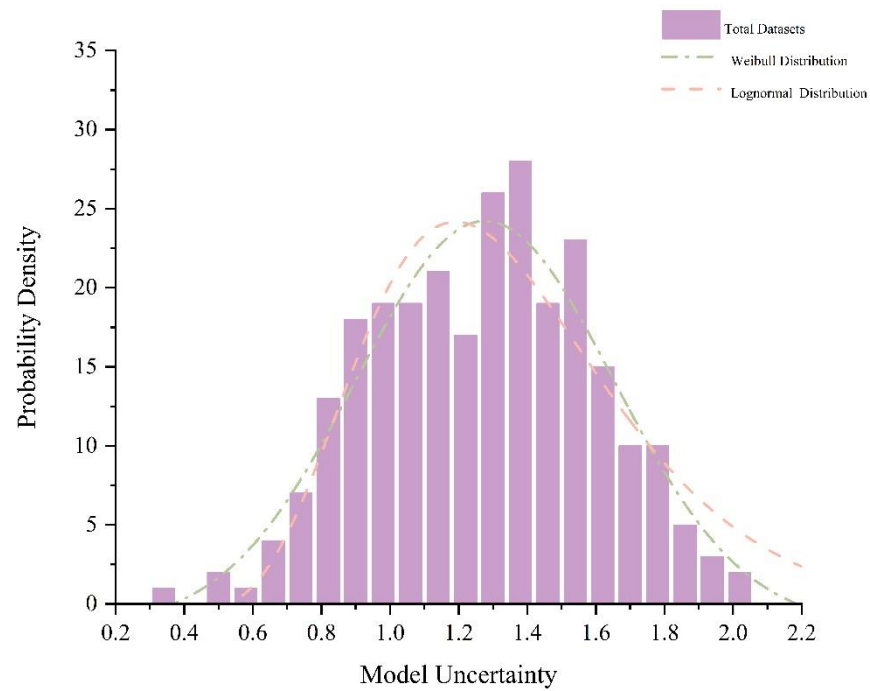
(f) HSFRC for Tarawneh model (CDF)



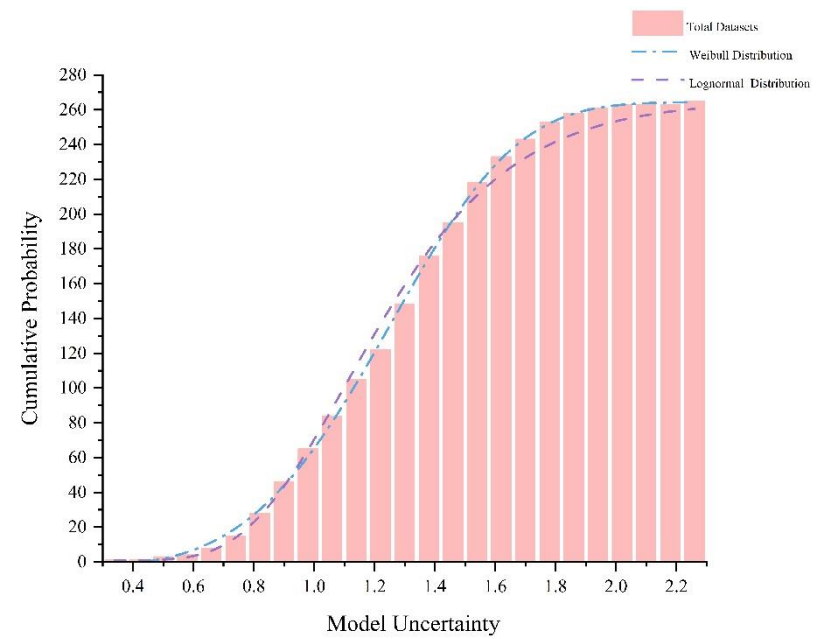
(g) HSFRC for AI-Ta'an model (PDF)



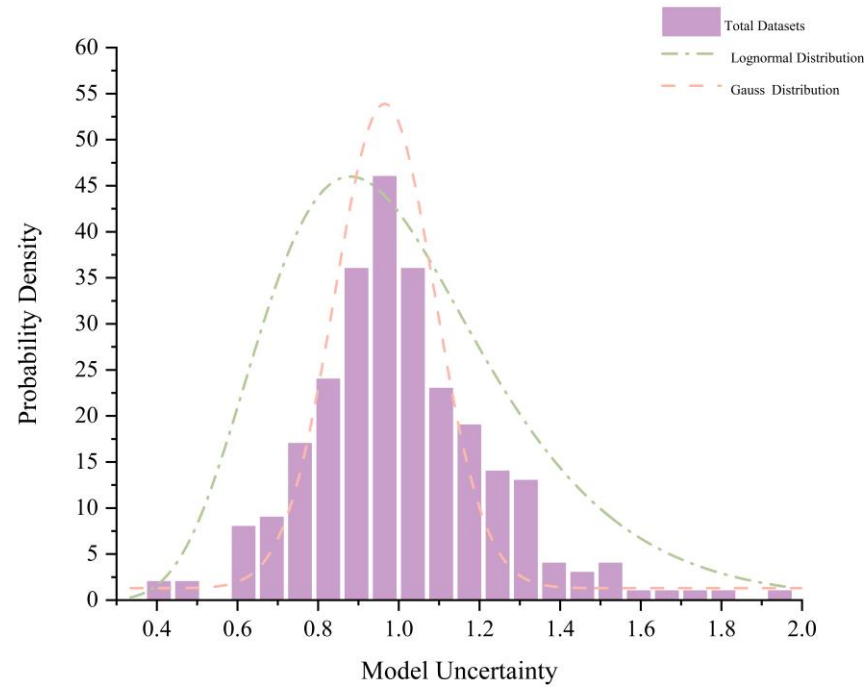
(h) HSFRC for AI-Ta'an model (CDF)



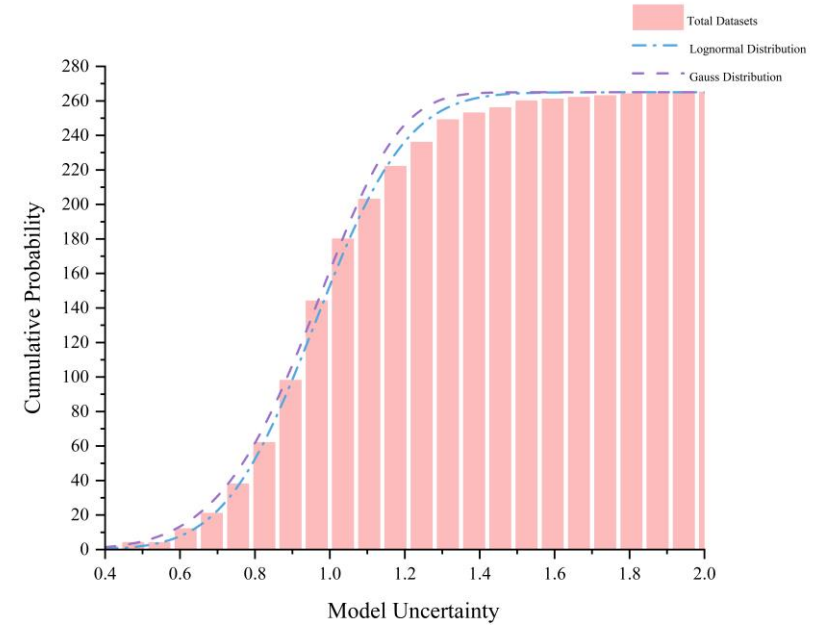
(a) NSFRC for Mansur model (PDF)



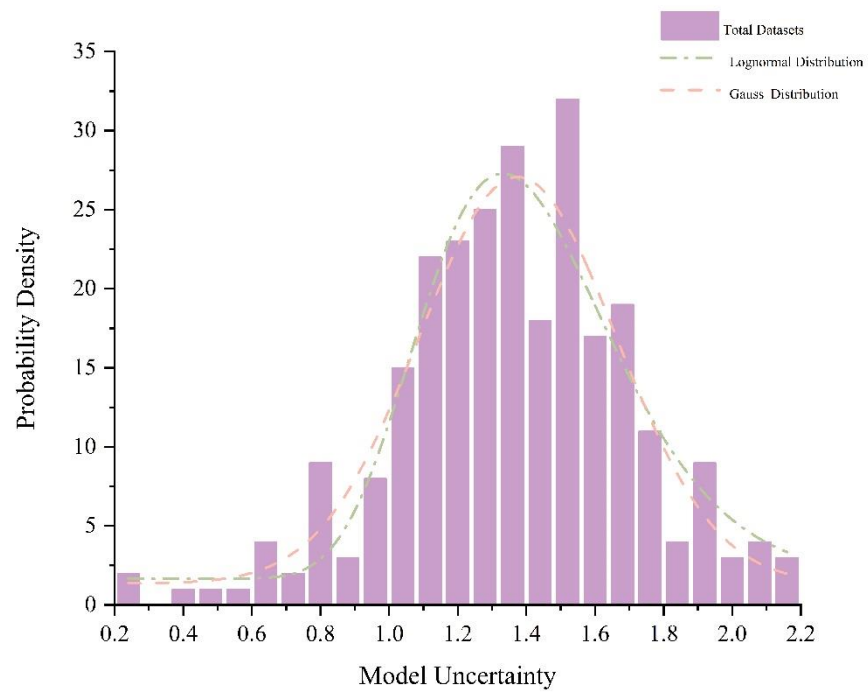
(b) NSFRC for Mansur model (CDF)



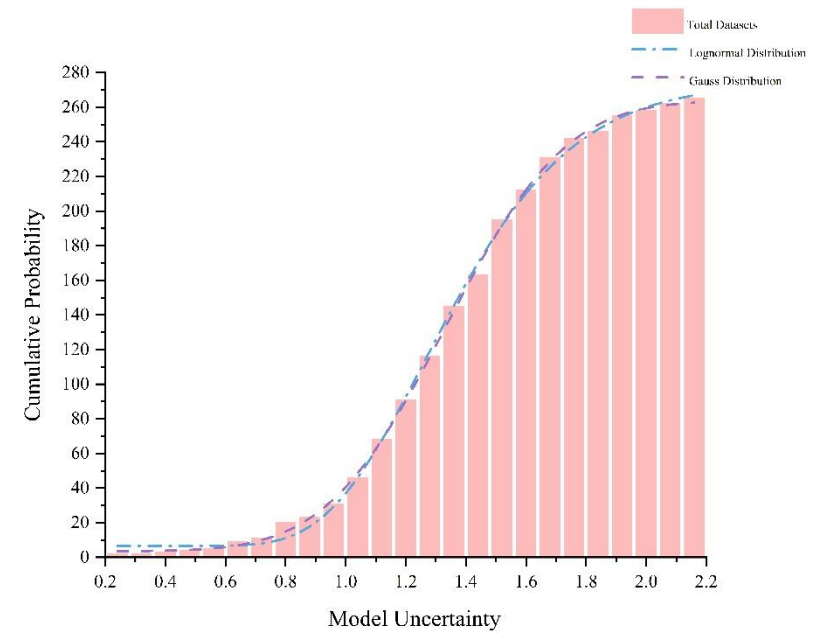
(c) NSFRC for Tarawneh model (PDF)



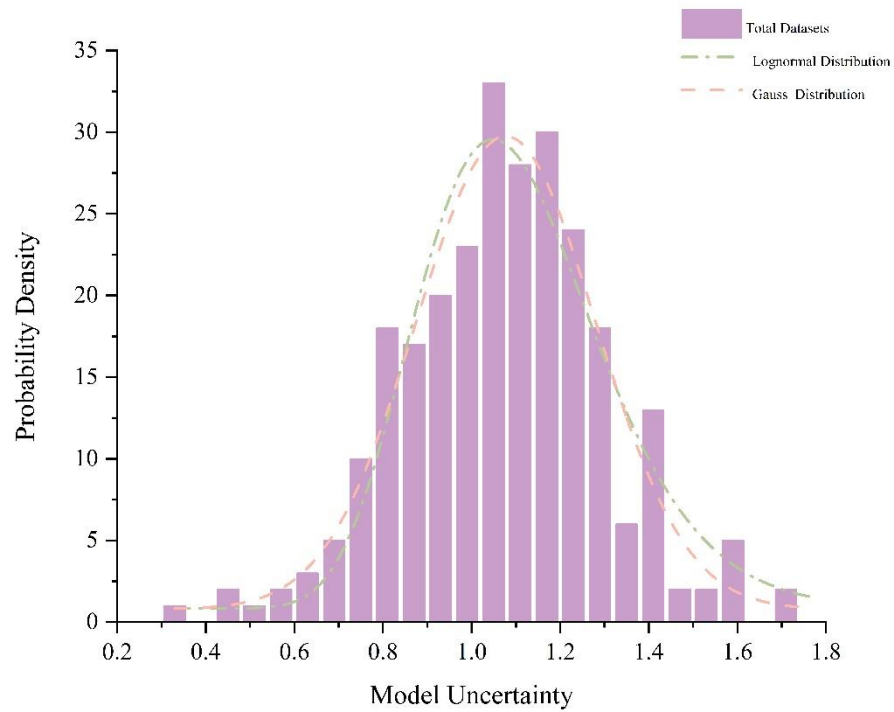
(d) NSFRC for Tarawneh model (CDF)



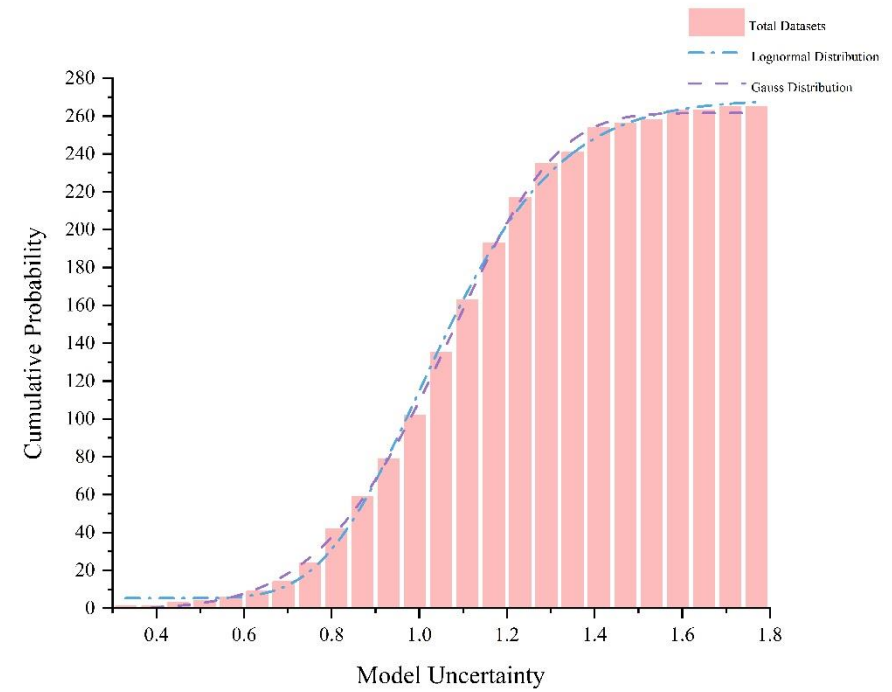
(e) NSFRC for Khuntia model (PDF)



(f) NSFRC for Khuntia model (CDF)



(g) NSFRC for Kara model (PDF)



(h) NSFRC for Kara model (CDF)

Figure 9-2 PDF and CDF graph for different models

Table 9-2 Anderson-Darling test results.

	Model Uncertainty			Distribution			
	Average	SD	COV	Gauss	Lognormal	Weibull	Gumbel
HSFRC Prediction Model							
Ashour et al.	1.17	0.19	0.16	0.02	0.08	0.27	6.15E-07
Kara	1.03	0.17	0.16	0.29	0.09	0.41	1.04E-4
Tarawneh	1.08	0.20	0.18	0.08	0.15	0.62	2.00E-10
Al-Ta'	1.04	0.19	0.18	0.61	0.44	0.23	5.20E-08
NSFRC Prediction Model							
Khuntia	1.36	0.33	0.24	0.52	0.65	0.07	1.52E-07
Kara	1.08	0.22	0.20	0.66	0.71	0.21	2.31E-10
Tarawneh	1.01	0.21	0.20	0.03	0.26	0.02	7.75E-16
Mansur et al.	1.27	0.33	0.26	0.52	0.58	0.61	1.26E-08

9.3 Reliability Analysis

9.3.1 Limit State Function

The Probability of Component Failure analysis investigates the probability of component failure by defining both load (Q) and resistance (R) as random variables with probability density functions. The Introduction the limit state function g , which is expressed in **Equation 9-5**, appraises this analysis:

$$g(R, Q) = R - Q \quad (9 - 5)$$

In this context, g signifies the safety margin. Assuming resistance (R) and load (Q) follow normal distributions, the reliability index β is determined using the formula:

$$\beta = \frac{m_R - m_Q}{\sqrt{\sigma_R^2 + \sigma_Q^2}} \quad (9 - 6)$$

where m_R and m_Q denote the mean values of resistance and total load effect, respectively, which respectively represent the standard deviations of the resistance and total load. Therefore, the reliability index can be viewed as a function of the probability of failure P_f as shown below:

Here, m_R and m_Q represent the mean values of resistance and total load effect, respectively, and σ_R and σ_Q denote their standard deviations. The reliability index is thus a function of the failure probability P_f expressed as:

$$\beta_1 = -\Phi^{-1}(P_f) \quad (9 - 7)$$

In this study, the shear resistance can be described as:

$$R = R_n \times M \times F \times P \quad (9 - 8)$$

where R_n is the nominal resistance, influenced by material (M), fabrication (F), and professional (P) factors. The formulation for P includes the ratio of experimental shear ability and the projected shear strength from the refined relationships. Consequently, various statistics are utilized for refined shear equations, including biases, standard deviations, and coefficients of variation. The structural analysis codes and design criteria we follow usually adhere to risk-oriented design requirements. The assurance inspections are conducted to figure out the likelihood that the necessary strength is equivalent or less than the design durability while recognizing the uncertainties associated with the properties of the structure and the load it bears. Using Equation 9-9, the safety and dependability of the five models are determined using the load and resistance factor approach (LRFD) method:

$$\phi R_n \geq \sum_i^m \gamma_i Q_{ni} \quad (9 - 9)$$

where R_n refers to the nominal resistance, Q_{ni} as the i th nominal load effect, ϕ as the resistance factor, and γ_i as the load factor for Q_i . Considering the joint action of live (L) and dead load (D) only, the LRFD gives:

$$\phi R_n = \gamma_D D_n + \gamma_L L_n \quad (9 - 10)$$

The limit state function is as follows:

$$G = R - D - L = B \times R_n - D - L \quad (9 - 11)$$

where B stands for the bias factor of resistance. **Equation 9-12** is obtained as follow based on previous Equations:

$$G = B \frac{\gamma_D D_n + \gamma_L L_n}{\phi} - \frac{D}{D_n} - \frac{L}{L_n} \cdot \frac{L_n}{D_n} \quad (9 - 12)$$

9.3.2 Load Combination

In order to accurately determine beam reliability in all circumstances, researchers are exploring diverse load mixes. When it comes to several loads on a structure, the component's largest load impact is assessed (Q) is deemed the critical load combination. Multiple possible load mixes are recommended for structures and their elements, according to the ACI 318 [143] and ASCE 7 [186] standards, which involve dead and live load, as seen in **Table 9-3**.

Table 9-3 Load combinations

Load Type	Load Combinations	Distribution	Bias	COV
Dead	-	Gauss	1.050	0.100
Live	1.2D + 1.6L	Extreme Value Type I	1.000	0.180
Snow	1.2D + 1.6S	Lognormal	0.820	0.260
Wind	1.2D + 1.6 W	Extreme Value Type I	0.780	0.370
Earthquake	1.2D + 1.0E	Extreme Value Type I	0.660	0.560

9.3.3 Target Reliability Index and Resistance Factor

Given that there are no firmly established resistance values intended for use in SFRC beams lacking stirrups, this study identifies values stated in [187]. This source provides these values for beams with limited shear reinforcement. The resistance values for beam shear strength are contingent on reinforcement pattern and achieve target reliability index of 3.5 indicated in [187]. The resistance value is 0.52 for beams devoid of stirrups, while it is between 0.6 and 0.64 for

those with minimum stirrups. Beams with $PvFy=150$ are assigned resistance values between 0.66 and 0.7. Given that this study focuses on SFRC beams lacking stirrups, it is essential to recognize the shear resistance offered by the fibres. The research thus adopts a resistance value between 0.6 and 0.64, drawing from the idea that the fibbers' impact on the shear strength is comparable to that of minimum stirrups.

9.3.3 FORM and SORM

This study offers a thorough evaluation of the trustworthiness of NSFRC and HSFRC beams, by utilizing FORM and the SORM. These processes provide robust frameworks in structural analysis since they make it easier to generate limit state functions by approximating them using a Taylor series expansion around a specific point intentionally selected to facilitate design.

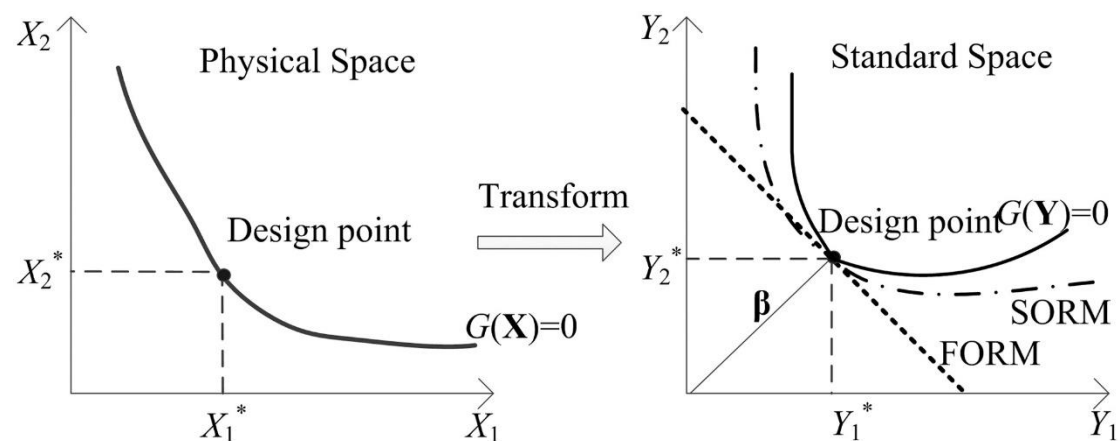


Figure 9-3 FORM and SORM

According to **Figure 9-3** [188] The point of design is the where the Limit Interactive Surface and the origin intersect [189]. Therefore, it is correct that we describe the parameters in the reduced normal space as having no mean and a single standard deviation because this places them on equal footing for comparison [190]. This the process of normalizing these parameters is reflected in **Equation 9-13**:

$$F_y(y) = F_x(x) \quad (9 - 13)$$

This equation involves both the standard normal and original cumulative distributions of the parameters. However, it applies specifically to independent, non-normal random parameters, with the transformation's Jacobian represented by a diagonal matrix with specific elements.

This transformation relies on both standard normal and original distribution probability density functions. It's essential to employ an iterative algorithm to find the exact design point on the risk surface since the performance function, $G(x)$, is understood as an implied function based on the random vector [233]. Therefore, this study utilized Python software integrated with Pystra package to analyse the reliability of NSFRC alongside HSFRC beams. We tapped Python's computational power, as well as Pystra's customized features for structural reliability check, to obtain reliability results by averaging the outcomes from both FORM and SORM.

9.4 Reliability Results

9.4.1 The Combination of Live and Dead Loads

Integrating reliability into the calibration of HSFRC and NSFRC beam shear models involves using multiple resistance factors. Various resistance factor values are derived by adjusting target reliability levels. These values are detailed in **Figures 9-4 and 9-5** and **Tables 9-4 and 9-5**.

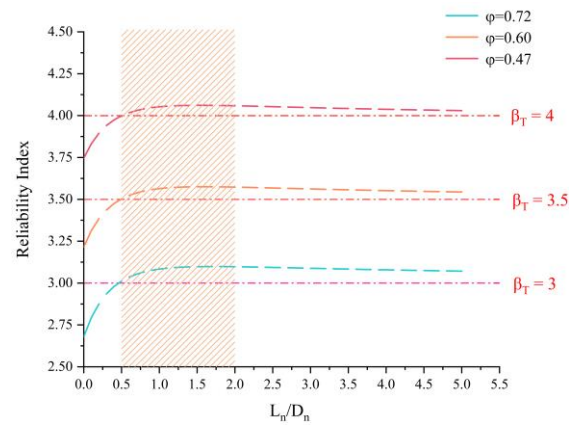
Table 9-4 Results for HSFRC group

Resistance Factor For L/D = [0.5, 2]				
	Ashour [182]	Kara [184]	Tarawneh [185]	Al-Ta'an [183]
$\beta_T = 3$	0.72	0.60	0.61	0.58
$\beta_T = 3.5$	0.60	0.48	0.49	0.47
$\beta_T = 4$	0.47	0.37	0.37	0.36

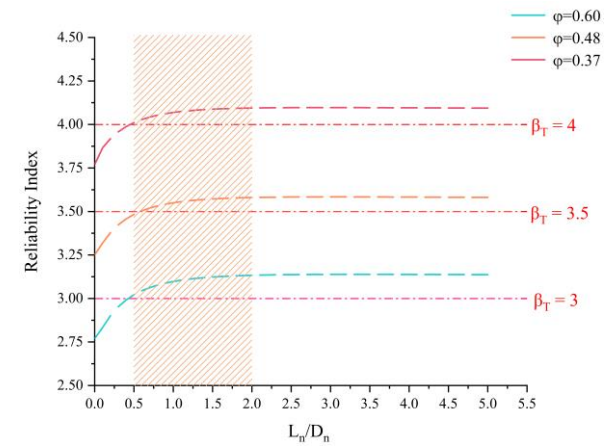
1 **Table 9-5** Results for NSFRC group

Resistance Factor For L/D = [0.5, 2]				
	Khuntia [183]	Kara [184]	Tarawneh [185]	Mansur [182]
$\beta_T = 3$	0.78	0.71	0.69	0.42
$\beta_T = 3.5$	0.66	0.62	0.60	0.30
$\beta_T = 4$	0.55	0.55	0.56	0.18

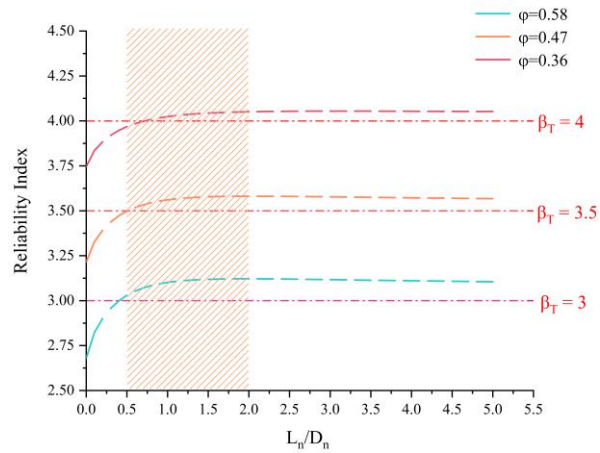
2



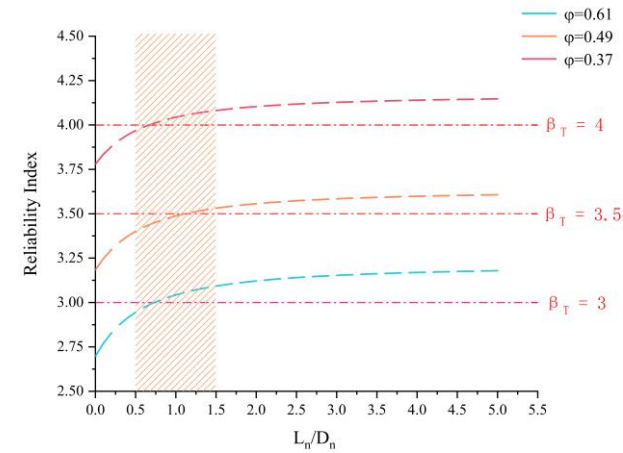
(a) Ashour



(b) Kara



(c) AI



(d) Tarawneh

Figure 9-4 HSFRC with live and dead loading combination

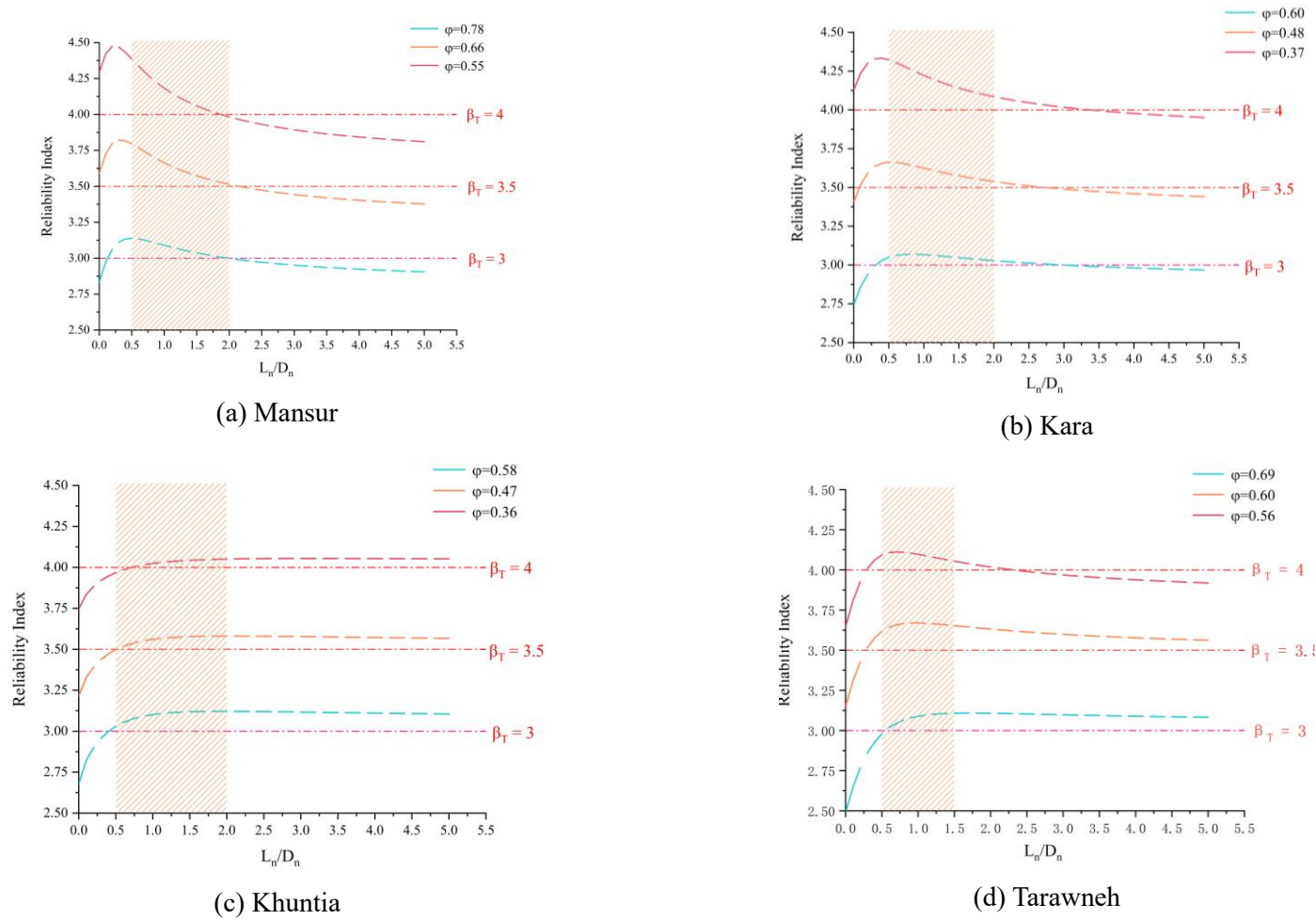


Figure 9-5 NSFRCC with live and dead loading combination

In the HSFRC beam model, not all shear forecast models can be sufficiently trusted. An example is the Ashour[182] formula, which assigns the most substantial resistance element a 0.6 quotient when the target reliability coefficient is 3.5. This only meets the recommended resistance interval's minimum value of 0.6 to 0.64, considering concrete beams with the least stirrups. Conversely, Kara [184] and Al-Ta'an [183] models seem to be too cautious, indicating resistance coefficients of between 20% and 21.7%, which fall short of the optimum shear resistance quotient of 0.6. Al-Ta'an's excessively cautious forecasts may be due to the formula satisfying both NSFRC and HSFRC beams, thus the shear resistance could be overvalued for HSFRC beams. Whereas the Kara [184] model is derived from a database using machine learning, it is mainly built on NSFRC beams and has few HSFRC beams. This has reduced its prediction accuracy for HSFRC beams, leading to untrustworthy predictions.

The Kara model, especially for NSFRC beams, outperforms other shear models mainly due to its ML forecast equation. For the targeted reliability index value of 3.5, the resistance factor is 0.62, which meets the suggested resistance factor. The reliability of NSFRC beam models is substantially more mature than HSFRC beam models. Specifically, at 3.5 for the reliability index value, the Khuntia model [183] has a resistance factor that is 3% above the maximum 0.64 recommendation. This represents only a 0.02 difference from the most desirable target resistance vs. threshold. Nonetheless, the Mansur's [182] overly simple model has a relatively weak reliability prediction because of its limited dataset and early development, which only included 24 test beams and their relevant mechanical data. The general simplification of its conditions has caused weak coefficients of uncertainty and scope. Given this, the NSFRC beams and the Kara model for it perform significantly better than HSFRC and Mansur. Both are optimized for balancing financial efficiency and safety.

The Tarawneh [185] model is better at predicting results than the Kara [184] model because it uses more detailed and complete prediction data. Even though the Kara [184] model has seven variables, Tarawneh's model only uses five, which is more effective. The Tarawneh [185] approach simplifies complicated structural responses by using simple formulas. However, the

Tarawneh [185] model's main weakness is that it emphasizes accuracy and simplification more than safety. When compared to the ACI's recommendation, a partial factor of 0.5 is much lower, which indicates a significant difference in safety precautions. Furthermore, Tarawneh [185] proposes a partial factor of 0.667 in the end of paper to improve the safety, there is a possibility of compromising prediction accuracy. It may be tricky to maintain a good balance between accurate predictions and safety concerns with formulas based on machine learning because they mostly depend on the quality and breadth of the databases used. In the future, researchers should focus on improving beam functions by considering parameters like shear span, beam type, and other combined variables to enhance the accuracy and applicability of these formulas.

In comparison of the two ML models, the Tarawneh [185] solution fares better in forecast capacity when contrasted to the Kara [184] model because it has broad and improved prediction data reserve. Tarawneh [185] makes use of only five factors to outperform Kara [184] who uses seven. Tarawneh's strategy is targeted at making it easy to interpret big design reactions via basic mathematical formulas. However, a potential caveat of the Tarawneh [185] model is its focus on accuracy and simplicity at the expense of security. Unlike the recommendation by the ACI for a decrease factor of 0.75, Tarawneh [185] calls for 0.5, revealing a significant difference in security margins. Amada discussed a 0.667 partial reduction in factor for forthcoming solution proposals to balance prediction accuracy and safety. But cutting the partial factor might hinder the predictability. It is hard to create designs that balance prediction accuracy and safety using machine learning-driven equations that hinge largely on the calibre and range of data they use. By concentrating on specifying beam functions by shear scope, beam design, and various groups, subsequent research should aim at enhancing the dependability and flexibility of these solutions.

9.4.2 Other Load Combinations

Because there are no recommended coefficient of resistance to snow, wind or earthquake load, it is vital to examine the resistance factors of different load combinations using comparative

analysis. **Tables 9-6** and **9-7** show the reliability index of the different beam models. The findings indicate that the HSFRC beam models demonstrate consistent stability across different loads. The shear models under live loads demonstrate nearly the same resistance factors as those of shear models under snow and wind loads at practical load thresholds, suggesting that guaranteeing shear strength for fundamental dead and live loads also means safety under snow and wind conditions.

For NSFRC beams, the Kara [184] model demonstrates superior prediction ability and stability. The resistance coefficient changes with a reliability index of 3.5 are minimal, at -9% and 2% for wind and snow load combinations, respectively. In comparison, the Mansur [182] model shows changes of -9.1% and 9.2%, highlighting the enhanced prediction capacity and reliability of data-driven machine learning models. Although the Tarawneh [185] model exhibits lower resistance factors compared to the Kara [184] model, it performs better under earthquake load combinations due to its median value being closer to 1, which enhances performance under highly unstable loads. Overall, machine learning models demonstrate higher accuracy and cost-effectiveness, particularly in the prediction of NSFRC beams, where they excel in accuracy, economy, and safety.

Kara [184] model is a better predictor of performance and has improved consistency compared to other models; this model is more resilient with minimal reduction coefficients of -9 % and 2 % for wind and snow load combinations when considering 3.5 reliability index. In contrast, Mansur [182] shows stability in data post-processing at -9.1 % and 9.2 % for wind and snow load combinations. It is apparent from the models' resistance factors that data-driven algorithms tend to show superior predictive ability and improved resilience, contributing to their heightened reliability in various experimental conditions. The model created by Tarawneh [185], albeit showing a more depleted resistance factor compared to the Kara [184] model, seems to offer improved performance with earthquake load combinations. As its median value is close to 1, it means that the Tarawneh [185] model is reliable in unstable conditions. It is recommended to use machine learning models for the assessment of NSFRC beams that need

- 1 to balance precision, cost, and safety. These models will be effective in similar applications as
 2 the pre-discussed frameworks, offering enhanced accuracy and the capability to balance
 3 different performance elements in terms of science, costs, and public safety.

4 **Table 9-6** Reliability Index for HSFRC Beams with Different Load Combination

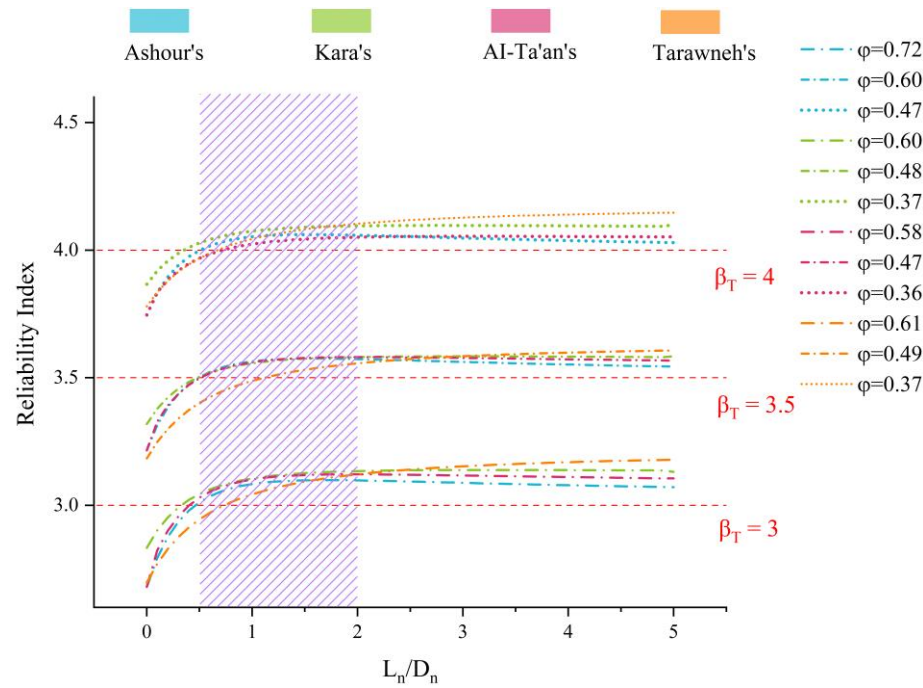
HSFRC Beams				
	Ashour [182]	Kara [184]	Al-Ta'an [183]	Tarawneh [185]
E/D = [0.5, 2]				
$\beta_T = 3$	0.43	0.40	0.37	0.39
$\beta_T = 3.5$	0.33	0.31	0.29	0.29
$\beta_T = 4$	0.25	0.24	0.21	0.22
W/D = [0.5, 2]				
$\beta_T = 3$	0.69	0.65	0.60	0.62
$\beta_T = 3.5$	0.57	0.53	0.50	0.48
$\beta_T = 4$	0.43	0.42	0.40	0.36
S /D = [0.5, 2]				
$\beta_T = 3$	0.70	0.63	0.62	0.62
$\beta_T = 3.5$	0.56	0.53	0.48	0.52
$\beta_T = 4$	0.43	0.43	0.37	0.41

5 **Table 9-7** Reliability Index for NSFRC Beams with Different Load Combination

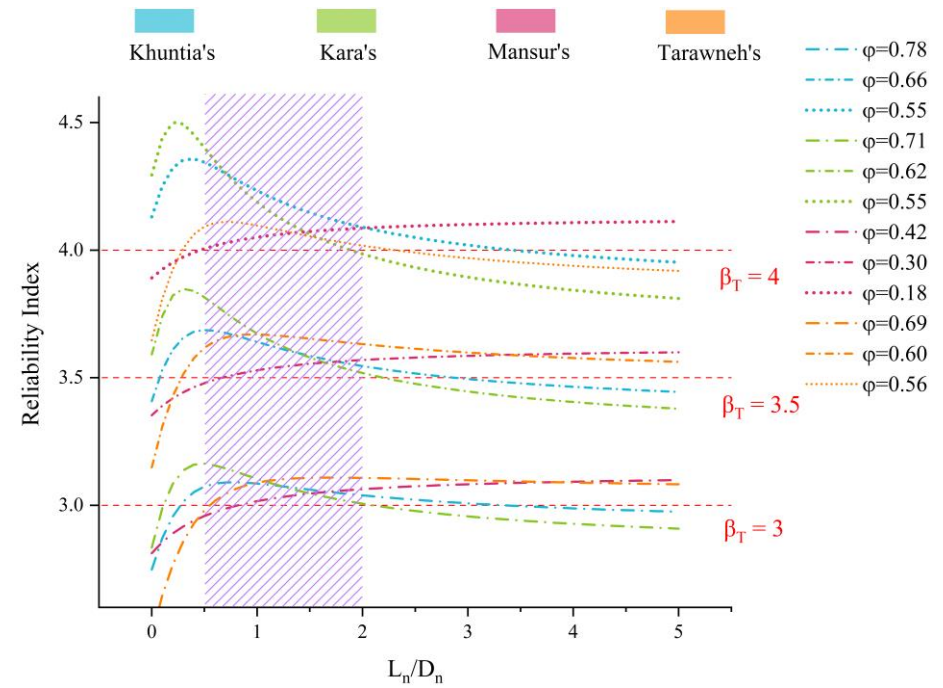
NSFRC Beams				
	Khuntia [183]	Kara [184]	Mansur [182]	Tarawneh [185]
E/D = [0.5, 2]				
$\beta_T = 3$	0.46	0.40	0.32	0.43
$\beta_T = 3.5$	0.36	0.31	0.21	0.37
$\beta_T = 4$	0.28	0.25	0.13	0.30
W/D = [0.5, 2]				
$\beta_T = 3$	0.75	0.67	0.42	0.63

$\beta_T=3.5$	0.61	0.55	0.28	0.52
$\beta_T=4$	0.50	0.45	0.18	0.42
$S/D=[0.5,2]$				
$\beta_T=3$	0.82	0.72	0.43	0.70
$\beta_T=3.5$	0.72	0.63	0.29	0.61
$\beta_T=4$	0.63	0.54	0.18	0.52

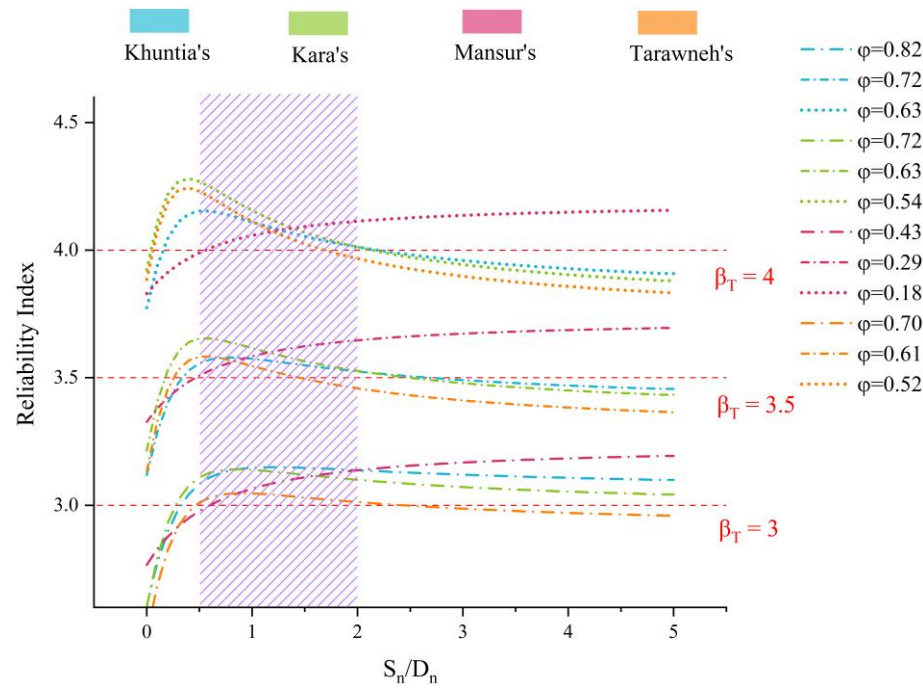
1



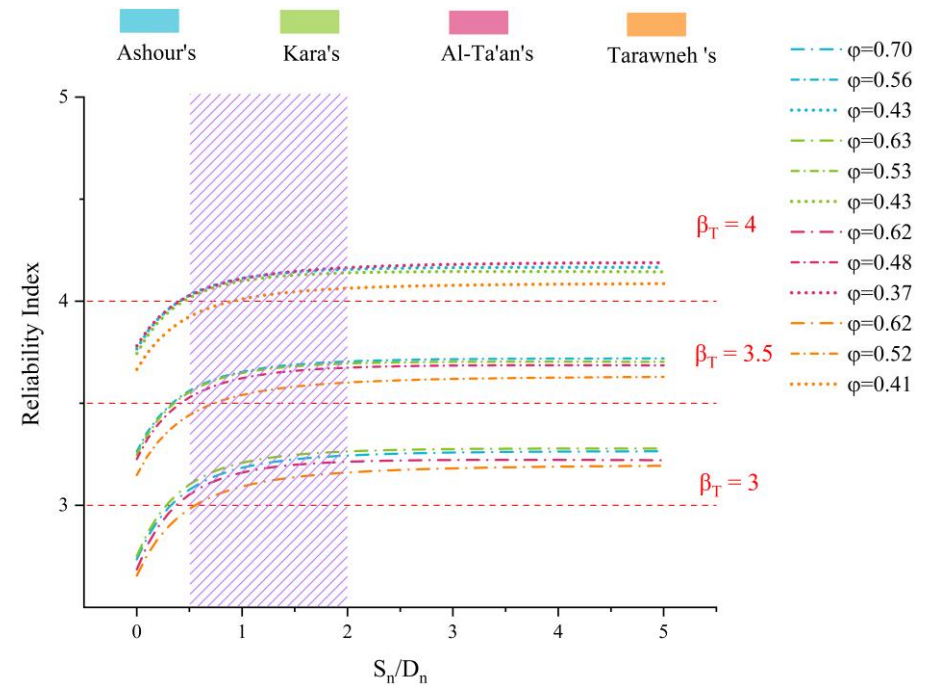
(a) NSFRC Live and Dead Load Combination 1.2L+1.6D



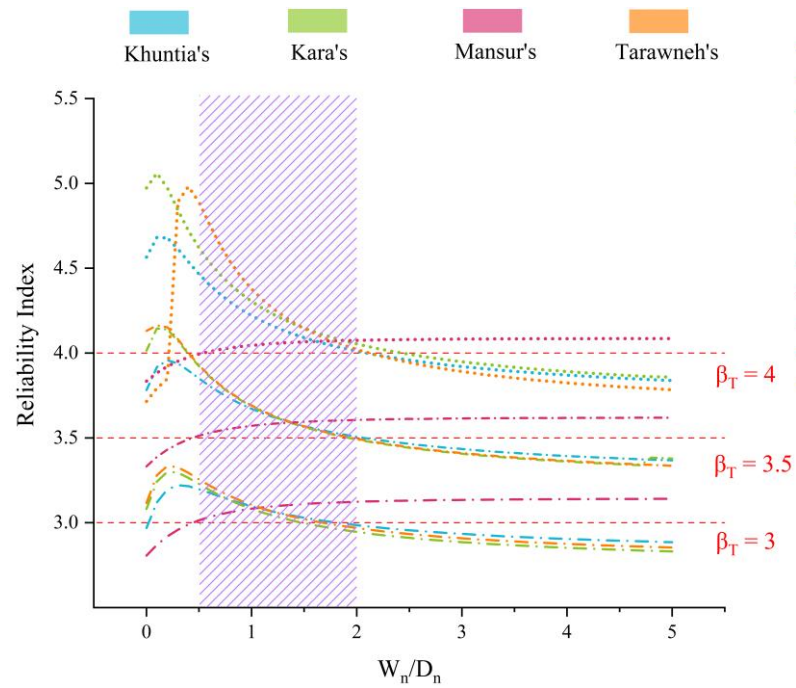
(b) HSFRC Live and Dead Load Combination 1.2L+1.6D



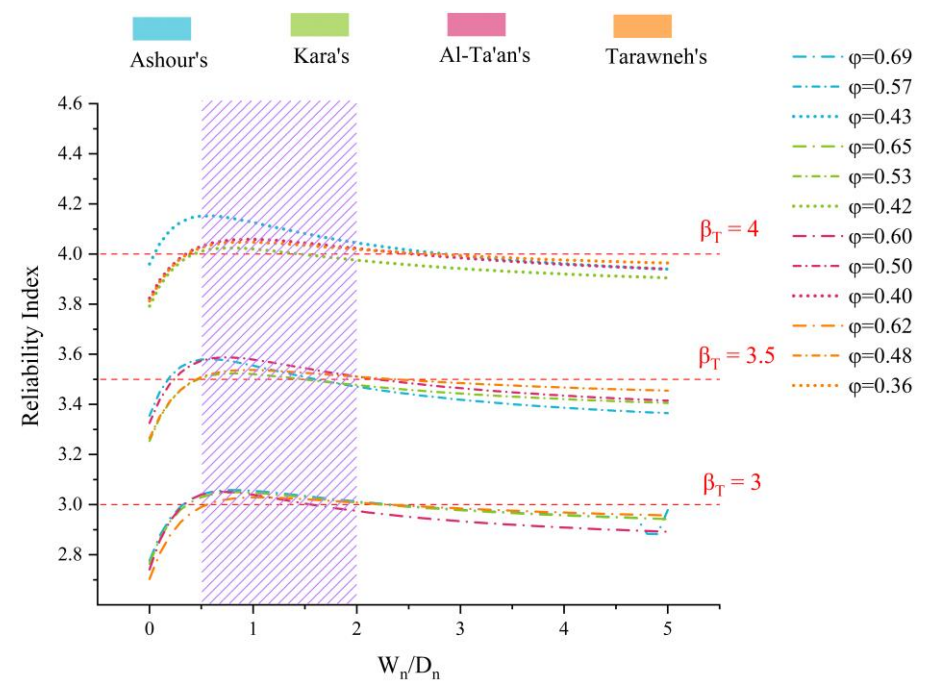
(c) NSFRC Snow and Dead Load Combination 1.2L+1.6S



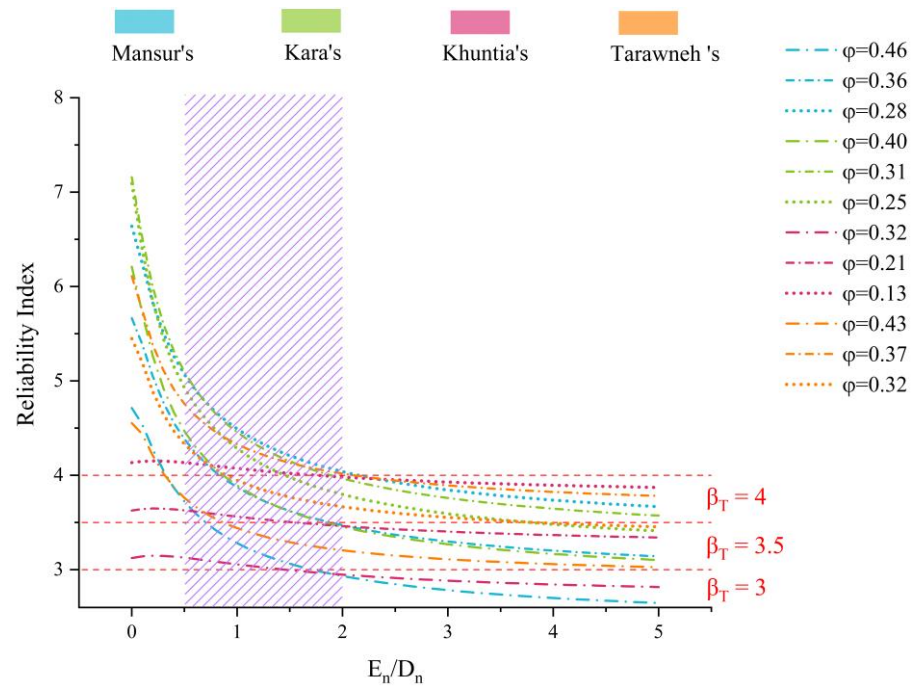
(d) HSFRC Snow and Dead Load Combination 1.2L+1.6S



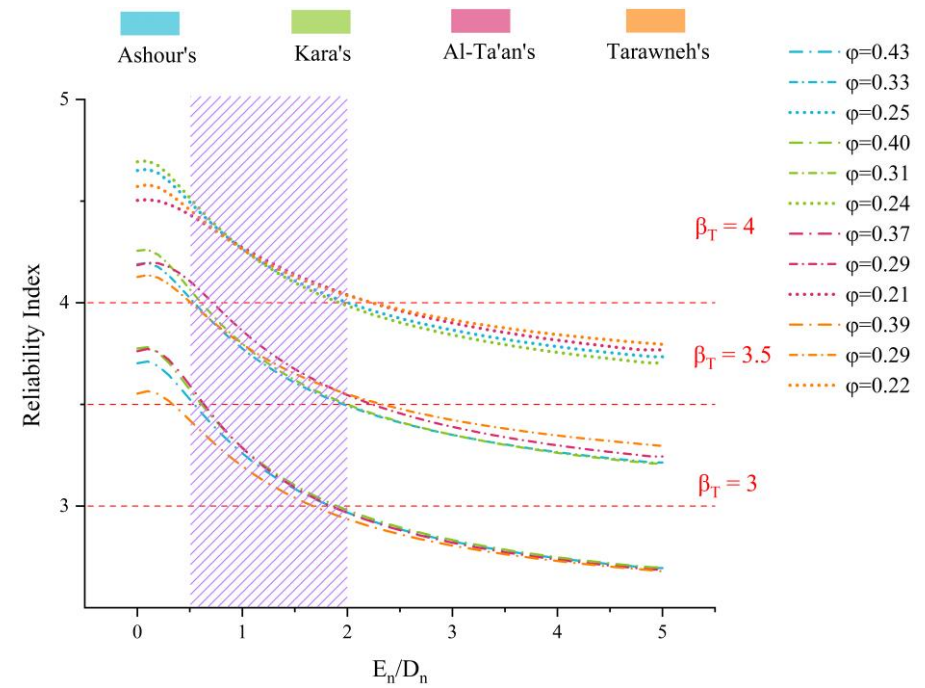
(e) NSFRC Wind and Dead Load Combination 1.2L+1.6W



(f) HSFRC Wind and Dead Load Combination 1.2L+1.6W



(g) NSFRC Earthquake and Dead Load Combination 1.2L+1E



(h) HSFRC Earthquake and Dead Load Combination 1.2L+1E

Figure 9-6 Reliability Index for different load combination

9.5 Sensitivity Analysis

A sensitivity study is employed to ascertain how probable an occurrence is to occur or not due to the standard deviation adjusting when handling unvarying and inconsistent variables, such as those in this study. This examination generates two bounds (PLf for the lower bound and PUf for the upper bound) for failure likelihood. The variance between these bounds identifies how affected the occurrence's likelihood is by unchecked variables. To perform this study and set a departure point for possible examination development, particularly concerning the dataset, the resistance factor or safety index is held steady while adjusting the standard deviation via various values, as presented in **Table 9-8** [182, 184].

Table 9-8 Sensitivity analysis

Target Reliability index $\beta = 3.5$						
	$\Delta_{+0\%}$	$\Delta_{+10\%}$	$\Delta_{+20\%}$	$\Delta_{+30\%}$	$\Delta_{+40\%}$	$\Delta_{+50\%}$
ϕ for Kara [184]	0.63	0.60	0.57	0.54	0.51	0.48
Φ for Ashour's[182]	0.60	0.55	0.50	0.45	0.40	0.35
Target Resistance Factor $\phi = 0.63$ (Ashour) and $\phi = 0.59$ (Ilker)						
	$\Delta_{+0\%}$	$\Delta_{+10\%}$	$\Delta_{+20\%}$	$\Delta_{+30\%}$	$\Delta_{+40\%}$	$\Delta_{+50\%}$
β for Kara [184]	3.51	3.30	3.12	2.96	2.82	2.69
ϕ for Ashour's[182]	3.5	3.32	3.16	2.99	2.86	2.72

While the dataset remains the largest and most comprehensive, the standard deviation is expected to fluctuate with more data added in the future. This adjustment could impact the reliability index. As noted by Table 9, the resistance coefficient decreases consistently with a growing standard deviation while the target reliability index remains unchanged. When comparing models, the Ashour [182] model shows more variations than the Kara [184] model. The Kara [184] model, using a logarithmically normal distribution, exhibits less fluctuation in resistance predictions, while the Ashour model, using the Weibull distribution, is more impacted by standard deviation changes.

The sensitivity analysis results suggest that the Kara model is less sensitive to data change than the Ashour formula. This can be attributed to the models' different methodologies. The Ashour formula relies on the original ACI model with minor regression analysis limitations based on a small subset of data. In comparison, the Kara model utilizes machine learning, which can investigate the complex relationship between different variables more effectively using a wide dataset. These findings indicate that machine learning models may provide superior results to conventional shear models acquired from mechanical analysis.

9.6 Conclusion Remark

This study introduces a reliability-based design procedure utilizing FORM and SORM to establish resistance factors for both NSFRC and HSFRC beams under various loading conditions, including dead, live, wind, snow, and seismic loads. The analysis involves comparing five widely used shear models and conducting sensitivity analyses, leading to the following key findings:

Shear Model Uncertainty: The uncertainty in shear models for SFRC beams was found to follow lognormal and Weibull distributions. For high-strength SFRC (HSFRC), Ashour's and Kara's models are consistent with the Weibull distribution, while Al-Ta'an's model aligns with a Gaussian distribution. For normal-strength SFRC (NSFRC), Ashour's and Khuntia's models follow a lognormal distribution, and Mansur's model fits the Weibull distribution.

Optimal Models for Reliability: To achieve a balance between safety and cost, Ashour's model is recommended for HSFRC, with a resistance coefficient of 0.59, and Kara's model is preferred for NSFRC, with a resistance coefficient of 0.61. These models are selected based on a target reliability index of 3.5. For non-structural beams, a reliability index of 3 is also acceptable, where Ashour's and Kara's models continue to provide effective balance.

Sensitivity Analysis: The sensitivity analysis indicates that HSFRC models are more responsive to dataset fluctuations than NSFRC models. Specifically, Ashour's model maintains a reliability index of around 3.1 with a 20% standard deviation fluctuation, but this index drops to 3 with a 30% fluctuation.

This analysis highlights the critical role of reliability assessment in selecting shear models for SFRC beams, ensuring they meet safety standards while optimizing cost-effectiveness. This analysis underscores the essential role of reliability assessment in choosing appropriate shear models for SFRC beams, ensuring safety while optimizing cost. However, to further refine these models, it is crucial to consider time-dependent reliability, which addresses durability concerns, especially under extreme environmental conditions such as coastal areas where corrosion is a significant factor. Given the limited research in this area, the next sections will delve into time-dependent reliability

analysis, focusing on the long-term performance and durability of SFRC beams, to better understand and predict their behaviour in challenging environments.

10. Time-Dependent Reliability Analysis

Because of the escalating alarm about corrosion issues, sustainability, and the cost of retrofitting, research in the last year about ISF's resistance has received substantial attention [191]. Durability is key in reinforced concrete structures, where they face long-term influences and outcomes on their safety and trust. During the long haul, the key kinds of damage are chloride ion intrusion and concrete carbonation. When exposed to chloride environments, chloride ions are highly harmful to concrete. They permeate the concrete and react with the steel reinforcements, causing rust. Building materials must be robust, meaning they must be durable throughout their life cycle. The subjected should have enough reliability to be repaired, maintained, renovated, or restored during their service cycle despite either natural or human-induced risks, uncertainties, or events [192]. Chloride ions are among the most corrosive chemical compounds formed as a result of concrete-covered alkali metals like those discussed in the alkali metals laboratory and during the cement hydration research. As a result, HSFRC's durability performance in terms of time-varying behaviour and corrosion elements should be investigated in more detail in order to optimize and use it in construction applications. The highlighted content raises alarms concerning sustainability, durability, and retrofitting costs, which must be greatly concerned [193]. However, the corrosion, and time-changing properties of ISFRC as well as RSFRC structures are not extensively researched. Therefore, more research and arguments are required to assess the durability of HSFRC in different environmental conditions.

10.1 Corrosion Mechanisms Analysis

The proposed Modified TR63 method which been described in **Section 5.2** will be used in this study. Steel reinforcement in reinforced concrete beams mainly experiences corrosion. In concrete frameworks, these beams extensively take compression and tensile loads [194]. Nevertheless, the elastic strength contributed by steel reinforcement plays a crucial role in the overall shear and flexural strength of the beam. Previous research has analysed the deterioration of overall shear strength as the flexural performance of the concrete beams due to corrosion degradation. It is worth noting that corrosion degradation reactions usually involve changes in a variety of variables. As a result, corrosion may lead to the deterioration of the relationship between steel reinforcement and concrete, possibly hurting the general structural performance [195]. In the same way, reinforcing bars and ISF in ISFRC beams can also cause bond slip in this concrete due to corrosion issues. This slip can lessen the overall shear strength of the structure because of this decay. Still, an essential approach is not there to carefully describe the slip condition during corrosion. This paper presents a general corrosion parameter degradation equation. It puts forward a list of parameter equations where the corrosion level impacts individual parameters. Finally, these parameter equations are combined to create an integrated time-to-failure reliability analysis method for HSFRC beams, demonstrating the likelihood of structural failure under normal conditions.

10.2 Study of Parameters

By analysing and describing **Formulas 5-25 to 5-28**, there are four important structural parameters play an essential role in the structure's shear capacity: compressive strength, shear

span ratio, and the effect of fibre and longitudinal ratio. This paper will examine how the parameters change as the corrosion process unfolds based on corrosion mechanisms. This study aims to improve the understanding of alterations in the structural dependability of HSFRC beams in deteriorating environments.

10.2.1 Corrosion Effect in Dimension

Shear span proportion reflects the effect of corrosion-induced structural damage on shear resistance [196]. While corrosion typically causes superficial spalling, the weakening of shear stress in large, eroded beams is relatively contained [197]. It is probably that corrosion will have a minor effect on structures' shear span ratios. In certain cases, thorough corrosion can cause significant injury in isolated parts of the structure, altering the location of concentrated loads and changing the structural shear span [198]. These changes occur when the structure's cross-sectional area varies, affecting its general shear resistance. Consequently, because severe spalling and loss of quality are rare, this paper does not cover these issues.

10.2.2 Corrosion Effect in Steel Rebars

The decline in shear and bending strength of concrete structures can affect their safety. Exposure to environments with high chloride levels leads to the corrosion of these structures. The concentration of defect in the reinforcement increasingly becomes irregular over time due to chloride contamination leading to failure of the beams. Chloride build-up in the reinforcing bars of the structure leads to a local low in reinforcement strength, thus preventing the building from accommodating the calculated load, thus collapsing. The increasing chloride concentration in reinforcement bars and the core will cause the structures to suffer chloride

diffusing corrosion, pitting, and massive structural problems [199]. Hence, the corresponding mathematical model that displays the environment of cross-section reinforcement variation because of pitting corrosion at different times is denoted by **Equation 10-1** [199]:

$$A_{pit}(\Delta t) = \begin{cases} A_1 + A_2 p_{max} \leq \frac{D_0}{\sqrt{2}} \\ \frac{\pi D_0^2}{4} - A_1 + A_2 \frac{D_0}{\sqrt{2}} \leq p_{max} \leq D_0 \\ \frac{\pi D_0^2}{4} p_{max} \geq \frac{D_0}{\sqrt{2}} \end{cases} \quad (10 - 1)$$

Where A_1 and A_2 are the corroded cross-sections calculated based on **Equation 10-2** to **10-6**.

$$A_1 = \frac{1}{2} \left[\theta_1 \left(\frac{D_0}{2} \right)^2 - a \left| \frac{D_0}{2} - p_{max} \right| \right] \quad (10 - 2)$$

$$A_2 = \frac{1}{2} \left[\theta_2 p_{max}^2 - a \frac{p_{max}^2}{D_0} \right] \quad (10 - 3)$$

$$\theta_1 = 2 \arcsin \left(\frac{a}{D_0} \right) \quad (10 - 4)$$

$$\theta_2 = 2 \arcsin \left(\frac{a}{2 p_{max}} \right) \quad (10 - 5)$$

$$a = 2 p_{max} \sqrt{1 - \left(\frac{p_{max}}{D_0} \right)^2} \quad (10 - 6)$$

Where D_0 and ‘a’ are the initial diameter of the reinforcement at the onset of chloride pitting and the depth of pitting, respectively, and A_1 and A_2 are the corroded areas associated with angles θ_1 and θ_2 . To evaluate the effect of time the maximum penetration rate of pitting corrosion over time (Δt) be used, which can be estimated using **Equation 10-7**:

$$p_{max}(t) = 0.0116 \eta i_{corr}(\Delta t) \quad (10 - 7)$$

Finally, the remaining reinforcement area $A_{Re-s}(t)$ is defined as **Equation 10-8**

$$A_{Re-s}(t) = \left(\frac{\pi D_0^2}{4} \right) - A_{pit}(t) \quad (10 - 8)$$

Based on the area of the corroded reinforcement, the time function for the longitudinal ratio parameter can be defined as follows:

$$\rho(t) = \rho_0 \frac{A_{Re-s}(t)}{\frac{\pi D_0^2}{4}} \quad (10 - 9)$$

10.2.3 Corrosion Effect of SFRC

Even if there's a small crack on its surface, experimental data indicate that SFRC tends to have a constant or insignificant difference in compressive stability and residual stress [200]. In a review of evidence on reinforced concrete degradation in chloride environments, sample field findings suggested insignificant weakening of both flexural and compressive strength in reinforced concrete without cracks. Only minor surface degradation (up to a few millimetres deep) due to outward-facing rust was observed, causing thin damage layers [201]. It was also noted that an increase in the tensile strength of residual fibres can be explained by keeping fibre erosion to a minimum and allowing the medium to thicken, which ultimately boosts the bond between the fibres [202]. The results were consistent even with slight cracks of ≤ 0.20 , indicating enhancements in persistent tensile robustness related to self-healing and the restrained corrosion of the fibre cracks. [200].

The results of this study suggest that not much attention is paid to the decline of concrete's compressive strength linked to chloride ion erosion because concrete with minimal or no cracking does not degrade significantly. Additionally, there is an improved level of material resistance due to higher friction between the fibre and concrete matrix owing to rust.

Nonetheless, there is potential for corrosion to affect the overall quantity of fibre, its cross-sectional area condition, as well as its length-to-width ratio in the concrete structure. This can ultimately lead to reduction of residual stress for SFRC. This paper utilizes a standard corrosion model to mathematically demonstrate the corrosion of fibres over time because ISF and RSF reinforcements are composed of iron and belong to the same substance, as shown in **Equations 10-10 to 10-13**.

$$A_{Re-f}(t) = \frac{\pi(D_f - 2P_{av})^2}{4} \quad (10 - 10)$$

$$p_{av}(t) = 0.0116i_{corr}(\Delta t) \quad (10 - 11)$$

$$V_f(t) = V_{f_{max}} \frac{A_{Re-f}(t)}{\frac{\pi D_f^2}{4}} \quad (10 - 12)$$

$$RI(t) = RI_{max} \frac{D_f}{D_f - 2P_{av}} \quad (10 - 13)$$

In an effort to assess the shear ability of HSFRC beams in corrosive conditions and predict and evaluate the shear capacity of HSFRC beams in corrosion environments based on trial outcomes and theoretical principles, this research sought to establish a new shear model. It fills an insufficiency in the quantitative examination of corrosion tendencies in research of HSFRC beams, offering a key framework for engineering endeavours. Nonetheless, although the model has such benefits, it features notable drawbacks. It incorporates only the deterioration factors' impact on vital shear ability parameters without analysing the interdependence among these parameters. Such research gaps should prompt innovative investigation. Moreover, the new method does not incorporate the structural and substantial impacts of significant, wide cracks, especially those causing more severe deformations. Specialized structural characteristics and

certain extreme corrosion environments necessitate corresponding adjustments. This new model offers crucial methodological and theoretical guidance for comprehending and using HSFRC beam shear ability. However, there is always room for advancement. Researchers should be conscious of these constraints when executing and enhancing future research endeavours.

10.3 Design Space

Among the problems that impact the endurance of reinforced concrete structures, chloride-induced corrosion is a significant issue. The passivation film formerly established on the steel surface is easily destroyed by concrete's alkalinity, allowing chloride ions to penetrate the contaminated mixture or its surroundings, resulting in localised failure. The filtration of the chloride ion clipped on hardened concrete can be idealised by diffusion, migration, penetration, and capillary absorption processes [203]. due to environmental exposure factors specified in ACI 440.2R-17. Corrosion-induced reduction in shear capacity of two types of HSFRC beams is predicted using various chloride concentrations. **Table 10-1** shows the important parameters.

Table 10-1 Environmental deterioration

Corrosion Degree	Degradation Parameters
Extreme	Cs = 7.35 kg/m3
	RH = 90%
	Temp = 40 °C

High

$$C_s = 2.95 \text{ kg/m}^3$$

$$RH = 75\%$$

$$\text{Temp} = 40^\circ\text{C}$$

The study simulates a coastal surroundings susceptible to intense rusting. The risk of corrosion is real when the surface chloride concentration thresholds are exceeded ($C_s > C_{th} = 1.2 \text{ kg/m}^3$). In this study, the structures were examined in time-dependent analysis exposed to corrosion-related to chloride in the initial part of their lifespan, after they were constructed, and before they reach the total life span of 100 years. Here, T_{ini} represents the beginning of corruption, marking the point when damage starts due to chloride penetration. The times in which exposure and corrosion start decide the length of corrosion, which calculates Δt with **Equation 10-14** and **10-15**.

$$T_{ini} = \frac{e^2}{4D_c \left(\text{erfc}^{-1} \left(\frac{C_{th}}{C_s} \right) \right)} \quad (10 - 14)$$

$$\ln(i_{corr}) = 0.0312RH - 4736/T + 1.695w_c - 0.0391e + 14.589 \quad (10 - 15)$$

Where D_c is the diffusion coefficient of chloride ions in concrete (mm^2/yr), erfc^{-1} is the inverse complementary error function, RH is the air relative humidity (%), T is the air temperature (K), w_c is the water-cement ratio, and e is the depth of concrete cover (mm). Since the fibres are random spread inside the concrete, the time when the fibres begin to corrode cannot be determined. To minimize the calculation complexity, this paper establishes the time to initiation of fibre corrosion as more than half of the fibres be affected by corrosion. In this paper, the statistical characteristics of geometric and material properties are based on previous studies, as

shown in **Table 10-2**.

Table 10-2 Parameters of random variable

Parameter	Symbol	Unit	Distribution	Mean	COV	Ref
Cover Depth	E	mm	Lognormal	40	0.15	[204]
Chloride Diffusion Coefficient	D_c	cm^2/s	Normal	2.0×10^{-8}	0.2	[205]
Threshold for Chloride Concentration	C_{th}	kg/m^3	Uniform	1.2	0.19	[206]
Surface Chloride Concentration,	C_s	kg/m^3	Lognormal	Table 2	0.5	[207]
Relative Humidity	RH	%	Normal	Table 2	0.1	[207]
Temperature	T	oC	Normal	Table 2	0.025	[207]
Diameter of Longitudinal Rabar	D_0	Mm	Normal	16	0.125	[208]
Water Cement Ratio	W_c	-	Normal	0.4	0.05	[209]
Width	B	mm	Normal	300	0.01	[210]
Hight	h	Mm	Normal	600	0.02	[210]
Diameter of Fibre	D_f	Mm	Normal	1	0.125	[211]
Fibre Volume	P_f	%	Normal	0.04	0.5	Assumed
Aspect Ratio of Fibre	AR	-	Normal	50	0.15	Assumed

10.4 Case Study

This research paper draws upon previous experimental studies that made for shear capacity analysis. The study employs the experimental HSFRC beams from the previous research, while the beams from the lab-based experiment are inadequate for coastal sites because they lack adequate corrosion resilience. Consequently, a new group of more extensive beams was brought in to replicate actual conditions and analyse the most critical design parameters. The original lab beams have metrics of 100 x 200mm, while the new beams have measurements of 300 x 600mm, as shown in **Table 10-2** and **Figure 10-1**, and their material and geometric properties are demonstrated.

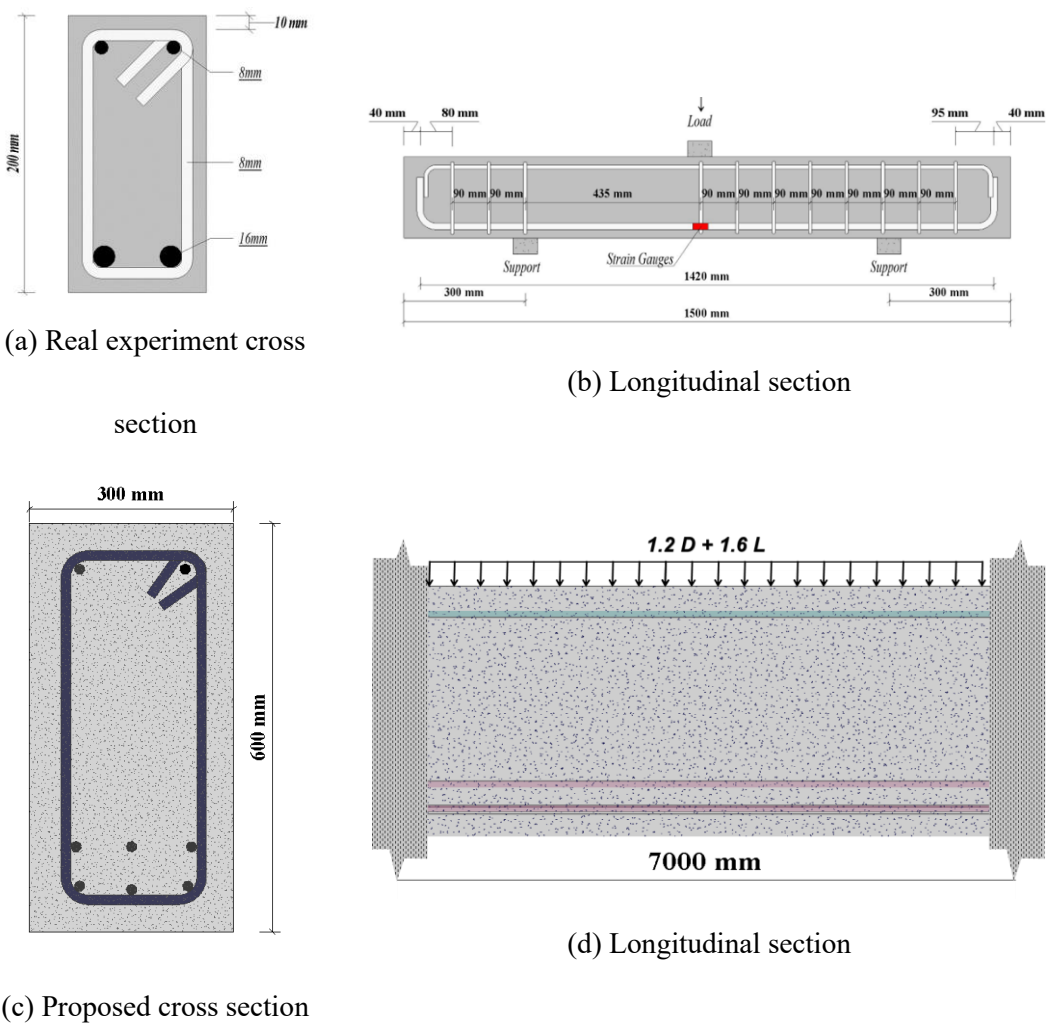


Figure 10-1 Detail of case study

The study will examine factors that may result from environmental degradation and cause changes in material properties and structural stability over time. It will take advantage of a model developed before to compute and examine these factors. By performing a material property degradation simulation and evaluating the change in load-carrying capacity over time, the article hopes to simulate and evaluate these changes. In addition, the proposed formulas assess shear strength's vulnerability due to the reinforcement of steel bars and fibre corrosion. These potential shear failures result in sudden, haphazard, and significant structural damage. Thus, an evaluation threshold is necessary for evaluating structural reliability. According to the modern structural design standards, the reliability index, β , of 3.5 is accepted for shear and must lead to sudden structural failures or severe consequences [212, 213].

10.4.1 Corrosion Environment

Environmental factors are of paramount importance in corrosion development, particularly in areas close to the sea. The harmful effects of chloride ion corrosion are particularly observed in reinforced concrete infrastructure, with the reaction rate being affected by factors such as temperature and ambient humidity. This research undertakes a detailed examination of how various environmental elements affect corrosion conditions in the region. To this end, the researchers established five distinctive corrosion environments to comprehensively investigate the corrosion characteristics of reinforced concrete structures in various environmental contexts and their possible implications for structural reliability, as shown in **Table 10-2**.

This paper has identified three additional conditions prone to severe corrosion to discuss

parameters noted in **Table 10-2** extensively. A few of the additional corrosion conditions added include high temperature, low-humidity, and coastal erosion situations. The chloride ion concentration in maritime environments is assessed, with emphasis placed on structures situated in direct contact with seawater. The chloride ion concentration in seawater is believed to be 90%, equating to 17.1 kg/m³. Concurrently, the humidity settings have been established to create an ambient moisture level that achieves approximately 60%. Though it is not yet universally agreed upon what amounts to a high-temperature environment, several interpretations include long periods of high temperatures. Based on available materials, many studies establish a threshold for a heatwave to occur at a daily maximal temperature (T_{max}) range of $\geq 35^{\circ}\text{C}$ persisting for ≥ 3 days. As such, this study understands a high-temperature environment as being $\geq 35^{\circ}\text{C}$. Also, the results are illustrated in **Figures 10-2** and **10-3** to visually clarify how variations in the environment influence structural reliability.

The lifecycle of laboratory-made concrete beams is shorter than that of the proposed beams, with the former lasting one-fourth the duration of the latter. This disparity is mainly due to the thinner protective concrete layer in the laboratory beams. Although the degradation trends are similar in both concrete beams, the trend is more pronounced in the laboratory ones. The significant reduction in the fibre content and the beam's failure to support the primary load cause rapid reliability loss after 18 years of corrosion in the laboratory beams. As degradation gradually advances, reliability gradually decreases over time. In contrast, the reliability of the large beams remains significantly high even as they approach the end of their lifecycle. Therefore, because the model resembles the laboratory beams in various ways, subsequent analyses will concentrate on it.

According to **Figure 10-2**, plates corrode and wear away a little each year, which deteriorates the structure. However, when steel fibres also suffer from corrosion (50 years after the start), the rate at which structure degrades increases. Basically, it's only seen after fifty years of using the structure. Temperature affects the structure more than humidity and concentration of chloride ions. A five-degree decrease in temperature can make a building last a further 18 years. Reducing humidity and chloride ion concentration isn't as beneficial since they don't change the lifespan that much. The importance of temperature is clear for structures in hot places. The tropical and subtropical environments' high temperatures really impact structures.

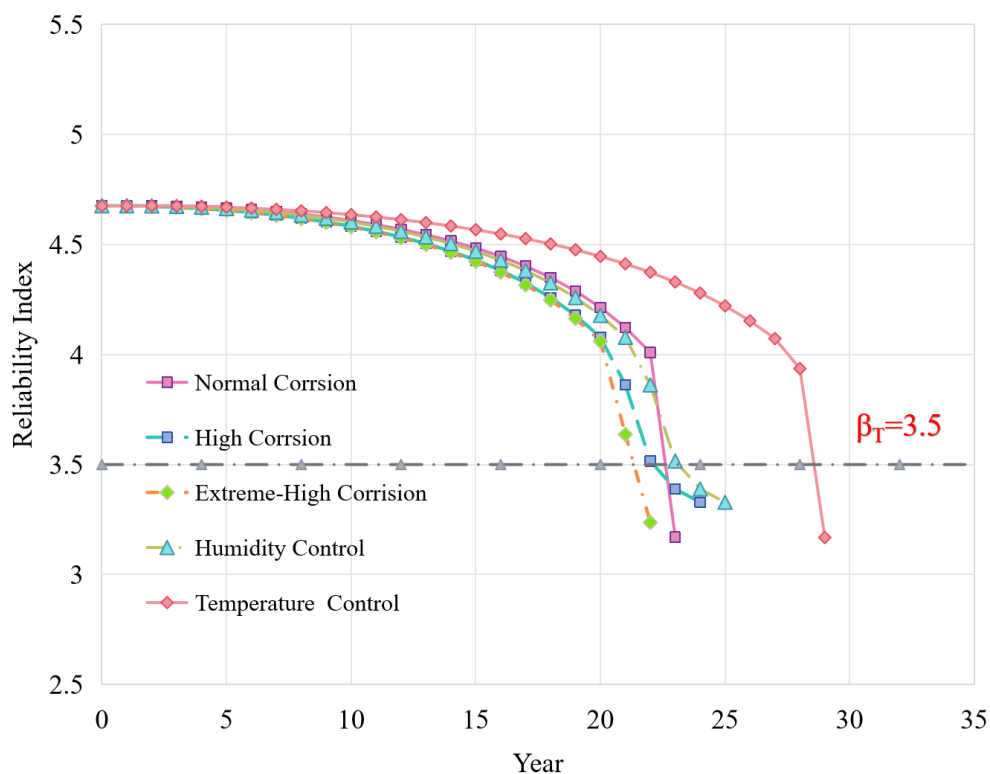


Figure 10-2 Experimental case study

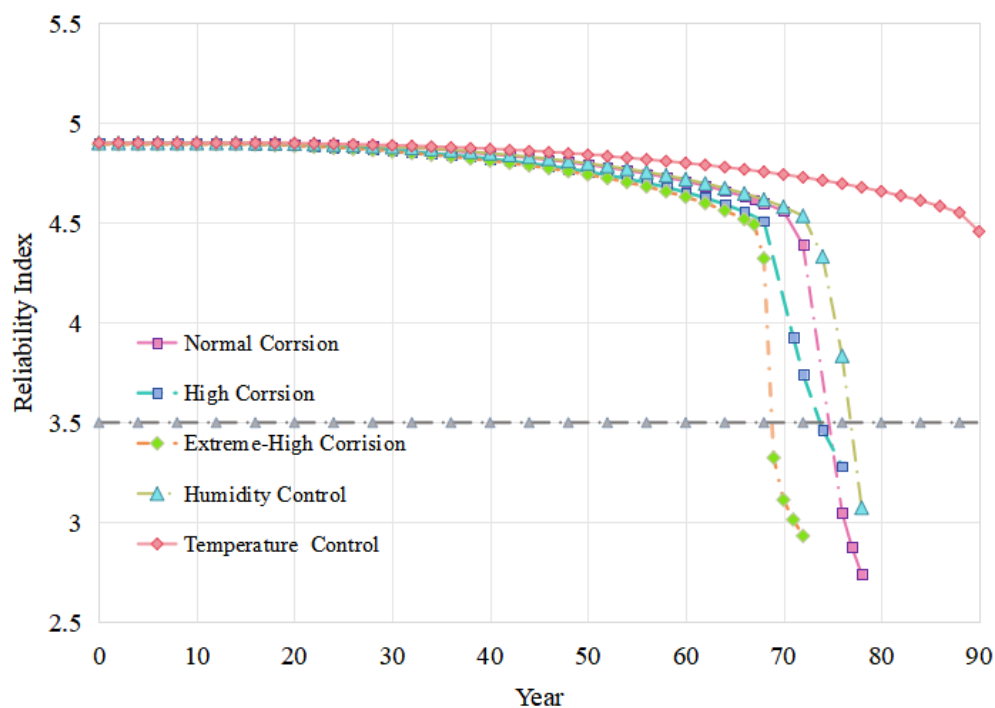


Figure 10-3 Proposed case study

10.4.2 Concrete Cover Depth

The conventional approach to structural protection athwart the coastal region is to augment the breadth of the concrete protective coating. This measure helps decelerate chloride ion ingress, thus ensuring the longevity of the steel reinforcement. The outcomes of the analysis in **Figure 10-4** indicate a significant and progressively improving relationship between the construction's longevity and the expansion of concrete protective layer thickness. With a reliability threshold of 3.5, there's a 31-year span extension when the thickness of the protective layer is increased from 30mm to 45mm. This is a 31-year lifespan expansion. On the other hand, a thickness of 50mm for the concrete protective layer can extend the structural lifespan to over 100 years. In general, augmenting the thickness of concrete protective layers provides a substantial uptick in

longevity for the construction, a slower breakdown caused by chloride ion corrosion, and a lesser degree of internal corrosion damage. This study complements designing and maintaining structures found in coastal areas, emphasizing the advantages of increases to the lens' thickness. However, augmenting thickness should consider a variety of factors such as the price, construction design, and environmental aspects.

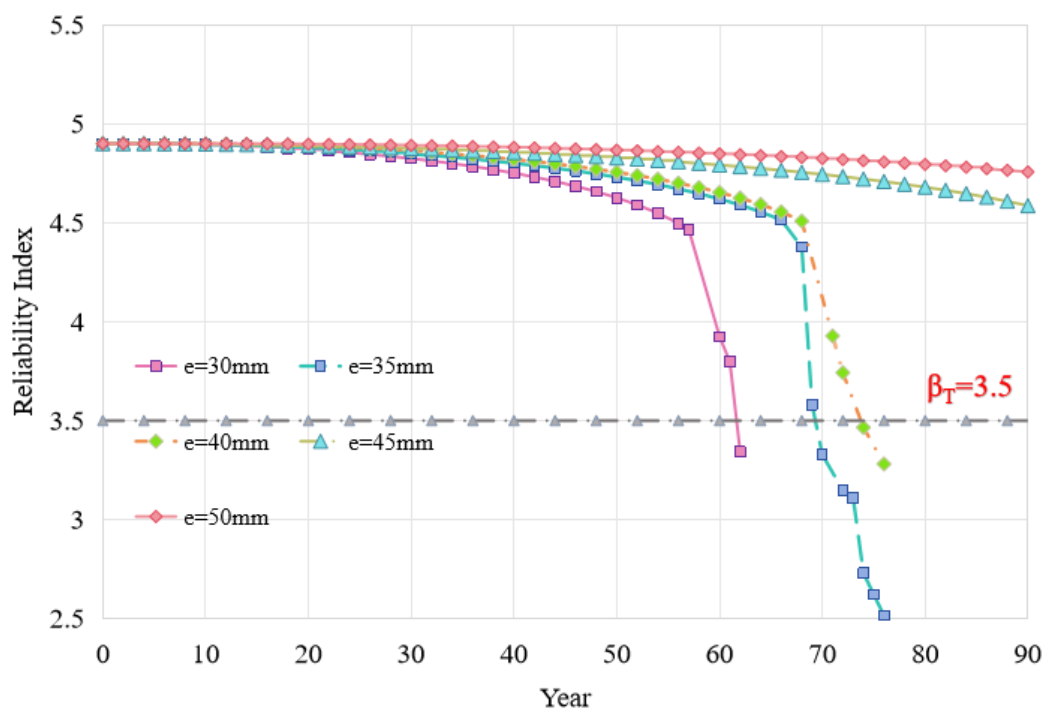


Figure 10-4 Effect of concrete cover depth

10.4.3 Steel Rebar

The initial structural reliability may strongly depend on the magnitude of the longitudinal reinforcement ratio, as shown in **Figure 10-5**. The initial reliability can increase by 140% with an increase in the reinforcement ratio from 0.22% to 1.1%. Even with a considerable rise in the ratio, the overall structure lifespan doesn't enhance significantly. Structural reliability drops significantly after around 70 years due to cross-sectional steel reinforcement loss. In reality,

when the cross-sectional steel reinforcement reaches a specific loss level, it approaches the load combination threshold, leading to a sharp rise in instability coefficients and causing a drop in structural reliability. Consequently, some instability coefficient values in the calculation matrix may surpass the load combination, resulting in rapid reliability reduction.

Increasing the reinforcement ratio in a corrosive environment has no impact on extending structural life, but it diminishes the effectiveness of elevating the structure's initial reliability. Therefore, the study underscores the need for proper control of the longitudinal reinforcement ratio during structural design and upkeep to guarantee the structure's long-term reliability and durability. It also underscores that, given the corrosive environment, selectively increasing the reinforcement ratio is not enough to ensure the structure's safe operation. It is critical to consider various factors.

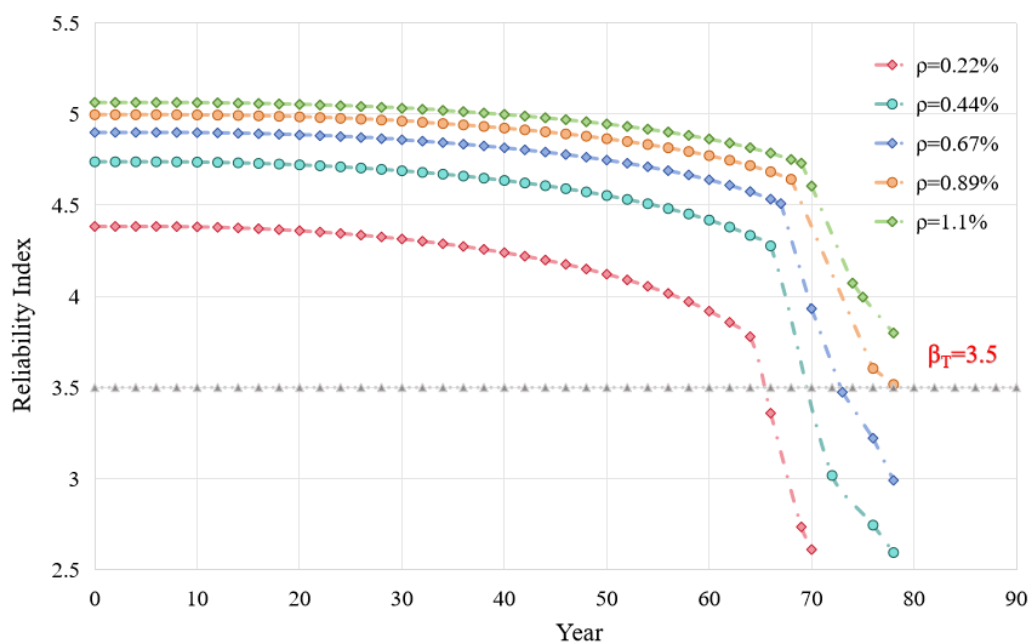


Figure 10-5 Effect of longitudinal ratio

10.4.4 Fibre Type

The impact of ISF content on structural reliability is shown in **Figure 10-16**. As the amount of ISF increases the original structural reliability is threatened especially due to the uncertainty of fibre. Fibres tend to redistribute unevenly in the structure, leading to a complex and disorganised system. This complex distribution may raise the overall load-distribution capacity in the structure but also leads to additional unpredictability which results in a reduction in the structural reliability. The decrease in structural reliability notwithstanding, adding steel fibres substantially lengthens the lifespan of the structure. The structure's lifespan increases by 15years when adding ISF from 1% to 3%, which shows that adding ISF raises the structural complexity and unpredictability while the potential impacts on extending the structure's lifespan are still significant.

The study evaluated the credibility shift of five eco-friendly RSF compared to ISF over time. It is crucial to note that the data from ref [214] was used to approximate RSF's corrosion process differences in ISF. As noted, ISF have chloride ion presence of 2.0, which increases to 2.472 in RSF. The data presented in **Figures 10-3** and **10-7** underlines RSF's weak performance compared to ISF in the past and present as well as their reliability increase over time. However, it is worth noting that further experiments and theoretical support are needed for fatigue stress analysis of environmentally friendly RSFs. As a secondary material, RSFs display greater uncertainty. Nevertheless, their high fatigue resistance comes from recycled steel wire from used tyres, their raw material

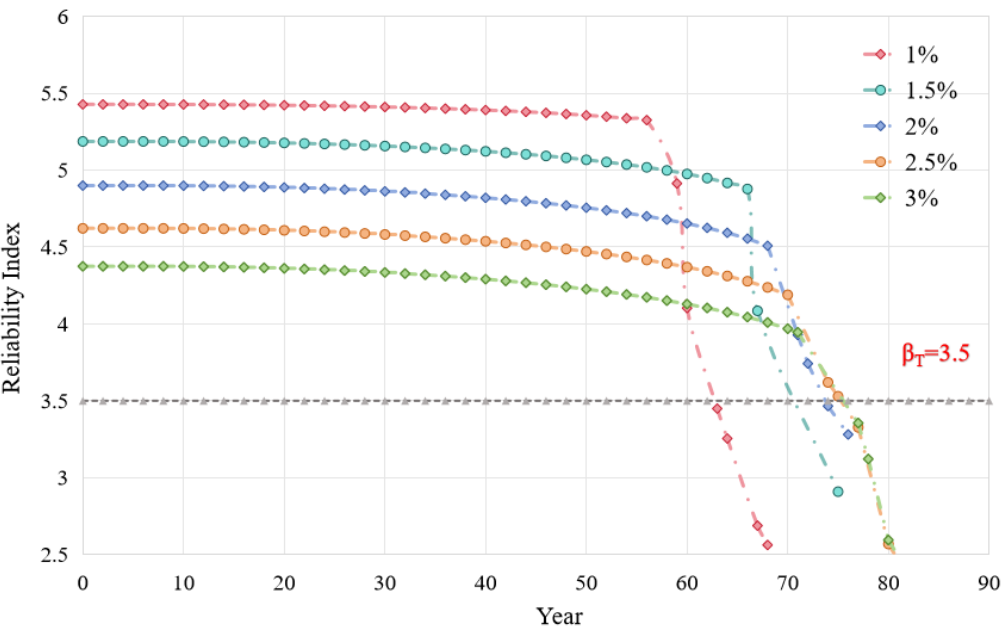


Figure 10-6 Effect of fibre content

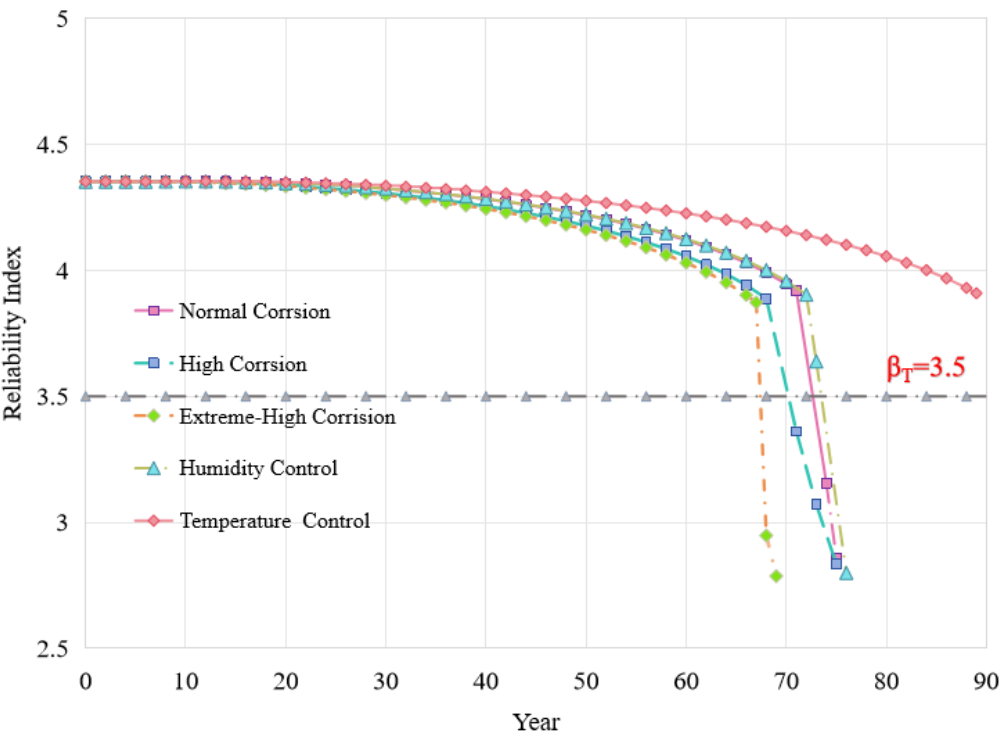


Figure 10-7 Effect of adding RSF in concrete

10.5 Conclusion Remark

This study presents a detailed analysis of HSFRC beams in corrosive environments. A new shear model tailored for corrosion conditions is proposed, filling a research gap by quantitatively assessing shear performance and providing essential engineering insights. The study also evaluates the durability of reinforced concrete in coastal settings, focusing on chloride-induced corrosion. It introduces a method to estimate corrosion onset and examines how increasing the thickness of protective concrete layers can extend structural lifespan and reduce corrosion risks. Comparative analyses reveal that while ISF generally enhance structural reliability more effectively than RSF, RSF can still partially replace ISF due to their environmental benefits.

In summary, this research offers critical guidance for evaluating HSFRC beams in corrosive environments and acknowledges the need for further model improvements. The following section will explore time-dependent reliability analysis, addressing the long-term durability of SFRC beams under extreme conditions such as coastal corrosion.

11. Conclusion and Recommendations

The thesis thoroughly explores the ability of collecting RSF from ELT tires for different engineering applications. It synthesizes a combination of experiments, numerical, and reliability analysis for ISFRC and HSFRC structures. The main findings outlined below:

11.1 Experimental Analysis

The experimental research parts examine the possibility of using RSF to replace the ISF in concrete. The study focuses on the fundamental properties of concrete and structural components' performance. Fundamentally, this study created seven different concrete mixtures with different fibre replacement contents and performed a series of experiments ranging from compressive, splitting tensile, CMOD, modal testing, and shear capacity.

In terms of fundamental properties, the experimental results indicate that with an increase in RSF content, the compressive strength, splitting tensile strength, and flexural strength of RSFRC significantly improve. Although the performance of RSFRC is slightly inferior to that of ISFRC, RSF can still effectively enhance concrete properties when its content is below 0.8%. For example, the use of 1.2% RSF can increase the compressive strength, splitting tensile strength, and flexural strength of concrete by 11.2%, 32.5%, and 82.3%, respectively. However, tensile test results show that due to limitations in the RSF manufacturing process, it is less effective than ISF in improving the residual stress of concrete. The hooked ends of RSF, weakened by high fatigue damage, reduce the strength, thereby diminishing its ability to restrain large cracks, which affects the overall mechanical performance of SFRC. Additionally, with an increase in RSF content, the natural frequency of concrete slightly increases from

1343.0 Hz to 1385.9 Hz at 1.2% fibre content, an increase of approximately 3.19%. By analysing the dynamic performance in conjunction with mechanical performance, a significant correlation was found between the two properties, with a prediction accuracy R^2 exceeding 0.97, providing a theoretical basis for future non-destructive testing.

Regarding the performance of structural components, this study assessed the shear behaviour of RSFRC and ISFRC beams under different shear span ratios and fibre properties. The experimental results show that although the shear capacity of ISFRC beams is slightly higher than that of RSFRC beams, the difference in strength is relatively small, particularly at a fibre content of 0.8%, where the difference is only 3.05 MPa. Specimens with smaller shear span ratios (e.g., 1.5) exhibited typical shear-compression failure modes. However, after RSF or ISF reinforcement, the peak load of the specimens significantly increased, and the original failure mode changed to shear-tension failure. In specimens with larger shear span ratios ($\lambda = 2.5, 3.5, 4$), diagonal tensile failure was observed. The bridging effect of fibres significantly enhanced the load-bearing capacity and deformability of concrete beams, particularly with RSF, which, despite its slightly lower performance compared to ISF, still demonstrated considerable structural enhancement. Further analysis revealed that the load-displacement curves of RSFRC and ISFRC beams exhibited similar trends, and the fibres had comparable effects on improving the load-bearing capacity and stiffness of the beams, indicating that RSF can be used as a substitute for ISF in practical engineering under certain conditions.

The finding in experimental research shown that RSF has shown good potential in both fundamental mechanical properties and structural component performance. Although it is

slightly inferior to ISF in some aspects, it can still provide an effective alternative for engineering applications.

11.2 Numerical Analysis

This study conducted a systematic qualitative and quantitative analysis of the structural performance of HSFRC beams, leading to an advanced formulation of the existing TR63 and Eurocode 2 standards. By incorporating the shear span ratio as a critical parameter, the new formula significantly improves the accuracy of predicting the shear capacity of both ISFRC and RSFRC beams. This formula is not only based on extensive experimental data but also derived from precise regression analysis, integrating experimental results with the best practices of existing formula designs.

In terms of machine learning numerical analysis, the study employed three ML models (ANN, Xgboost, and BNN) to accurately predict the shear strength, flexural capacity, and stiffness of HSFRC beams. Notably, the BNN model performed best in predicting flexural capacity and stiffness, while the Xgboost model, despite showing the lowest error and highest R^2 during training, exhibited relatively weaker generalization ability on test data. Additionally, sensitivity analysis further confirmed that fibre content and shear span ratio are the primary factors influencing shear strength, whereas compressive strength has a lesser impact. The results also indicate that increasing the fibre content in the structure not only improves structural performance but also offers significant environmental and economic benefits, particularly in balancing sustainability goals with structural performance.

Regarding FEM numerical analysis, this study developed a nonlinear analysis model for

different fibre contents, shear span ratios, and fibre types (RSF and ISF) to explore in detail the shear performance of HSFRC beams. By employing the RILEM TC 162-TDF CDP model and integrating residual stress testing, the study successfully optimized the prediction of shear capacity, demonstrating FEM's exceptional ability to capture the interaction between SFRC and reinforcement. The analysis shows that as the shear span ratio increases, the ultimate strength of the beam significantly improves, particularly when the shear span ratio exceeds 2.5, where the contribution of fibre content to enhancing shear resistance is especially pronounced. While the model exhibited good predictive ability across different types of HSFRC, the inherent uncertainty of RSF resulted in slightly lower predictive accuracy compared to ISF. Further model development included the proposal of a new KSM model based on FEM results, and modifications to the TR63 formula, leading to an improved predictive model with a higher R^2 value (0.97), thereby significantly enhancing the accuracy and applicability of the model.

In summary, this study presents a comprehensive and innovative set of tools for predicting the shear performance of HSFRC beams by combining formula-based predictions, ML models, and FEM analysis. These models not only enhance the precision and efficiency of structural design but also provide more efficient, economical, and environmentally friendly solutions for the construction industry by balancing structural performance with sustainability demands. The findings will contribute to optimizing resource utilization, reducing material waste, and promoting more sustainable engineering practices.

11.3 Reliability Analysis

This study developed a reliability-based design procedure within the framework of FORM and

SORM to determine the resistance factors for HSFRC and NSFRC beams under various load types, including dead load, live load, wind load, snow load, and seismic load. A comparative analysis was conducted on five commonly used shear models, followed by a sensitivity analysis of the optimal model. The results indicate that the uncertainty factor θ_R of the shear models for HSFRC beams follows log-normal and Weibull, the Ashour model was identified as the optimal model, with a resistance factor of 0.59, while for NSFRC, the Kara model was deemed most suitable, with a resistance factor of 0.61. The sensitivity analysis revealed that the shear model for HSFRC is more sensitive to dataset variations, indicating that its design is less mature. Nevertheless, the Ashour model maintained a high reliability index even with a standard deviation fluctuation of 20% to 30%.

Further research delved into the time-dependent reliability of HSFRC beams in corrosive environments. A new shear model was proposed to assess the shear performance of HSFRC beams under corrosion conditions, addressing a gap in existing studies. The investigation into the effects of chloride ingress on the durability of reinforced concrete structures in coastal environments found that appropriately increasing the thickness of the concrete cover can effectively extend the structure's lifespan and reduce corrosion risk. Additionally, the study evaluated the roles of ISF and RSF in concrete structures. The results showed that although ISF outperforms RSF in enhancing structural reliability, RSF offers unique environmental benefits, making it a viable partial substitute for ISF.

11.3 Conclusion Remark

This study systematically analysed the structural performance of HSFRC beams, focusing on

the formulation and prediction of shear capacity, and proposed improved formulas based on the TR63 and Eurocode 2 standards. Additionally, the research employed three machine learning models and developed high-precision predictive tools through finite element analysis to evaluate the effectiveness of different types of fibre in concrete beams. Through reliability analysis and time-dependent reliability analysis, the study further explored the performance of SFRC beams under various environmental conditions, particularly the time-dependent reliability in corrosive environments, providing robust theoretical support for optimizing structural design and enhancing material applicability.

In summary, this research offers comprehensive theoretical foundations and practical guidance for the design and application of HSFRC beams. By integrating formula-based prediction, ML, FEM, and reliability analysis, the study not only improved the accuracy of structural performance predictions but also laid the groundwork for sustainable engineering practices, holding significant academic and practical engineering value.

11.4 Advice for Future Research

Future research should delve deeper into the mechanisms of corrosion of SFRC including electrochemical reactions, chloride ion penetration, and the formation of corrosion products. Additionally, durability analysis should encompass freeze-thaw cycles, high temperatures, and other extreme environmental conditions. These studies require not only theoretical exploration but also long-term exposure experiments to ensure sustained structural performance in real-world applications.

The nonlinear behaviour of SFRC beams under complex loading conditions, such as cyclic

loading, dynamic impacts, and seismic loads, requires further investigation. Future studies should employ more sophisticated numerical simulations and experimental testing to understand the mechanical responses of these structures under complex scenarios. This will enable the refinement of existing predictive models, making them more accurate in reflecting the complexities encountered in real-world engineering, which is crucial for enhancing structural resilience and safety.

While significant theoretical advancements have been made in the study of SFRC, challenges remain in translating these theories into practical engineering applications. Future research should focus on bridging the gap between theory and practice, exploring how laboratory findings can be transformed into actionable engineering technologies. This will ensure that innovative materials and structural designs can be effectively implemented in real-world construction projects, meeting the practical demands of the industry.


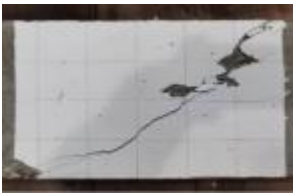





Future research should prioritize the collection of extensive experimental data and the development of advanced models to guide the production and application of SFRC. These models need to be highly accurate and supported by a comprehensive database that covers a wide range of conditions. Emphasizing the precision of models and the completeness of data is crucial for improving the reliability and practicality of structural design and decision-making processes.

Given the increasing frequency of seismic activities worldwide, it is essential to study the behaviour of SFRC beams under seismic conditions. Future research should conduct comprehensive analyses of the material's seismic performance through experiments and

numerical simulations, focusing on energy absorption, crack propagation, and structural failure modes. Additionally, developing design codes and standards tailored to different seismic conditions will ensure that these structures can effectively enhance the earthquake resilience and safety of buildings in practical applications.

Appendix A

Table A-1 Failure mode analysis

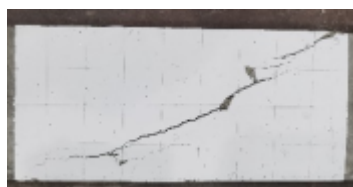
Beam	Failure Mode
M0-1.5	
M1-ISF-1.5	
M2-ISF-1.5	
M1-RSF-1.5	
M2-RSF-1.5	
M0-2.5	
M1-ISF-2.5	

Appendix

M2-ISF-2.5



M1-RSF-2.5



M2-RSF-2.5



M0-3.5



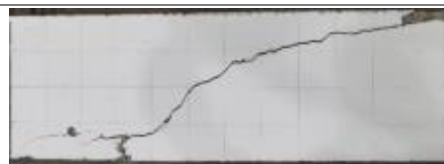
M1-ISF-3.5



M2-ISF-3.5




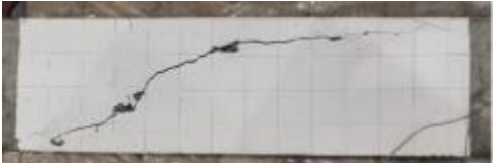

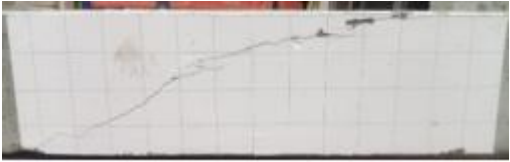
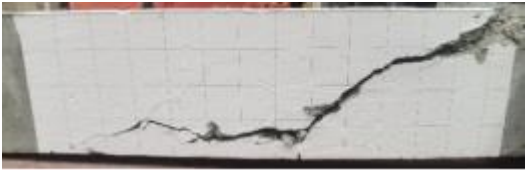
M1-RSF-3.5



M2-RSF-3.5



Appendix

M0-4	
M1-ISF-4	
M2-ISF-4	
M1-RSF-4	
M2-RSF-4	

Appendix

Table A-2 Datasets for shear capacity analysis

Number of Beam	Compressive Strength MPa	Fibre Content %	Shear Span	Fibre Type	Ref
18	92 ~101.32	0.5~1.5	1, 2, 4, 6	Hooked	[182]
3	62.3	0.75	2, 4, 6	Hooked	[215]
6	82~83.8	0.5~1.5	1.5, 2.5	Hooked	[216]
16	63.1~65	0~3	2.2	Hooked	[217]
9	62.6~68.6	0~0.75	2, 3, 4	Hooked	[218]
6	61.6~73	0~0.75	3	Hooked	[219]
9	53.4~64.6	0.75~1. 5	3.49	Hooked	[220]
16	108.5~112	0~0.75	1.75, 2.5, 3.5, 4.5	Hooked	[124]
14	54.3~89.9	0~2	1.05	Hooked	[221]
20	57.3~65.8	0.25~3	2, 2.5, 3	Crimped	[222]
13	80	0~1	2, 3, 4.5, 6	Plain	[223]
17	72~93.3	0.5~1	2.77~3.33	Plain and Hooked	[224]
4	54	1.5	1.5~2.5	Plain	[225]
3	58~88	0.5~1	3	Hooked	[226]

Appendix

10	62.6	1	1~3	Crimped	[227]
----	------	---	-----	---------	-------

Table A-3 Datasets for ML analysis

Number of Beam	Compressive Strength MPa	Fibre Content %	Shear Span	Fibre Type	Ref
18	92 ~101.32	0.5~1.5	1, 2, 4, 6	Hooked	[182]
3	62.3	0.75	2, 4, 6	Hooked	[215]
6	82~83.8	0.5~1.5	1.5, 2.5	Hooked	[216]
16	63.1~65	0~3	2.2	Hooked	[217]
1	58.87	1	1.5	Hooked	[228]
9	62.6~68.6	0~0.75	2, 3, 4	Hooked	[218]
6	61.6~73	0~0.75	3	Hooked	[219]
9	53.4~64.6	0.75~1.5	3.49	Hooked	[220]
16	108.5~112	0~0.75	1.75, 2.5, 3.5, 4.5	Hooked	[124]
14	54.3~89.9	0~2	1.05	Hooked	[221]
20	57.3~65.8	0.25~3	2, 2.5, 3	Crimped	[222]
13	80	0~1	2, 3, 4.5, 6	Plain	[223]
17	72~93.3	0.5~1	2.77~3.33	Plain and Hooked	[224]

Appendix

4	54	1.5	1.5~2.5	Plain	[225]
3	58~88	0.5~1	3	Hooked	[226]
11	62.6	1	1~3	Crimped	[227]
2	54.1~54.8	0.4~0.75	1.63	Hooked	[229]
1	59.4	0.5	3.77	Hooked	[230]
2	109.2~110.9	0.75	2.75	Hooked	[231]

Table A-4 Datasets for ML analysis

Number of Beam	Compressive Strength MPa	Fibre Content %	Fibre Type	Author
11	34.2 ~78.1	0~1.5	Hooked	[177]
6	64.2~65	0.5~3	Hooked	[232]
3	34~42.4	0~2	Plain	[233]
4	40.85~43.23	1~2	Hooked	[234]
6	36.5~65	1~2	Hooked	[235]
15	36.97~40.88	0~1	Crimped	[236]
6	80.2~95.2	0.5~2	Hooked	[237]
39	37~90	0~1.75	Hooked	[238]
8	108.5~111.5	0.75	Hooked	[239]
9	40.3~47.8	0~2	Plain	[240]
52	10.04~90.5	0~1.75	Hooked	[241]
24	79.7~92.1	0~1	Crimped	[222]

Appendix

Table A-5 NSFRC beams datasets for reliability analysis

Author	Number of Beam	Compressive Strength MPa	Fibre Content %	Shear Span	Fibre Type
[242]	3	24.1~32.9	0.75~1.25	3.45	Hooked
[243]	3	22~31	1	3	Hooked
[244]	10	31~49.2	1~1.5	3.4~3.5	Hooked
[245]	17	37.7~48.3	0.25~0.76	1.5~4	Hooked
[246]	3	35	0.75	1.59~2.95	Hooked
[247]	28	30.6~53.55	0.25~2	2.02~3.11	Crimped
[234]	4	40.85~43.23	1~2	2~2.8	Hooked
[233]	2	38.69~42.4	1~2	3.08	Straight smooth
[248]	21	29.6~44.9	0.75~1.5	3.44	Hooked
[249]	4	19.6~21.3	0.5~1	3	Hooked
[250]	4	24.8~38.6	0.38~0.57	2.5	Hooked

Appendix

[251]	3	44.6	0.5	2~4	Hooked
[252]	7	34	0.5~1	1.5~3.5	Hooked
[180]	9	20.6~29.9	0.5~0.75	2~3.6	Hooked
[253]	5	33~36	0.75~1	1.5~2.5	Hooked
[254]	2	21~56	0.75	4	Hooked
[255]	1	48.6	0.96	1.81	Hooked
[227]	11	22.7~53	1~2	1.5~3	Crimped&H ooked
[256]	7	33.9~41.9	1	2~4.91	Crimped
[257]	9	38~53.7	0.5~1	3	Hooked& flat end
[258]	20	27.2~47.6	0.25~0.75	1.5~3.5	Hooked
[259]	5	36.4~40.8	0.8~1.2	4.5	Hooked
[260]	41	33.22~40.21	0.22~1.76	3.2~4.8	Crimped&Ro und

Appendix

[261]	4	34.45~37.13	0.5~2	2	Mill-cut
[262]	4	33.1	1~2	2.5	Hooked
[226]	5	35.5~40	0.5~2	3.02~3.14	Hooked
[263]	4	49.6~54.5	0.5~1	3.77~3.81	Hooked
[264]	11	36	0.5~0.75	1~2.5	Hooked
[265]	7	49.3~54.8	0.5~2	3.52	Crimped
[266]	2	39.8~41.2	1~1.5	3	Hooked
[267]	2	30	0.5	1.8	Hooked
[88]	3	50	0.769	2.56	Recycled
[268]	2	23~41	1	3	Hooked
[269]	3	31.9	0.2~0.6	1.13	Corrugated

Reference

- [1] Mohajerani A, Burnett L, Smith JV, Markovski S, Rodwell G, Rahman MT et al. Recycling waste rubber tyres in construction materials and associated environmental considerations: A review. *Resources, Conservation and Recycling*. 2020;155.
- [2] Hamdi A, Abdelaziz G, Farhan KZ. Scope of reusing waste shredded tires in concrete and cementitious composite materials: A review. *Journal of Building Engineering*. 2021;35.
- [3] Fedroff D, Ahmad S, Savas BZJTRR. Mechanical properties of concrete with ground waste tire rubber. 1996;1532:66-72.
- [4] Liew KM, Akbar A. The recent progress of recycled steel fiber reinforced concrete. *Construction and Building Materials*. 2020;232.
- [5] Samarakoon SMSMK, Ruben P, Wie Pedersen J, Evangelista L. Mechanical performance of concrete made of steel fibers from tire waste. *Case Studies in Construction Materials*. 2019;11.
- [6] El-Gammal A, Abdel-Gawad A, El-Sherbini Y, Shalaby AJJoETiE, Sciences A. Compressive strength of concrete utilizing waste tire rubber. 2010;1:96-9.
- [7] Sienkiewicz M, Kucinska-Lipka J, Janik H, Balas AJWm. Progress in used tyres management in the European Union: A review. 2012;32:1742-51.
- [8] Aderemi AO, Otitoloju AAJJJoEP. An assessment of landfill fires and their potential health effects-a case study of a municipal solid waste landfill in Lagos, Nigeria. 2012;2:22-6.
- [9] Shulman VL. Tire recycling. *Waste: Elsevier*; 2019. p. 489-515.

- [10] Lin H-M. A scenario study on end-of-life tyre management in 2020. 2011.
- [11] Roychand R, Gravina RJ, Zhuge Y, Ma X, Youssf O, Mills JE. A comprehensive review on the mechanical properties of waste tire rubber concrete. *Construction and Building Materials*. 2020;237.
- [12] Burchart-Korol D. Life cycle assessment of steel production in Poland: a case study. *Journal of Cleaner Production*. 2013;54:235-43.
- [13] Shih P-H, Wu Z-Z, Chiang H-LJWm. Characteristics of bricks made from waste steel slag. 2004;24:1043-7.
- [14] Centonze G, Leone M, Aiello MA. Steel fibers from waste tires as reinforcement in concrete: A mechanical characterization. *Construction and Building Materials*. 2012;36:46-57.
- [15] Centonze G, Leone M, Aiello MJC, Materials B. Steel fibers from waste tires as reinforcement in concrete: A mechanical characterization. 2012;36:46-57.
- [16] Bisegna P, Luciano RJMom. Bounds on the overall properties of composites with debonded frictionless interfaces. 1998;28:23-32.
- [17] Feo L, Greco F, Leonetti L, Luciano RJCS. Mixed-mode fracture in lightweight aggregate concrete by using a moving mesh approach within a multiscale framework. 2015;123:88-97.
- [18] Yazıcı Ş, Arel HŞ. The effect of steel fiber on the bond between concrete and deformed steel bar in SFRCs. *Construction and Building Materials*. 2013;40:299-305.
- [19] Won J-P, Lee J-H, Lee S-JJCS. Predicting pull-out behaviour based on the bond mechanism of arch-type steel fibre in cementitious composite. 2015;134:633-44.

- [20] Carpinteri A, Fortese G, Ronchei C, Scorza D, Vantadori SJT, Mechanics AF. Mode I fracture toughness of fibre reinforced concrete. 2017;91:66-75.
- [21] Vantadori S, Carpinteri A, Guo L-P, Ronchei C, Zanichelli AJCPBE. Synergy assessment of hybrid reinforcements in concrete. 2018;147:197-206.
- [22] Shah AA, Ribakov Y. Recent trends in steel fibered high-strength concrete. Materials & Design. 2011;32:4122-51.
- [23] Düzgün OA, Gül R, Aydın ACJML. Effect of steel fibers on the mechanical properties of natural lightweight aggregate concrete. 2005;59:3357-63.
- [24] Benaïmeche O, Carpinteri A, Mellas M, Ronchei C, Scorza D, Vantadori SJCPBE. The influence of date palm mesh fibre reinforcement on flexural and fracture behaviour of a cement-based mortar. 2018;152:292-9.
- [25] Vantadori S, Carpinteri A, Zanichelli AJT, Mechanics AF. Lightweight construction materials: Mortar reinforced with date-palm mesh fibres. 2019;100:39-45.
- [26] Leone M, Centonze G, Colonna D, Micelli F, Aiello MA. Fiber-reinforced concrete with low content of recycled steel fiber: Shear behaviour. Construction and Building Materials. 2018;161:141-55.
- [27] Mastali M, Dalvand A, Sattarifar AR, Ilkainen M. Development of eco-efficient and cost-effective reinforced self-consolidation concretes with hybrid industrial/recycled steel fibers. Construction and Building Materials. 2018;166:214-26.
- [28] Isa M, Pilakoutas K, Guadagnini M, Angelakopoulos HJC, Materials B. Mechanical performance of affordable and eco-efficient ultra-high performance concrete (UHPC) containing recycled tyre steel fibres. 2020;255:119272.

- [29] Fazli A, Rodrigue DJJoCS. Recycling waste tires into ground tire rubber (GTR)/rubber compounds: A review. 2020;4:103.
- [30] Crane G, Elefritz R, Kay E, Laman JJRC, Technology. Scrap tire disposal procedures. 1978;51:577-99.
- [31] Reschner KJAsopd, recycling methods. Entire-Engineering B. Scrap tire recycling. 2008.
- [32] Dobrotă D, Dobrotă G, Dobrescu TJJoCP. Improvement of waste tyre recycling technology based on a new tyre markings. 2020;260:121141.
- [33] Li X, Xu X, Liu ZJPt. Cryogenic grinding performance of scrap tire rubber by devulcanization treatment with ScCO₂. 2020;374:609-17.
- [34] Barros JAO, Frazão C, Caggiano A, Folino P, Martinelli E, Xargay H et al. Cementitious Composites Reinforced with Recycled Fibres. Recent Advances on Green Concrete for Structural Purposes2017. p. 141-95.
- [35] Islam M, Joardder M, Hasan S, Takai K, Haniu HJWm. Feasibility study for thermal treatment of solid tire wastes in Bangladesh by using pyrolysis technology. 2011;31:2142-9.
- [36] Turer A. Recycling of scrap tires. Material Recycling-Trends Perspectives. 2012:195-212.
- [37] Islam MR, Parveen M, Haniu H, Sarker MIJJoES, Development. Innovation in pyrolysis technology for management of scrap tire: a solution of energy and environment. 2010;1:89.

- [38] Nkosi N, Muzenda E. A review and discussion of waste tyre pyrolysis and derived products. Proceedings of the world congress on engineering 2014. p. 2-4.
- [39] Alsaleh A, Sattler MLJCSRER. Waste tire pyrolysis: influential parameters and product properties. 2014;1:129-35.
- [40] Barbooti MM, Mohamed TJ, Hussain AA, Abas FOJJoA, Pyrolysis A. Optimization of pyrolysis conditions of scrap tires under inert gas atmosphere. 2004;72:165-70.
- [41] Rutherford Sr D. Process for recycling vehicle tires. Google Patents; 1992.
- [42] Martinelli E, Caggiano A, Xargay HJC, Materials B. An experimental study on the post-cracking behaviour of Hybrid Industrial/Recycled Steel Fibre-Reinforced Concrete. 2015;94:290-8.
- [43] Danso H, Martinson DB, Ali M, Williams J. Effect of fibre aspect ratio on mechanical properties of soil building blocks. Construction Building Materials. 2015;83:314-9.
- [44] Yazıcı Ş, İnan G, Tabak V. Effect of aspect ratio and volume fraction of steel fiber on the mechanical properties of SFRC. Construction and Building Materials. 2007;21:1250-3.
- [45] Johnston CD, Zemp RWJMJ. Flexural fatigue performance of steel fiber reinforced concrete--influence of fiber content, aspect ratio, and type. 1991;88:374-83.
- [46] Hu H, Papastergiou P, Angelakopoulos H, Guadagnini M, Pilakoutas K. Mechanical properties of SFRC using blended Recycled Tyre Steel Cords (RTSC) and

- Recycled Tyre Steel Fibres (RTSF). Construction and Building Materials. 2018;187:553-64.
- [47] Grzymiski F, Musiał M, Trapko T. Mechanical properties of fibre reinforced concrete with recycled fibres. Construction and Building Materials. 2019;198:323-31.
- [48] Sudhikumar G, Prakash K, Rao MS. Effect of aspect ratio of fibers on the strength characteristics of slurry infiltrated fibrous ferrocement. Journal of civil structural engineering. 2014;3:29-37.
- [49] Peng GF, Niu XJ, Long QQ. Experimental Study of Strengthening and Toughening for Recycled Steel Fiber Reinforced Ultra-High Performance Concrete. Key Engineering Materials. 2014;629-630:104-11.
- [50] Skarżyński Ł, Suchorzewski J. Mechanical and fracture properties of concrete reinforced with recycled and industrial steel fibers using Digital Image Correlation technique and X-ray micro computed tomography. Construction and Building Materials. 2018;183:283-99.
- [51] Bjegovic D, Baricevic A, Lakusic S, Damjanovic D, Duvnjak I. Positive Interaction of Industrial and Recycled Steel Fibres in Fibre Reinforced Concrete. Journal of Civil Engineering and Management. 2014;19:S50-S60.
- [52] Lee DJ, Ryu SR. The Influence of Fiber Aspect Ratio on The Tensile and Tear Properties of Short-Fiber Reinforced Rubber. ICCM12. 1999.
- [53] Nakagawa T. Steel fiber for reinforced concrete. Google Patents; 1981.
- [54] Figueiredo ADd, Ceccato MR. Workability Analysis of Steel Fiber Reinforced Concrete Using Slump and Ve-Be Test. Materials Research. 2015;18:1284-90.

- [55] Hoang N-D, Pham A-D. Estimating Concrete Workability Based on Slump Test with Least Squares Support Vector Regression. *Journal of Construction Engineering*. 2016;2016.
- [56] Acikgenc M, Alyamac KE, Ulucan ZC. Fresh and hardened properties of steel fiber reinforced concrete produced with fibers of different lengths and diameters. 2013.
- [57] Leone M, Centonze G, Colonna D, Micelli F, Aiello MA. Experimental Study on Bond Behavior in Fiber-Reinforced Concrete with Low Content of Recycled Steel Fiber. *Journal of Materials in Civil Engineering*. 2016;28.
- [58] Rossli SA, Ibrahim IS. Mechanical properties of recycled steel tire fibres in concrete. Technical Report, Faculty of Civil Engineering, University Technology Malaysia; 2012.
- [59] Boulekbache B, Hamrat M, Chemrouk M, Amziane S. Flowability of fibre-reinforced concrete and its effect on the mechanical properties of the material. *Construction Building Materials*. 2010;24:1664-71.
- [60] Li P, Yu Q, Brouwers H, Yu R. Fresh behaviour of ultra-high performance concrete (UHPC): an investigation of the effect of superplasticizers and steel fibres. *Proceedings of the 9th International Concrete Conference 2016, Environment, Efficiency and Economic Challenges for Concrete*, July 4-6, 2016, Dundee, Scotland, United Kingdom 2016, p. 635-44.
- [61] Mezzal SK, Al-Azzawi Z, Najim KBJFSJ. Effect of discarded steel fibers on impact resistance, flexural toughness and fracture energy of high-strength self-compacting concrete exposed to elevated temperatures. 2021;121:103271.

- [62] Richardson A, Coventry K, Wilkinson S. Freeze/thaw durability of concrete with synthetic fibre additions. *Cold regions science and technology*. 2012;83:49-56.
- [63] Guerini V, Conforti A, Plizzari G, Kawashima S. Influence of steel and macro-synthetic fibers on concrete properties. *Fibers*. 2018;6:47.
- [64] Smrkić MF, Damjanović D, Baričević A. Application of recycled steel fibres in concrete elements subjected to fatigue loading. *Građevinar*. 2017;69:893-905.
- [65] Zhang P, Li D, Qiao Y, Zhang S, Sun C, Zhao TJJoMiCE. Effect of air entrainment on the mechanical properties, chloride migration, and microstructure of ordinary concrete and fly ash concrete. 2018;30:04018265.
- [66] Wang W, Wang L, Shi Q, Yu H, Chen T, Wang C et al. Progress of the surface modification of PP fiber used in concrete. 2006;45:29-34.
- [67] Baricevic A, Bjegovic D, Skazlic M. Hybrid Fiber-Reinforced Concrete with Unsorted Recycled-Tire Steel Fibers. *Journal of Materials in Civil Engineering*. 2017;29.
- [68] Wu H, Lin X, Zhou A. A review of mechanical properties of fibre reinforced concrete at elevated temperatures. *Cement and Concrete Research*. 2020;135.
- [69] Song P, Hwang S. Mechanical properties of high-strength steel fiber-reinforced concrete. *Construction Building Materials*. 2004;18:669-73.
- [70] Neves RD, Fernandes de Almeida JJSc. Compressive behaviour of steel fibre reinforced concrete. 2005;6:1-8.

- [71] Usman M, Farooq SH, Umair M, Hanif A. Axial compressive behavior of confined steel fiber reinforced high strength concrete. *Construction Building Materials*. 2020;230:117043.
- [72] Usman M, Farooq SH, Umair M, Hanif AJC, Materials B. Axial compressive behavior of confined steel fiber reinforced high strength concrete. 2020;230:117043.
- [73] Society C. Fibre Concrete. 2020.
- [74] Sengul O. Mechanical properties of slurry infiltrated fiber concrete produced with waste steel fibers. *Construction and Building Materials*. 2018;186:1082-91.
- [75] Vistos L, Galladini D, Xargay H, Caggiano A, Folino P, Martinelli E. Hybrid Industrial/Recycled SFRC: Experimental Analysis and Design. *Proceedings of Italian Concrete Days 2016* 2018. p. 98-112.
- [76] Bong SH, Nematollahi B, Nazari A, Xia M, Sanjayan J. Efficiency of different superplasticizers and retarders on properties of ‘one-Part’ Fly ash-slag blended geopolymers with different activators. *Materials & Design*. 2019;12:3410.
- [77] Pająk M, Ponikiewski T. Flexural behavior of self-compacting concrete reinforced with different types of steel fibers. *Construction and Building Materials*. 2013;47:397-408.
- [78] Mastali M, Dalvand A. Fresh and Hardened Properties of Self-Compacting Concrete Reinforced with Hybrid Recycled Steel–Polypropylene Fiber. *Journal of Materials in Civil Engineering*. 2017;29.
- [79] Bartolac M, Damjanović D, Krolo J, Duvnjak I, Baričević A. Punching of slabs reinforced with recycled steel fibres from used tyres. 2016.

- [80] Abdul Awal ASM, Kadir MAA, Yee LL, Memon N. Strength and Deformation Behaviour of Concrete Incorporating Steel Fibre from Recycled Tyre. InCIEC 20142015. p. 109-17.
- [81] Shi X, Brescia-Norambuena L, Grasley Z, Hogancamp J. Fracture Properties and Restrained Shrinkage Cracking Resistance of Cement Mortar Reinforced by Recycled Steel Fiber from Scrap Tires. Transportation Research Record: Journal of the Transportation Research Board. 2020;2674:581-90.
- [82] Khor W. Crack tip opening displacement (CTOD) in single edge notched bend (SEN (B)): Brunel University London; 2018.
- [83] Caggiano A, Said Schicchi D, Etse G, Martinelli E. Meso-Scale Modeling of Hybrid Industrial/Recycled Steel Fiber-Reinforced Concrete. Proceedings of the VII European Congress on Computational Methods in Applied Sciences and Engineering (ECCOMAS Congress 2016)2016. p. 2353-62.
- [84] Najim KB, Saeb A, Al-Azzawi Z. Structural behaviour and fracture energy of recycled steel fibre self-compacting reinforced concrete beams. Journal of Building Engineering. 2018;17:174-82.
- [85] Jeng F, Lin M-L, Yuan S-CJT, technology us. Performance of toughness indices for steel fiber reinforced shotcrete. 2002;17:69-82.
- [86] Tlemat H, Pilakoutas K, Neocleous K. Flexural toughness of SFRC made with fibres extracted from tyres. Proceedings of International Symposium on Advances in Waste Management and Recycling (in Recycling and Reuse of Waste Materials), Dundee2003. p. 365-74.

- [87] Vandewalle L, Nemegeer D, Balazs L, Barr B, Barros J, Bartos P et al. RILEM TC 162-TDF: Test and design methods for steel fibre reinforced concrete'-sigma-epsilon-design method-Final Recommendation. 2003;36:560-7.
- [88] Zamanzadeh Z, Lourenço L, Barros J. Recycled steel fibre reinforced concrete failing in bending and in shear. *Construction and Building Materials*. 2015;85:195-207.
- [89] Tlemat H, Pilakoutas K, Neocleous KJM, structures. Stress-strain characteristic of SFRC using recycled fibres. 2006;39:365-77.
- [90] Surfaces BN. Tire Materials Testing for Harsh Environments. 2018.
- [91] Sienkiewicz M, Kucinska-Lipka J, Janik H, Balas A. Progress in used tyres management in the European Union: A review. *Waste management*. 2012;32:1742-51.
- [92] Mehdipour S, Nikbin IM, Dezhampanah S, Mohebbi R, Moghadam H, Charkhtab S, Moradi A. Mechanical properties, durability and environmental evaluation of rubberized concrete incorporating steel fiber and metakaolin at elevated temperatures. *Journal of Cleaner Production*. 2020;254:120126.
- [93] Piotrowska K, Kruszelnicka W, Bałdowska-Witos P, Kasner R, Rudnicki J, Tomporowski A et al. Assessment of the environmental impact of a car tire throughout its lifecycle using the lca method. *Materials & Design*. 2019;12:4177.
- [94] Yepes V, Martí Albiñana JV, García-Segura T. Design optimization of precast-prestressed concrete road bridges with steel fiber-reinforcement by a hybrid evolutionary algorithm. *International Journal of Computational Methods*. 2017;5:179-89.

- [95] Turner DA, Williams ID, Kemp S. Greenhouse gas emission factors for recycling of source-segregated waste materials. *Resources, Conservation Recycling*. 2015;105:186-97.
- [96] Neocleous K, Angelakopoulos H, Pilakoutas K, Guadagnini M. Fibre-reinforced roller-compacted concrete transport pavements. *Proceedings of the institution of civil engineers-transport*: Thomas Telford Ltd; 2011. p. 97-109.
- [97] Razak HA, Choi F. The effect of corrosion on the natural frequency and modal damping of reinforced concrete beams. *Engineering structures*. 2001;23:1126-33.
- [98] Kot P, Muradov M, Gkantou M, Kamaris GS, Hashim K, Yeboah D. Recent advancements in non-destructive testing techniques for structural health monitoring. *Applied Sciences*. 2021;11:2750.
- [99] Qin X, Kaewunruen S. Environment-friendly recycled steel fibre reinforced concrete. *Construction and Building Materials*. 2022;327:126967.
- [100] Zakaria M, Ahmed M, Hoque MM, Islam S. Scope of using jute fiber for the reinforcement of concrete material. *Textiles and Clothing Sustainability*. 2017;2:1-10.
- [101] Ospitia N, Korda E, Kalteremidou K-A, Lefever G, Tsangouri E, Aggelis DG. Recent developments in acoustic emission for better performance of structural materials. *Developments in the Built Environment*. 2022:100106.
- [102] Belli A, Mobili A, Bellezze T, Tittarelli F. Commercial and recycled carbon/steel fibers for fiber-reinforced cement mortars with high electrical conductivity. *Cement and Concrete Composites*. 2020;109:103569.

- [103] Faris MA, Abdullah MMAB, Muniandy R, Abu Hashim MF, Błoch K, Jeż B et al. Comparison of hook and straight steel fibers addition on malaysian fly ash-based geopolymer concrete on the slump, density, water absorption and mechanical properties. *Materials*. 2021;14:1310.
- [104] Roychand R, Gravina RJ, Zhuge Y, Ma X, Youssf O, Mills JE. A comprehensive review on the mechanical properties of waste tire rubber concrete. *Construction and Building Materials*. 2020;237:117651.
- [105] Rossli SA, Ibrahim IS. Mechanical properties of recycled steel tire fibres in concrete. 2012.
- [106] Johnston C, Skarendahl Å. Comparative flexural performance evaluation of steel fibre-reinforced concretes according to ASTM C1018 shows importance of fibre parameters. *Materials and Structures*. 1992;25:191-200.
- [107] Niş A, Eren NA, Çevik A. Effects of recycled tyre rubber and steel fibre on the impact resistance of slag-based self-compacting alkali-activated concrete. *European Journal of Environmental and Civil Engineering*. 2023;27:519-37.
- [108] El-Hassan H, Elkholy S. Enhancing the performance of Alkali-Activated Slag-Fly ash blended concrete through hybrid steel fiber reinforcement. *Construction and Building Materials*. 2021;311:125313.
- [109] Zhong H, Chen M, Zhang M. Effect of hybrid industrial and recycled steel fibres on static and dynamic mechanical properties of ultra-high performance concrete. *Construction and Building Materials*. 2023;370:130691.

- [110] Baricevic A, Bjegovic D, Skazlic M. Hybrid fiber–reinforced concrete with unsorted recycled-tire steel fibers. *Journal of materials in civil engineering*. 2017;29:06017005.
- [111] Zia A, Zhang P, Holly I. Effectiveness of hybrid discarded tire/Industrial steel fibers for improving the sustainability of concrete structures. *Construction and Building Materials*. 2023;378:131226.
- [112] Chen G, Gao D, Zhu H, Yuan JS, Xiao X, Wang W. Effects of novel multiple hooked-end steel fibres on flexural tensile behaviour of notched concrete beams with various strength grades. *Structures: Elsevier*; 2021. p. 3644-54.
- [113] Venkateshwaran A, Tan KH, Li Y. Residual flexural strengths of steel fiber reinforced concrete with multiple hooked-end fibers. *Structural Concrete*. 2018;19:352-65.
- [114] Kato M, Shimada S. Vibration of PC bridge during failure process. *Journal of Structural Engineering*. 1986;112:1692-703.
- [115] Fayyadh MM, Razak HA. Experimental assessment of dynamic and static based stiffness indices for RC structures. *Structures: Elsevier*; 2022. p. 459-74.
- [116] Zhang Q, Luan C, Yu C, Huang Y, Zhou Z. Mechanisms of carbon black in multifunctional cement matrix: Hydration and microstructure perspectives. *Construction and Building Materials*. 2022;346:128455.
- [117] Letelier V, Bustamante M, Olave B, Martínez C, Ortega JM. Properties of mortars containing crumb rubber and glass powder. *Developments in the Built Environment*. 2023;14:100131.

- [118] Mohajerani A, Burnett L, Smith JV, Markovski S, Rodwell G, Rahman MT et al. Recycling waste rubber tyres in construction materials and associated environmental considerations: A review. *Resources, Conservation and Recycling*. 2020;155:104679.
- [119] Liu X, Thermou GE. A review on the shear performance of reinforced concrete (RC) beams strengthened with externally bonded mortar-based composites. *Structures: Elsevier*; 2023. p. 105474.
- [120] Song P, Hwang S. Mechanical properties of high-strength steel fiber-reinforced concrete. *Construction and Building Materials*. 2004;18:669-73.
- [121] Behbahani H, Nematollahi B, Farasatpour M. Steel fiber reinforced concrete: a review. 2011.
- [122] Lantsoght EO. How do steel fibers improve the shear capacity of reinforced concrete beams without stirrups? *Composites Part B: Engineering*. 2019;175:107079.
- [123] Ahmad SH, Khaloo A, Poveda A. Shear capacity of reinforced high-strength concrete beams. *Journal Proceedings*1986. p. 297-305.
- [124] Vamdewalle MI, Mortelmans F. Shear capacity of steel fiber high-strength concrete beams. *Special Publication*. 1994;149:227-42.
- [125] Balaha M, Badawy A, Hashish M. Effect of using ground waste tire rubber as fine aggregate on the behaviour of concrete mixes. 2007.
- [126] Bockstal L, Berchem T, Schmetz Q, Richel A. Devulcanisation and reclaiming of tires and rubber by physical and chemical processes: A review. *Journal of Cleaner Production*. 2019;236:117574.

- [127] Anderson J, Moncaster A. Embodied carbon of concrete in buildings, Part 1: Analysis of published EPD. *Buildings and Cities*. 2020;1.
- [128] Ouellet-Plamondon C, Habert G. Life cycle assessment (LCA) of alkali-activated cements and concretes. *Handbook of alkali-activated cements, mortars and concretes*: Elsevier; 2015. p. 663-86.
- [129] Özdemir A, Günkaya Z, Özkan A, Ersen O, Bilgiç M, Banar M. Lifecycle assessment of steel rebar production with induction melting furnace: Case study in Turkey. *Journal of Hazardous, Toxic, and Radioactive Waste*. 2018;22:04017027.
- [130] Araujo-Morera J, Verdejo R, López-Manchado MA, Santana MH. Sustainable mobility: The route of tires through the circular economy model. *Waste Management*. 2021;126:309-22.
- [131] Hay R, Ostertag CP. Life cycle assessment (LCA) of double-skin façade (DSF) system with fiber-reinforced concrete for sustainable and energy-efficient buildings in the tropics. *Building and Environment*. 2018;142:327-41.
- [132] Formela K. Sustainable development of waste tires recycling technologies—recent advances, challenges and future trends. *Advanced industrial and engineering polymer research*. 2021;4:209-22.
- [133] Okoye CO, Zhu M, Jones I, Zhang J, Zhang Z, Zhang D. An investigation into the preparation of carbon black by partial oxidation of spent tyre pyrolysis oil. *Waste Management*. 2022;137:110-20.
- [134] ECOTECH G. GEP ECOTECH.

- [135] DIANYAN. High Performance Waste Tire Shredder Waste Tire Recycling Machine 75×kWPower.
- [136] Björkman B, Samuelsson C. Recycling of steel. Handbook of recycling: Elsevier; 2014. p. 65-83.
- [137] Khaloo AR, Dehestani M, Rahmatabadi P. Mechanical properties of concrete containing a high volume of tire–rubber particles. Waste management. 2008;28:2472-82.
- [138] Fiksel J, Bakshi BR, Baral A, Guerra E, DeQuervain B. Comparative life cycle assessment of beneficial applications for scrap tires. Clean technologies and environmental policy. 2011;13:19-35.
- [139] Zamani B, Svanström M, Peters G, Rydberg T. A carbon footprint of textile recycling: A case study in Sweden. Journal of industrial ecology. 2015;19:676-87.
- [140] Mäkelä M, Rissanen M, Sixta H. Machine vision estimates the polyester content in recyclable waste textiles. Resources, Conservation and Recycling. 2020;161:105007.
- [141] Mungyeko Bisulandu B-JR, Marias F. Numerical Modeling of Thermochemical Conversion of Biomass and Tires as Fuels for Cement Clinker Production. Recycling. 2023;8:41.
- [142] Wu Q, Leng S, Zhang Q, Xiao J. Resource and environmental assessment of pyrolysis-based high-value utilization of waste passenger tires. Waste Management. 2021;126:201-8.
- [143] Boiler. How much CO₂ does a tree absorb?

- [144] Zhang X, Li Z-X, Shi Y, Wu C, Li J. Fragility analysis for performance-based blast design of FRP-strengthened RC columns using artificial neural network. *Journal of Building Engineering*. 2022;104364.
- [145] Mangalathu S, Jang H, Hwang S-H, Jeon J-S. Data-driven machine-learning-based seismic failure mode identification of reinforced concrete shear walls. *Engineering Structures*. 2020;208:110331.
- [146] Qian Y, Sufian M, Hakamy A, Farouk Deifalla A, El-said A. Application of machine learning algorithms to evaluate the influence of various parameters on the flexural strength of ultra-high-performance concrete. *Frontiers in Materials*. 2023;9:1114510.
- [147] Pakzad SS, Roshan N, Ghalehnovi M. Comparison of various machine learning algorithms used for compressive strength prediction of steel fiber-reinforced concrete. *Scientific Reports*. 2023;13:3646.
- [148] Kang M-C, Yoo D-Y, Gupta R. Machine learning-based prediction for compressive and flexural strengths of steel fiber-reinforced concrete. *Construction and Building Materials*. 2021;266:121117.
- [149] Alzabeebee S, Al-Hamd RKS, Nassr A, Kareem M, Keawsawasvong S. Multiscale soft computing-based model of shear strength of steel fibre-reinforced concrete beams. *Innovative Infrastructure Solutions*. 2023;8:63.
- [150] Rahman J, Ahmed KS, Khan NI, Islam K, Mangalathu S. Data-driven shear strength prediction of steel fiber reinforced concrete beams using machine learning approach. *Engineering Structures*. 2021;233:111743.

- [151] Shatnawi A, Alkassar HM, Al-Abdaly NM, Al-Hamdany EA, Bernardo LFA, Imran H. Shear Strength Prediction of Slender Steel Fiber Reinforced Concrete Beams Using a Gradient Boosting Regression Tree Method. *Buildings*. 2022;12:550.
- [152] Shahnewaz M, Alam MS. Genetic algorithm for predicting shear strength of steel fiber reinforced concrete beam with parameter identification and sensitivity analysis. *Journal of Building Engineering*. 2020;29:101205.
- [153] Kara IF. Empirical modeling of shear strength of steel fiber reinforced concrete beams by gene expression programming. *Neural Computing and Applications*. 2013;23:823-34.
- [154] Adhikary BB, Mutsuyoshi H. Prediction of shear strength of steel fiber RC beams using neural networks. *Construction and Building Materials*. 2006;20:801-11.
- [155] Yaseen ZM. Machine learning models development for shear strength prediction of reinforced concrete beam: a comparative study. *Scientific Reports*. 2023;13:1723.
- [156] Vu NS, Li B, Beyer K. Effective stiffness of reinforced concrete coupling beams. *Engineering Structures*. 2014;76:371-82.
- [157] Sadati Tilebon SM, Emamian SA, Ramezanpour H, Yousefi H, Özcan M, Naghib SM et al. Intelligent modeling and optimization of titanium surface etching for dental implant application. *Scientific Reports*. 2022;12:1-16.
- [158] Mangalathu S, Heo G, Jeon J-S. Artificial neural network based multi-dimensional fragility development of skewed concrete bridge classes. *Engineering Structures*. 2018;162:166-76.

- [159] Jahangir H, Eidgahee DR. A new and robust hybrid artificial bee colony algorithm–ANN model for FRP-concrete bond strength evaluation. *Composite Structures*. 2021;257:113160.
- [160] Dong W, Huang Y, Lehane B, Ma G. XGBoost algorithm-based prediction of concrete electrical resistivity for structural health monitoring. *Automation in Construction*. 2020;114:103155.
- [161] Bentz EC. Sectional analysis of reinforced concrete members: University of Toronto Toronto; 2000.
- [162] Amin MN, Ahmad W, Khan K, Ahmad A, Nazar S, Alabdullah AA. Use of Artificial Intelligence for Predicting Parameters of Sustainable Concrete and Raw Ingredient Effects and Interactions. *Materials*. 2022;15:5207.
- [163] Yapar O, Basu P, Nordendale N. Accurate finite element modeling of pretensioned prestressed concrete beams. *Engineering Structures*. 2015;101:163-78.
- [164] Zheng X, Li W, Huang Q, Wang B. Finite element modeling of steel-concrete composite beams with different shear connection degrees. *International Journal of Steel Structures*. 2021;21:381-91.
- [165] Lee J, Fenves GL. Plastic-damage model for cyclic loading of concrete structures. *Journal of engineering mechanics*. 1998;124:892-900.
- [166] Lubliner J, Oliver J, Oller S, Oñate E. A plastic-damage model for concrete. *International Journal of solids and structures*. 1989;25:299-326.

- [167] Ouyang X, Wu Z, Shan B, Chen Q, Shi C. A critical review on compressive behavior and empirical constitutive models of concrete. *Construction and Building Materials*. 2022;323:126572.
- [168] Khan M, Cao M, Ali M. Cracking behaviour and constitutive modelling of hybrid fibre reinforced concrete. *Journal of Building Engineering*. 2020;30:101272.
- [169] Vandewalle L, Nemegeer D, Balazs L, Barr B, Barros J, Bartos P et al. RILEM TC 162-TDF: Test and design methods for steel fibre reinforced concrete'-sigma-epsilon-design method-Final Recommendation. *Materials and Structures*. 2003;36:560-7.
- [170] Song C. The scaled boundary finite element method: introduction to theory and implementation: John Wiley & Sons; 2018.
- [171] Kudela J, Matousek R. Recent advances and applications of surrogate models for finite element method computations: a review. *Soft Computing*. 2022;26:13709-33.
- [172] Wei P, Lu Z, Song J. Regional and parametric sensitivity analysis of Sobol' indices. *Reliability Engineering & System Safety*. 2015;137:87-100.
- [173] Shi J, Chu L, Braun R. A kriging surrogate model for uncertainty analysis of graphene based on a finite element method. *International journal of molecular sciences*. 2019;20:2355.
- [174] Rosolem R, Gupta HV, Shuttleworth WJ, Zeng X, de Gonçalves LGG. A fully multiple-criteria implementation of the Sobol' method for parameter sensitivity analysis. *Journal of Geophysical Research: Atmospheres*. 2012;117.

- [175] Tsvetkova O, Ouarda TB. A review of sensitivity analysis practices in wind resource assessment. *Energy Conversion and Management*. 2021;238:114112.
- [176] Homma T, Saltelli A. Importance measures in global sensitivity analysis of nonlinear models. *Reliability Engineering & System Safety*. 1996;52:1-17.
- [177] Kim W, Kim J, Kwak Y-K. Evaluation of flexural strength prediction of reinforced concrete beams with steel fibres. *Journal of Structural Integrity and Maintenance*. 2016;1:156-66.
- [178] Sandeep MS, Tiprak K, Kaewunruen S, Pheinsusom P, Pansuk W. Shear strength prediction of reinforced concrete beams using machine learning. *Structures: Elsevier*; 2023. p. 1196-211.
- [179] Qin X, Kaewunruen S. Eco-Friendly Design and Sustainability Assessments of Fibre-Reinforced High-Strength Concrete Structures Automated by Data-Driven Machine Learning Models. *Sustainability*. 2023;15:6640.
- [180] Mansur M, Ong K, Paramasivam P. Shear strength of fibrous concrete beams without stirrups. *Journal of structural engineering*. 1986;112:2066-79.
- [181] Khuntia M, Stojadinovic B, Goel SCJSJ. Shear strength of normal and high-strength fiber reinforced concrete beams without stirrups. 1999;96:282-9.
- [182] Ashour SA, Hasanain GS, Wafa FF. Shear behavior of high-strength fiber reinforced concrete beams. *Structural Journal*. 1992;89:176-84.
- [183] Al-Ta'an S, Al-Feel J. Evaluation of shear strength of fibre-reinforced concrete beams. *Cement Concrete Composites*. 1990;12:87-94.

- [184] Kara IF. Empirical modeling of shear strength of steel fiber reinforced concrete beams by gene expression programming. *Neural Computing Applications*. 2013;23:823-34.
- [185] Tarawneh A, Almasabha G, Alawadi R, Tarawneh M. Innovative and reliable model for shear strength of steel fibers reinforced concrete beams. *Structures: Elsevier*; 2021. p. 1015-25.
- [186] Simiu E. Design of buildings for wind: A guide for ASCE 7-10 standard users and designers of special structures: John Wiley & Sons; 2011.
- [187] Ellingwood B. Development of a probability based load criterion for American National Standard A58: Building code requirements for minimum design loads in buildings and other structures: Department of Commerce, National Bureau of Standards; 1980.
- [188] Guo Q, Jeffers AE. Finite-element reliability analysis of structures subjected to fire. *Journal of Structural Engineering*. 2015;141:04014129.
- [189] Haldar A, Mahadevan S. Reliability assessment using stochastic finite element analysis: John Wiley & Sons; 2000.
- [190] Papaioannou I, Straub D. Variance-based reliability sensitivity analysis and the FORM α -factors. *Reliability Engineering & System Safety*. 2021;210:107496.
- [191] Renne N, Kara De Maeijer P, Craeye B, Buyle M, Audenaert A. Sustainable assessment of concrete repairs through life cycle assessment (LCA) and life cycle cost analysis (LCCA). *Infrastructures*. 2022;7:128.

- [192] Yang W, Baji H, Li C-Q. Time-dependent reliability method for service life prediction of reinforced concrete shield metro tunnels. *Structure and Infrastructure Engineering*. 2018;14:1095-107.
- [193] Lehner P, Kubzová M, Křivý V, Konečný P, Bujdoš D, Rovnaníková P. Correlation between surface concentration of chloride ions and chloride deposition rate in concrete. *Construction and Building Materials*. 2022;320:126183.
- [194] Huang L, Ye H, Jin X, Jin N, Xu Z. Corrosion-induced shear performance degradation of reinforced concrete beams. *Construction and building materials*. 2020;248:118668.
- [195] Fu X, Chung D. Effect of corrosion on the bond between concrete and steel rebar. *Cement and Concrete Research*. 1997;27:1811-5.
- [196] Bazant ZP, Kim J-K. Size effect in shear failure of longitudinally reinforced beams. American Concrete Institute Farmington Hills, MI; 1984.
- [197] Stewart MG, Rosowsky DV. Structural safety and serviceability of concrete bridges subject to corrosion. *Journal of Infrastructure systems*. 1998;4:146-55.
- [198] Biondini F, Vergani M. Deteriorating beam finite element for nonlinear analysis of concrete structures under corrosion. *Structure and Infrastructure Engineering*. 2015;11:519-32.
- [199] Stewart MG, Al-Harthy A. Pitting corrosion and structural reliability of corroding RC structures: Experimental data and probabilistic analysis. *Reliability engineering & system safety*. 2008;93:373-82.

- [200] Marcos-Meson V, Michel A, Solgaard A, Fischer G, Edvardsen C, Skovhus TL. Corrosion resistance of steel fibre reinforced concrete-A literature review. *Cement and Concrete Research*. 2018;103:1-20.
- [201] Bernard E. Durability of cracked fibre reinforced shotcrete. *Shotcrete: more engineering developments*: CRC Press; 2004. p. 59-66.
- [202] Mangat P, Gurusamy K. Corrosion resistance of steel fibres in concrete under marine exposure. *Cement and Concrete Research*. 1988;18:44-54.
- [203] Kiese TS, Bonnet S, Amiri O, Ventura A. Analysis of corrosion risk due to chloride diffusion for concrete structures in marine environment. *Marine structures*. 2020;73:102804.
- [204] Bigaud D, Ali O. Time-variant flexural reliability of RC beams with externally bonded CFRP under combined fatigue-corrosion actions. *Reliability Engineering & System Safety*. 2014;131:257-70.
- [205] Bastidas-Arteaga E, Bressollette P, Chateauneuf A, Sánchez-Silva M. Probabilistic lifetime assessment of RC structures under coupled corrosion-fatigue deterioration processes. *Structural safety*. 2009;31:84-96.
- [206] Kato Y, Uomoto T. Proposal for quantitative evaluation methodology of inspection value in maintenance of concrete structures based on repair-risk. *Journal of Advanced Concrete Technology*. 2005;3:363-70.
- [207] El Hassan J, Bressollette P, Chateauneuf A, El Tawil K. Reliability-based assessment of the effect of climatic conditions on the corrosion of RC structures subject to chloride ingress. *Engineering Structures*. 2010;32:3279-87.

- [208] Mirza SA, MacGregor JG. Variability of mechanical properties of reinforcing bars. *Journal of the Structural Division*. 1979;105:921-37.
- [209] Atadero RA, Karbhari VM. Calibration of resistance factors for reliability based design of externally-bonded FRP composites. *Composites Part B: Engineering*. 2008;39:665-79.
- [210] Mirza SA, MacGregor JG. Probabilistic study of strength of reinforced concrete members. *Canadian Journal of Civil Engineering*. 1982;9:431-48.
- [211] Simwanda L, De Koker N, Viljoen C. Structural reliability of ultra high-performance fibre reinforced concrete beams in flexure. *Engineering Structures*. 2021;244:112767.
- [212] Shahnewaz M, Machial R, Alam MS, Rteil A. Optimized shear design equation for slender concrete beams reinforced with FRP bars and stirrups using Genetic Algorithm and reliability analysis. *Engineering Structures*. 2016;107:151-65.
- [213] Nasrollahzadeh K, Aghamohammadi R. Reliability analysis of shear strength provisions for FRP-reinforced concrete beams. *Engineering Structures*. 2018;176:785-800.
- [214] Frazão CM, Barros JA, Bogas JA. Durability of recycled steel fiber reinforced concrete in chloride environment. *Fibers*. 2019;7:111.
- [215] Yoo D-Y, Yang J-M. Effects of stirrup, steel fiber, and beam size on shear behavior of high-strength concrete beams. *Cement Concrete Composites*. 2018;87:137-48.

- [216] Manju R, Sathya S, Sylviya B. Shear strength of high-strength steel fibre reinforced concrete rectangular beams. *Int J Civ Eng Technol*. 2017;8:1716-29.
- [217] Tahenni T, Chemrouk M, Lecompte T. Effect of steel fibers on the shear behavior of high strength concrete beams. *Construction Building Materials*. 2016;105:14-28.
- [218] Kwak Y-K, Eberhard MO, Kim W-S, Kim J. Shear strength of steel fiber-reinforced concrete beams without stirrups. *ACI Structural journal*. 2002;99:530-8.
- [219] Alzahrani F. Shear behaviour of steel fibre-reinforced high strength lightweight concrete beams without web reinforcement: Memorial University of Newfoundland; 2018.
- [220] Singh B, Jain K. Appraisal of Steel Fibers as Minimum Shear Reinforcement in Concrete Beams. *ACI Structural Journal*. 2014;111.
- [221] Cho S-H, Kim Y-I. Effects of steel fibers on short beams loaded in shear. *Structural journal*. 2003;100:765-74.
- [222] Narayanan R, Darwish I. Shear in mortar beams containing fibers and fly ash. *Journal of Structural Engineering*. 1988;114:84-102.
- [223] Shin S-W, Oh J-G, Ghosh S. Shear behavior of laboratory-sized high-strength concrete beams reinforced with bars and steel fibers. *Special Publication*. 1994;142:181-200.
- [224] Noghabai K. Beams of fibrous concrete in shear and bending: experiment and model. *Journal of Structural Engineering*. 2000;126:243-51.
- [225] Uomoto T, Weeraratne R, Furukoshi H, Fujino H. Shear strength of reinforced concrete beams with fiber reinforcement. *Proc RILEM Symp FRC1986*. p. 553-62.

References

- [226] Hwang J-H, Lee DH, Kim KS, Ju H, Seo S-Y. Evaluation of shear performance of steel fibre reinforced concrete beams using a modified smeared-truss model. Magazine of Concrete Research. 2013;65:283-96.
- [227] Li VC, Ward RJ, Hamza AM. Steel and synthetic fibers as shear reinforcement. 1992.
- [228] de Lima Araújo D, Nunes FGT, Toledo Filho RD, de Andrade MASJAST. Shear strength of steel fiber-reinforced concrete beams. 2014;36:389-97.
- [229] Adebar P, Mindess S, Pierre DS-, Olund B. Shear tests of fiber concrete beams without stirrups. Structural Journal. 1997;94:68-76.
- [230] Cohen M, Aoude H. Shear behavior of SFRC and SCFRC beams. Proceedings of the 3rd International Structural Specialty Conference, Edmonton, AB, Canada 2012. p. 6-9.
- [231] Pansuk W, Nguyen TN, Sato Y, Den Uijl J, Walraven J. Shear capacity of high performance fiber reinforced concrete I-beams. Construction Building Materials. 2017;157:182-93.
- [232] Tahenni T, Chemrouk M, Lecompte T. Effect of steel fibers on the shear behavior of high strength concrete beams. Construction and Building Materials. 2016;105:14-28.
- [233] Lim D, Oh B. Experimental and theoretical investigation on the shear of steel fibre reinforced concrete beams. Engineering structures. 1999;21:937-44.
- [234] Cucchiara C, La Mendola L, Papia M. Effectiveness of stirrups and steel fibres as shear reinforcement. Cement and concrete composites. 2004;26:777-86.

- [235] Tahenni T, Bouziadi F, Boulekbache B, Amziane S. Experimental and numerical investigation of the effect of steel fibres on the deflection behaviour of reinforced concrete beams without stirrups. Structures: Elsevier; 2021. p. 1603-19.
- [236] Swamy F, Sa'ad A. Deformation and ultimate strength in flexure of reinforced. ACI JOURNAL. 1981.
- [237] Cardoso DC, Pereira GB, Holtz Filho JJ, Silva FA, Pereira EV. FLEXURAL BEHAVIOR OF UNDER-REINFORCED STEEL FIBER CONCRETE (R/SFRC) BEAMS.
- [238] Beshara F, Shaaban I, Mustafa T. Nominal flexural strength of high strength fiber reinforced concrete beams. Arabian Journal for Science and Engineering. 2012;37:291-301.
- [239] Imam M, Vandewalle L, Mortelmans F. Shear–moment analysis of reinforced high strength concrete beams containing steel fibres. Canadian Journal of Civil Engineering. 1995;22:462-70.
- [240] Oh BH. Flexural analysis of reinforced concrete beams containing steel fibers. Journal of structural engineering. 1992;118:2821-35.
- [241] Rjoub M, Muhammad I. Moment capacity of steel fiber reinforced concrete beams. JES Journal of Engineering Sciences. 2006;34:413-22.
- [242] Sahoo DR, Sharma A. Effect of steel fiber content on behavior of concrete beams with and without stirrups. ACI Structural Journal. 2014;111:1157.

- [243] Shoaib A, Lubell AS, Bindiganavile VS. Shear response of lightweight steel fiber reinforced concrete members without stirrups. *Materials and Structures*. 2015;48:3141-57.
- [244] Parra-Montesinos G, Wight J, Dinh H, Libbrecht A, Padilla C. Shear strength of fiber reinforced concrete beams without stirrups. University of Michigan: Ann Arbor, MI, USA. 2006:39.
- [245] Rosenbusch J, Teutsch M. Trial beams in shear brite/euram project 97-4163 final report sub Task 4.2. Tech Univ Braunsch. 2003;1:105-17.
- [246] Sahoo DR, Bhagat S, Reddy TCV. Experimental study on shear-span to effective-depth ratio of steel fiber reinforced concrete T-beams. *Materials and Structures*. 2016;49:3815-30.
- [247] Narayanan R, Darwish I. Use of steel fibers as shear reinforcement. *Structural Journal*. 1987;84:216-27.
- [248] Dinh HH. Shear behavior of steel fiber reinforced concrete beams without stirrup reinforcement: University of Michigan; 2009.
- [249] Aoude H, Belghiti M, Cook WD, Mitchell D. Response of Steel Fiber-Reinforced Concrete Beams with and without Stirrups. *ACI Structural Journal*. 2012;109.
- [250] Minelli F, Plizzari GA. On the Effectiveness of Steel Fibers as Shear Reinforcement. *ACI Structural Journal*. 2013;110.
- [251] Kang TH, Kim W, Kwak Y-K, Hong S-G. Shear testing of steel fiber-reinforced lightweight concrete beams without web reinforcement. *ACI Structural Journal*. 2011;108:553.

- [252] Lim T, Paramasivam P, Lee S. Shear and moment capacity of reinforced steel-fibre-concrete beams. *Magazine of concrete research*. 1987;39:148-60.
- [253] Tan K, Murugappan K, Paramasivam P. Shear behavior of steel fiber reinforced concrete beams. *Structural Journal*. 1993;90:3-11.
- [254] Kim C-G, Lee H, Park H-G, Hong G-H, Kang S-M. Effect of Steel Fibers on Minimum Shear Reinforcement of High-Strength Concrete Beams. *ACI Structural Journal*. 2017;114.
- [255] Sharma A. Shear strength of steel fiber reinforced concrete beams. *Journal Proceedings*1986. p. 624-8.
- [256] Swamy RN, Jones R, Chiam AT. Influence of steel fibers on the shear resistance of lightweight concrete I-beams. *Structural Journal*. 1993;90:103-14.
- [257] Greenough T, Nehdi M. Shear behavior of fiber-reinforced self-consolidating concrete slender beams. *ACI materials Journal*. 2008;105:468.
- [258] Dupont D, Vandewalle L. Shear capacity of concrete beams containing longitudinal reinforcement and steel fibers. *Special Publication*. 2003;216:79-94.
- [259] Swamy R, Bahia H. The effectiveness of steel fibers as shear reinforcement. *Concrete International*. 1985;7:35-40.
- [260] Batson G, Jenkins E, Spatney R. Steel fibers as shear reinforcement in beams. *Journal Proceedings*1972. p. 640-4.
- [261] Zhao J, Liang J, Chu L, Shen F. Experimental study on shear behavior of steel fiber reinforced concrete beams with high-strength reinforcement. *Materials*. 2018;11:1682.

- [262] Kwak K-H, Suh J, Hsu C-TT. Shear-fatigue behavior of steel fiber reinforced concrete beams. *Structural Journal*. 1991;88:155-60.
- [263] Aoude H, Cohen M. Shear response of SFRC beams constructed with SCC and Steel Fibers. *Electronic Journal of Structural Engineering*. 2014;14:71-83.
- [264] Qissab MA, Salman MM. Shear strength of non-prismatic steel fiber reinforced concrete beams without stirrups. *Struct Eng Mech*. 2018;67:347-58.
- [265] Furlan Jr S, de Hanai JB. Shear behaviour of fiber reinforced concrete beams. *Cement and concrete composites*. 1997;19:359-66.
- [266] Krassowska J, Kosior-Kazberuk M. Failure mode in shear of steel fiber reinforced concrete beams. *MATEC Web of Conferences: EDP Sciences*; 2018. p. 02003.
- [267] Gali S, Subramaniam KV. Shear behavior of steel fiber reinforced concrete using full-field displacements from digital image correlation. *MATEC Web of Conferences: EDP Sciences*; 2017. p. 04003.
- [268] Shoaib A, Lubell AS, Bindiganavile VS. Size effect in shear for steel fiber-reinforced concrete members without stirrups. *ACI Structural Journal*. 2014;111:1081.
- [269] Abdul-Zaher AS, Abdul-Hafez LM, Tawfic YR, Hammed O. Shear behavior of fiber reinforced concrete beams. *JES Journal of Engineering Sciences*. 2016;44:132-44.

References
